Provenance and metamorphic evolution of high-pressure rocks from the Malpica-Tuy zone (MTZ) in NW Spain

Von der Fakultät Chemie der Universität Stuttgart
zur Erlangung der Würde eines Doktors der
Naturwissenschaften (Dr. rer. nat.) genehmigte Abhandlung

Vorgelegt von

Botao Li

aus Nei Mongol, VR China

Hauptberichter: Prof. Hans-Joachim Massonne
Mitberichter: Prof. Joris van Slageren
Vorsitzender des Prüfungsausschusses: Prof. Thomas Schleid

Tag der mündlichen Prüfung: 22. August 2016

Universität Stuttgart

Institut für Mineralogie und Kristallchemie
2016

Erklärung über die Eigenständigkeit der Dissertation

Ich versichere, dass ich die vorliegende Arbeit mit dem Titel

"Provenance and metamorphic evolution of high-pressure rocks from the Malpica-Tuy zone (MTZ) in NW Spain"

selbständig verfasst und keine anderen als die angegebenen Quellen und Hilfsmittel benutzt habe; aus fremden Quellen entnommene Passagen und Gedanken sind als solche kenntlich gemacht.

Declaration of Authorship

I hereby certify that the dissertation entitled

"Provenance and metamorphic evolution of high-pressure rocks from the Malpica-Tuy zone (MTZ) in NW Spain"

is entirely my own work except where otherwise indicated. Passages and ideas from other sources have been clearly indicated.

Name/Name: Botao Li_____

Unterschrift/Signed: _____

Datum/Date: _____

Provenance and metamorphic evolution of high-pressure rocks from the Malpica-Tuy zone (MTZ) in NW Spain

Zusammenfassung

Das Verständnis der Kontinent-Kontinent Kollisionsprozesse der Erde lässt sich am besten an der Naht zwischen den kollidierenden Kontinentalplatten untersuchen. Eine relativ gut untersuchte Nahtzone ist die Malpica-Tuy (auch Tui) Scherzone (MTZ) im Nordwesten Spaniens. Frühere Arbeiten in diesem Bereich haben zu einer zunehmend detaillierteren Karte der Region geführt. Einige Arbeiten zu der Datierung von Gesteinen wurden durchgeführt (Protolith auf metamorphen Alter). Es ist jedoch nur wenig über die Entwicklung der Gesteine des MTZ bekannt. Aus diesem Grund wurde eine Untersuchung der verschiedenen metamorphen Gesteine aus der MTZ begonnen. Das Ziel war ihre zeitliche Druck-Temperatur (P-T) Entwicklung zu entschlüsseln und damit zu das Verständnis der Kontinent-Kontinent Kollisionsprozesse zu vertiefen. Um dieses Ziel zu erreichen, wurden folgende Analysenmethoden eingesetzt. Die Anzahl der Analysen für jede Probe, die detailliert untersucht wurde, ist in Tabelle 1 aufgeführt:

(1) Optische Mikroskopie: Es wurden Dünnschliffe der häufig vorkommenden Gesteinsproben ausgewählt, die im Detail überprüft, untersucht werden sollten. Strukturelle Beziehungen von Mineralien konnten erkannt werden.

(2) Elektronenmikrosonde (EMP) Analytik: Die chemische Zusammensetzung von Mineralen wurde bestimmt. Strukturelle Beziehungen wurden durch rückgestreute Elektronenbilder dokumentiert. Röntgenkarten wurden angefertigt, um die Verteilung der Elemente in Mineralen sichtbar zu machen. Die U, Th und Pb Gehalte von Monazit wurden zur Altersbestimmung der Minerale herangezogen.

(3) Röntgenfluoreszenz (XRF) Spektrometrie: Bulk-Gestein-Zusammensetzungen wurden für die wichtigsten Elemente aus Gesteinsmehl und Spectromelt (Li-Borat: $Li_2B_4O_7$) unter Verwendung von Glasscheiben bestimmt. Spurenelemente wurden auf Scheiben durch Pressen von Gesteinsmehl mit Wachs analysiert.

(4) Laser-Ablation induktiv gekoppelte Plasma-Massenspektrometrie (LA-ICP-MS): Spurenelemente wurden zusätzlich durch Ablation der für XRF benutzen Proben auf Glassscheiben analysiert. Ein wesentlicher Teil der Bewertung der analytischen Arbeit und ihre Verwendung zur Bestimmung der P-T Pfade war verbunden mit der

Berechnung der P-T, P-O_2 und T-O_2 pseudosections. Zu diesem Zweck wurde das Programmpaket PERPLE_X für das chemische System Si-Ti-Al-Fe-Mn-Mg-Ca-Na-K-O-H eingesetzt. Diese Pseudosections wurden durch Isoplethen für diverse modale und chemische Parameter konturiert, wie zum Beispiel vol.% von Granat, Si-Gehalt in kaliumhaltigem Weissglimmer pro Formeleinheit. Die vorliegende Arbeit ist in drei Teile untergliedert. Der erste Teil wurde in dem European Journal of Mineralogy (EJM) veröffentlicht. Der zweite Teil wird zum Einreichen an ein internationales Journal vorbereitet. Der dritte Teil ist beim Verlag zur Überprüfung eingereicht.

Teil 1 (EJM): Eklogit (Probe 18149) und der umgebende Gneis (Probe 18159) aus dem nördlichen MTZ wurden untersucht. Eine Reihe von P-T pseudosections wurden für die Bulk-Rock-Zusammensetzung dieser Gesteine berechnet und konturiert. Die P-T pfade wurden zumeist mittels der variablen Granat und Phengit Zusammensetzung und deren Isoplethen berechnet. Der Pfad für Eklogit ist durch die isotherme Erdlagerung bei Spitzendrücken von 22.5 kbar bei 540 °C charakterisiert. Die nachfolgende Erosion findet bei bei P-T-Bedingungen von 21 kbar bei 575 °C und 13.5 kbar bei 625 °C statt. Die letzteren Daten repräsentieren auch die Spitzen-P-T-Bedingungen des Gneis. Allerdings beginnt der frühe P-T Pfad des Gneis bereits bei 11.5-13.7 kbar und 520-570 °C. Obwohl beide Gesteine in direkten Kontakt miteinander stehen, war der frühe P-T Verlauf unterschiedlich. Die häufig geäußerte Meinung, dass ein solcher Kontakt eine gemeinsame P-T Entwicklung von Eklogit und Gneis beweist, wurde widerlegt. Nur der Erosionsvorgang der untersuchten Gesteine aus einer Tiefe von 45 bis 50 km entsprechend einem Druck von 13.5 kbar war übereinstimmend.

Teil 2 (beim Vorbereiten der Einreichung): Fünf Proben, drei verschiedene Eklogite (Proben: 130893, 18193, Sp96-41a), ein granathaltiger Glaucophanite (Sp96-41b) und ein tonalitischer Gneis (18195), wurden bei 'La Pioza' im zentralen MTZ gesammelt und ihre P-T Entwicklung sowie die Art der Protolithe bestimmt. Eine Reihe von P-T, P-O_2 und T-O_2 Pseudosectionen wurden berechnet und konturiert, insbesondere durch Isoplethen der Molenbrüche von Granat-Komponenten. Unter Verwendung solcher Isoplethen und der Zr-in-Rutil Geothermometrie, wurden drei gegensätzliche P-T Pfade abgeleitet. (1) Zwei Eklogite und Gneise ergaben einen ähnlichen P-T Pfad im Gegenuhrzeigersinn. Speziell einer der Eklogite war durch

einen Pfad ausgezeichnet, der von 565-590 °C/5-8.5 kbar zu Spitzentemperaturen von 650 °C bei 17-20 kbar und zu anschliessenden Spitzendrücken von 23-26 kbar bei 610-645 °C führte. (2) Eine im Uhrzeigersinn verlaufende P-T-Schleife wurde abgeleitet für einen Eklogit, die bei 565-590 °C/16-19 kbar beginnt und bei 595-640 °C/22-25 kbar endet. (3) Der im Uhrzeigersinn verlaufende P-T Pfad des Glaucophanits zeigte eine Temperaturerhöhung von 590 bis 610 °C bis 665 °C im Druckbereich von 18 bis 22 kbar. Geochemische Eigenschaften der Haupt- und Spurenelemente zeigen, dass die Protolithe der Eklogite eine kalk-alkalische Affinität aufweisen und der Gneis mit einem magmatischen Bogen in Beziehung steht. Die Protolithe der Eklogite mit tholeiitischer Affinität stehen in Beziehung zu Basalt/Gabbros der verdickten ozeanischen Kruste (Inselbogen im Rheischen Ozean). Für den Eklogit 130893, für den ein nahezu isothermer Einbettungspfad bei etwa 5-8.5 kbar beginnt, wurde eine kontinentale protolitische Signatur abgeleitet. Es wird zudem angenommen, dass er in die Subduktion durch tektonische Erosion miteinbezogen wurde (analaog zu Eklogit aus dem nördlichen MTZ (Teil 1). Die gegensätzlichen P-T Pfade und unterschiedliche Natur der Protolithe werden durch leicht verschiedene aufwärts gerichtete Massenströme erklärt. Somit ergibt sich eine Vermischung unterschiedlicher Arten von Gesteinen in einem Subduktionskanal.

Teil 3 (ist eingereicht): Zwei Chloritoidschiefer und eine staurolith-andalusithaltige Lagerstätte aus dem Ceán-Bereich und des nördlichen MTZ wurden untersucht, um ihre P-T Entwicklung zu erforschen. Eine Serie von P-T, P-O_2 und T-O_2 pseudosections, wurden berechnet und durch Isoplethen verschiedener Parameter konturiert, einschließlich Molenbrüche von Granat Komponenten, Si (pfu) in Phengit und XMg (Mg / (Mg + Fe^{2+}) in Chloritoid. Diese Isoplethen wurden verwendet um P-T Pfade abzuleiten. Die beiden untersuchten Chloritoid Schiefer wiesen Spitzenwerte im P-T Diagramm bei rund 21 kbar und 570 °C und einer nachfolgenden isothermen Ferilegung durch Erosion. Der entgegen dem Uhrzeigersinn durchlaufene Weg ist durch einen Druckanstieg von etwa 8 kbar gekennzeichnet, bei Startwerten der Temperatur von 450-500 °C. Dies weist auf eine tektonische Erosion hin, verursacht durch eine abtauchende (ozeanische) Platte. Der Staurolith-Andalusithaltige Lagerschiefer erfuhr nur Spitzendrücke von 9 kbar bei einer Temperatur von etwa 570 °C. Diese Gesteine könnten metamorphosierte Sedimente sein, die sich ursprünglich auf der Oberfläche der sich abwärts

bewegenden Kontinentalplatte befanden. Zusätzlich wurden mit EMP Altersbestimmungen für Monazit auf dem Staurolith tragenden Metapelite durchgeführt. Das Alter des Monazits von 307-385 Ma bestätigt vorher bestimmte oberdevonische bis spätkarbonische metamorphe Vorgänge.

Die vorgenannten Ergebnisse haben zu neuen grundlegenden Erkenntnissen geführt:

1) Hochdruck (P > 10 kbar) Gesteine aus dem MTZ sind nicht Teil der kohärenten Krustenabschnitte wie in früheren Arbeiten vorgeschlagen. Diese Gesteine wurden tektonisch noch bei HP Bedingungen vermischt.

(2) In Bezug auf Gesteine, die Drücke über 18 kbar erfahren hatten, trat diese Vermischung bereits im Subduktionskanals auf.

(3) Einige der hier untersuchten Gesteine wurden durch tektonische Erosion in die Subduktionszone transportiert.

Table 1. The studied samples and their corresponding analytical work. “Parts1 to 3”: See text. Abbreviations: amphibole (Am), biotite (Bt), chlorite (Ch), chloritoid (Ctd), epidote (Ep), garnet (Gt), K-feldspar (Kf), monazite (Mo), omphacite (Om), paragonite (Pa), phengite (+ muscovite) (Ph), plagioclase (Pl), rutile (Rt), staurolite (St), and tourmaline (Tour).

	Samples	**XRF**		**LA-ICP-MS**	**EMP**		
		major element analyses	trace element analyses	trace element analyses	spot analyses	X-ray maps	monazite Analyses for dating
Part 1	Eclogite (18149)	1	1	1	226 Gt, 97 Ph,128 Am, 126 Om, 8 Ep, 25 Ch, 6 Pl	4 Gt, 3 Ph 3 Am, 3 Om	
	Gneiss (18159)	1			107 Gt, 120 Ph, 11 Ep, 20 Bt, 7 Pl, 7 Kf, 20 Ch	4 Gt, 2 Ph	
Part 2	Eclogite (130893)	1	1	1	268 Gt, 165 Am, 113 Om, 54 Ep, 21 Ch, 10 Pl, 15 Pa, 196 Rt	3 Gt, 2 Am 3 Om	
	Eclogite (Sp96-41a)	1	1	1	205 Gt, 119 Ph, 134 Am, 126 Om, 58 Ep, 11 Ch, 6 Pl, 72 Rt	4 Gt, 2 Ph 3 Am, 3 Om	
	Eclogite (18193)	1	1	1	140 Gt, 82 Ph, 90 Am, 171 Om, 9 Ep, 10 Ch, 13 Pl, 163 Rt	4 Gt, 2 Ph 3 Am, 3 Om	
	Tonalitic gneiss (18195)	1			121 Gt, 89 Ph, 22 Pa, 45 Am, 17 Bt, 52 Om, 46 Ep, 20 Ch, 32 Pl, 101 Rt	4 Gt, 2 Ph	
	Glaucophanite (Sp96-41b)	1	1	1	260 Gt, 30 Pa, 124 Am, 18 Om, 13 Ep, 22 Ch, 50 Pl, 76 Rt	3 Gt, 3 Am	
Part 3	Chloritoid schist (Sp96-39j)	1			107 Gt, 81 Ctd, 150 Ph, 14 Pa, 5 Ep, 17 Ch, 20 Tour	3 Gt, 2 Ph 2 Ctd	
	Chloritoid schist (Sp96-39k)	1			92 Gt, 90 Ctd, 132 Ph, 20 Pa, 11 Ep, 30 Ch, 12 Tour	3 Gt, 2 Ph 2 Ctd	
	Staurolite-andalusite-bearing schist (Sp96-38w)	1			52 Ph, 30 Bt, 18 Ch, 20 Tour, 25 St, 12 Pl, 15 Kf	2 Ph	111 Mo

Summary

The understanding of continent-continent collisional processes on Earth can best be studied in suture zones between the colliding continental plates. A relatively well studied suture zone is the Malpica-Tuy (also Tui) shear zone (MTZ) in northwestern Spain. Previous work in this zone has resulted in a continuous detailed map of the area. Several works on dating of rocks (protolith on metamorphic ages) have been achieved. However, little is known about the evolution of the rocks of the MTZ. For this reason, a study of various metamorphic rocks from the MTZ was started to decipher their pressure-temperature (P-T) - time evolution and, thus, to better understand continent-continent collisional processes.

To reach the goal, the following analytical methods were applied. The numbers of analyses achieved on each sample studied in detail are listed in Table 1:

(1) Optical microscopy: Thin sections of abundant rock samples were checked for the selection of samples to be studied in detail. Textural relations of minerals could be recognized.

(2) Electron-microprobe (EMP) analytics: Chemical compositions of minerals were determined. Textural relations were documented by back scattered electron images. X-ray maps were produced to recognize the chemical zonation of minerals. Monazite was analyses to date this mineral using its U, Th, and Pb contents.

(3) X-ray fluorescence (XRF) spectrometry: Bulk-rock compositions were determined for major elements using glass discs prepared from rock powder and Spectromelt (Li-borate: $Li_2B_4O_7$). Trace elements were analyzed on discs obtained by pressing rock powder with wax.

(4) Laser-ablation inductively-coupled plasma mass-spectrometry (LA-ICP-MS): trace elements were also analyzed by ablation of glass discs used for XRF spectrometry.

A major part of the evaluation of the analytical work and its use to determine P-T paths was related to the calculation of P-T, P-O_2, and T-O_2 pseudosections. For this purpose, the computer program package PERPLE_X was applied to the chemical system Si-Ti-Al-Fe-Mn-Mg-Ca-Na-K-O-H. These pseudosections were contoured by isopleths for diverse modal and chemical parameters such as vol.% of garnet, Si content in potassic white mica per formula unit.

The achieved work could be easily subdivided into three parts. The first part is published on the European Journal of Mineralogy (EJM). The second is prepared for submission to an international journal. The third part is in submission.

Part 1 (EJM): Eclogite (sample 18149) and its surrounding gneiss (sample 18159) from the northern MTZ were studied. A series of P-T pseudosections were calculated for the bulk-rock compositions of these rocks and contoured. Using mainly the variable garnet and phengite compositions and these isopleths, P-T paths were derived. This path for the eclogite is characterized by isothermal burial to peak pressures of 22.5 kbar at 540 °C. The subsequent exhumation path passes through P-T conditions of 21 kbar at 575 °C and 13.5 kbar at 625 °C. The latter data also represent the peak P-T conditions of the gneiss. However, the early P-T path of the gneiss starts already at 11.5-13.7 kbar and 520-570 °C. Thus, the P-T paths for both rocks, although now in direct contact with each other, had experienced a different early P-T evolution. The frequently uttered opinion that such a contact proves a common P-T history of eclogite and gneiss was disproved. Only the exhumation history of the studied rocks from depths of 45-50 km corresponding to 13.5 kbar was a common one.

Part 2 (In preparation for submission): Five samples, three different eclogites (samples: 130893, 18193, Sp96-41a), a garnet-bearing glaucophanite (Sp96-41b) and a tonalitic gneiss (18195), were collected at the 'La Pioza' land site in the central MTZ, and their P-T evolution and kind of protoliths were determined. A series of P-T, P-O2, and T-O2 pseudosections were calculated and contoured especially by isopleths of molar fractions of garnet components. Using such isopleths and Zr-in-rutile geothermometry, three contrasting P-T paths were derived. (1) Two eclogites and the gneiss yielded a similar anticlockwise P-T path. Especially one of these eclogites recorded an extended path from 565-590 ºC and 5-8.5 kbar to peak temperatures of 650 ºC at 17-20 kbar and further to peak pressures of 23-26 kbar at 610-645 ºC. (2) A clockwise P-T loop was derived for an eclogite starting at 565-590 ºC and 16-19 kbar and ending at 595-640 ºC and 22-25 kbar. (3) The clockwise P-T path of the glaucophanite showed a temperature increase from 590-610 ºC to 665 ºC in the pressure range 18-22 kbar. Major and trace element geochemical features demonstrate that the protoliths of the eclogites with calc-alkaline affinity and the gneiss can be related to a magmatic arc. The protoliths of

the eclogites with tholeiitic affinity were related to basalt/gabbro of thickened oceanic crust (island arc in the Rheic Ocean). Eclogite 130893 with a continental protolith signature, for which a nearly isothermal burial path starting at a pressure of about 5-8.5 kbar was derived, is hypothesized to be involved in the subduction by tectonic erosion as the eclogite from the northern MTZ (Part 1). The contrasting P-T paths and different nature of the protoliths are explained by slightly different upwards-directed mass flows and, thus, mixing of various types of rocks in a subduction channel.

Part 3 (In submission): Two chloritoid schists and a staurolite-andalusite bearing schist from the Ceán unit of the northern MTZ were studied to decipher their P-T evolution. A series of P-T, P-O_2, and T-O_2 pseudosections, were calculated and contoured by isopleths of various parameters, including molar fractions of garnet components, Si (pfu) in phengite, and XMg ($Mg/(Mg + Fe^{2+})$) in chloritoid. These isopleths were used to derive P-T paths. The two studied chloritoid schists experienced peak P-T conditions around 21 kbar at 570 °C and a subsequent isothermal exhumation. The prograde path is characterized by a pressure increase of about 8 kbar starting at temperatures of 450-500 °C and, thus, points to a tectonic erosion event caused by a subducting (oceanic) slab. The staurolite-andalusite bearing schist experienced only peak pressures of 9 kbar at a temperature around 570 °C. This rock might represent metamorphosed sediments that were originally at the surface of the downgoing continental plate. In addition, monazite ages were determined with EMP on the staurolite-bearing metapelite. The monazite ages of 307-385 Ma confirm previously determined Upper Devonian to late Carboniferous metamorphic events.

The aforementioned results have resulted in the following new major findings: 1) high-pressure (P > 10 kbar) rocks from the MTZ are not part of coherent crustal sections as suggested in previous works. These rocks were tectonically mixed still at HP conditions. (2) Concerning rocks which had experienced pressures in excess of 18 kbar, this mixing occurred already in the subduction channel. (3) Some of the rocks studied here were transported into the subduction zone by tectonic erosion.

Table of contents

1. Introduction

1.1. Motivation

Various geodynamic models for the European part of the Variscan orogeny exist. However, all models consider the closure of the Rheic Ocean and the subsequent collision of Gondwana and Laurussia. Furthermore, concerning the closure of the Rheic Ocean, two types of tectonic models exist. The first type suggests that this ocean completely developed at the margin of Laurussia based on the appearance of diverse ophiolite sequences in northern Spain (Martínez Catalán et al., 1996, 2007, 2009; Arenas et al., 2009; Díez Fernández et al., 2011, 2012a, 2012b; Díez Fernández & Martínez Catalán, 2012). Another type of these models proposes that the Rheic Ocean was subducted below Laurussia followed by continental (Gondwana) subduction (Rodríguez et al., 2003; Ballèvre et al., 2012; Rubio Pascual et al., 2013). However, the timing of this process and the way how this ocean was subducted is still a matter of debate. The Malpica-Tuy shear zone (MTZ) in northwestern Spain is a key area for the understanding of the collisional process, because the tectonic construction of this zone is relatively simple but the rock types (metamafic rocks and orthogneisses and metasediments) in the MTZ are variable. In general, metamorphic rocks are interpreted as the result of continental subduction (e.g. Guillot et al., 1997; Jahn, 1999; Pullen et al., 2008; Nakano et al., 2010; Ravna et al., 2010; López-Carmona et al., 2014a) or collision between continental crust and oceanic crust (e.g. Klemd et al., 2011; Endo et al., 2012; Nakano et al., 2015). Detailed mass-flow paths in terms of pressure (P) and temperature (T) for different types of rocks and their original nature are required to better understand the collisional situation in Variscan times.

In the MTZ, lenses/blocks of co-occurring high-pressure (HP: > 10 kbar) metatonalites and metamafic (eclogite) rocks are distributed in host orthogneisses. The area with such metamorphic lenses is classified as eclogite-facies terrane (Díez Fernández et al., 2011). Usually, the whole eclogite-facies terrane was treated as one tectonic block that has moved as a whole during the Variscan collision (Rodríguez et al., 2003; López-Carmona et al., 2010, 2013; Díez Fernández et al., 2011). However, country-rocks, such as gneisses, and embedded eclogite bodies can show similar (e.g. NW Spain: Albert et al., 2012) or different P-T evolutions (e.g. Willner et al., 2000;

Săbău & Massonne, 2003; Massonne, 2012). In the latter cases, the eclogite bodies must have been tectonically inserted in the country rocks. On the contrary, geoscientists often believe that country rocks and eclogite bodies embedded therein must have experienced the same P-T evolution (Krogh, 1980; 1981; Kaneko et al., 2003; Xu et al., 2006). Due to the lack of well-constrained P-T data of HP country-rock gneisses and embedded eclogite bodies in the MTZ, it is not clear if both rock types were subject to similar P-T conditions. With this study, we want to demonstrate that (1) the metamorphic evolution of HP eclogite bodies and adjacent gneisses can be successfully derived and (2) important conclusions can be drawn to characterize the geodynamic processes behind such occurrences of HP rocks.

Furthermore, it should be figured out if metamafic lenses/blocks located in different places of the MTZ have experienced a similar P-T history. Even, the tectonic evolution of the same type of rocks with diverse mineral assemlages (e.g. with or without phengite) from the same locality could be different. For example, Kadarusman et al. (2007) and Krebs et al. (2011) have shown that eclogite bodies, occurring in a single unit, could show different P-T paths. The cited authors reported that the studied blocks of eclogite and blueschist occur in a serpentinite melange. In only km^2-large gneiss areas, but possibly in different units, eclogite bodies with different P-T evolutions were also found (e.g. in the Sulu terrane, E China: Zhu et al., 2007; in a limited area of the southern Dabie Shan, E China: compare Massonne, 2012, and Wei et al., 2015; in the Tian Shan of NW China: Tian & Wei, 2013). In other instances, bodies of eclogite can have experienced similar P-T conditions in an extended gneiss area (e.g. in NE Sardinia, Italy: Giacomini et al., 2005; Cruciani et al., 2011; Cruciani et al., 2012).

In order to decipher the collision-related tectonic setting, it is necessary to know the original setting and provenance of the protoliths of the orthogneisses, metamafic rocks (eclogites and amphibolites) and metasediments. The protoliths of orthogneisses and metasediments have been studied by Abati et al. (2010) and Fuenlabrada et al. (2012), but the protoliths of metamafic rocks have not studied in detail. There are two possible settings for metamafic rocks in the MTZ. One setting is related to calc-alkaline or subalkaline magmatism of a continental back-arc basin formed after the Iapetus Ocean had been subducted under Gondwana before the Variscan collision (Abati et al., 2010;

Andonaegui et al., 2015). Another possibility is that the metamafic rocks had formed by metamorphism of oceanic crust.

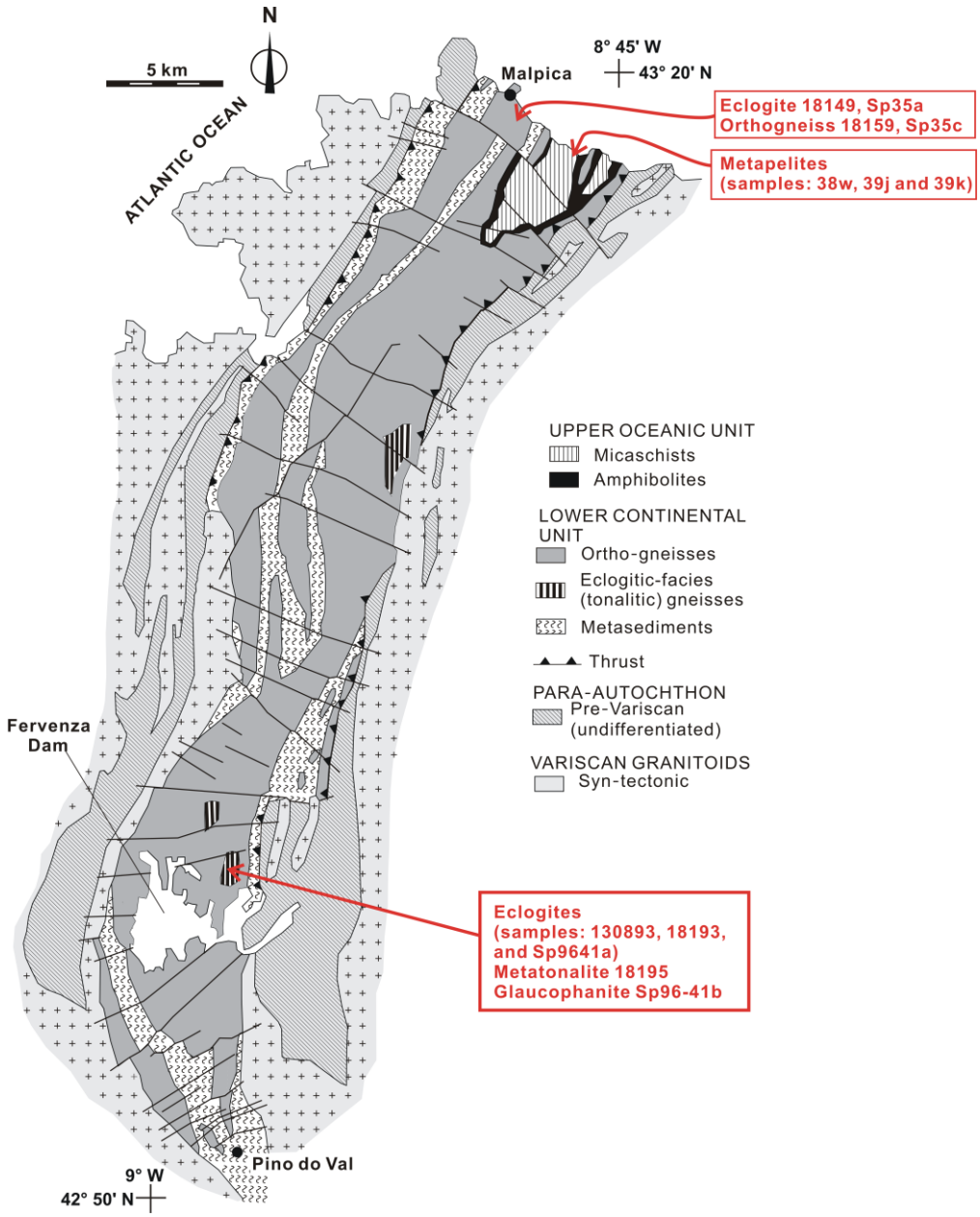

Fig. 1.1. Geological map of the MTZ after Rodríguez et al. (2003) showing sample localities.

An important type of metamorphic rock is metasediment. Blueschist facies metapelites have been studied to derive their P-T-t paths using chemical phase diagrams and Ar-Ar phengite dating by López-Carmona et al. (2010; 2013; 2014a). However, the Ar-Ar technique can be challenging because excess Ar is common in HP metamorphic

rocks and difficult to detect due to too high $^{40}Ar/^{39}Ar$ ratios for precise measurements (de Jong, 2003; Platt et al., 2006; Smye et al., 2013; Kirchner et al., 2016). A geochronologic technique that has recently achieved with great success in constraining the timing of HP metamorphism is U-Th-Pb dating of monazite (Williams et al., 1999; Foster et al., 2000; Möller et al., 2003; Horváth et al., 2010; Massonne, 2014; Balen et al., 2015). Monazite growth and P-T conditions can eventually be correlated by trace-element changes (Massonne et al., 2014; Deburah et al., 2016; van Leeuwen et al., 2016). In this thesis, monazite ages and P-T paths of corresponding rocks are presented in an effort to refer metamorphic ages to rocks of the Ceán Unit.

1.2. Aims of the thesis and studied rocks

The primary aim of the doctoral thesis was to derive P-T paths of eclogite bodies, orthogneisses and metapelites combining the thermodynamic calculation of pseudosections and analyzed chemical compositions of minerals, which can be chemically zoned such as garnet. In addition, the protolith character of metamafic rocks should be recognized. Monazite dating should be performed on metapelite. These methods provide information for the better understanding of the collisional situation of the target area in Variscan times.

Detailed research objectives:

(1) Careful study of mineral chemistry and mineral paragenesis in metamafic rocks and surrounding gneisses from different locations. Finally, their P-T paths and tectonic evolutions should be reconstructed.

(2) Comparison of the P-T evolutions of eclogites from different localities (in the north and center of the MTZ).

(3) Tectonic settings of protoliths of metamafic rocks should be recognized.

(4) Determination of U-Th-Pb ages on monazite from metapelites.

In order to reach these goals, 5 eclogites, 3 orthogneisses, 3 metapelites and 1 glaucophanite from the MTZ were studied. These samples cover almost all types of metamorphic rocks in this zone (Fig. 1.1). Two eclogites, two surrounding gneisses and three metapelites are from northern the MTZ. Three eclogites, one glaucophanite and a gneiss (metatonalite) were collected from the central part of the MTZ.

2. Geological background

2.1. Variscan orogeny in Europe

The European Variscan belt was formed by the collision between Gondwana and Laurussia following the closure of the Rheic Ocean (Fig.2.1) (Matte, 1991; Fuenlabrada et al., 2010; Casini & Oggiano, 2008; Nance et al., 2010; Kroner & Romer, 2013) in Devonian and Carboniferous times (420-300 Ma) (Franke, 1989; Finger et al., 1997). This belt extends from southern Iberia to northeastern Bohemia, and outcrops in various stable massifs (Iberian, Armorican, French Massif Central, Rhenish and Bohemian) (Matte, 1986). These massifs include a succession of allochthonous complexes, which are considered to be remnants (klippen) of a large nappe pile (Fig. 2.2) (Fuenlabrada et al., 2010).

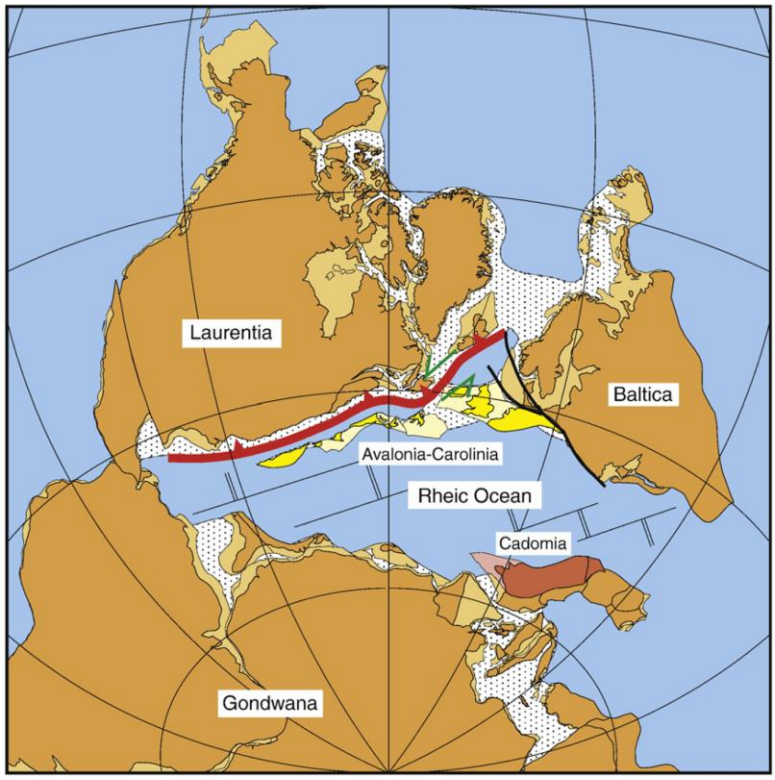

Fig. 2.1. Early Silurian reconstruction of the Rheic Ocean immediately prior to the closure of the Iapetus ocean by its subduction beneath Laurentia (toothed red line) (Nance et al., 2010). Stippled areas denote inferred regions of thinned and/ or anomalous thickness of continental and arc crust. Rheic ridge-transform systems are purely schematic. Heavy black lines trace the Tornquist suture zone.

Variscan orogeny: The Variscan or Hercynian orogeny is a geological mountain-buiding event caused by late Late Palaeozoic (420-300 Ma) continental collision between Laurussia and Gondwana to finally form the supercontinent Pangaea.

Rheic Ocean: Laurussia was separated from Gondwana after closure of the Iapetus by the Rheic Ocean, one of the principal oceans of the Palaeozoic. Its suture extends over 10,000 km from Mexico to Turkey (Nance et al., 2010). The evolution of the Rheic Ocean is consequently not only important for the history of the Late Palaeozoic, but also a broader issue for supercontinental assembly (Nance et al. 2010; Krs et al., 2001).

Laurussia: North of the boundary of the Variscan realm in Europe, Laurussia formed during the Caledonian collision of Laurentia and Baltica, in Ordovian and Silurian times (Franke, 1989). The large Palaeozoic continent of Laurentia was largely in North America, but included parts of modern Europe. It was independent from late Neoproterozoic times on (at about 570 Ma) until it merged with Avalonia-Baltica in the 430-420 Ma Silurian Caledonide Orogeny (Cocks & Torsvik, 2011).

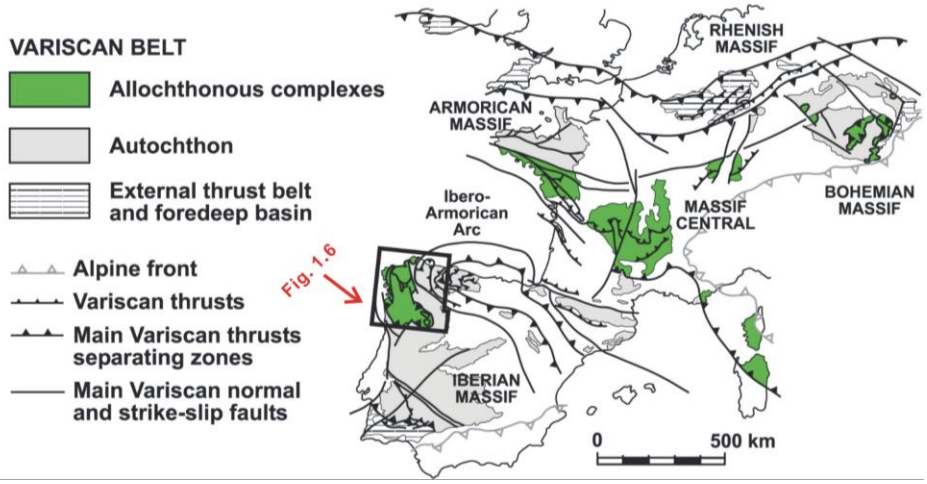

Fig. 2.2. Synthesis of the major domains of the Variscan belt and location of the study area (Díez Fernández et al., 2012c).

Gondwana: Gondwana was a large continent that originated in very late Precambrian times by amalgamation of Africa, South America, India, Antactica and Australia. In Cambrian times, it included all of Europe, south of Avalonia and Baltica. In late Ordovician times the South Pole was in North Africa and, although the terranes of southern Europe had separated from Gondwana, they were still far enough south to carry periglacial deposits (McKerrow et al., 2000).

2.2. Tectonic evolution of the Variscan orogeny in Europe

Two options exist for the tectonic evolution of the Variscan orogeny in Europe, which are distinguished by the fate of Gondwanan island arcs (upper allochthonous unit) formed during the late Cambrian-middle Ordovician (500-460 Ma).

One model (Fig. 2.3) (Abati., 2010; Martínez Catalán et al., 2009; Díez Fernández et al., 2012b; Barreiro et al., 2007) suggests that an island arc (upper allochthonous unit) was caused by calc-alkaline and alkaline plutons during 470-495 Ma (Abati et al., 2010), and then drifted away to open the Rheic Ocean during the middle Ordovician at ca. 465-440 Ma (Martínez Catalán et al., 2009) (Fig. 2.3b, c). At ca. 425-390 Ma, the arc accreted to Laurussia while the Rheic Ocean was still open (Fig. 2.3c). Subduction of a part of the arc involved tectonometamorphic events in the high-P and high-T units. The last stage of subduction related to early Variscan convergence happened between 375 and 365 Ma (Rodríguez et al., 2003; Santos Zalduegui et al., 1995). The Rheic Ocean closed and Gondwana and Laurussia collided. At ca. 350 Ma, the Laurussia-Gondwana convergence continued, the Variscan orogen formed finally (Fig. 2.3d) (Martínez Catalán et al., 2009).

Another type of tectonic model does not involve drifted Gondwana arcs (Arenas et al., 2014). The Variscan orogen resulted from two collisions. In NW Spain, three units (upper units, ophiolitic units and basal units) formed by two HP events during 370-395 Ma (Fig. 2.4). The detailed tectonic process is the following: (1) the Rheic Ocean between Laurussia and Gondwana started to be diminished by subduction at ca. 420 Ma (Fig. 2.4a); (2) The closure of the Rheic Ocean was followed by a first continental collision between Laurussia and Gondwana at ca. 400-410 Ma. The first collision caused deep subduction of the most external margin of Gondwana and the generation of a HP-UHP metamorphic belt (upper unit of the Variscan suture) (Fig. 2.4b); (3) The renewed dextral motion between Gondwana and Laurussia favored the rapid generation of a rather wide pull-apart basin at ca. 400-395 Ma (Fig. 2.4c); (4) The rapid closure of this basin started at ca. 380 Ma and caused the accretion of buoyant oceanic lithosphere below the northern continent. This oceanic lithosphere is represented by the most common ophiolites found in the European Variscan suture (ophiolitic unit). Finally, renewed dextral convergence led to a new collision with the Gondwana margin at ca. 370 Ma and the generation of a second

HP belt (basal unit) (Fig. 2.4d).

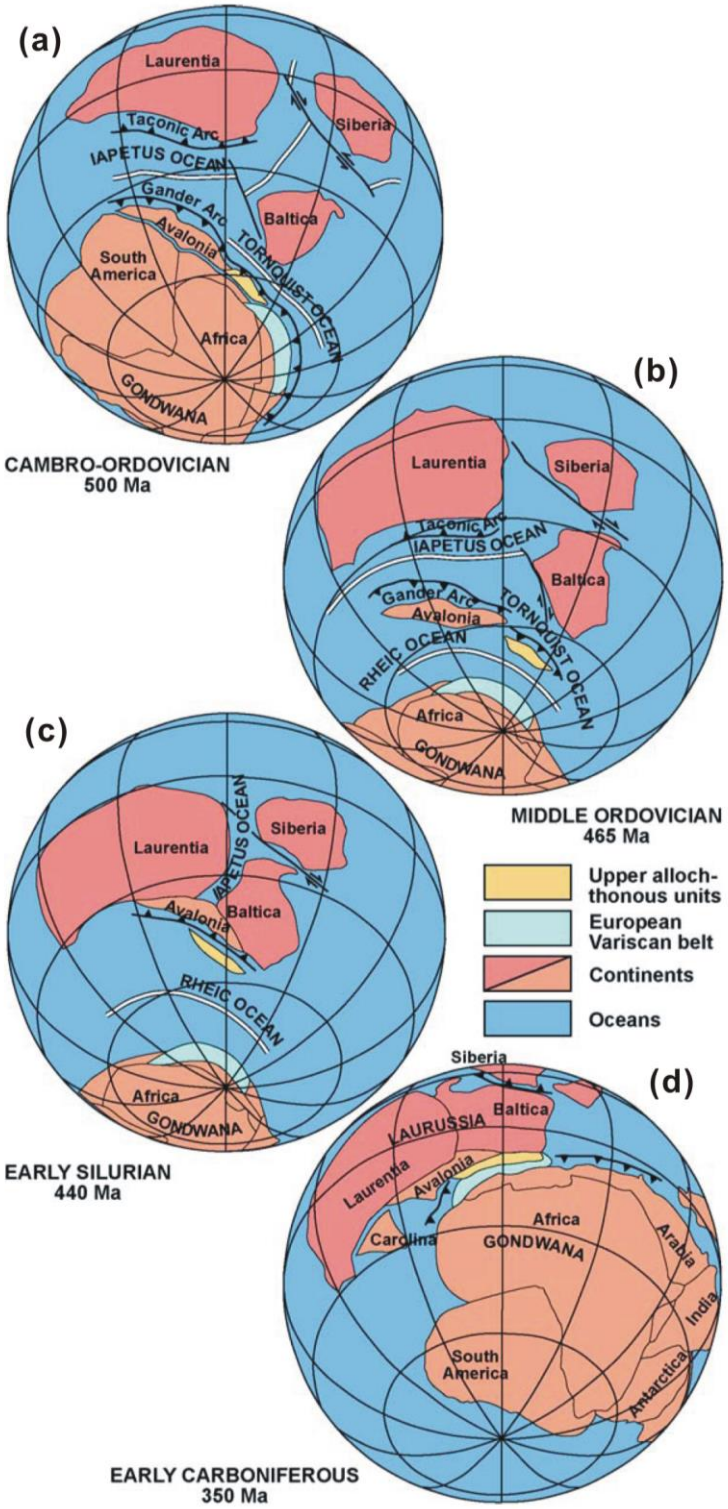

Fig. 2.3. Distribution of continental masses during the Palaeozoic, showing the suggested palaeopositions of the European Variscides and the ensialic arc preserved in the upper allochthonous units (Barreiro et al., 2007; Winchester & Team, 2002; Martínez Catalán et al., 2009).

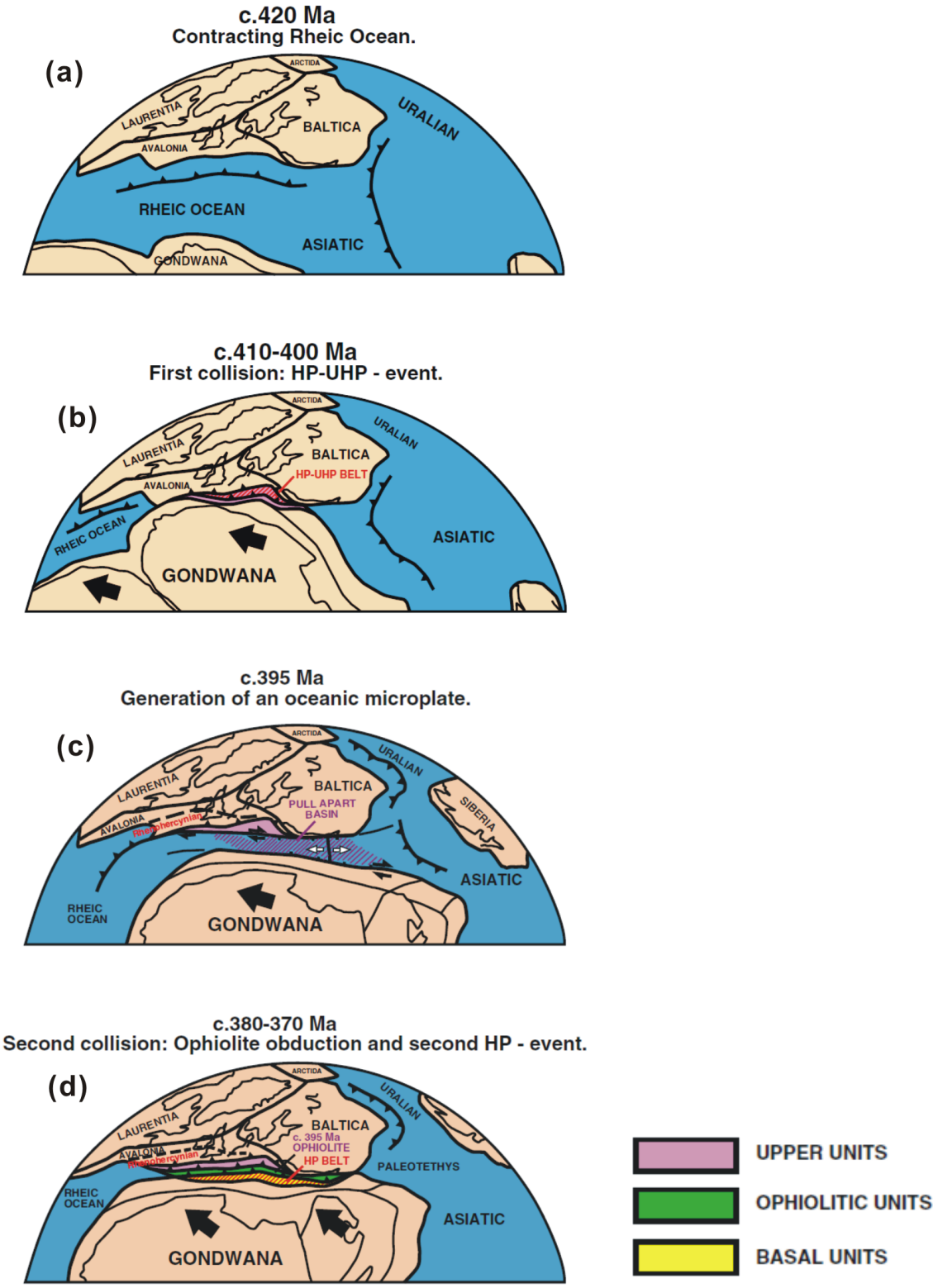

Fig. 2.4. Another type of Variscan evolution (Arenas et al., 2014). (a) The realm of the Rheic Ocean at the Silurian-Devonian boundary. (b) The initial collision between Gondwana and Laurussia at ca. 410-400 Ma. (c) Dextral motion between Gondwana and

Laurussia, which favored the opening of a rather ephemeral pull-apart basin at ca. 395 Ma with generation of new oceanic lithosphere. (d) The second and final collision at ca. 380-370 Ma.

2.3. Variscan orogeny in the Iberian Massif

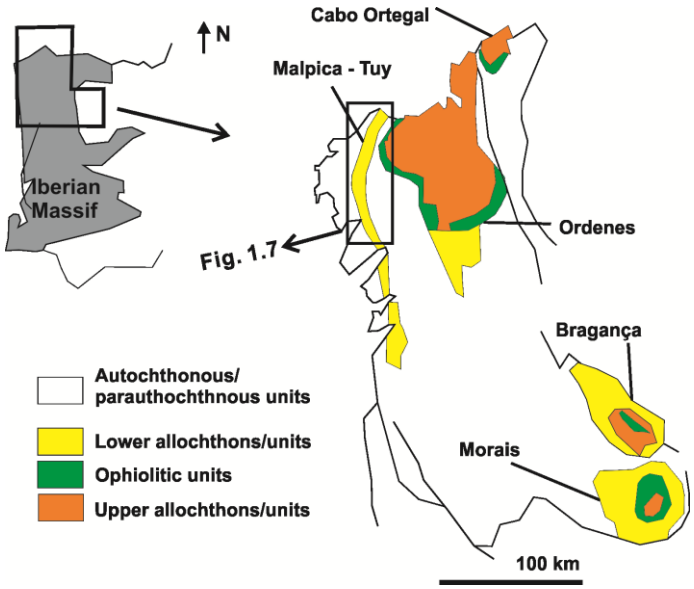

Fig. 2.5. Geological frame of the Malpica-Tuy allochthon located in the Palaeozoic orogenic belt of NW Iberia (after Santos Zalduegui et al., 1995).

The Iberian Massif is located in southwestern Europe involving a large fragment of the Variscan orogen (Andonaegui et al., 2012; Díez Fernández et al., 2011, 2012a; Díez Fernández & Martínez Catalán, 2012). In the northwestern Iberian Massif, five allochthonous complexes are preserved in late synformal structures: three of them outcropping in Galicia (Cabo Ortegal, Órdenes, and MTZ) and two in the Portuguese region of Trás-os-Montes (Bragança and Morais complexes) (Fig. 2.5). The allochthonous complexes include three main terranes designated, from top to bottom, the upper unit, ophiolitic unit and basal unit (Fuenlabrada et al. 2010). The upper unit is interpreted to be an arc-derived terrane. The arc also has a peri-Gondwanan provenance, and it either was separated from the main continent at ca. 465 Ma (Fig. 2.3) (Martínez Catalán et al., 2009) and drifted north contemporaneously with the opening of the Rheic ocean, or it never drifted away and formed by the first collision between Gondwana and Laurussia at ca. 395 Ma (Fig. 2.4b). The basal units are considered to be the most

external margin of Gondwana subducted beneath Laurussia at the onset of Variscan deformation (Abati et al., 2010; Andonaegui et al., 2012), which is related by Arenas et al. (2014) to the second collision at ca. 370 Ma. The ophiolitic units are considered as collisional suture, and they are the remnant of the Rheic Ocean.whereas the upper unit is interpreted to be the most external continental margin of Gondwana.

2.4. Malpica-Tuy zone/complex (MTZ)

The MTZ is the westmost exposure of the basal unit in the allochthonous complexes of NW Iberia. It crops out as an enlongated synformal structure oriented N-S, the axis of which plunges slightly to the north. The MTZ is about 150 km long and 10 km wide, stretching from Malpica in A Coruña, to Tuy/Tui in Pontevedra (López-Carmona et al., 2010) (Fig. 2.5).

2.4.1. Lower continental subunit and upper oceanic subunit

The MTZ is mainly composed of the basal unit (Fig. 2.6a) (Díez Fernández et al., 2012b; Díez Fernández and Martínez Catalán, 2012). However, some authors subdivided the MTZ in a lower continental subunit (Malpica-Tuy unit = MTU) and an upper oceanic subunit (Ceán unit) (Rodríguez et al., 2003; López-Carmona et al., 2013). The contact between upper and lower subunits is marked by a several meter thick zone of mylonites and ultramylonites located at the base of the Cambre amphibolites (Díez Fernández et al., 2011; López-Carmona et al., 2013) (Fig. 2.6).

The Ceán unit, which is ascribed to the aforementioned ophiolitic unit, has oceanic affinity, and may correspond to an outboard sequence of that margin. After metamorphism this oceanic subunit was thrust over the continental subunit. The Ceán unit is exposed along the coastal strip of the MTZ (Fig. 2.6) and composed of a sequence of massive, finely foliated amphibolites with lawsonite-pseudomorphs and a thicker metasedimentary sequence consisting of pelitic schists and minor intercalations of ampelites, lydites and carbonates (Arps 1981; López-Carmona et al., 2010).

The lower continental subunit (MTU) is formed by thick metasedimentary rock sequences, with detritus derived from Gondwana (Díez Fernández et al., 2010), containing mafic rocks. These sequences were intruded by granitoids ranging in composition from calc-alkaline or subalkaline (protolith ages of ca. 493 Ma; see Abati et

al., 2010; Díez Fernández et al., 2012b; Fuenlabrada et al., 2012) to minor alkaline-peralkaline (ca. 470-475 Ma; Rodríguez et al., 2007; Díez Fernández et al., 2012b; Fuenlabrada et al., 2012). The granitoids were transformed into variably deformed orthogneisses (Fig. 2.6c). The associated mafic rocks were metamorphosed to amphibolites, blueschists, and eclogites during an Eo-Variscan HP event (Gil Ibarguchi & Ortega Gironés, 1985; Fuenlabrada et al., 2012).

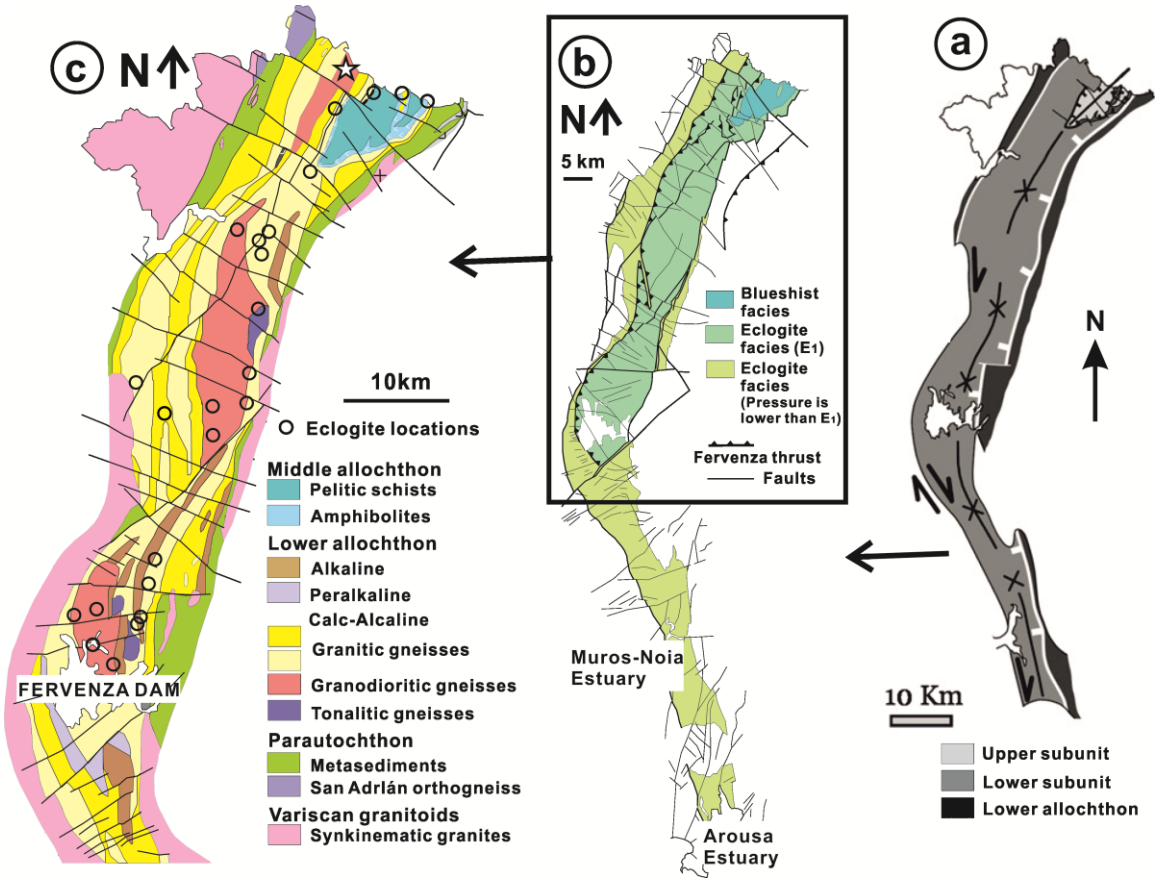

Fig. 2.6. (a) Simplified tectonic map of the MTZ (López-Carmona et al., 2010). (b) The distribution of rocks of different metamorphic facies in the MTZ after (Díez Fernández et al., 2011). (c) Geological map of the MTZ after López-Carmona et al. (2013) showing eclogite locations (Gil Ibarguchi & Ortega Gironés, 1985).

2.4.2. The concept of eclogite and eclogite facies

Eclogite as a petrographic rock name is restricted to rocks of broadly basaltic composition which lack primary plagioclase and are characterized by a predominant assemblage of omphacite and garnet. Small amounts of other anhydrous minerals are

widely recognized in eclogites. Quartz, kyanite, orthopyroxene and rutile are the most common of such minerals. Coesite, diamond and aragonite are very rare, but notably are indicative of high confining pressures (Carswell, 1990). The status of accessory hydrous silicates such as glaucophanitic, barroisitic or pargasitic amphibole, phengite, paragonite, phlogopite, talc, zoisite and clinozoisite is more debatable (Smith et al., 1982).

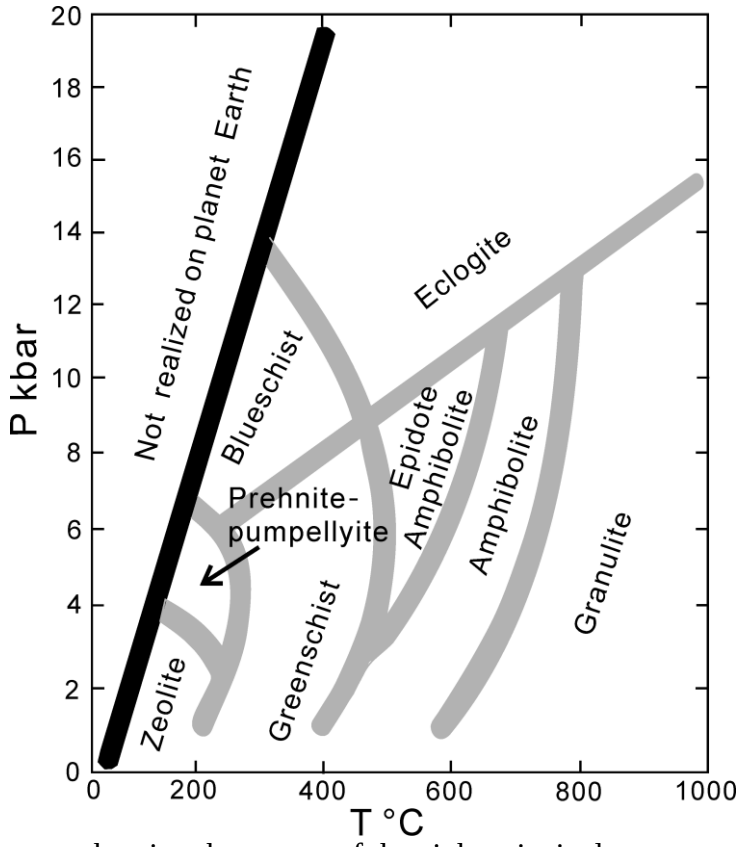

Fig. 2.7. P-T diagram showing the ranges of the eight principal metamorphic facies (Spear, 1995).

The eclogite facies is the facies at the highest metamorphic pressure at high temperature (Fig. 2.7). The eclogite facies is characterized by the following silicate assemblages: omphacite + garnet (± kyanite, quartz, barroisitic to Na-amphibole , zoisite, talc, phengite) in eclogite, quartz + phengite + jadeite/omphacite + garnet (± K-feldspar, epidote) in metagranodiorite, and phengite + garnet + quartz, (± kyanite, chloritoid, talc, jadeite, epidote) in metapelite.

2.4.3. Eclogites and metamorphic facies in the MTZ

Eclogites in the Malpica-Tuy unit (MTU, precisely defined as the lower subunit of the MTZ) are often included in orthogneiss (Figs. 2.6c, 2.8) as lenses and boudins with

different intensities of deformation (Gil Ibarguchi & Ortega Gironés, 1985; Santos Zalduegui et al., 1995; Rodríguez et al., 2003; Abati et al., 2010), from simply foliated to ultramylonitic. Sometimes, pristine contacts can be observed between eclogite and the surrounding orthogneiss. The eclogite lenses can often be traced along several meters resulting from boudinage of a tabular body, most probably a dike (see for example Fig. 3a in Díez Fernández and Martínez Catalan, 2012; Fig. 4e in Díez Fernández et al., 2012a). The interpretation of basic rocks as dikes in the MTU dates back to the pioneer Ph.D. thesis of Peter Floor (1967, p. 164), although he only studied the southern part of the MTZ, where no eclogites were found. However, not all ecologitized basic rocks in the MTU were dikes, neither all of them are included in orthogneiss, as they may also occur in metasediments too. Some bodies are big enough to be mapped to scales of 1:200 000 and less (the largest of which is 0.5 km long). These bodies occur between 25-40 km south of the Atlantic coast, where they are spatially associated to four different types of orthogneiss: peralkaline, alkaline, granodioritic, and tonalitic, the latter of which appears to be eclogitized (Rodríguez Aller, 2005; Abati et al., 2010; Díez Fernández & Martínez Catalan, 2012).

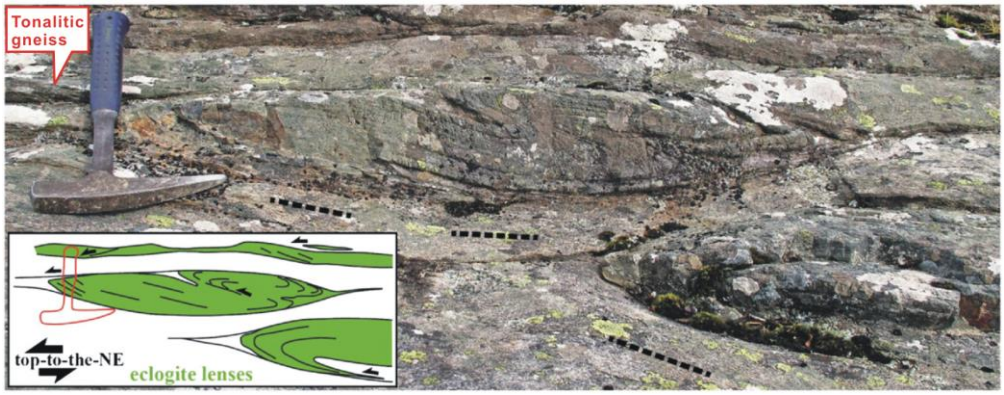

Fig. 2.8. Eclogite lenses in tonalitic orthogneiss of the MTZ (from Díez Fernández et al., 2012a).

According to structural research in the MTZ, three metamorphic facies are designated (Díez Fernández et al., 2011) (Fig. 2.6b): blueschist facies, eclogite facies (E_1) and eclogite facies (E_2) characterized by lower peak pressure compared to E_1. Rocks of the Ceán unit can be assigned to the blueschist facies. The northern and southern parts of the MTU are characterized by eclogite facies (E_1) and eclogite facies (E_2) rocks, respectively (Fig. 2.6b).

2.5. Existing pressure and temperature estimates in the MTZ

P-T conditions in the MTZ have been published in several scientific papers using methods of geothermobarometry (Gil Ibarguchi & Ortega Gironés, 1985; Gil Ibarguchi, 1995 (Table 2.1); Rodríguez et al., 2003; López-Carmona et al., 2010) and chemical phase diagrams (Rodríguez et al., 2003; López-Carmona et al., 2010; 2013; 2014a).

Table 2.1. Summary of previous thermobarometric calculations (Fe^{2+}-Mg exchange thermometry; GRIPS = the equilibrium of garnet-plagioclase-rutile-ilmenite-quartz; and the reaction of albite = jadeite + quartz) on rocks from the MTU (Gil Ibarguchi and Ortega Gironés, 1985; Gil Ibarguchi, 1995. Abrevations: Ab (albite), Bt (biotite), Cpy (clinopyroxene), Gt (garnet), Jd (jadeite), Min (minimum) and Max (Maximum).

Reference	Rock type	Geobaro-metry	Geother-mometry	Pressure (P)	Temperature (T)
Gil Ibarguchi & Ortega Gironés (1985)	Eclogite	Ab = Jd + Q	Gt-Cpy	Min P: 10.5 ± 0.5 kbar for Gt core and 11.5 ± 1 kbar for Gt rim.	Min T: 525 ± 20 °C for Gt core and 570 ± 40 °C for Gt rim.
Gil Ibarguchi (1995)	Jd bearing rocks	Ab = Jd + Q	Gt-Bt	Min P: 18 ± 1 kbar	630 ± 40 °C
	Orthogneisses lacking Jd	GRIPS	Gt-Bt	15.5 ± 1 kbar	655 ± 30 °C
	Elogite	Ab = Jd + Q	Gt-Cpy	16 ± 1 kbar	675 ± 30 °C

Gil Ibarguchi & Ortega Gironés (1985) published minimum P-T conditions of 525 ± 20 °C at 10.5 ± 0.5 kbar and 570 ± 40 °C at 11.5 ± 1 kbar for garnet core and rim domains, respectively, in eclogite (Table 2.1) from the MTU. These date were derived using the garnet-clinopyroxene (Ellis & Green et al., 1979) geothermometer, combined with the lower stability limit of omphacite (Jd_{45}) and the albite = jadeite + quartz boundary determined by authors such as Johannes et al. (1971) and Holland (1980). Gil Ibarguchi (1995) published P-T conditions of 630 ± 20 °C and minimum pressure of 18 ± 1 kbar for jadeite-bearing rocks from the MTU. The pressure was again estimated by jadeite + quartz geobarometry. The temperature was calculated using the experimental calibration of the garnet-biotite Fe^{2+}-Mg exchange equilibrium (Lavrenteva & Perchuk, 1981; Aranovich et al., 1988). P-T conditions of orthogneisses lacking jadeite were also

estimated by Gil Ibarguchi (1995). P-T conditions of 570 ± 40 °C and 11.5 ± 1 kbar resulted using the garnet-biotite equilibrium and GRIPS (the equilibrium of garnet-plagioclase-rutile-ilmenite-quartz) geobarometry (Bohlen & Liotta, 1986). Gil Ibarguchi (1995) also gave P-T conditions for eclogite with 675 ± 30 °C and 16 ± 1 kbar, using published (Gil Ibarguchi & Ortega, 1985) and new data. The latter were based on jadeite in omphacite geothermobarometry (Holland, 1980, 1990) and garnet-clinopyroxene thermometry (Krogh, 1988).

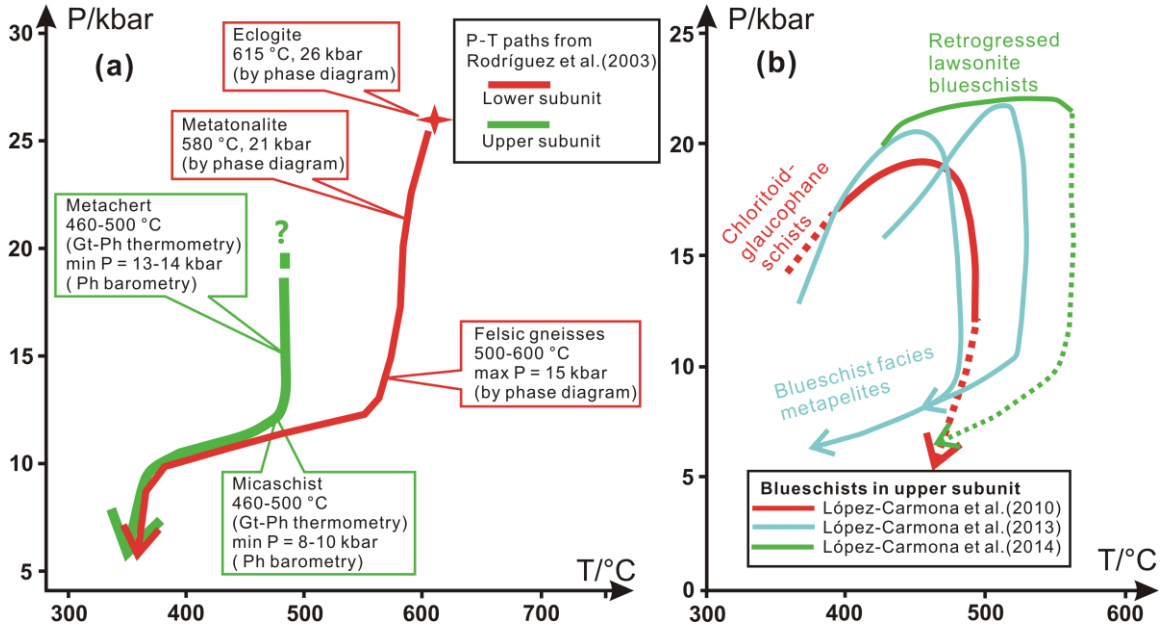

Fig. 2.9. P-T trajectories. (a) Two P-T paths for different rocks from the lower continental subunit and upper oceanic subunit (Rodríguez et al., 2003). (b) P-T paths for different blueschist facies metapelites in the upper oceanic unit (López-Carmona et al., 2010; 2013; 2014a). Solid and dashed lines refer to certain and uncertain sections of the P-T path.

Rodríguez et al. (2003) studied metamorphic conditions of various rocks located in both Ceán unit and MTU (Fig. 2.9a). For the Ceán unit, temperatures of 460-500 °C and minimum pressures of 13-14 kbar (Table 2.1) were obtained for metachert by garnet-phengite geothermometry (Krogh & Råheim, 1978; Hynes & Forest, 1988) and phengite geobarometry (Massonne and Schreyer, 1987). The garnet-phengite thermometer and the Si-in-phengite barometer yielded temperatures of 460-500 °C at minimum pressures of 8-10 kbar for micaschist. For rocks of the MTU, phase diagrams were produced with the Thermocalc software (Powell & Holland, 1988; version 2.7, with

the updated dataset of Holland & Powell, 1998). Maximum P-T conditions of eclogite were calculated to 26 kbar and 615 °C. For metatonalite such P-T conditions were 21 kbar and 580 °C. Felsic gneisses were metamorphosed at 500-600 °C and maximum pressures of 15 kbar. Finally, two P-T paths were reconstructed using P-T conditions obtained for different rocks of the Ceán unit and the MTU (Fig. 2.9a).

López-Carmona et al. (2010; 2013; 2014a) worked on blueschist facies metapelites from the Ceán unit using Thermocalc 3.26 (Powell and Holland, 1988) with the internally consistent thermodynamic dataset of Holland and Powell (1998; updated 22 Nov. 2003). Chloritoid-glaucophane schists experienced peak conditions between P = 19-20 kbar and T = 425-430 °C (López-Carmona et al., 2010). These data were checked by conventional thermobarometry and P-T pseudosections calculated with PERPLE_X. Retrogressed lawsonite blueschists experienced peak conditions of ca. 22 kbar and 560 °C (López-Carmona et al., 2014a). Another two blueschist-facies metapelites reached peak conditions of ca. 21-22 kbar at 520 °C and 21 kbar at 460 °C (López-Carmona et al., 2013). Finally, four similarly shaped P-T paths were constrained (Fig. 2.9b), and the difference of their P-T conditions were explained by the occurrence of the studied rocks at different locations in a subduction channel (López-Carmona et al., 2014a).

2.6. Geochronology and previous protolith studies of the MTZ rocks

A range of 340-370 Ma for the metamorphism of the MTZ has been reported (van Calsteren et al.,1979; Santos Zalduegui et al., 1995; Rodríguez et al., 2003; Rodríguez et al., 2007; Abati et al., 2010; and López-Carmona et al., 2014a). The age range 360-370 Ma was related to HP or peak pressure metamorphism. Ages around 350 Ma were explained as cooling age or the age of juxtaposition of Ceán unit and MTU during exhumation (Table 2.2). According to López-Carmona et al. (2014a), the $^{40}Ar/^{39}Ar$ step heating of phengitic muscovite from blueschist yielded a plateau age of ca. 363 ± 2 Ma. This is consistent with published 362-370 Ma, 365 Ma Rb-Sr, and 365 ± 1 Ma $^{40}Ar/^{39}Ar$ mica ages for eclogite, associated eclogite-facies gneiss and another eclogite, respectively (van Calsteren et al., 1979; Santos Zalduegui et al., 1995; Rodríguez et al., 2003). A cooling age has been determined at ca. 350 Ma by $^{40}Ar/^{39}Ar$ step heating of phengitic muscovite in micaschist, blueschist, and orthogneiss and by Rb-Sr in biotite and plagioclase in metagranodiorite (Table 2.2). For the magmatism, concerning the

protoliths of metamorphic rocks, Abati et al. (2010) used U-Pb geochronology in zircon to obtain 495 ± 5 Ma and 498 ± 6 Ma on calc-alkaline gneiss and eclogite, respectively. For eclogite, 498 ± 6 Ma was considered as the best estimate for the age of the mafic-intermediate magmatism of the MTU (Abati et al., 2010), whereas alkaline magmatism was dated by TIMS (U-Pb dating on zircon by Thermal Ionization Mass Spectrometry) at 472 ± 2 Ma (Rodríguez et al., 2007).

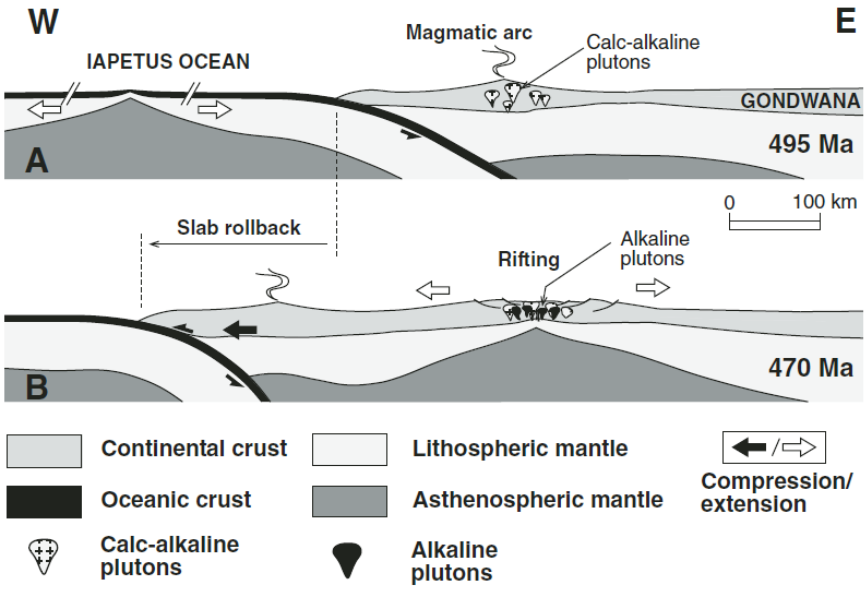

Fig. 2.10. Proposed model for the evolution of magmatism in the basal units of the allochthonous complexes of the NW Iberian Massif (Abati et al., 2010). The calc-alkaline association is related to an active plate margin at the northern Gondwana margin at ca. 495 Ma. (A) Evolving through a slab-rollback process that produced the migration of the arc oceanward and the initiation of a backarc rift and concomitant ascent of alkaline magmas intruding the previous calcalkaline plutons at ca. 470 Ma. (B) The rift progressed to form the Rheic Ocean.

According to Abati et al., 2010, calc-alkaline magmas crystallized in a continental magmatic arc (Fig. 2.10). This arc was produced at ca. 490-500 Ma as suggested by Abati et al. (2010) and Díez Fernández et al. (2012b). These authors also proposed that an alkaline to peralkaline magma suite formed at 472 ± 2 Ma, which is 20 Ma younger than the calc-alkaline magmatism, in the same tectonic unit. Because of similar magmatic ages of calc-alkaline magmatism and mafic-intermediate magmatism, metamafic rocks (eclogite and amphibolite) were also assigned to the calc-alkaline suite.

Table 2.2. Previous age dating and interpretations.

Locality	Rock type	Age[Ma]	Method	Interpretation	Reference
Ceán unit	micaschist	348 ± 8	$^{40}Ar/^{39}Ar$ in phengite	Juxtaposition of two subunits	Rodríguez et al., 2003
Ceán unit	blueschist	363 ± 2	$^{40}Ar/^{39}Ar$ in phengite	HP metamorphism.	López-Carmona et al., 2014a
Ceán unit	blueschist	354 ± 1	$^{40}Ar/^{39}Ar$ in phengite	Cooling age	López-Carmona et al, 2014a
MTU	eclogite	362-370	Rb-Sr in mica	HP metamorphism	van Calsteren et al.,1979
MTU	orthogneiss	365	Rb-Sr in garnet and phengite	HP metamorphism	Santos Zalduegui et al., 1995
MTU	metagranodiorite	352 ± 3	Rb-Sr in whole rock, biotite and plagioclase	Cooling below ca. 320 °C	Santos Zalduegui et al., 1995
MTU	amphibolite	352 -372	$^{40}Ar/^{39}Ar$ in phengite	Indicating incomplete Ar resetting during retrograde amphibolitization of the mafic rocks.	Rodríguez et al., 2003
MTU	tonalitic gneiss	353 ± 2 357 ± 3	$^{40}Ar/^{39}Ar$ in phengite	Argon loss and rapid regional cooling	Rodríguez et al., 2003
MTU	eclogite	365 ± 1	$^{40}Ar/^{39}Ar$ in phengite	HP metamorphism	Rodríguez et al., 2003
MTU	alkaline gneiss	472 ± 2	TIMS	Alkaline magmatism	Rodríguez et al., 2007
MTU	calc-alkaline gneiss	494 ± 5	U-Pb in zircon	Calc-alkaline magmatism	Abati et al., 2010
MTU	eclogite	498 ± 6	U-Pb in zircon	Mafic-intermediate magmatism	Abati et al., 2010

2.7. Published tectonometamorphic models for the MTZ

Two types of tectonic models were proposed for the closure of the Rheic Ocean in the range of the MTZ. One type (Fig. 2.11 left) suggests that the Rheic Ocean was subducted below Laurussia followed by continental (Gondwana) subduction (Rodríguez et al., 2003). Another type of the models (Fig. 2.11 right) hypothesizes that this ocean completely developed at the Laurussia margin based on the appearance of diverse ophiolite sequences in northern Spain (Martínez Catalán et al., 1996; López-Carmona et al., 2014). Both models consider the same maximum depth attained during continental

subduction and subsequent continental breakup at eclogite-facies conditions at 360-370 Ma. Then the continental slice (MTU) continued exhumation and was juxtaposed with the partially exhumed oceanic subunit (Ceán unit) at ca. 350 Ma.

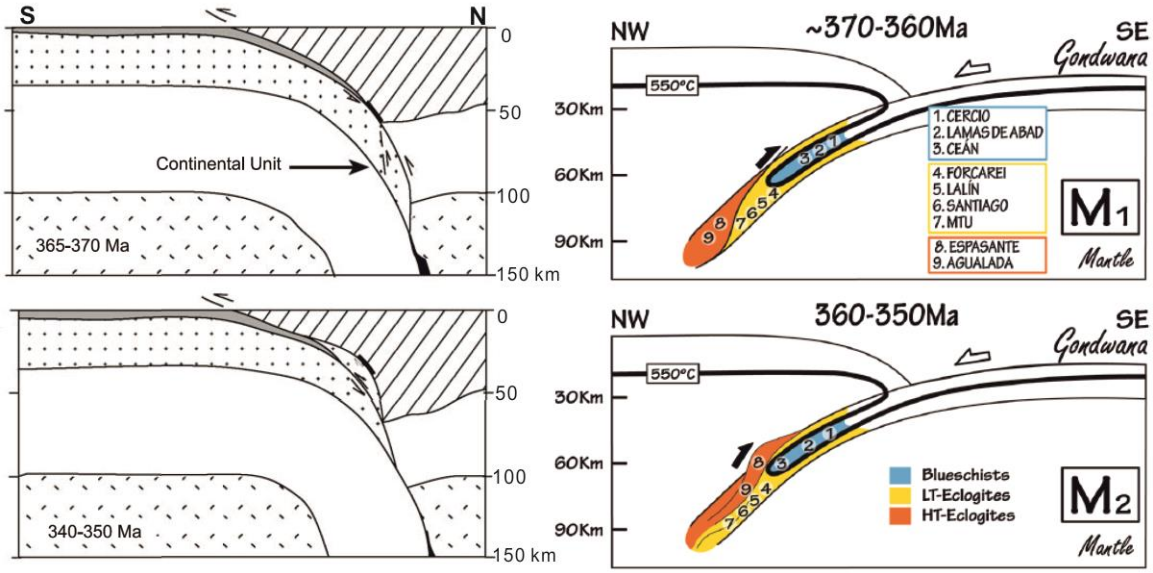

Fig. 2.11. Proposed tectonic models (left: Rodríguez et al., 2003; right: López-Carmona et al., 2014) for the final stages of plate subduction as recorded in the northwestern Iberian Massif. Model 1: (Left up): maximum depth attained during continental subduction, subsequent continental breakup at eclogite-facies conditions at 365-370 Ma. (Left down): Continued exhumation of the continental slice (MTU) and juxtaposition with the partially exhumed oceanic subunit (Ceán unit) at ca. 340-350 Ma. Model 2: (Right up): 370-360 Ma: maximum depth attained. (Right down): 360-350 Ma: exhumation stage.

3. Methods

Field work (Fig. 3.1a-b) in NW Spain was undertaken by Prof. Hans-Joachim Massonne in 1989, 1993 and 1996. Approximately 130 samples (Fig. 3.1c) from the MTZ were collected, including eclogite, amphibolite, metagranite, metagranodiorite, metatonalite, paragneiss, metapsammite, metapelite, and mylonite. These samples represent almost all types of rocks occurring in different tectonic settings. From the collected samples, thirteen were chosen from the MTZ (Fig. 1.1) for further study.

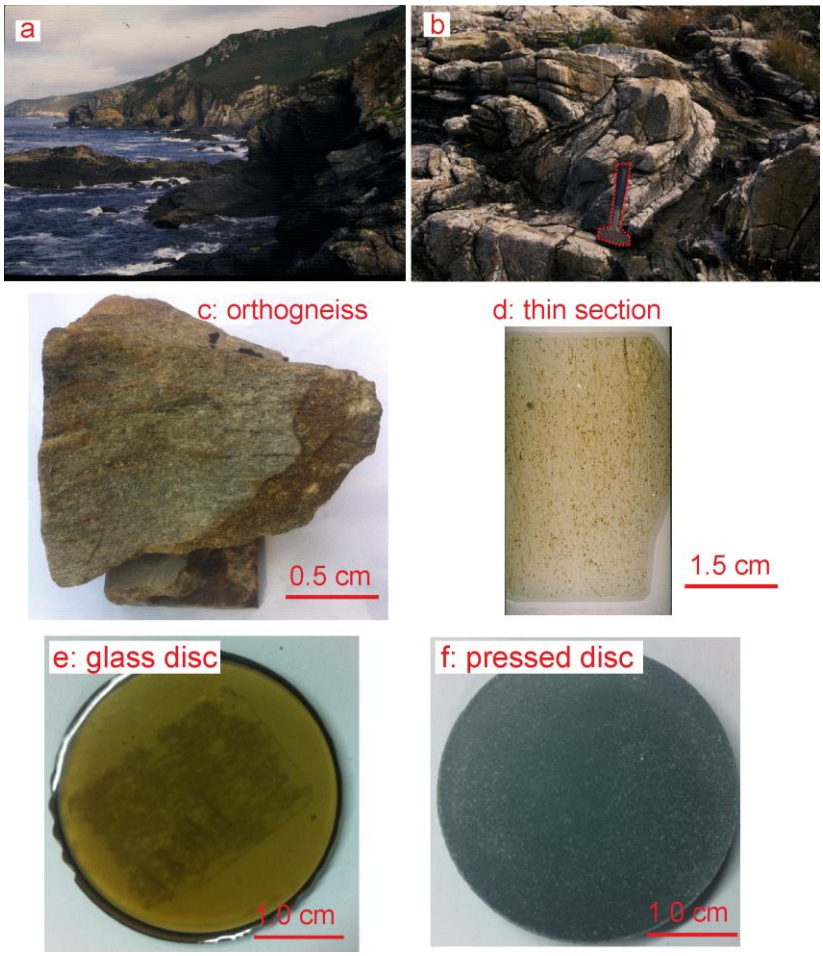

Fig. 3.1. Sample collection and preparation process. (a) Field overview near Punta Palerón (also Pelerón or Peterón); (b) Orthogneiss in the field near Punta Palerón; (c) Collected respective orthogneiss (sample 18159); (d) Orthogneiss thin-section (sample 18159); (e) Glass disc prepared for major element analysis and trace element analysis using XRF and LA-ICP-MS, respectively. (f) Pressed disc prepared for trace element analysis using XRF.

3.1. Optical microscope

Polished thin sections (Fig. 3.1d) with an average thickness of 30 µm were prepared for mineral identification and microtextural observations using polarizing optical microscopy (Fig. 3.2).

Fig. 3.2. Polarizing optical microscopy with a digital camera at the Institut für Mineralogie und Kristallchemie (IMK) at Universität Stuttgart.

3.2. Mineral chemistry

The chemical compositions of minerals were obtained with a CAMECA SX100 electron microprobe (EMP). This instrument was used for silicate analysis, rutile thermometry, monazite dating, and as an aid to identify unknown mineral phases.

3.2.1. Sample preparation

As the polished thin-sections used for ordinary microscopy were prepared using lead disks with embedded microdiamonds, hand-polished (lead-free) thin sections were also produced for metapelites, such as sample Sp96-38w, for Th-U-Pb monazite dating. Conventional lead disks are not suitable for the production of thin sections for Th-U-Pb dating with the EMP, because they deposit lead at grain boundaries and fill surface irregularities, thus contaminating the sample (Scherrer et al., 2000). The analytical

parameters and procedures are reported in sections 4.3.1, 5.3.2 and 6.4.

Before EMP analysis, the conventional and lead-free thin sections were coated with a ca. 20-30 nm carbon film to make the surface conductive. This is to prevent the sample from charging during electron bombardment. The carbon coating was achieved in a vacuum chamber where a carbon yarn was burned by an electric impuls. The thickness of the coating was controlled by the interference colour produced on a polished brass plate in the chamber (Ogenhall, 2010).

3.2.2. An introduction to electron-microprobe (EMP) analysis

A typical arrangement of an EMP is a vertical electron-beam column, an array of detectors placed around the sample chamber block, a sample entry vacuum lock, a console to control operating conditions, screens to view control interfaces and sample output, and a computer for control of data acquisition (Fig. 3.3).

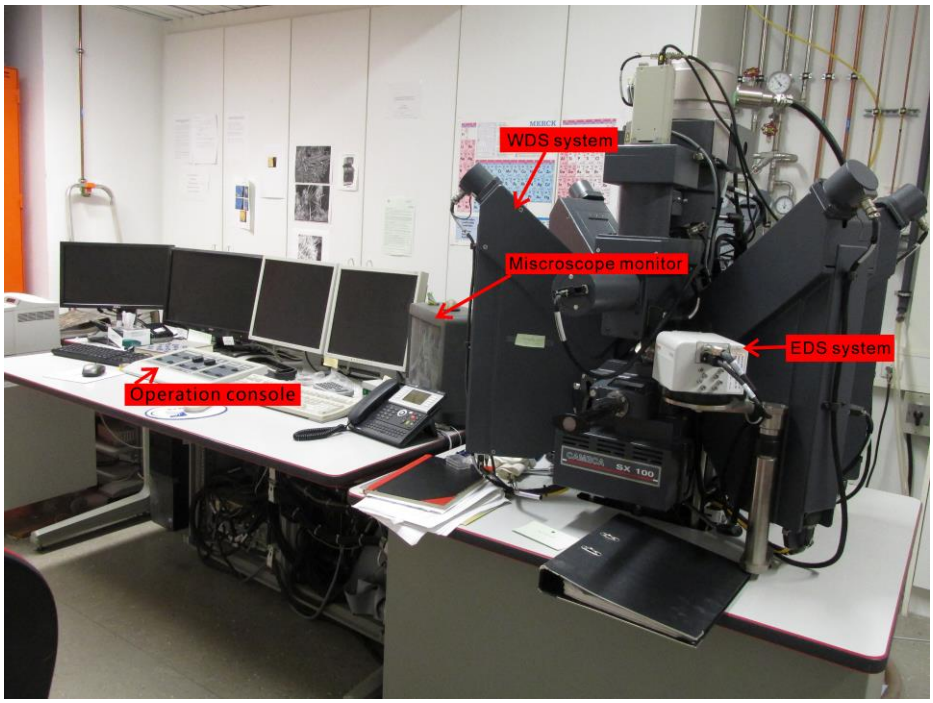

Fig. 3.3. Electron microprobe (Cameca SX100) at IMK at Universität Stuttgart.

The used EMP was a Cameca SX100 equipped with (Figs. 3.3, 3.4):

1. Five wavelength dispersive spectrometers (WDSs) around the sample chamber for quantitative mineral chemical analysis.

2. An energy dispersive spectrometer (EDS) used for (semi-)quantitative mineral

chemical analysis.

3. A tungsten filament was used as electron source.

4. A series of alignment coils, two condenser lenses, and objective lens located in the column of the instrument were adjusted to condense and focus the electron beam.

5. A sample chamber houses a brass stage to move specimens in X, Y, and Z direction.

6. An optical microscope was used to focus and view the area to be analyzed.

7. The EPM was operated under constant vacuum to reduce the influence of molecules from the atmosphere from interfering with the electron beam.

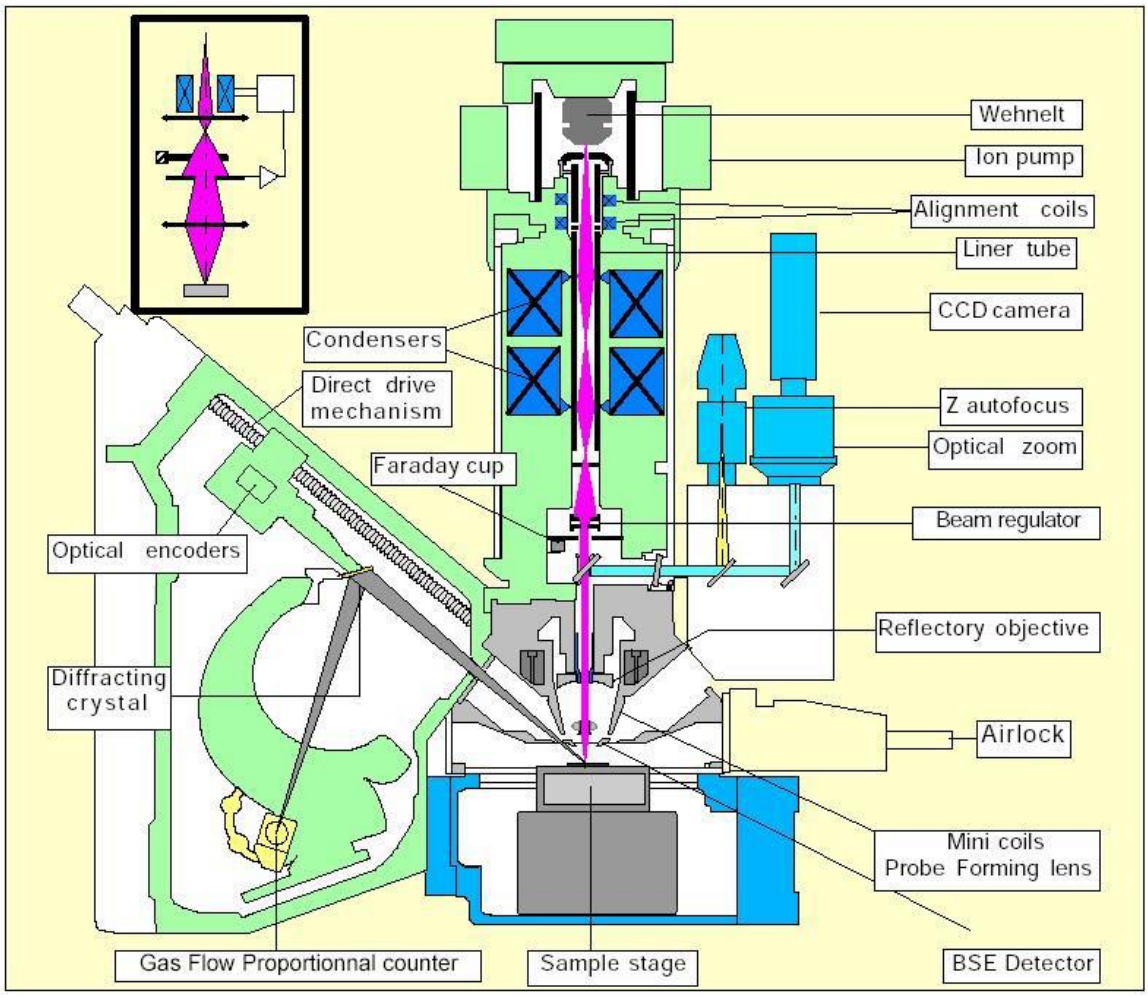

Fig. 3.4. Cross section of an electron microprobe (Cameca SX100), modified from a Cameca leaflet printed in 1999.

3.2.3. Electron-sample interactions

Electrons are produced by heating a tungsten filament to high temperatures (in the

gun). These electrons are accelerated from the filament towards the sample surface. The electrons as charged particles can be directed and focused on this surface by using electron static lenses (gun alignment, condensers) (Fig. 3.4).

The electron beam colliding with the sample surface excites mainly backscattered electrons (eleastic scattering at the nucleus partially with low energy loss = Bremsstrahlung) and characteristic X-rays (at the electron shell: high energy loss). The intensity of backscattered electrons contains information on the mean atomic number. The characteristic X-rays, having a specific wavelength, are used to analyze the concentration of elements in the specimen.

The intensity of X-rays with a specific wavelength is statistically counted using either an EDS or the system with WDSs. The EDS accumulates all wavelengths produced by interaction of a volume of the specimen with the electron beam, whereas the WDS system uses X-ray diffraction at an analyzing crystal to select and count a specific X-ray wavelength of interest. At the IMK, TAP, PET, and LIF (Table 3.1) were used as analyzing crystal. In fact, multi-elemental analyses can be much faster obtained with an EDS but the WDS system is significantly better for obtaining high-quality analyses.

Table 3.1. The applied analyzing crystals and elements commonly analyzed with them (from: http://web.mit.edu/e-probe/www/courses.shtml).

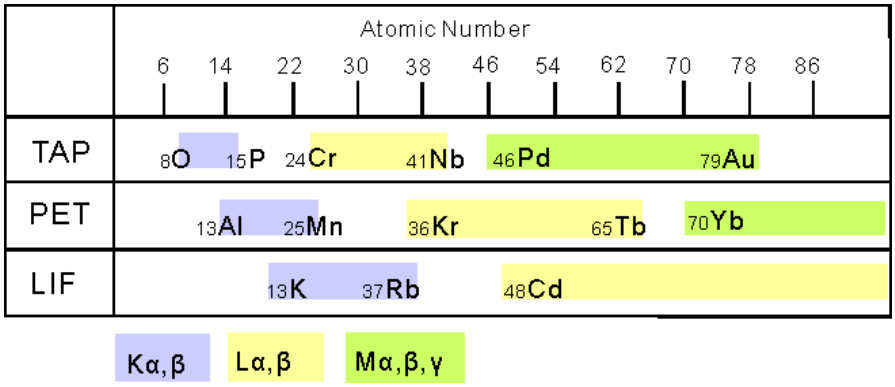

3.2.4. Characteristic X-ray spectra

Characteristic X-rays are emitted as a result of the transition of an electron from an outer to an inner electron shell of an atom (Fig. 3.5 left) (Reed et al., 1996). The corresponding energy difference depends on the shells and the element. When irradiating an atom with an electron beam, an electron from this atom can be expelled. Thus, a ‘hole’

in a shell, for instance, the K-shell is generated. The atom wants to restore the original configuration, which is achieved by transferring an electron from an outer shell such as the L-shell to the hole in the K-shell. An L-shell electron has a higher energy than a K-shell electron. Thus, when an L-shell electron is transferred to the K-shell, the energy surplus can be emitted as an X-ray photon (Brouwer, 2006). The X-ray photon energy is equal to the difference between the energies of the initial and final levels for the relevant transition of electrons (Reed et al., 1996) (Fig. 3.5). In a spectrum, this is seen as a specific line (Fig. 3.6).

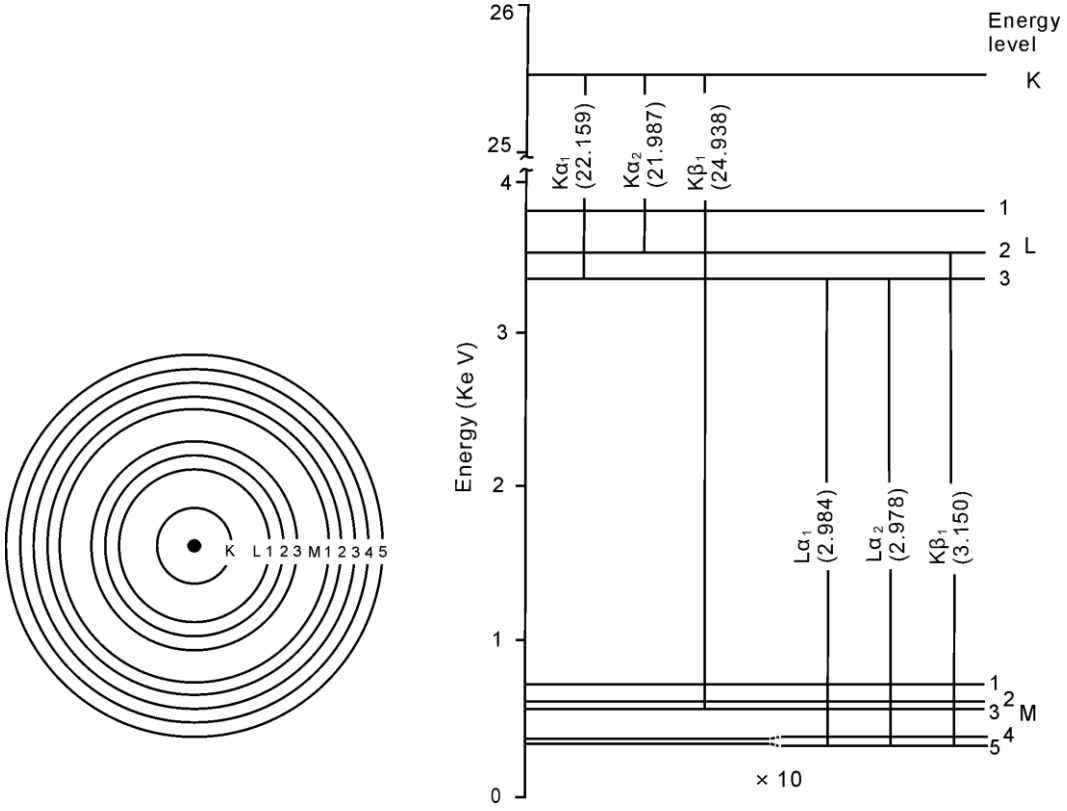

Fig 3.5. Left: Schematic diagram of inner atomic electron shells. Right: Energy level diagram for silver (the number of electrons: Z = 47); characteristic X-ray energy (given in kiloelectronvolts) is equal to the difference in energy between the levels involved in the transition (Reed, 1996).

In EMP analytics, one is mainly concerned with X-ray energies up to about 10 keV, and the $K\alpha_1$-line is used for the analysis of elements of atomic number up to about 30. For atoms with higher atomic number, the $L\alpha_1$ line is usually used (or the M α_1 line for the heaviest elements) (Reed, 1996).

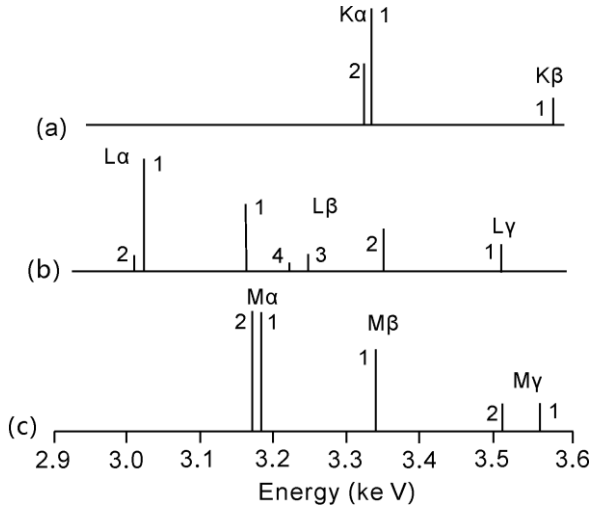

Fig. 3.6. Typical examples of characteristic X-ray spectra (principal lines only shown) (Reed, 1996): (a) K spectrum of potassium (Z = 19); (b) L spectrum of silver (Z = 47); (c) M spectrum of uranium (Z = 92).

3.3. Bulk-rock analyses

The concentrations of major elements were determined for all selected samples, but the concentrations of trace element were determined only for 5 eclogites and 1 glaucophanite. X-ray fluorescence (XRF) spectrometry and laser ablation inductively coupled plasma mass spectrometry (LA-ICP-MS) were used for bulk-rock analysis.

3.3.1. X-ray fluorescence (XRF) spectrometry

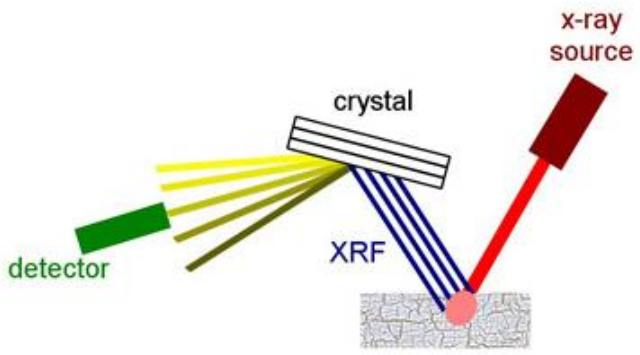

Fig. 3.7. The key components of a typical WD-XRF spectrometer (http://www.horiba.com/scientific/products/x-ray-fluorescence-analysis/tutorial/).

X-ray fluorescence (XRF) spectrometry is a widely-used technique for the routine determination of the major elements as well as a large number of geochemically

important trace elements in geological samples. Here, a PHILIPS PW2400 XRF spectrometer was used with a WDS system.

The WDS system physically separates the X-rays according to their wavelengths as in the EMP (Fig. 3.7). However, the detector is placed at a fixed position, but the analyzing crystal is rotated so that different wavelengths are diffracted into the detector.

Rocks were crushed and milled to obtain homogeneous powders for whole-rock analyses. A glass disc was prepared by melting 0.6 g sample powder + 3.6 g Li-borate = Spectromelt® or 0.5 g sample powder and 5 g Spectromelt®) (Fig. 3.1e). Other discs were produced by pressing 12 g sample powder and 3 g wax-C (Fig. 3.1f). Before analyses, the calibration of the XRF spectrometer was checked using geostandards. Bulk-rock major elements were analyzed on glass discs. Trace elements were determined on pressed discs.

3.3.2. Laser ablation inductively coupled plasma mass spectrometer (LA-ICP-MS)

Spectrometry with a LA-ICP-MS is a powerful analytical technology that enables highly sensitive elemental and isotopic analysis to be performed directly on solid samples. The technique is capable of determining many trace elements down to low ppm or even ppb levels.

The general configuration of a LA-ICP-MS instrument (Figs. 3.8, 3.9) comprises:

(1) An LA system, for sample desintegration and transport into the plasma.

(2) ICP-MS equipment (Agilent 7700s).

The aforementioned glass-disc (Fig. 3.1e) was ablated with a Cetac LSX-213 system using a wavelength of 213 nm. Laser sampling was performed by an energy-controlled pulsed laser beam. This beam is transmitted through an optical lens, which is also used to focus the beam onto the sample surface. The high-energy photons generated in the laser are converted into thermal energy, which is responsible of the ablation and the vaporization of the material. As a consequence, an aerosol composed of vapor and microscopic particles and agglomerates from the ablated solid sample is generated and transferred by the continuous gas stream of a He-Ar atmosphere (He: 300 ml/min, Ar: 800 ml/min) of the ablation cell into the plasma source. The spot size, laser shot frequency, and laser energy were 150 μm, 20 Hz, and 20 %, respectively. For each analysis 450 shots were achieved. The external standards for calibration were DLH-7

glass from the P&H company and a NIST 612 glass. Silicon was used as the internal standard, employing the SiO_2 concentration previously measured by XRF spectrometry. For a quality check of the applied method, diorite (DR-N) and zinnwaldite (ZW-C) reference standards from the Service d'Analyse des Roches et des Minéraux du CNRS were used.

Fig. 3.8. Laser-ablation inductively-coupled plasma-mass spectrometer (LA–ICP–MS) combining a Cetac LSX-213 system with an Agilent 7700s ICP-MS (from: http://www.uni-stuttgart.de/imi/institut/ausstattung.html).

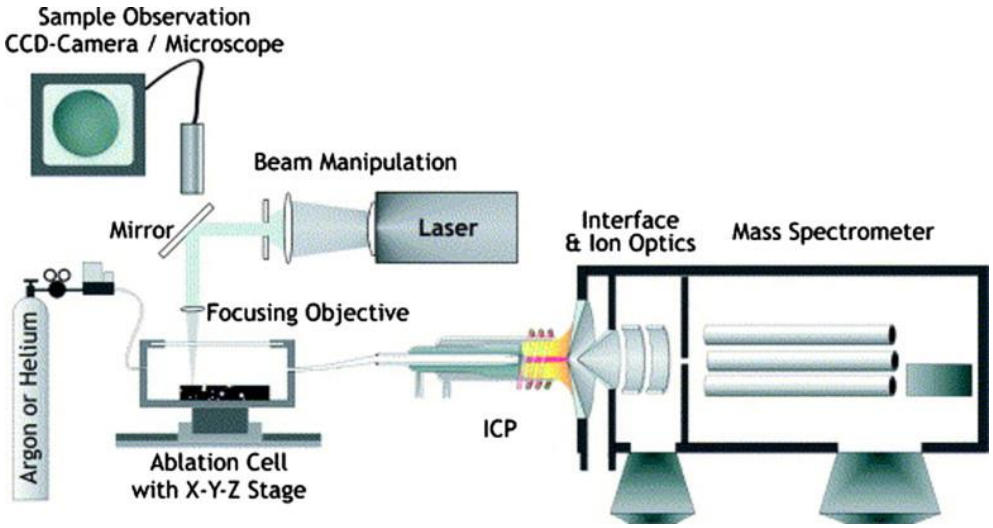

Fig. 3.9. Set-up of an instrument for spectrometry with a LA-ICP-MS (Orellana et al., 2013).

The inductively-coupled plasma (ICP) works as an atomization and ionization system (Orellana et al., 2013). The ions, formed by hot plasma, are introduced to a quadrupole mass spectrometer (filter) through the ICP-MS interface. The quadrupole mass filter consists of four parallel metal rods, connected in pairs. A radio-frequency voltage applied to these rods allows the separation of ions according to their *m*/*z* value. After passing through the filter, the ions with a specific *m*/*z* value are detected by a detector equipped with a channeltron electron multiplier.

3.4. Geochronology

Monazite in the sample of metapelite Sp96-38w was dated (see: section 6.7). This dating was undertaken on a lead-free thin section using the EMP (see section 3.2). The analytical procedure is reported in section 6.4.

Monazite, $(Ce,La,Nd)PO_4$, is a light rare earth element (LREE)-bearing phosphate mineral that is present in a wide variety of rock types and contains some Th and U (Th+Ca substitute 2 Ce,La) but virtually no common Pb. Therefore, it turned out to be a powerful mineral for age dating in metamorphic rocks (Bingen & van Breemen, 1998; Braun et al., 1998; Allaz et al., 2013). In addition, because diffusion of major and trace components appears to be slow (Parrish, 1990; Cherniak et al., 2004), monazite has the potential to retain chemical and geochronological information through young metamorphic events (Williams, et al., 1999). Age calculations use the measured Th, U and Pb contents. Corrected Pb, Th and U concentrations (ppm) are used to iteratively solve an age equation (Eq. 1), assuming no uncertainty on the decay constants (Suzuki & Adachi. 1991):

$$0 = a\,Th\,(e^{\lambda 232 Tht}-1) + b\,U(e^{\lambda 238 Ut}-1) + c\,U(e^{\lambda 235 Ut}-1) - Pb. \quad (1)$$

Where a, b, c are 'molecular constants' (a = 208/232, b = (0.9928×206)/238.04, c = (0.0072×207)/238.04), λ^k are decay constants, t is age in Ma, and Th, U, Pb are measured concentrations in ppm. In this way, an age is derived for each EMP spot analysis. Minimum age uncertainties are calculated for every analysed spot, derived by propagating X-ray counting errors through the age equation, analytical uncertainties (1σ) being taken as equal to the square root of the total counts (Poisson statistics) (Kelsey et al., 2003).

3.5. Geothermometry

In the chapter 4, Garnet-clinopyroxene thermometry was used for calculating metamorphic temperature at peak pressure of eclogite. Garnet-biotite thermometry was used for calculating metamorphic temperature of orthogneiss. In the chapter 5, Zr-in-rutile thermometry was used for 3 eclogites, 1 metatonalite and 1 glaucophanite.

3.5.1. Garnet-clinopyroxene thermometry

Garnet and clinopyroxene can occur in a wide variety of rocks. Therefore, several calibrations of the garnet-clinopyroxene geothermometer have been undertaken partially by high-pressure experiments (Pattison & Newton, 1989; Green & Adam, 1991; Ai, 1994; Ravna, 2000; Nakamura, 2009). This thermometer is based on the exchange reaction:

$MgAl_{2/3}SiO_4 + CaFe^{2+}SiO_6 = Fe^{2+}Al_{2/3}SiO_4 + CaMgSi_2O_6$

pyrope hedenbergite almandine diopside

The applied calibration is based on experimental data including 333 garnet-clinopyroxene pairs (Nakamura, 2009). The regressed and obtained thermometer formulation is as follows:

$T(°C) = \{2784 + 14.52\ P + (2601 + 1.44\ P)(2X_{grs}X_{prp} - A) + (1183 + 6.98\ P)\ (X_{grs}^2 - A) - 105(2X_{grs}X_{alm} + B) + (814.6 + 3.61P)(X_{grs}^2 + B) - (254.6 + 8.42\ P)(2X_{prp}X_{alm} - X_{alm}^2 + C) - 83.6(X_{prp}^2 - 2X_{prp}X_{alm} + C) + 1388X_{sps} - 462(X_{Mg}^{Cpx} - X_{Fe}^{Cpx})\}/\{\ln K_D + 1.431 + 0.695(2X_{grs}X_{prp} + X_{grs}^2 - 2A) + 0.203(X_{grs}^2 - 2X_{grs}X_{alm}) + 0.922X_{sps}\} - 273,$

where T = temperature, P = pressure (kbar), $A = 0.5\ X_{grs}\ (X_{prp} - X_{alm} - X_{sps})$, $B = 0.5\ X_{grs}\ (X_{prp} - X_{alm} + X_{sps})$, $C = 0.5\ (X_{grs} + X_{sps})(X_{prp} - X_{alm})$, $X_{prp} = Mg/(Fe^{2+} + Mn + Mg + Ca)^{Grt}$, $X_{alm} = Fe/(Fe^{2+} + Mn + Mg + Ca)^{Grt}$, $X_{sps} = Mn/(Fe^{2+} + Mn + Mg + Ca)^{Grt}$, $X_{grs} = Ca/(Fe^{2+} + Mn + Mg + Ca)^{Grt}$, $X_{Mg}^{Cpx} = Mg/(Al + Fe^{total} + Mg)^{Cpx}$, $X_{Fe}^{Cpx} = Fe^{2+}/(Al + Fe^{total} + Mg)^{Cpx}$, $K_D = (Fe^{2+}/Mg)^{Grt}/(Fe^{2+}/Mg)^{Cpx}$, Grt = Garnet, Cpx = clinopyroxene, alm = almandine, grs = grossular, prp = pyrope, sps=spessartine.

3.5.2. Garnet-biotite thermometry

Partitioning of Fe^{2+} and Mg is also known between coexisting biotite and garnet ($Fe_3Al_2Si_3O_{12} + KMg_3AlSi_3O_{10}(OH)_2 = Mg_3Al_2Si_3O_{12} + KFe_3AlSi_3O_{10}(OH)_2$ or almandine component in garnet + phlogopite component in biotite = pyrope component in garnet + annite component in biotite) and significantly depends on temperature as well.

Because of the common occurrence of this mineral pair in medium to high grade metamorphic rocks, the garnet-biotite Fe-Mg exchange geothermometer was also calibrated by several studies (Ferry & Spear, 1978; Krogh, 1988; Pattison & Newton, 1989; Dasgupta et al., 1991; Kleemann & Reinhardt, 1994).

The calibration of Kleemann & Reinhardt (1994) was applied because it is acknowledged to show small errors in reproducing experimental temperatures and good accuracy (see, e.g., Wu & Zhao, 2006; Wu & Chen, 2006). These authors refined the garnet-biotite thermometry by taking into account the effects of octahedral Al and Ti in biotite.

3.5.3. Zr-in-rutile thermometry

Due to the slow diffusion rate of Zr in rutile (e.g., Zr contents will be preserved for ca. 50 Ma at 700 °C in the center of 500 μm rutile grains, and for somewhat more than a million years at 900 °C; Cherniak et al., 2007), the shielding effect by porphyroblasts such as garnet or pyroxene (Zack et al., 2004), and because of the common occurrence of rutile in HP rocks the Zr-in-rutile (TiO_2) thermometer was established. Zr contents in rutile increase with rising temperature dependent and this thermometer is believed to be capable of recording high to ultra-high-T conditions (e.g. Zhang et al., 2010; Ewing et al., 2013).

Four calibrations of the Zr-in-rutile thermomer (Zack et al., 2004; Watson et al., 2006; Ferry & Watson, 2007; Tomkins et al., 2007) have been published. The first three ones focus exclusively on the effect of temperature on the Zr content in rutile. However, the calibration by Tomkins et al. (2007) has considered a minor pressure dependence of the Zr content in rutile. This content decreases with increasing pressure as a result of substituting Ti^{4+} by the larger Zr^{4+} cation. In this study, due to roughly known pressure conditions (see: section 5.7.3), the calibration by Tomkins et al. (2007) was used. The applied thermometric equation for the α-quartz field is: $T(°C) = \frac{83.9 + 0.410P}{0.1482 - R\ln\phi} - 273$, in which φ is ppm Zr, P is in kbar and R is the gas constant: 0.0083144 kJ K^{-1}.

3.6. Phase equilibria modeling (PERPLE_X)

3.6.1. Introduction

THERMOCALC and PERPLE_X are commonly used software packages for the calculation of phase diagrams, pseudosections, and mineral and rock properties.

THERMOCALC (Powell & Holland 1988) is based on the solution of a system of nonlinear equations and can directly calculate field boundaries of stable mineral assemblages. But because of abundant mineral reactions within a broader P-T frame, the use of THERMOCALC to create a phase diagram is quite laborious: each curve must be calculated by hand and the Schreinemaker's analysis must be achieved manually.

PERPLE_X (Connolly, 2005) uses the approach to equilibrium by Gibbs free energy minimization (linear programming), and its main strength is the very rapid ability to produce an output. Complete pseudosections for a broader P-T frame can be created in a few minutes with an ordinary personal computer and little understanding of the thermodynamic calculation process. The disadvantage of PERPLE_X can be the lacking pedagogical drawback, i.e. the applying scientist is able to run the program without a deep consideration of its actions and choices, e.g. the thermodynamic properties when using specific solid-solution models.

Pseudosections obtained from different software are virtually identical when the same thermodynamic database is utilized. Differences in calculated metamorphic assemblages arise from the choice of different solid solution models (Massonne, 2013).

In the thesis, PERPLE_X was used for calculation of pseudosections and mineral properties.

3.6.2. The basic principles of PERPLE_X

PERPLE_X is written and maintained by James Connolly (Zürich) (Connolly & Kerrick, 1987; Connolly, 1990; 2005; Connolly & Petrini, 2002), and is written in FORTRAN with the source code available. In order to produce a phase diagram, a gridded minimisation is used.

3.6.2.1. Gridded minimisation

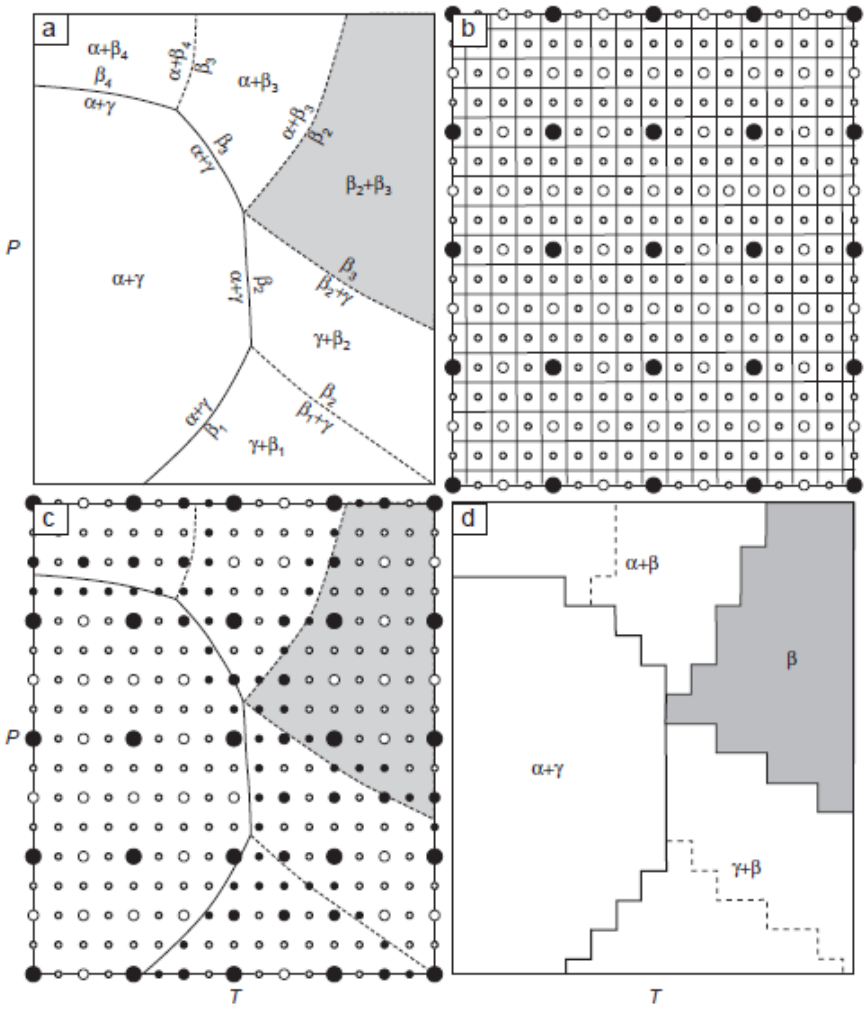

Fig. 3.10. Schematic phase pressure-temperature diagram section for a binary system with phases α, γ and β (Connolly, 2005). Only β is a solid-solution phase subdivided in a number of so-called pseudocompounds β_1, β_2 etc. (a) Small fields are defined by unique pseudocompound assemblages. (b) A four level grid. Higher levels are indicated by circles of decreasing size. (c) Phases computed by the mapping strategy are indicated by filled circles. (d) The final map is constructed by assuming that each node of the grid represents a finite area of the diagram.

Isochemical phase diagrams (so-called pseudosections) usually comprise several phase fields characterized by a particular phase assemblage. Within these fields the chemical composition and physical properties of the stable phases may vary continuously, but are uniquely determined at any point. A consequence of the pseudocompound approximation is that the continuous compositional variation of the individual phases

becomes discrete, so that the phase fields of a true section decompose into a continuous polygonal mesh of smaller pseudodivariant fields each of which is defined by a unique pseudocompound assemblage (Fig. 3.10a).

At the lowest level of resolution the grid has n_x and n_y data sampling points on the horizontal and vertical axes. Grids of successively higher levels of resolution are generated by halving the nodal spacing (Fig. 3.10b). Partially and entirely heterogeneous cells are marked for investigation in the next step, in which each of these marked cells is split into four cells at the next higher level. The stable assemblages at any of these nodes that are not known from the previous step are determined by free energy minimization, and heterogeneous cells are again marked for investigation. This process is repeated until the highest level is reached (Fig. 3.10c). A continuous map of the phase relations can then be constructed by associating a representative area with each point of the $N_x \times N_y$ grid (Fig. 3.10d) (Connolly, 2005). Finally, this map (pseudosection) (Fig. 3.10d) should be redrawn using, for instance, the computer software Coreldraw. All phase boundaries are smoothed to straight or simply curved lines. Individual P-T field should be filled by a designated background, marking the variance of the assemblage, and labelled.

4. Early Variscan P-T evolution of an eclogite body and its adjacent orthogneiss from the northern Malpica-Tuy shear-zone in NW Spain

by

Botao Li and Hans-Joachim Massonne*

Institut für Mineralogie und Kristallchemie, Universität Stuttgart, Azenbergstr. 18, D-70174 Stuttgart, Germany

*corresponding author: H.-J. Massonne, Tel.: +49-711-68581225,

Fax: +49-711-68581222, * e-mail: h-j.massonne@mineralogie.uni-stuttgart.de

European Journal of Minerology

(DOI: 10.1127/ejm/2016/0028-2569, First Published on July 17, 2016)

Abstract: An eclogite and its surrounding gneiss from the Malpica-Tuy zone, northwestern Spain, were studied. The eclogite contains besides garnet and omphacite, barroisitic amphibole, quartz, phengite with Si contents between 3.27 and 3.45 per formula unit (pfu), rutile, and accessory phases such as talc and (clino)zoisite-epidote. Garnet exhibits a chemical zonation with $Alm_{59}Prp_{13}Grs_{24}Sps_{4}$, $Alm_{57}Prp_{13}Grs_{27}Sps_{3}$, $Alm_{56.6}Prp_{12.5}Grs_{30.2}Sps_{0.7}$, and $Alm_{54}Prp_{20}Grs_{25}Sps_{1}$ as inner core, outer core, inner rim, and outermost rim compositions, respectively. The gneiss is a former granodiorite now mainly composed of quartz, plagioclase, K-feldspar, biotite, garnet, (clino)zoisite-epidote, and phengite with Si contents between 3.27 and 3.38 pfu. Garnet shows inner core, outer core, and rim compositions of $Alm_{26.9}Prp_{0.2}Grs_{70}Sps_{2.9}$, $Alm_{33.8}Prp_{0.7}Grs_{64}Sps_{1.5}$, and $Alm_{42.6}Prp_{1.4}Grs_{54}Sps_{2}$, respectively. P-T pseudosections, which were calculated with PERPLE_X for the bulk-rock compositions of the studied eclogite and gneiss, were contoured by isopleths of various parameters such as molar fractions of garnet components. Mainly based on the variable garnet and phengite compositions and these isopleths, P-T paths were derived. After an isothermal burial path the eclogite reached peak pressure conditions of 22.5 kbar at 540 °C. The subsequent exhumation path passed through P-T conditions of 21 kbar and 575 °C and 13.5 kbar and 625 °C. The latter data represent the peak P-T conditions of the gneiss. These P-T data

suggest that the protolith of the eclogite, a basic rock of an island-arc setting, underwent high-pressure metamorphism in a subduction zone. During its exhumation it came in contact with the buried metagranodiorite, representing the tip of a descending continental plate, at depths of 45-50 km probably ca. 350-355 Ma ago.
Keywords: Eclogite; Orthogneiss; Malpica-Tuy zone; Garnet zonation; P-T path; Continental collision.

4.1. Introduction

High-pressure (HP: P > 10 kbar) rocks such as eclogite- and blueschist-facies rocks often occur in major suture zones of collided continental plates. These rocks are frequently interpreted as the result of continental subduction (e.g. Guillot et al., 1997; Jahn, 1999; Pullen et al., 2008; Nakano et al., 2010; Ravna et al., 2010; López-Carmona et al., 2014a). However, these interpretations are often based on a few studied rocks only. In addition, HP metabasites are the dominant rock-types in these studies although gneisses usually predominate in the field. Studies which considered the pressure-temperature (P-T) evolution of both eclogites and adjacent gneissic country-rocks (e.g. Krogh, 1981; Willner et al., 2000; Godard, 2009) are rare. In general, these studies came to the conclusion that the gneisses experienced HP conditions. However, there are examples where the related eclogites had experienced significantly higher pressures than the country rocks (Willner et al., 2000; Massonne, 2012). A similar conclusion was drawn by Massonne (2009) for the Triassic Dabie-Sulu collisional belt based on the paucity of garnet in the country-rocks which proves rather low pressures. Nevertheless, this belt with abundant eclogite bodies, partially with evidence for metamorphism at ultrahigh pressure (UHP) conditions (e.g. Xiao et al., 2000; Gao et al., 2012; Groppo et al., 2015), is generally assigned to an extended HP-UHP terrane (Xu et al., 2006). Also the Himalayan belt with only three major occurrences of eclogite bodies, partially showing coesite relics, in its central and western part of the Greater Himalayan Sequence, was also related to a HP-UHP terrane formed by continental subduction (e.g., Lanari et al., 2013) although studies of various gneisses prove peak pressures around 13 kbar only (e.g., Liu et al., 2007; Iaccarino et al., 2015). Such examples for contrasting peak pressure conditions between metabasites, as typical representatives of oceanic crust, and gneisses, representing continental crust, could be continued for so-called HP-UHP

zones of other continent-continent collisional belts (see, e.g., Massonne, 2016 and references therein). Among the few examples of well studied HP rocks of basic and acidic nature, which seem to have experienced the same P-T evolution, those from Ecuador are noteworthy. The occurrence of these rocks is related to the collision of a microcontinent with the South American plate and to peak pressures of only 13 kbar (Massonne & Toulkeridis, 2012).

Due to the lack of well-constrained P-T data of HP country-rock gneisses, the understanding of a corresponding collisional process is limited. With this study, we want to demonstrate that (1) the metamorphic evolution of HP-UHP eclogite bodies and adjacent gneisses can be successfully derived and (2) important conclusions can be drawn to characterize the geodynamic processes behind such occurrences of HP-UHP rocks. Our target area (Fig. 4.1) is the already well-studied Malpica-Tuy (also written Tui) Zone (MTZ), a prominent suture zone in the Variscan orogen of southwestern Europe. In this zone abundant eclogite bodies occur, for which peak pressures in excess of 12 ± 2 kbar were already determined long time ago (Gil Ibarguchi & Ortega Gironés, 1985). We selected such a body in the northern portion of the MTZ close to the Atlantic coast. Garnet-bearing orthogneiss surrounds this eclogite occurrence. Both rock-types were carefully studied and finally evaluated for their P-T paths using isochemical phase diagrams (commonly called pseudosections) and especially the variable compositions of garnet and phengite in the rocks (for the method see, e.g., Massonne, 2013). We will demonstrate that the studied rocks have experienced clearly different peak pressures. This finding is interpreted by a geodynamic collisional scenario.

4.2. Geological setting

The Variscan orogeny is a mountain-building event caused by Late Paleozoic continental collision of Laurussia and Gondwana. However, different models, concerning timing and involvement of (micro) plates, exist in the literature for this orogeny (e.g. Matte, 1998; Shelley & Bossière, 2000; Kroner & Romer, 2013). The Iberian Massif in southwestern Europe involves a large fragment of the Variscan orogen (Andonaegui et al., 2012; Díez Fernández et al., 2011, 2012a; Díez Fernández & Martínez Catalán, 2012).

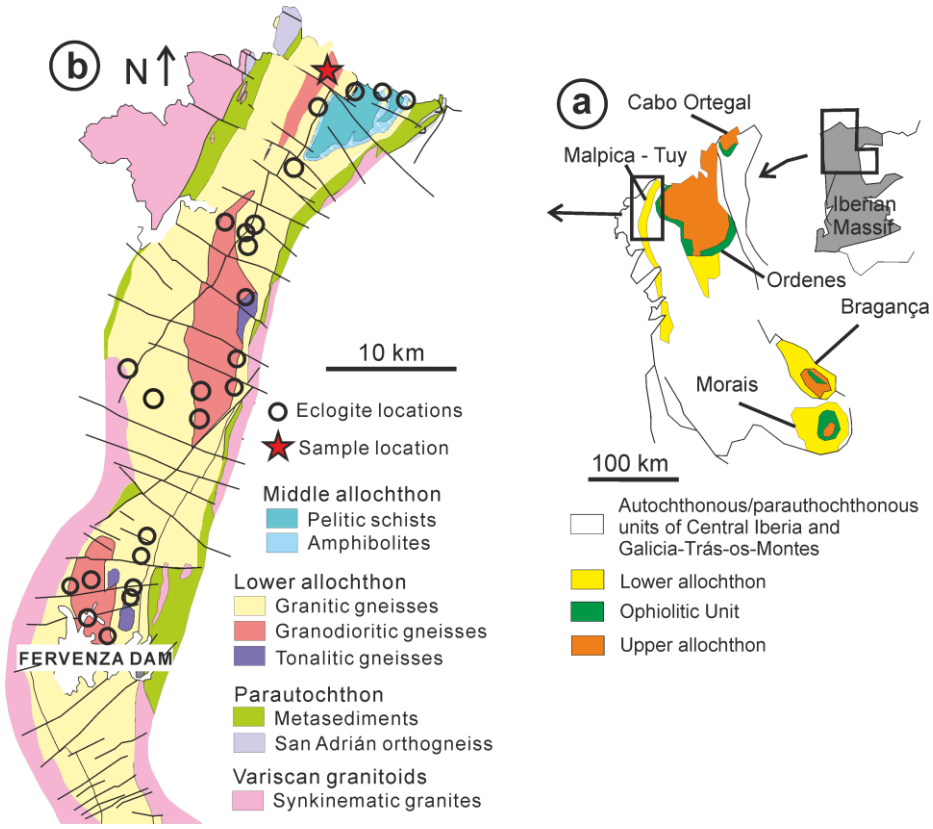

Fig. 4.1. (a) Geological frame of the Malpica-Tuy allochthon located in the Palaeozoic orogenic belt of NW Iberia (after Santos Zalduegui et al., 1995). (b) Geological map of the Malpica-Tuy Zone (after López-Carmona et al., 2013) showing eclogite locations (Gil Ibarguchi & Ortega Gironés, 1985) and the sample locality.

In the northwestern Iberian Massif, five allochthonous complexes are preserved in late synformal structures: three of them outcropping in Galicia (Cabo Ortegal, Órdenes, and MTZ units) and two in the Portuguese region of Trás-os-Montes (Bragança and Morais complexes) (Fig. 4.1a). In these allochthonous complexes, it is possible to distinguish several crustal slices with different origin, which are assigned from the top to the bottom to so-called upper, ophiolitic, and basal units. The upper unit represents exotic terranes with Gondwanan affinity; the ophiolitic unit is considered as a collisional suture, whereas the basal unit is interpreted to be the most external continental margin of Gondwana (Abati et al., 2010; Andonaegui et al., 2012). The basal unit of the allochthonous complexes of NW Iberia is formed by thick metasedimentary rock sequences, with detritus derived from Gondwana (Díez Fernández et al., 2010), containing mafic rocks. These sequences were intruded by granitoids ranging in

composition from calc-alkaline or subalkaline (protolith ages of ca. 493 Ma; see Abati et al., 2010; Díez Fernández et al., 2012b; Fuenlabrada et al., 2012) to minor alkaline-peralkaline (ca. 470-475 Ma; Rodríguez et al., 2007; Díez Fernández et al., 2012b; Fuenlabrada et al., 2012). The granitoids were transformed into variably deformed orthogneisses. The associated mafic rocks were metamorphosed to amphibolites, blueschists, and eclogites during an Eo-Variscan HP event (Gil Ibarguchi & Ortega Gironés, 1985; Fuenlabrada et al., 2012).

The MTZ is the westernmost of the European Variscan allochthonous complexes. It contains an upper unit of oceanic affinity (Ceán unit) composed of pelitic schists and N-MORB-derived metabasic rocks (Rodríguez et al., 2003; López-Carmona et al., 2013) (Fig. 4.1b). The underlying continental unit (called here Malpica-Tuy unit) is made of variably deformed and recrystallized granitoids, metasediments and sparse metabasites. Peak metamorphic conditions of rocks from the Malpica-Tuy unit are in the intermediate temperature eclogite-facies whereas the Ceán unit is considered as a highly condensed metamorphic succession with a lower part in the blueschist facies and an uppermost part containing rocks that have experienced metamorphic peak pressures of 21-22 kbar at 520 °C (López-Carmona et al., 2010, 2013).

Pods and relicts of eclogites and blueschists, well preserved in the NW Iberian massif, are considered to be the best record of the Variscan subduction at the northern Gondwana margin (Gil Ibarguchi et al., 1990, Arenas et al., 1997; Rubio Pascual et al., 2002). The blueschists of the MTZ have been studied in detail resulting in P-T-t paths using conventional geothermobarometry (Rodríguez et al., 2003) and P-T pseudosections (López-Carmona et al., 2010, 2014a). For eclogites, Gil Ibarguchi & Ortega Gironés (1985) pointed to two types existing in the Malpica-Tuy unit: glaucophane-bearing eclogites and those without glaucophane. Van der Wegen (1978) and Abati et al. (2010) suggested that the protoliths of these eclogites were Ti-rich alkaline and sub-alkaline basalts of a mafic-intermediate magmatism as old as 498 ± 6 Ma (Abati et al., 2010). The HP event was dated at 365-370 Ma (Van Calsteren et al., 1979; Santos Zalduegui et al., 1995; Martínez Catalán et al., 1996; Rodríguez et al., 2003; Abati et al., 2010).

Gil Ibarguchi (1995) calculated metamorphic peak conditions of 630 ± 40 °C (garnet-biotite Fe-Mg exchange geothermometry) and a minimum pressure of 16.5 ± 1

kbar (jadeite-quartz) for the HP event experienced by a metagranite. Rodríguez et al. (2003) estimated that the peak conditions of the HP metamorphic event was at ca. 21 kbar and 580 °C based on the assemblage garnet-phengite-omphacite.

Tectonic research addressed mainly the relation between different tectonic units and rock types, without any detailed consideration of eclogite bodies (Llana-Fúnez & Marcos, 2001; Rodríguez et al., 2003; Martínez Catalán et al., 2009; Díez Fernández et al., 2011; López-Carmona et al., 2014a). These works stress the character of the Malpica-Tuy unit as a major crustal-scale shear zone. According to Díez Fernández and Martínez Catalán (2012), this zone is the result of several shear zones superimposed in space and time. These authors related the preserved macrostructures in the Malpica-Tuy unit to exhumation and late-Variscan transcurrent tectonics.

Eclogites are present only in the central to northern part of the Malpica-Tuy unit and occur mostly as lenses and boudins within gneisses (Gil Ibarguchi & Ortega Gironés, 1985; Santos Zalduegui et al., 1995; Rodríguez et al., 2003; Abati et al., 2010). It is hypothesized that at least some eclogite bodies resulted from boudinage of a tabular body, possibly a dike (Díez Fernández and Martínez Catalan, 2012). Abundant eclogite bodies and adjacent rocks were sampled during three excursions in 1989, 1993, and 1996. Rocks from Punta Palerón (also Pelerón or Peterón, N43°18’40”, W8°48’07”), located ca. 2 km southeast of the town of Malpica near the Atlantic coast (Fig. 4.1b), seemed to be suitable for the envisaged study. A dekameter-sized eclogite body and the surrounding orthogneiss are outcropping at this locality. Abundant meter-sized blocks of gneiss are also lying on the ground around the eclogite boudin. We selected from the samples, which were taken from the Punta Palerón locality, two eclogite samples (18149, Sp35a) and two garnet-bearing gneiss samples (18159, Sp35c) for further detailed petrological studies.

4.3. Analytical methods

4.3.1. Electron microprobe study of minerals

Chemical analyses of minerals were carried out with a CAMECA SX100 electron microprobe (EMP) with 5 wavelength-dispersive spectrometers. For the eclogite sample, several larger grains of garnet, white mica, amphibole, and clinopyroxene were analyzed in detail. For the orthogneiss sample, the focus was on analyzing garnet and white mica.

Table 4.1. Representative EMP analyses (in wt%) of minerals in eclogite sample (18149).Structural formulae were calculated as follows: garnet (Gt) = 24 O, 10 six- and eight-fold coordinated cations; white mica (Wm), O = 11; amphibole (Am) = 46 valencies, sum of cations - (K+Ba+Ca+Na) = 13; clinopyroxene = 6 O, 4 cations; (clino)zoisite (Czs) = 25 valencies, Mn is trivalent. b.d.l, below the detection limit. Outerm.= outermost.

	Gt	Gt	Gt	Gt	Wm	Wm	Am	Am	Am	Om	Om	Om	Talc	Czs
SiO_2	37.65	37.86	37.89	38.32	52.47	50.78	46.04	52.28	48.33	56.10	56.83	56.31	63.56	37.25
TiO_2	0.14	0.16	0.11	0.04	0.27	0.53	0.38	0.12	0.26	0.08	0.06	0.05	0.02	0.07
Al_2O_3	21.45	21.41	21.43	21.80	26.60	28.94	13.36	7.45	11.17	8.51	11.25	9.28	0.07	28.51
Cr_2O_3	0.01	b.d.l	0.01	0.03	b.d.l	b.d.l	b.d.l	b.d.l	b.d.l	b.d.l	b.d.l	b.d.l	b.d.l	b.d.l
$(FeO)_{tot}$	27.69	27.00	27.46	25.99	1.40	1.28	13.61	7.79	8.96	4.37	3.21	3.43	2.87	5.96
MnO	1.52	0.60	0.29	0.62	0.00	0.03	0.01	0.01	0.01	0.01	0.02	b.d.l	0.05	0.09
MgO	3.40	3.27	3.06	5.13	4.22	3.29	11.27	16.72	14.52	10.71	8.97	10.19	28.18	0.03
CaO	9.17	10.22	10.93	9.11	0.01	0.02	10.65	9.19	8.56	16.09	14.05	15.95	b.d.l	24.42
Na_2O	0.04	0.03	b.d.l	0.01	0.59	0.90	2.72	2.89	3.42	5.15	6.66	5.72	b.d.l	0.02
K_2O					10.22	9.89	0.30	0.18	0.33	0.01	b.d.l	b.d.l	b.d.l	b.d.l
BaO					0.36	0.41	b.d.l	b.d.l	b.d.l	b.d.l	b.d.l	b.d.l	b.d.l	b.d.l
total	101.1	100.6	101.2	101.1	96.1	96.1	98.2	96.6	95.6	101.4	99.0	100.7	94.43	96.3
Si	5.817	5.896	5.850	5.855	3.448	3.342	6.630	7.340	6.917	1.985	1.990	1.984	4.071	2.932
Ti	0.016	0.019	0.013	0.005	0.013	0.027	0.041	0.012	0.028	0.002	0.002	0.002	0.001	0.004
Al	3.906	3.930	3.899	3.926	4.885	4.901	2.268	1.232	1.884	0.355	0.466	0.385	0.005	2.645
Cr	0.001	0.000	0.001	0.004			0.000	0.000	0.000					0.000
Fe^{3+}	0.093	0.070	0.101	0.070			0.288	0.480	0.590	0.025	0.002	0.035		0.392
Fe^{2+}	3.489	3.447	3.450	3.255	0.077	0.071	1.352	0.434	0.483	0.105	0.092	0.066	0.154	
Mn	0.199	0.079	0.038	0.081	0.000	0.002	0.001	0.002	0.001	0.000	0.001	0.000	0.003	0.006
Mg	0.783	0.759	0.704	1.169	0.413	0.323	2.419	3.500	3.097	0.565	0.468	0.535	2.691	0.003
Ca	1.518	1.706	1.808	1.492	0.001	0.002	1.643	1.382	1.313	0.610	0.528	0.602		2.060
Na	0.011	0.009	0.000	0.003	0.075	0.115	0.759	0.786	0.949	0.353	0.452	0.391		0.003
K					0.857	0.831	0.060	0.027	0.033	0.000	0.000	0.000		
Ba					0.010	0.011	0.000	0.000	0.000					

Table 4.2. Representative EMP analyses (in wt%) of minerals in gneiss sample 18159. Structural formulae of garnet (Gt), white mica (Wm), and clinozoisite-epidote (Ep) were calculated as given in Table 4.1. For biotite (Bt) 11 O were considered. Feldspar (Pl: plagioclase, Kf: K-feldspar) was calculated with 8 O. b.d.l, below the detection limit.

	Gt	Gt	Gt	Wm	Wm	Bt	Bt	Ep	Ep	Ep	Pl	Kf
SiO_2	38.29	37.11	37.51	49.47	49.37	34.66	33.83	38.94	37.41	37.00	68.05	63.51
TiO_2	0.13	0.18	0.11	0.32	0.30	1.75	1.09	0.03	0.11	0.17	0.00	0.00
Al_2O_3	21.45	20.47	20.46	26.90	27.69	17.31	18.38	31.06	26.11	25.78	19.07	18.04
Cr_2O_3	b.d.l	0.03	b.d.l	b.d.l	b.d.l	b.d.l	b.d.l	b.d.l	b.d.l	b.d.l	b.d.l	b.d.l
(FeO)tot	15.26	17,19	20.57	4.65	5.34	25.39	25.95	3.21	8.85	9.28	b.d.l	0.07
MnO	1.13	0.63	0.28	0.03	b.d.l	0.23	0.29	0.07	0.03	0.16	0.03	0.01
MgO	0.20	0.17	0.30	2.35	2.15	5.35	5.28	0.06	0.02	0.20	b.d.l	0.01
CaO	23.81	22.62	20.13	b.d.l	0.03	b.d.l	0.07	24.56	23.63	23.12	0.08	b.d.l
Na_2O	b.d.l	b.d.l	0.01	0.09	0.15	0.03	0.03	0.01	b.d.l	b.d.l	11.74	0.37
K_2O				10.68	11.39	9.29	8.89	b.d.l	b.d.l	b.d.l	0.11	16.80
BaO				0.44	0.50	0.14	0.02	b.d.l	b.d.l	b.d.l	b.d.l	0.44
total	100.3	98.40	99.36	94.90	96.92	93.91	93.54	97.94	96.14	95.71	99.06	99.18
Si	5.906	5.833	5.904	3.365	3.323	2.764	2.709	2.980	2.986	2.951	3.002	2.984
Ti	0.015	0.021	0.013	0.017	0.015	0.105	0.065	0.002	0.009	0.010	0.000	0.000
Al	3.898	3.792	3.795	2.156	2.196	1.626	1.735	2.801	2.417	2.424	0.991	0.999
Cr	0.000	0.004	0.000	0.000	0.000	0.000	0.000	0.000	0.000	0.000	0.000	0.000
Fe^{3+}	0.102	0.204	0.205	0.000	0.014	0.000	0.000	0.205	0.573	0.619		0.003
Fe^{2+}	1.872	2.066	2.496	0.265	0.287	1.693	1.737					
Mn	0.148	0.084	0.038	0.002	0.000	0.015	0.020	0.004	0.002	0.010	0.001	
Mg	0.045	0.040	0.070	0.236	0.216	0.636	0.630	0.007	0.002	0.024	0.000	0.000
Ca	3.934	3.809	3.394	0.000	0.002	0.000	0.006	2.013	2.008	1.976	0.004	0.000
Na	0.001	0.001	0.002	0.012	0.019	0.005	0.004	0.002	0.000	0.000	1.004	0.034
K				0.927	0.978	0.945	0.908				0.006	1.007
Ba				0.012	0.013	0.004	0.001				0.000	0.008

For both rock samples, we also paid particular attention to inclusion minerals mainly in garnet. The analyses of the minerals included the element concentrations of F, Na, Mg, Al, Si, K, Ca, Ti, Cr, Mn, Fe, and Ba. The conditions for these analyses were 15 kV acceleration voltage, 10 or 15 nA beam current, and approximately 2 minutes total counting time (a detailed description of the analytical conditions and errors are given by Massonne, 2012). Back-scattered electron (BSE) images were taken with the EMP to document specific textural features.

For the calculation of structural formulae of minerals and the molar fractions of mineral components from EMP analyses, the computer program CALCMIN (Brandelik, 2009) was used. Representative EMP analyses of minerals in the studied eclogite and gneiss are given in Tables 4.1 and 4.2, respectively.

X-ray maps for specific mineral grains were produced with the EMP. For the mapping, Mn, Ca, Mg, Fe, and Y were considered for garnet. Magnesium, Fe, Ti, Na, and Ba concentrations were mapped for white mica. For clinopyroxene and amphibole Ca instead of Ba was considered. The parameters for the X-ray mapping were 1 or 2 µm step width, 50-100 ms per step, 15 kV accelerating voltage, and 30 nA beam current for white mica, 50 nA for clinopyroxene and amphibole, and 60 nA for garnet.

4.3.2. Whole-rock analyses

Major and trace elements were determined for eclogite sample 18149. Only major elements were analyzed for gneiss sample 18159. The results are given in Table 4.3.

Both samples were crushed and milled to obtain homogeneous powders for whole-rock analyses. Bulk-rock major elements were analyzed on lithium borate glass-disks (prepared with 0.5 g sample powder and 5 g Li-borate = Spectromelt®) by X-ray fluorescence (XRF) spectrometry with a PHILIPS PW2400 XRF spectrometer. This instrument had been calibrated by using numerous geostandards. Both, XRF and laser ablation inductively-coupled plasma mass spectrometry (LA–ICP–MS), were used for the determination of trace elements. A part of powder of sample 18149 was pressed to a disk (prepared with 12 g sample powder and 3 g wax-C) for the XRF determination. A lithium borate glass-disk (0.6 g sample powder + 3.6 g Spectromelt®) was analyzed by LA–ICP–MS employing a Cetac LSX-213 system with a wavelength of 213 nm combined with an Agilent 7700s ICP-MS. Laser sampling was performed in a He-Ar

Table 4.3. Bulk-rock analyses for the studied eclogite (Eg) and the relatively fine-grained gneiss (Gs) determined by X-ray fluorescence (XRF) spectrometry and laser-ablation ICP mass-spectrometry (LA-ICP-MS). b.d.l = below detection limit. The compositions used for PERPLE_X calculations (in the upper right) were modified as indicated in the text (section 7.1): modified1 refers to the bulk-rock composition of the eclogite, whereas modified 2 represents the composition after subtracting the eclogitic garnet core.

	XRF		**for pseudosection calculations**		
Sample	Eg:18149	Gs:18159	Eg modified 1	Eg modified 2	Gs modified
SiO_2 in wt.	48.46	72.24	46.25	48.46	70.60
Al_2O_3	14.28	13.70	13.63	12.43	13.39
MnO	0.23	0.03	0.22	0.05	0.03
MgO	7.10	0.41	6.78	7.42	0.40
CaO	10.01	2.13	9.26	9.34	2.01
Na_2O	2.47	3.37	2.36	2.82	3.29
K_2O	0.38	3.00	0.37	0.44	2.93
TiO_2	2.12	0.29	2.02	2.40	0.28
P_2O_5	0.24	0.05			
Fe_2O_3	13.97	2.90			
FeO			11.99	9.55	2.55
O_2			0.13	0.11	0.03
H_2O			7.00	7.00	4.50
Total	99.26	98.12	100.00	100.00	100.00

Minor and trace elements in eclogite 18149					
	XRF	LA-ICP-MS		XRF	LA-ICP-MS
Sc in ppm	16.3	47.9	Zr	150	196
Ti	13190	12706	Hf	b.d.l	4.88
Rb	10.4	7.16	Sm	4.3	6.44
Ba	157	119	Eu		1.75
K	3155	2186	Gd		7.41
Th	1.3	1.10	Tb		1.22
U	b.d.l	0.30	Dy		8.07
Nb	11	5.54	Y	42.7	44.6
Ta	1.7	0.36	Ho		1.73
La	13.27	12.2	Er		5.03
Pr	b.d.l	3.90	Tm		0.74
Ce	26	26.2	Yb	6.3	4.66
Sr	47	147	Lu		0.72
Nd	18	21.7			

atmosphere (He: 300 ml/min, Ar: 800 ml/min). The spot size, laser shot frequency, and laser energy were 150 μm, 20 Hz, and 20 %, respectively. For each analysis 450 shots were achieved. The external standards for calibration were DLH-7 glass from the P&H company and NIST 612 glass. Silicon was used as the internal standard, employing the SiO_2 concentration previously measured by XRF spectrometry. For a quality check of the applied method, we used the diorite (DR-N) and zinnwaldite (ZW-C) reference standards from the Service d'Analyse des Roches et des Minéraux du CNRS.

For plotting the obtained trace element concentrations in diverse discrimination diagrams, we applied the results from the LA-ICP-MS analyses for contents below 30 ppm as they are more precise than the corresponding results from the XRF spectrometry. For element concentrations above 30 ppm (except Sr for which the content obtained from LA-ICP-MS was applied), we used the mean values of both analytical methods.

4.4. Petrography

4.4.1. Eclogite

The investigated eclogite samples turned out to be nearly identical. Both are fine-grained amphibole eclogites, which are dark green and weakly to non-foliated displaying a granoblastic texture. The rocks are composed mainly of garnet (40 vol.%), amphibole (25 vol.%), and omphacite (20 vol.%) with minor amounts of phengite (5 vol.%), quartz (5 vol.%), and rutile (1.5 vol.%) (Fig. 4.2a, b). Talc, (clino)zoisite, apatite, zircon, ilmenite, and iron sulfides occur as accessories.

Garnet is fine-grained with grain sizes usually between 0.05 and 0.2 mm. It contains numerous inclusions of quartz, (clino)zoisite, amphibole, and rutile, and occasionally apatite, zircon, and ilmenite. A conspicuous regular distribution of the inclusions correlates with the chemical zonation of the garnet (see below). (1) The garnet core contains inclusions of quartz, (clino)zoisite, and amphibole (Fig. 4.2b, c) and also rare apatite inclusions. (2) Rutile is enclosed in the outer core, mantle, and rim of garnet. (3) The rim domain of garnet is almost free of inclusions. Amphibole has formed along cracks in garnet. Also ilmenite fills some cracks.Clinopyroxene, commonly with sizes between 0.1 and 0.5 mm, appears as subhedral crystals in the matrix or as irregularly shaped crystals frequently (partially) surrounded by amphibole (Fig. 4.2b), which seems

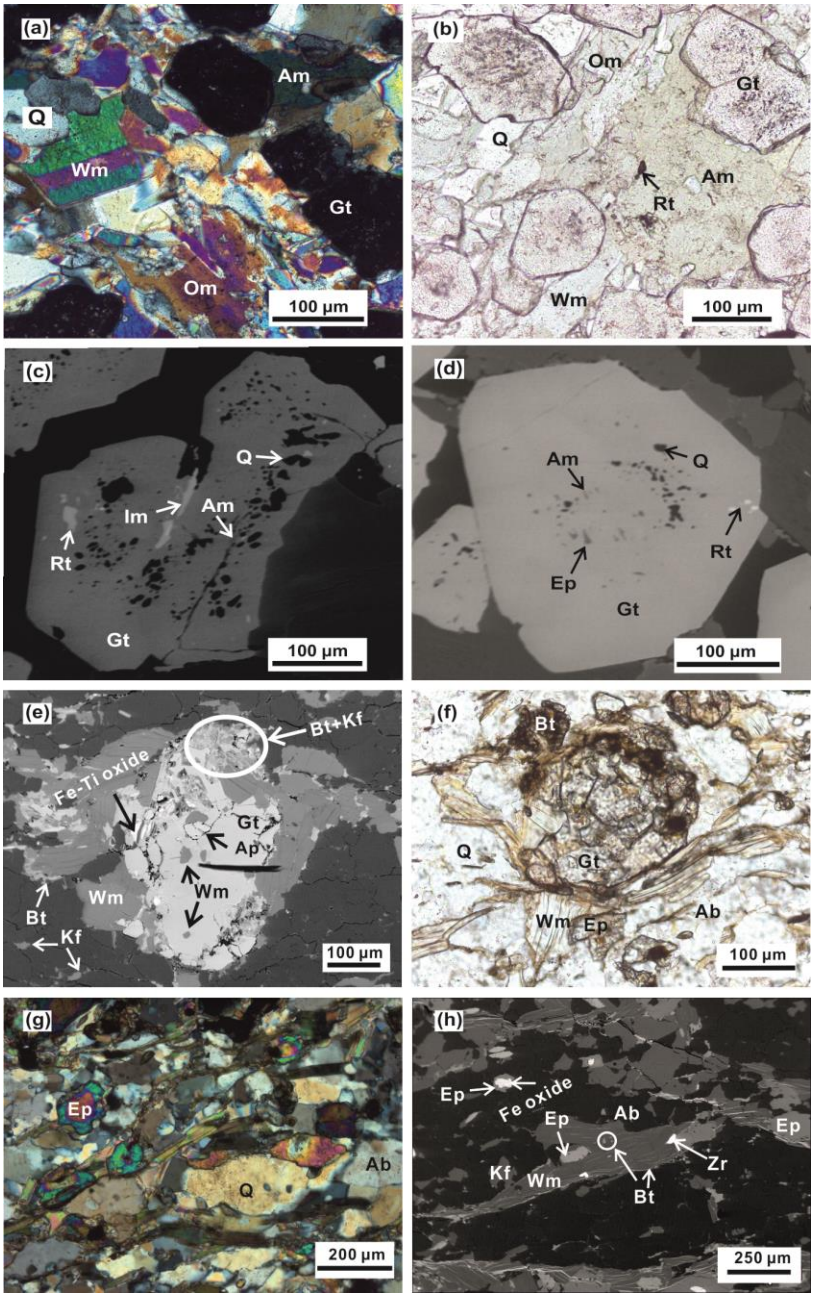

Fig. 4.2. Photomicrographs of the eclogite(a-d) and gneiss (e-h). (a) Under crossed polarized light (CPL): main minerals of eclogite with garnet (Gt), omphacite (Om), amphibole (Am), white mica (Wm), and quartz (Q). (b) Under plain polarized light (PPL): Am can be recognized by darker colors than Om; most Am grains are larger than grains of Om. Rt = rutile. (c) and (d) BSE images showing inclusions in Gt. Ep = clinozoisite-epidote, Im = ilmenite. (e) BSE image showing a strongly corroded Gt; Wm and Ap occur as inclusions; biotite (Bt) and K-feldspar (Kf) symplectites are around garnet; Kf grew interstitially among albite grains. (f) PPL: Bt appears as a retrograde product around Gt and along Wm cleavage planes. Ab = albite. (g) CPL: zoned Ep along foliations and Q with irregular boundaries. (h) BSE image showing Ep as corona around Fe oxide close to Ab. Zr: zircon.

to have replaced clinopyroxene. This type of amphibole, which forms mm-sized grains, locally shows a granular texture. Quartz, clinopyroxene, apatite, garnet, and rutile were found as rare inclusions in this amphibole. Occasionally, symplectites can also occur around clinopyroxene. They are composed of columns/plates of plagioclase, amphibole, and clinopyroxene which are usually only a few micrometers thick.

Phengite occurs as large subhedral grains or small grains in interstices (Fig. 4.2a). Clinopyroxene and rutile are enclosed in phengite. Rutile occurs as anhedral large grains (up to 0.03 mm × 0.06 mm in size) in the matrix and usually as significantly smaller grains enclosed in the major minerals. (Clino)zoisite only appears as inclusion in garnet (see above). Small grains of talc were found in direct contact with matrix phengite.

4.4.2. Granodioritic gneiss

The studied samples represent two types of garnet-bearing granodioritic gneiss surrounding the studied eclogite body. One type (sample 18159) is characterized by a well-developed foliation with relics of small flattened feldspar augen. The other type (sample Sp35c) shows a less strong foliation with significantly larger feldspar augen. As the mineral assemblage in both rock types is the same, only sample 18159 is described in more detail.

The main minerals in sample 18159 are quartz (35 vol.%), plagioclase (30 vol.%), K-feldspar (12 vol.%), white mica (10 vol.%), biotite (3 vol.%), clinozoisite-epidote (7 vol.%), garnet (0.5 vol.%), and Fe (Ti) oxide (0.5 vol.%). Further accessory minerals are chlorite, titanite, zircon, apatite, rutile, and monazite. The foliation is defined by aligned flakes of white mica and biotite (Fig. 4.2f, g) sandwiched between grains of feldspar and quartz.

Porphyroblastic garnet (Fig. 4.2e, f), frequently with sizes between 2 and 4 mm, is usually corroded and surrounded by white mica, biotite, and clinozoisite-epidote. Inclusions in garnet are quartz, white mica, biotite, clinozoisite-epidote, and apatite (Fig. 4.2e). Especially white mica appears in all garnet domains from core to rim and, thus, formed earlier than white mica surrounding garnet. Titanite, quartz, and zircon occur as inclusions in white mica. Biotite also crystallized in white mica-rich cleavage planes (Fig. 4.2f). Zoned porphyroclastic clinozoisite-epidote grains are distributed along these planes (Fig. 4.2g). Another type of clinozoisite-epidote appears as corona of Fe oxides along the

boundaries with plagioclase Fig. 4.2h).

Plagioclase augen (up to 1.5 mm) with and without exsolved K-feldspar occur in the rock. Anhedral K-feldspar with grain sizes around 50 μm grew interstitially together with anhedral plagioclase grains (30-300 μm in size) in the matrix (Fig. 4.2e, h). K-feldspar also appears in symplectites together with biotite around garnet. Quartz with irregular boundaries is the most common matrix phase. It recrystallized to aggregates of small grains (50-200 μm in size) (Fig. 4.2g). Titanite grains were found at corroded garnet boundaries.

4.5. Mineral chemistry

4.5.1. Eclogite

Garnet shows variable concentrations of spessartine (Sps: 0.4-5 mol %), almandine (Alm: 50-60), pyrope (Prp: 10-26), and grossular (Gros: 22-31) components (Table 4.1, Fig. 4.3). The growth zoning of porphyroblastic garnet is characterized by a relatively Mn rich core and an increase of the Ca content from the core towards the inner rim (Fig. 4.3). In most garnet grains, Mg and Fe contents are almost constant from the core to the inner rim. Occasionally, Mg and Fe are enriched compared to these constant values. However, this enrichment occurs along cracks so that such higher Mg and Fe contents are not representative for the original growth zoning. An outer rim in garnet is common. This garnet domain is characterized by Mg and Mn contents being higher and Ca and Fe contents being lower than those of the inner rim. A further generation of garnet (outermost rim) with straight phase boundaries discontinuously overgrew the irregular rim of the garnet of the previous generation. Thus, between these garnet generations a resorption event had happened. Altogether, the compositional zonation of garnet is characterized by the following compositions representative of particular domains: inner core $Alm_{59}Prp_{13}Grs_{24}Sps_{4}$ (Gt_1), outer core $Alm_{57}Prp_{13}Grs_{27}Sps_{3}$ (Gt_2), inner rim $Alm_{56.6}Prp_{12.5}Grs_{30.2}Sps_{0.7}$ (Gt_3), outermost (outer) rim $Alm_{54}Prp_{20}Grs_{25}Sps_{1}$ (Gt_4). There is almost no andradite component in garnet (Table 4.1) according to the applied calculation method for the garnet structural formula.

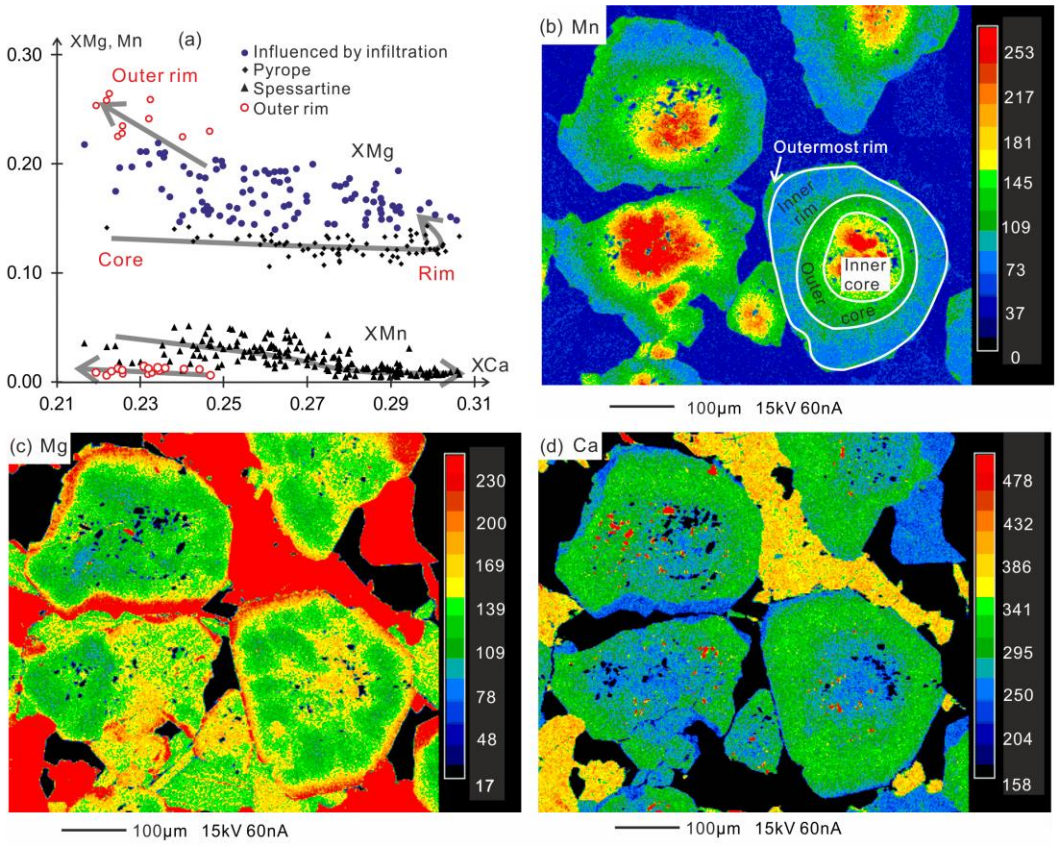

Fig. 4.3. (a) Analyses of garnet from eclogite sample 18149 obtained with an EMP in terms of molar fractions of pyrope (XMg) and spessartine (XMn) versus that of grossular (+ andradite) as XCa. The solid lines show the chemical trends from the core to the rim of garnet ignoring somewhat Mg-richer compositions probably due to fluid infiltration (see text). (b-d) Mn, Mg, and Ca concentration maps of garnet in eclogite also obtained with an EMP.

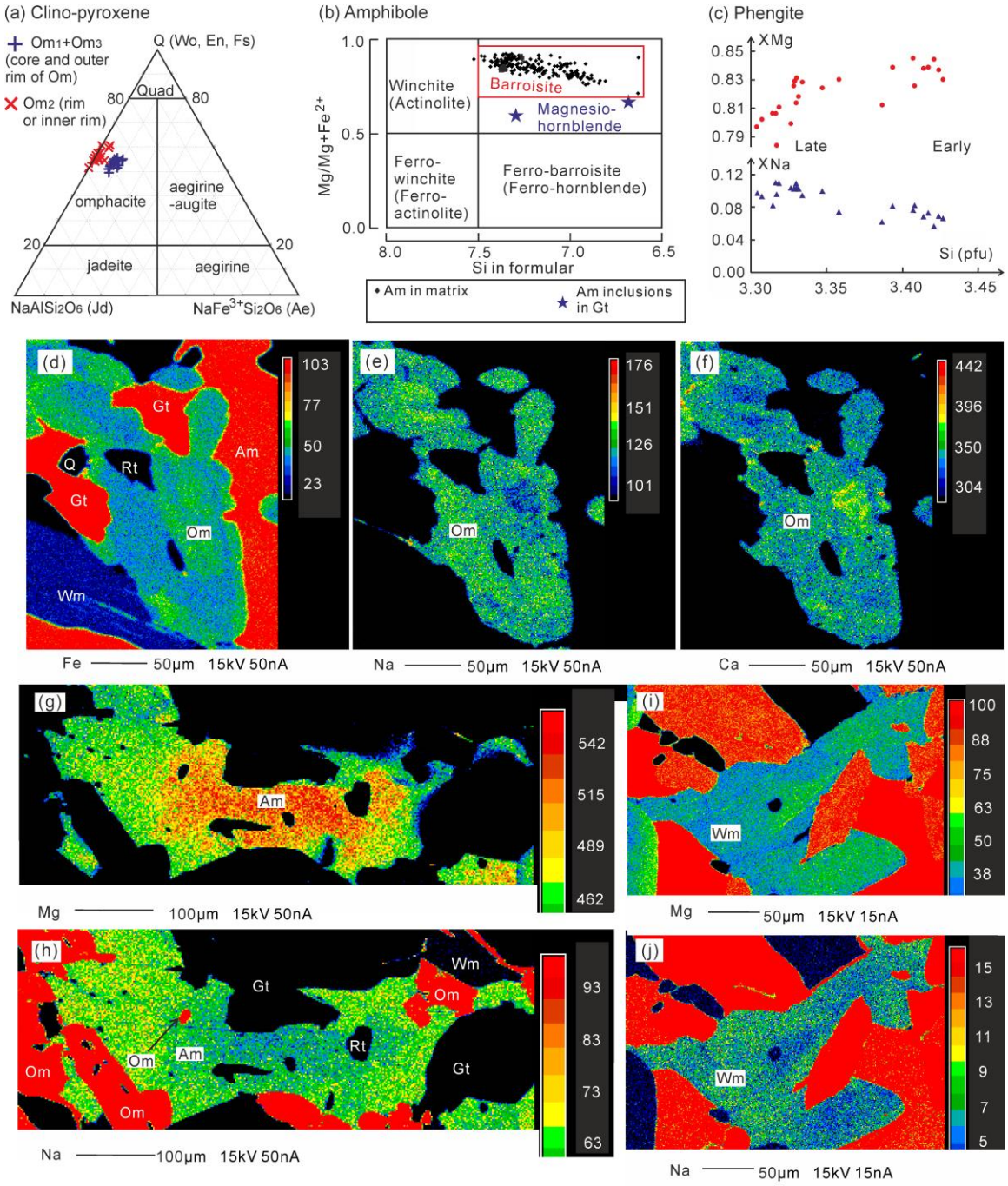

Fig. 4.4. (a) Classification of analyzed Ca-Na clinopyroxene after Morimoto et al. (1998). (b) Classification of the analyzed amphibole after Leake et al. (1997). (c) White mica analyses obtained with an EMP in terms of XMg and XNa versus Si pfu, (d-j) Concentration maps obtained with a CAMECA SX100 EMP of clinopyroxene (d-f), amphibole (g, h), and white mica (i, j) in eclogite. For abbreviations see legend of Figure 4.2.

Besides diopsidic clinopyroxene with 0.01-0.10 Na per formula unit (pfu) and XFe = Fe/(Fe + Mn + Mg) = 0.00-0.06 in symplectites, omphacite occurs as the dominant clinopyroxene: Omphacite grains (Fig. 4.4a) typically with embayed contacts contain 35-48 mol % jadeite+aegirine component. In general, these grains are zoned (Fig. 4.4d-f). Their core with XNa = 0.35-0.42 pfu (Om_1) is somewhat richer in Ca, Mg, and Fe compared to the rim (Om_2). The (inner) rim is characterized by XNa = 0.43-0.48 pfu and a higher Ti content compared to the core. Locally, a narrow outer rim with XNa = 0.38-0.40 pfu (Om_3) with higher Ca, Mg, and Fe and lower Na and Ti contents compared to Om_2 was observed. The calculated content of aegirine component in Om_1 and Om_3 is higher (7-11 mol %) than in Om_2 (0-4 mol %) (Fig. 4.4a).

According to textural position and composition, three types of amphibole were recognized. One type appears as inclusion in garnet. The two achieved analyses of this type refer to a hornblende (Am_1: Si = 6.63 pfu, XNa = $Na^{[8]}/2$ = 0.18 and Si = 7.22, XNa = 0.05; Tab. 4.1 and Fig. 4.4b). Another type (Am_2-Am_3) is a mainly sodic-calcic barroisitic amphibole (XNa between 0.29 and 0.37, Fig. 4.4b), which occurs as matrix grain and contains clinopyroxene inclusions (Fig. 4.4g, h). This amphibole is frequently zoned (Fig. 4.4g, h): Mg and Ca contents are higher and Fe, Na, and Ti contents are lower in the core (Am_2) compared to the rim (Am_3). In addition, the Si content changes from 7.5 (core) to 6.8 (rim) pfu. The composition of amphibole (Am_4) in the symplectites around omphacite is that of a tschermakite (Si = 6.2-6.5 pfu; XNa = 0.08-0.17).

All white mica is phengite, the silicon content of which ranges from 3.27 to 3.45 pfu (Fig. 4.4c). According to the produced X-ray maps, phengite can be easily subdivided into two generations (Fig. 4.4i, j). The older generation (core domain = Ph_1) is richer in Si and Mg and poorer in Na (Si = 3.36-3.45 pfu, Mg = 0.34-0.44 pfu, Na = 0.06-0.10 pfu) compared to the younger generation (rim domain = Ph_2: Si = 3.27-3.34 pfu, Mg = 0.29-0.35 pfu, Na = 0.09-0.14 pfu). (Clino)zoisite contains between 5 and 11 mol % pistacite, $Ca_2Al_2Fe^{3+}Si_3O_{10}(OH)$, component. Plagioclase in the symplectites is oligoclase-andesine with X_{An} = 0.20-0.35.

Based on the observed mineral assemblages, their microstructural characteristics, and the analyzed compositions of minerals of the eclogite, we propose five metamorphic stages for this rock: (1) According to inclusions in garnet, the (incomplete) assemblage,

representing the earliest metamorphic stage (M_1), is hornblende (Am_1) + (clino)zoisite + quartz + rutile. (2) The subsequent metamorphic stage (M_2) is characterized by the coexistence of early garnet (Gt_1-Gt_2), omphacite (Om_1-Om_2), quartz, and rutile. Probably phengite was already present. However, if a composition of Ph_1 represents such an early phengite is not clear. (3) The third metamorphic stage (M_3) resulted in the replacement of omphacite by relatively coarse-grained amphibole. Thus, Am_2-Am_3, garnet (Gt_3), phengite (Ph_1), quartz, and rutile probably coexisted. If (clino)zoisite was another coexisting phase at stage M_3 is not clear. (4) The fourth metamorphic stage (M_4) is defined by Om_3 which either formed rims around Om_1-Om_2 instead of amphibole or even replaced former Am_2. Thus, Om_3 coexisted with late amphibole (Am_3), garnet (Gt_4), and phengite (Ph_2) as well as quartz, rutile, and probably (clino)zoisite. (5) The fifth metamorphic stage (M_5) corresponds to the formation of symplectites with amphibole (Am_4) + plagioclase + diopsidic clinopyroxene at the expense of omphacite. Also ilmenite, as one of the replacement products of garnet, belongs to this (incomplete) assemblage.

4.5.2. Granodioritic gneiss

Two larger, moderately corroded garnet grains (diameter: 3.5 and 2.8 mm) in sample 18159 were studied for their compositional zonation in detail. The smaller grain displays a fairly regular zonation whereas the larger grain shows an irregular zonation (Fig. 4.5) suggesting two growth generations. Its core (generation I = GGt_1) is characterized by relatively low pyrope (0.2-0.5 mol %) and spessartine (0.4-3.0 mol %) contents and high grossular contents (60-71 mol %). Representative compositions of the inner and outer core are: $Alm_{26.9}Prp_{0.2}Grs_{70}Sps_{2.9}$ and $Alm_{34.7}Prp_{0.4}Grs_{64.1}Sps_{0.8}$ (Table 4.2, Fig. 4.5a). After a resorption event, suggested by the shape of the core, the garnet mantle of the studied larger grain formed. This mantle (generation II) shows a similar zonation as the entire somewhat smaller grain studied in detail as well as a few significantly smaller garnet grains investigated by X-ray mapping. Representative compositions for the inner and outer mantle (or core and rim of smaller grains) are $Alm_{33.8}Prp_{0.7}Grs_{64}Sps_{1.5}$ (GGt_2) and $Alm_{42.6}Prp_{1.4}Grs_{54}Sps_2$ (GGt_3), respectively.

All white mica is phengite with silicon contents between 3.27 and 3.38 pfu (GPh_1-GPh_3). The phengite inclusions in garnet of generations I and II show Si contents around 3.37

(GPh_1) and 3.34 (GPh_2) pfu, respectively. Phengite in the matrix is also characterized by these Si contents. The Si contents of phengite (GPh_3) replacing garnet are between 3.27 and 3.32. The 2 textural types of biotite (as inclusion in garnet = GBt_1, in the matrix also along the margin of phengite = GBt_2) are characterized by XFe = $Fe^{2+}/(Fe^{2+} + Mg)$ = 0.73-0.81 (GBt_1) and 0.66-0.73 (GBt_2).

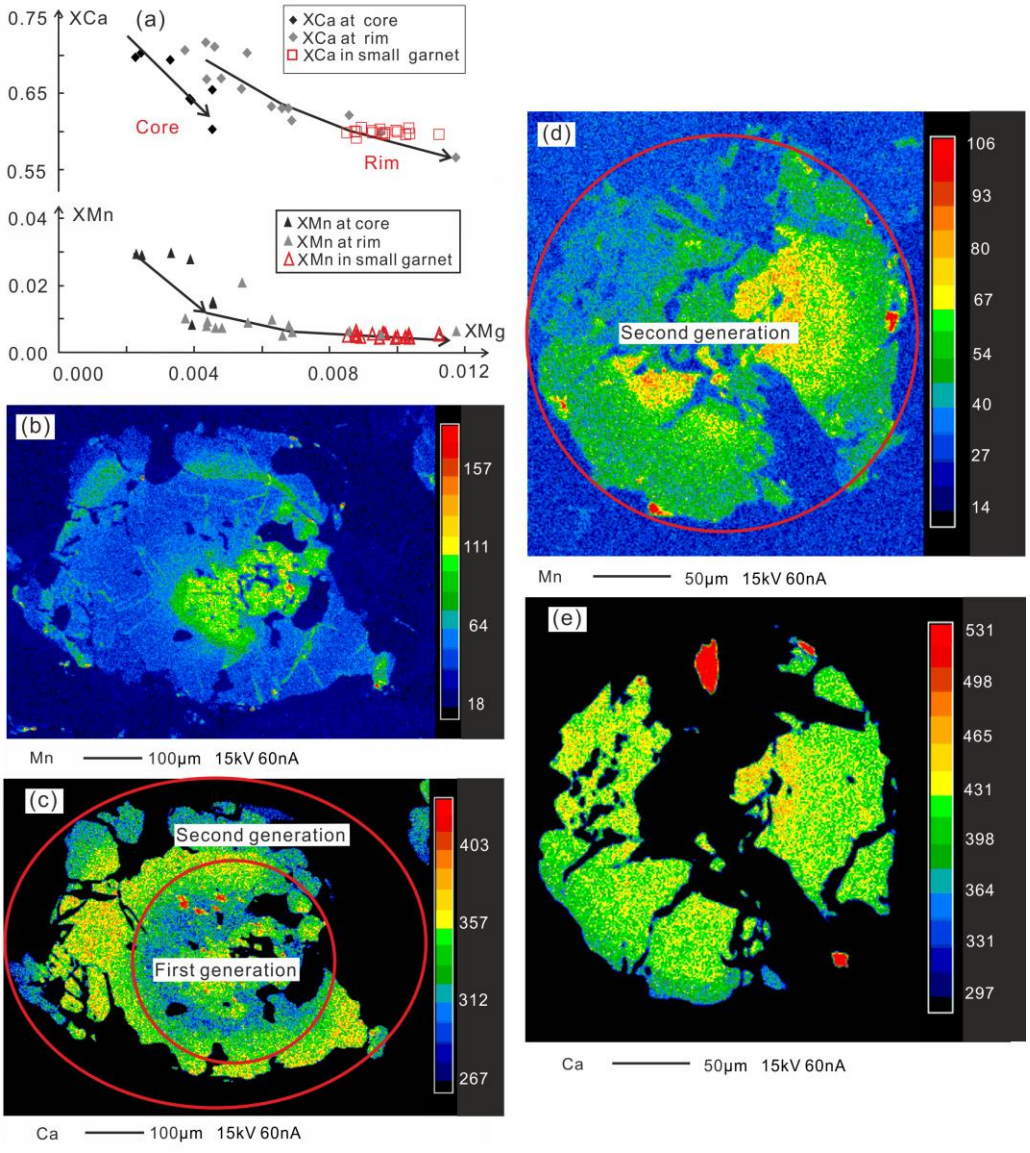

Fig. 4.5. (a) Analyses of garnet in orthogneiss 18159 obtained with an EMP in terms of molar fractions of grossular (+ andradite) as XCa and spessartine (XMn) versus that of pyrope (XMg). The solid lines show the chemical trends from the core to the rim of garnet. (b-e) Mn and Ca concentration maps of garnets in the orthogneiss also obtained with an EMP. For generations see text.

The composition of clinozoisite-epidote (GEp_1) enclosed in garnet is characterized by low Fe^{3+} contents with 5-8 mol % pistacite component. In the matrix, clinozoisite-epidote occurs as optically zoned grains (GEp_2) but its composition is fairly homogeneous (17-20 mol % pistacite component). The coronal clinozoisite-epidote (GEp_3) shows only slightly higher Fe^{3+} contents corresponding to 19-21 mol % pistacite components. Plagioclase of different grain size in the matrix is nearly pure albite (XNa = 0.98-1.0). K-feldspar contains ca. 95 mol % $KAlSi_3O_8$ component.

Petrographic relationships and the above mineral chemistry indicate at least three metamorphic stages for the gneiss: (1) According to inclusions in garnet, the early metamorphic stage (GM_1) is characterized by the assemblage GGt_1 + GPh_1 + GBt_1 + GEp_1+ quartz, albite, K-feldspar. (2) During the second metamorphic stage (GM_2), clinozoisite-epidote and white mica flakes seem to have grown. Thus, the coexisting mineral assemblage of GM_2 was probably GGt_2 + GGt_3 + GPh_2 + GEp_2 + quartz, albite, K-feldspar. (3) Retrograde phases are GPh_3, GBt_2, GEp_3, chlorite, and titanite which have formed during the late metamorphic stage (GM_3).

4.6. Bulk-rock compositions and protolith nature

On the basis of the observed feldspar augen in gneiss, especially large K-feldspar ones in sample Sp35c, the protolith of this rock type should be a granitoid. This was confirmed by the bulk-rock composition of the studied gneiss (Table 4.3). On the basis of a K_2O versus SiO_2 plot (Peccerillo & Taylor, 1976), the granitoid protolith of gneiss 18159 would belong to the calc-alkaline series.

Major element concentrations (Table 4.3) suggest that the protolith of the eclogite was originally a tholeiitic basalt or gabbro applying the classification plot of SiO_2 versus $Na_2O + K_2O$ (Le Bas et al., 1986) and the AFM ternary diagram (Irvine & Baragar, 1971). In the rare-earth element (REE) diagram of Fig. 4.6a, sample 18149 shows a pattern with light REEs enriched $(Ce/Yb)_N = 1.6$) and without Eu anomaly. The REE pattern is similar to a tholeiitic arc basalt or an enriched mid-ocean ridge basalt (MORB), but differs from that of a typical N-MORB. After normalization to primitive mantle (Sun & McDonough, 1989) the data for sample 18149 show negative anomalies of Nb-Ta, Sr, and Ti in the spider diagram of Figure 4.6b. Usually, a Nb-Ta negative anomaly points to island arcs and/or continental settings. In the applied discrimination diagrams (Ti-Zr-Y diagram after

Pearce & Cann, 1973; Th-Ta-Hf diagram after Wood et al., 1979) of Figure 4.6c and d, the composition of eclogite 18149 plots in the fields for island arc tholeiite (IAT) or MORB+IAT. A (normal) MORB can again be excluded. This is also supported by the analyzed TiO_2 content, which is significantly higher than maximal TiO_2 contents of MORBs (1.5 wt%, see Jakes & Gill, 1970; Perfit et al., 1980). In the TiO_2-K_2O-P_2O_5 diagram (Fig. 4.6e, Pearce et al., 1975), the eclogite 18149 shows oceanic affinity. Thus, it is concluded on the basis of the minor and trace element data that the basaltic/gabbroic protolith of the studied eclogite formed in an oceanic island-arc setting.

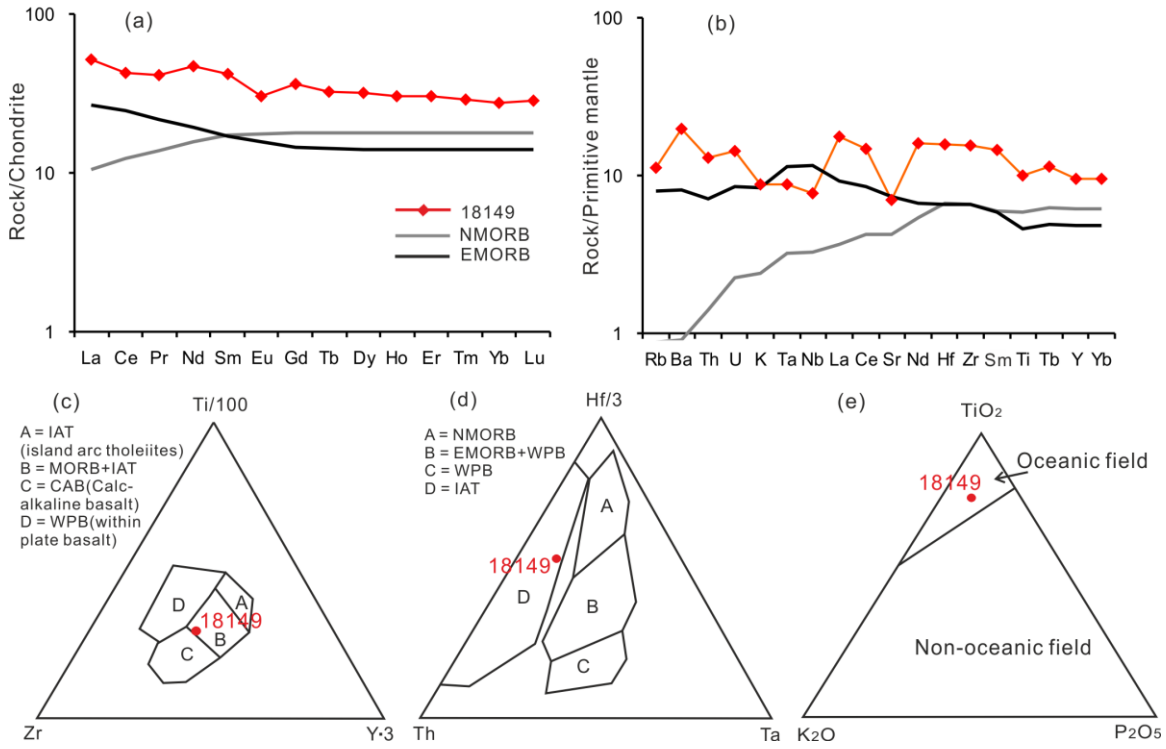

Fig. 4.6. (a-b) Data for the bulk rock composition of eclogite 18149 shown in chondrite-normalized spider diagrams. The element concentrations of chondrite, NMORB, and EMORB are from Sun & Mcdonough (1989). These data are also plotted in (c) a Ti-Zr- ternary diagram (Pearce & Cann, 1973), (d) a Th-Ta-Hf ternary diagram (Wood et al., 1979), and (e) a TiO_2–K_2O–P_2O_5 diagram (Pearce et al., 1975).

4.7. P-T Path

4.7.1. Calculation methods

P-T conditions were estimated using isochemical P-T phase diagrams and conventional geothermobarometry. P-T pseudosections were calculated with the

computer software package PERPLE_X (Connolly, 2005; version from August 2011 downloaded from the internet site http://www.perplex.ethz.ch/) and the thermodynamic dataset of Holland & Powell (1998 and updates) in the system Na_2O-K_2O-CaO-FeO-O_2-MnO-MgO-Al_2O_3-SiO_2-TiO_2-H_2O for the bulk-rock compositions of eclogite 18149 and orthogneiss 18159. The obtained pseudosections were contoured by isopleths of various parameters such as the molar fractions of garnet components. Before the calculations, the bulk-rock compositions were modified a bit (Table 4.3) following, for instance, Massonne (2012): (1) as thermodynamic data for phosphates are lacking in the available PERPLE_X data sets, phosphorus must be ignored. Assuming that all phosphorus is bound to apatite, $Ca_5(PO_4)_3(OH)$, CaO was reduced according to phosphorus contents of the bulk-rock compositions. (2) The H_2O content was set to 7 and 4.5 wt% for the studied eclogite and gneiss, respectively, in order to allow the formation of a free hydrous fluid at relatively low temperatures. (3) A certain amount of oxygen was considered for each bulk rock composition, which was related to a value corresponding to 10 % of the iron being trivalent during metamorphism. However, this oxygen value could be also somewhat lower for the orthogneiss as little amounts of Fe^{3+}-bearing minerals such as clinozoisite-epidote occur in this rock. The same might be true for the eclogite as the calculated amounts of aegirine component in omphacite, and Fe^{3+} contents in amphibole and (clino)zoisite are fairly low.

Two different pseudosections were produced for eclogite 18149. One was calculated for the entire bulk-rock composition, whereas the other one was modelled after subtracting the garnet core to obtain an effective bulk-rock composition for a late metamorphic stage (see, e.g., Marmo et al., 2002). For the purpose of subtraction, an image analysis has been used to calculate the modal abundance of garnet cores at 16 vol.%. Afterwards, the average composition of the garnet core was acquired based on the EMP analyses (Table 4.1). For the pseudosection of gneiss 18159 only the simplified bulk-rock composition was used as only very little amounts of garnet (0.5 vol.%) occur in this rock.

The following solid-solution models (see file solution model of the PERPLE_X software), which are based on works, for instance, by Anderson & Lindsley (1988), Fuhrman & Lindsley (1988), Powell & Holland (1999), and Massonne (2010), were used

for calculating the P-T pseudosection for the eclogite: Chl(HP) for chlorite, Ep(HP) for clinozoisite-epidote, feldspar for plagioclase and K-feldspar, GlTrTsPg as a frequently used model for amphibole, Gt(HP) for garnet, hCrd for cordierite, IlGkPy for ilmenite, MtUl(A) for magnetite, Mica(M) for paragonite, Omph(GHP) for clinopyroxene, Pheng(HP) for phengite, St(HP) for staurolite, Stlp(M) for stilpnomelane, T for talc, and TiBio(HP) for biotite. The components tip, tbi, ann1, qfm, mthm, h2oL, ab, rieb, mrb, cumm, grun, and mic were excluded partly because of their untrustworthiness (see, e.g., Massonne, 2012). For the gneiss, the model Opx(HP) for orthopyroxene was additionally used and Omph(HP) was applied instead of Omph(GHP) for clinopyroxene. The components tip, tbi, ann1, qfm, mthm, h2oL, ab, and mic were excluded.

Conventional Fe^{2+}-Mg exchange geothermometry was also applied. We used relatively recent calibrations of Nakamura (2009) and Green & Hellman (1982) for the garnet-clinopyroxene and the garnet phengite pair, respectively. For the garnet-biotite pair the calibration of Kleemann & Reinhardt (1994) was applied because it is acknowledged to show small errors in reproducing experimental temperatures and good accuracy (see, e.g., Wu & Zhao, 2006; Wu & Chen, 2006).

4.7.2. Results for the eclogite

The pseudosections for the modified eclogite compositions of Table 4.3 were calculated for the P-T range of 5-25 kbar and 300-800 °C (Fig. 4.7) and contoured by isopleths for the molar fractions of garnet components (XCa, XMg, and XMn: Fig. 4.8a), Si contents of phengite (Fig. 4.8b), the garnet modal contents (Fig. 4.8c), and the Na contents in clinopyroxene (Fig. 4.8d). Relevant boundaries of specific phases are shown in Fig. 4.8e. The intersections of specific isopleths of garnet components and the final P-T path are given in Fig. 4. 8f.

The observed mineral assemblage garnet + omphacite + phengite + quartz + rutile is stable over a wide P-T range (approximately 14-25 kbar, 500-800 °C) according to the calculated pseudosection (Fig. 4.7). The contouring with the isopleths for garnet components for the P-T fields of the assemblage garnet + omphacite demonstrates that the XCa parameter is broadly pressure sensitive at T < 520 °C. At T > 600 °C, this parameter is sensitive to temperature. Compared to XCa and XMn, XMg is a good indicator for temperature at HP conditions (Fig. 4.8a) as both XMg and temperature

increase simultaneously. The Mg concentration map for garnet (Fig. 4.3c) shows that the Mg contents are relative homogeneous in the core to the inner rim. This indicates that the early garnet grew within a narrow temperature range. From the inner rim to the outer rim a significant increase of XMg from 0.14 to 0.25 was observed implying that the outer rim formed at a higher temperature than the one at which the inner garnet part grew.

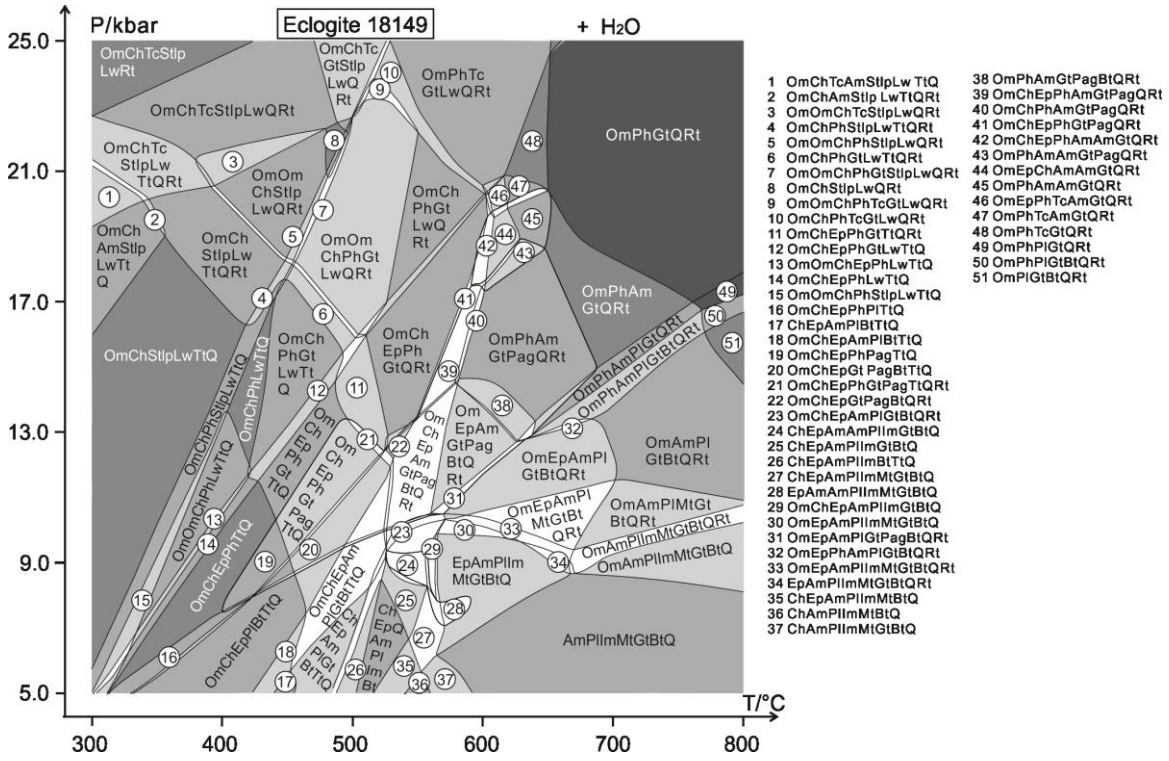

Fig. 4.7. P-T pseudosection calculated for the modified composition of eclogite 18149 (Eg modified 1 in Table 4.3) with the computer software package PERPLE_X. Abbreviations: Ch: chlorite, Lw: lawsonite, Pag: paragonite, Ph: Phengite, Pl: plagioclase, Sill: sillimanite, Stlp: stilpnomelane, Tc: talc, Tt: titanite, Mt: magnetite, and as in the legend of Figure 4.2. Note that the phase relations at high temperatures can be metastable with respect to silicate melt.

The intersections of isopleths of the garnet components grossular (+andradite), pyrope, and spessartine for a composition of an inner garnet core (see above: $Alm_{59}Prp_{13}Grs_{24}Sps_4$), including errors in the P-T position of these isopleths, point to a P-T range of 22-23.5 kbar and 530-590 °C (Fig. 4.8f) for early garnet formation. Correspondingly, the outer core composition of garnet (see above: $Alm_{57}Prp_{13}Grs_{27}Sps_3$) yielded a similar P-T range of 20-22 kbar and 540-600 °C.

When using the contouring for the pseudosection after subtracting the garnet core from the bulk-rock, which is very similar to the one without subtraction, solely the XMg and XCa isopleths were considered for this rim P-T estimate (in this effective bulk-rock composition only 0.05 wt% MnO is left). The inner rim composition (see above: $Alm_{56.6}Prp_{12.5}Grs_{30.2}Sps_{0.7}$), combined with the lowest Si content in phengite (3.27 pfu), signalizes a significant pressure release to 12-14 kbar at a temperature between 610 and 670 °C. Concerning the outer rim composition of garnet, we disclaimed a P-T estimate because the corresponding garnet domain only forms a very thin and incomplete envelope around garnet which could be due to a local chemical equilibrium.

The highest Si content in phengite (3.45 pfu) points to pressures around 21.5 kbar at a temperature of 595 °C, which is in the aforementioned temperature range (Fig. 4.8f) for an early metamorphic stage. Such high pressures are also required for the observed assemblage with talc (Fig. 4.8e). The isopleth for the lowest Si content in phengite (3.27 pfu) appears near the intersection of garnet isopleths for the inner rim composition (see above and Fig. 4.8b, f).

According to the determined and calculated Na contents in clinopyroxene (Fig. 4.8d), the omphacite with the highest Na content (Om_2 with XNa = 0.43-0.48 pfu, see above) formed at the early eclogite stage at 22-23.5 kbar and 530-590 °C (garnet inner core). The early omphacite Om_1 with a lower Na content (XNa = 0.35-0.42 pfu) could have formed before the garnet core during more or less isothermal burial. A burial, for instance, along a low geotherm should have resulted in the early formation of omphacite with a higher XNa than 0.5. The late omphacite, which also shows relatively low Na contents (Om_3: XNa = 0.38-0.40 pfu), grew together with the garnet rim as the isopleths for this Na content of clinopyroxene are compatible with the P-T conditions derived for the garnet rim (12-14 kbar, and 610-670 °C).

Based on compositions of garnet, clinopyroxene, and phengite, which could be in equilibrium according to the P-T positions of corresponding isopleths used above, conventional geothermometers confirm the above derived metamorphic temperatures. Applying the garnet-clinopyroxene geothermometer by Nakamura (2009), temperatures of 543 ± 25 °C at P = 22.7 ± 0.7 kbar (Fig. 4.8d) were obtained for the compositions of the garnet inner core and the clinopyroxene with the highest Na content. For the outer

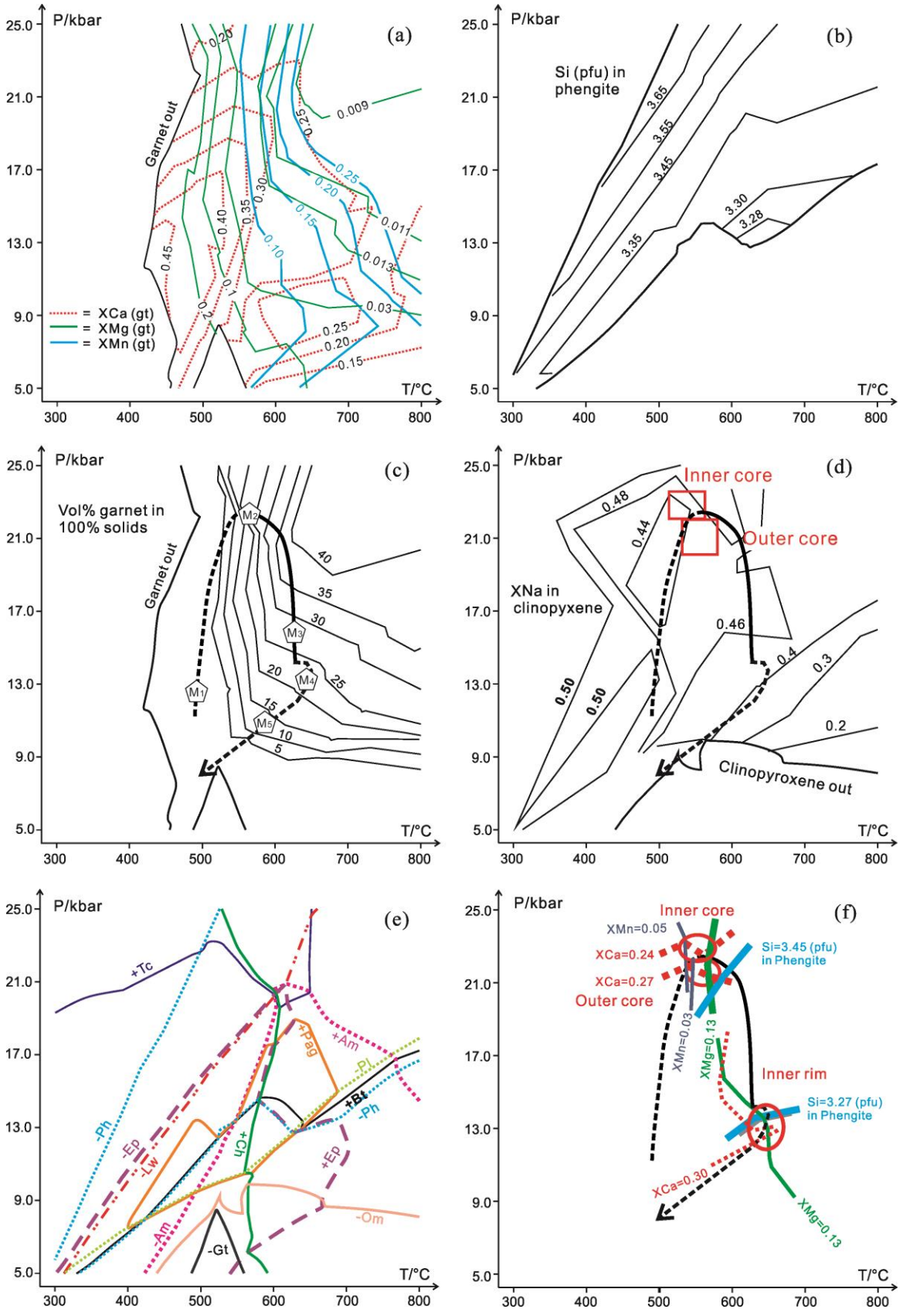
(a)
P/kbar
T/°C
Garnet out
= XCa (gt)
= XMg (gt)
= XMn (gt)
(b)
Si (pfu) in phengite
3.65
3.55
3.45
3.35
3.30
3.28
(c)
Vol% garnet in 100% solids
M1
M2
M3
M4
M5
(d)
Inner core
Outer core
XNa in clinopyxene
Clinopyroxene out
(e)
+Tc
-Ph
-Ep
-Lw
-Am
-Gt
+Pag
+Am
-Pl
+Bt
+Ch
+Ep
-Om
(f)
Inner core
XMn=0.05
XCa=0.24
XCa=0.27
Outer core
Si=3.45 (pfu) in Phengite
XMn=0.03
XMg=0.13
Inner rim
Si=3.27 (pfu) in Phengite
XCa=0.30
XMg=0.13

Fig. 4.8. Contoured P-T pseudosection of Figure 4.7 by various parameters: (a) molar fractions of garnet components, (b) Si contents (pfu) in phengite, (c) modal content of garnet in vol.% and the derived P-T path (broken lines: uncertain, solid line: constrained; also shown in d and f) with metamorphic stages M_1 to M_5, (d) Na content (pfu) in clinopyroxene and P-T conditions (red boxes) calculated by garnet-clinopyroxene and garnet-phengite geothermometry for the garnet inner and outer core, respectively, (e) boundaries of the P-T fields of relevant phases are shown by lines of different signature, (f) intersections of isopleths of garnet components and Si contents in phengite.

core of garnet and phengite with the highest Si content, temperatures of 561 ± 25 °C resulted from the garnet-phengite thermometer by Green & Hellman (1982) for a pressure of 21 ± 1 kbar (Fig. 4.8d).

According to the above results, the well constrained P-T path for the eclogite starts around 22.5 kbar and 540 °C (Fig. 4.8f), then shows a moderate T increase to 575 °C and more at slightly reduced pressures (21 kbar), and ends at P-T conditions around 13.5 kbar and 625 °C. This path is compatible with the growth of garnet from core to rim. At the peak pressure, a considerable amount of garnet (core) had formed (16 vol.%, see above). During the initial decompression, the rim of garnet grew by heating to temperatures above 600 °C, so that a total garnet volume of (almost) 40% was reached. For the metamorphic stage M_4 at which the outermost rim grew (12-15 kbar), the calculated garnet volume is between 20 and 25 vol.%, which is much lower than the observed content. This is explained by incomplete corrosion of the garnet before reaching pressures of ~13 kbar.

4.7.3. Results for the granodioritic gneiss

The pseudosection for the gneiss composition of Table 4.3 was calculated for the P-T range of 5-25 kbar and 300-800 °C (Fig. 4.9) and contoured by isopleths for the molar fractions of garnet components (XCa and XMg in Fig. 4.10a), Si contents of phengite (Fig. 4.10b), and garnet modal content (Fig. 4.10c). The intersections of isopleths of garnet components are shown in Fig. 4.10d. Relevant boundaries of specific phases are displayed in Fig. 4.10e. P-T conditions calculated by conventional garnet-biotite geothermometry are presented in Fig. 4.10f.

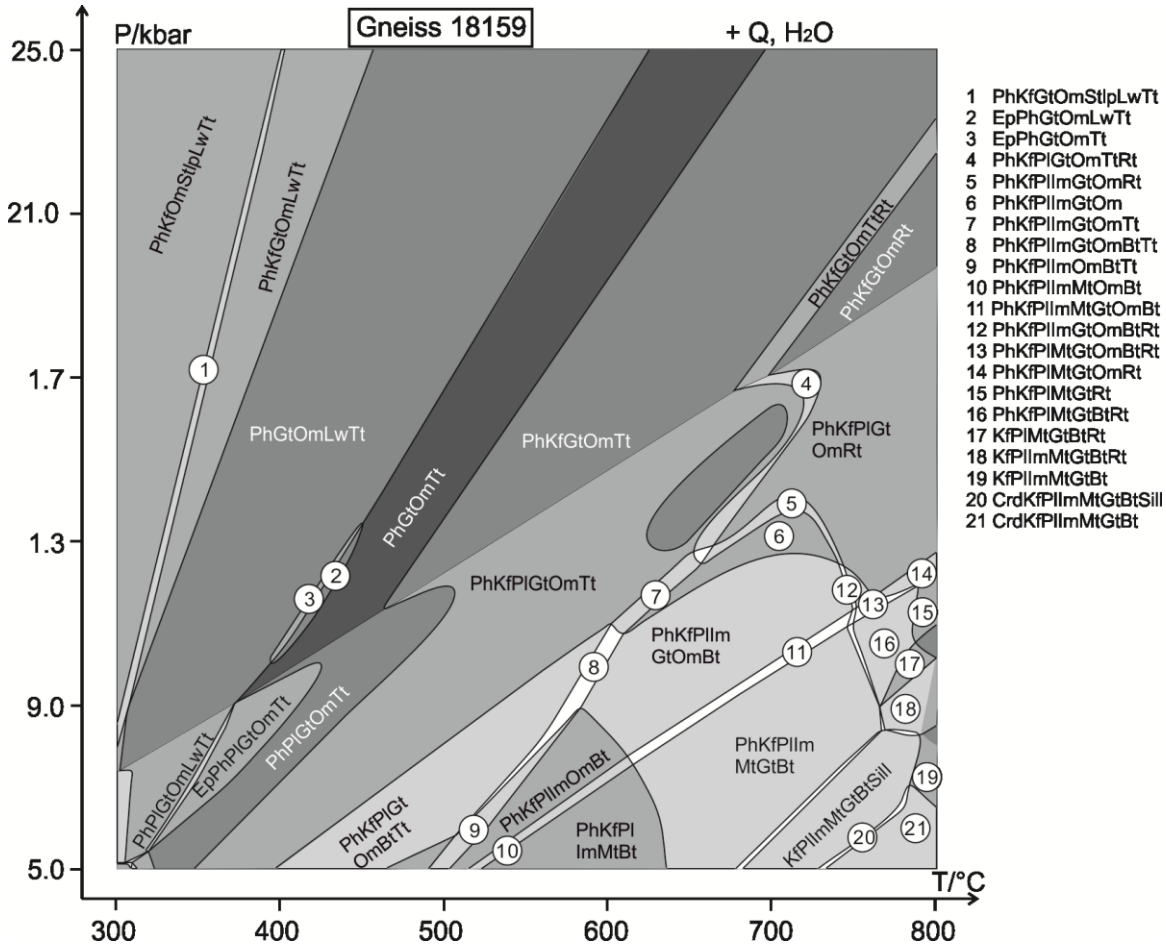

Fig. 4.9. P-T pseudosection calculated for the modified composition of orthogneiss 18159 (Table 4.3) with the computer software package PERPLE_X. Abbreviations are the same as in Figures 4.2 and 4.7. Note that the phase relations at high temperatures can be metastable with respect to granitic melt.

The observed mineral assemblage garnet + phengite + K-feldspar + plagioclase + quartz is stable over a wide P-T range (ca. 5-17 kbar, 450-800 °C) according to the calculated pseudosection (Fig. 4.9). With decreasing P and increasing T, XCa and XMg of garnet decrease and increase, respectively, in the temperature range 400-700 °C. We used these isopleths for the garnet core and its inner and outer rim compositions (Fig. 4.5a) to deduce the P-T evolution of the orthogneiss. However, the XCa and XMg isopleths (Fig. 4.10a) show a similar dP/dT slope, so that the P-T conditions could not be as precisely derived as for the eclogite. As we observed an XCa decrease and XMg increase from core to rim, the garnet must have grown at increasing temperature. The corresponding isopleths for the inner core ($Alm_{26.9}Prp_{0.2}Grs_{70}Sps_{2}$), inner rim ($Alm_{33.8}Prp_{0.7}Grs_{64}Sps_{1.5}$),

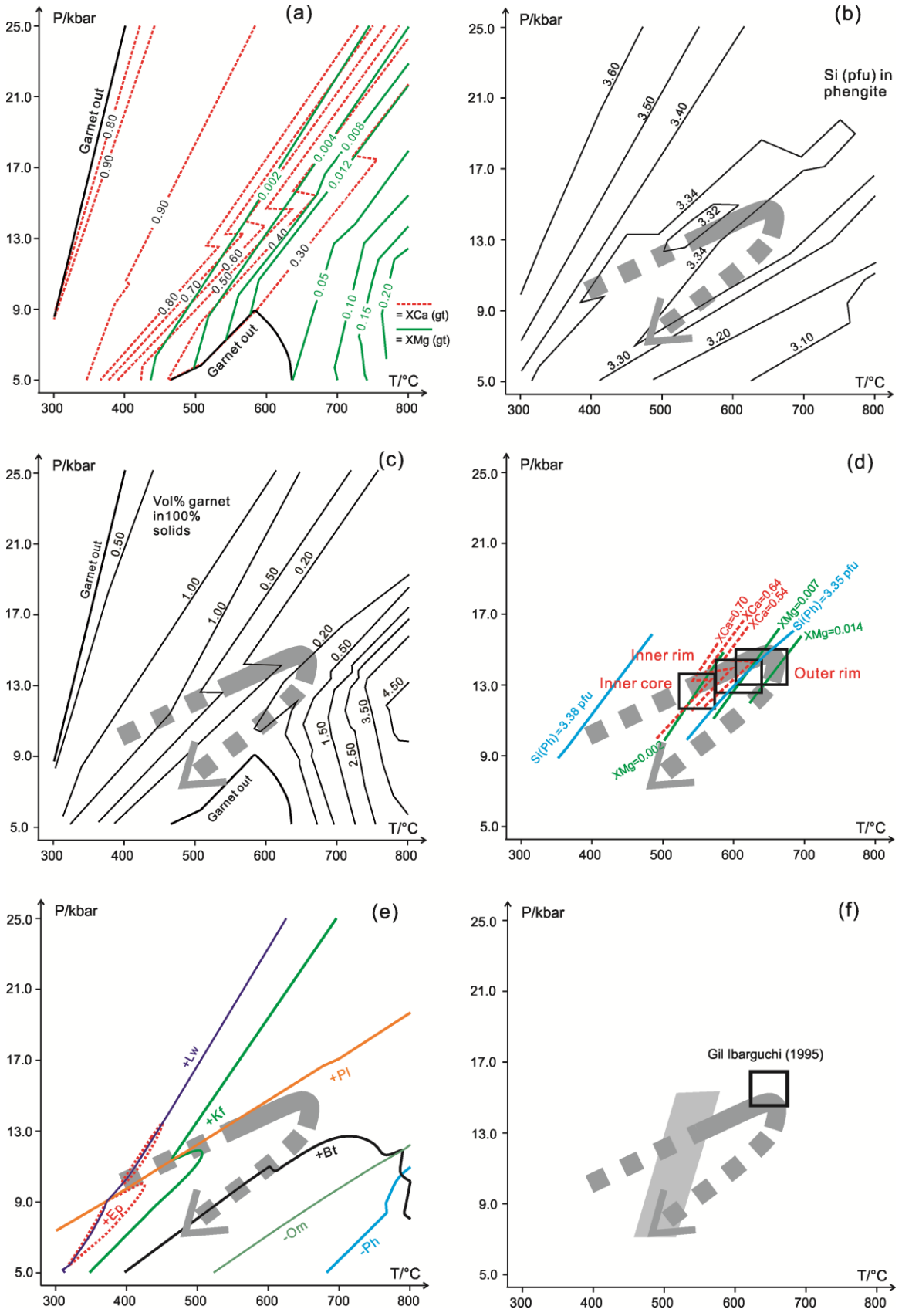
(a)
P/kbar
T/°C
Garnet out
= XCa (gt)
= XMg (gt)
(b)
Si (pfu) in phengite
(c)
Vol% garnet in100% solids
(d)
Inner rim
Inner core
Outer rim
Si(Ph)=3.38 pfu
Si(Ph)=3.35 pfu
XMg=0.002
XMg=0.007
XMg=0.014
XCa=0.70
XCa=0.64
XCa=0.54
(e)
+Lw
+Pl
+Kf
+Bt
+Ep
-Om
-Ph
(f)
Gil Ibarguchi (1995)

Fig. 4.10. Contoured P-T pseudosection of Figure 4.9 by various parameters: (a) molar fractions of garnet components. (b) Si contents (pfu) in phengite. (c) Modal content of garnet in vol.% as well as the derived P-T path (broken lines: uncertain, solid line: constrained), which is also shown in c)-f). (d) Intersections of isopleths of garnet components. (e) Boundaries of the P-T fields of relevant phases are shown by lines of different signature. (f) Temperatures calculated with garnet-biotite geothermometry for garnet core and enclosed biotite compositions (grey quadrangle). P-T conditions given by Gil Ibarguchi (1995) for the peak metamorphic conditions of an orthogneiss from the MTZ (black box).

and outer rim ($Alm_{42.6}Prp_{1.4}Grs_{54}Sps_{2}$) of the larger garnet intersect under consideration of P-T errors at 11.5-13.7 kbar and 520-570 °C, 12.5-14.5 kbar and 570-640 °C, and 13-15 kbar and 600-670 °C, respectively. Other P-T conditions for such intersections can be ruled out because of the compositions of coexisting plagioclase and phengite (see below). The outer core domain, which is characterized by a low Ca content and grew after the resorption inner core (Fig. 4.5b, c), was not used, because a true equilibrium composition of this domain was possibly not reached.

Connecting the above isopleth intersections related to the order of early (core) to late (rim) garnet, a prograde P-T path for the gneiss was defined (Fig. 4.10d). The retrograde P-T path could not be well constrained, but it must have crossed the limits for the biotite and clinozoisite-epidote fields (Fig. 4.10e). In this respect, it is worthy of note that increasing Fe^{3+} contents of the bulk-rock would increase the field for clinozoisite-epidote as we have checked it by tentative PERPLE_X calculations (see also Massonne, 2015).

Phengite with the highest Si contents (up to 3.38 pfu, see GPh_1 above) must have formed at a very early stage of the prograde evolution, because the corresponding isopleth passes through P-T conditions of the invoked P-T path before the garnet inner core formed. This is compatible with our observation that the phengite with the highest Si content is enclosed in this garnet domain (section 4.5.2.). However, phengite with Si contents between 3.32 and 3.35 pfu (GPh_2) is compatible (Fig. 4.10b) with the derived P-T conditions using intersections of garnet isopleths. Phengite with the lowest Si contents (down to 3.27 pfu) should have formed during the retrograde evolution of the gneiss.

Although the biotite field is outside the P-T range where garnet isopleths intersect (Fig. 4.10e), we chose the compositions of the garnet core (GGt_1) and biotite (GBt_1) included in garnet to calculate a temperature with the garnet-biotite geothermometer (Kleemann & Reinhardt, 1994). At the above noted pressure of 12 ± 1 kbar, we obtained temperatures around 532 ± 30 °C (Fig. 4.10f), which would be in agreement with the above results. Usig he compositions of the matrix biotite (GBt_2) and the garnet outer rim (GGt_3), yielded ca. 400 °C, which might be meaningless.

4.8. Discussion

4.8.1. Protoliths and their geodynamic environments

On the basis of various discrimination diagrams and the determined contents of minor and trace elements, the protolith of the eclogite was found to be a tholeiitic basalt or gabbro that had formed in an oceanic island-arc setting (section 4.6.). However, a different conclusion was drawn by Abati et al. (2010) based on U-Pb zircon dating. In fact, these authors admitted that an age difference of 20 Ma might exist between the formation of a calc-alkaline magmatic suite and an alkaline to peralkaline plutonic suite of the same tectonic unit, but because of similar ages of gneiss and eclogite the protolith of the two eclogites studied by Abati et al. (2010) were also assigned to the calc-alkaline suite. Our study disproves this idea because neither gneiss and eclogite studied here show the same early metamorphic evolution nor the trace element signature of our eclogite points to a calc-alkaline suite.

According to the existing tectonic models for acidic and basic magmatism at the margin of the here relevant continental plate (Gondwana: Abati et al., 2010; Andonaegui et al., 2015; Díez Fernández et al., 2012b; Fuenlabrada et al., 2012) the protoliths of both eclogite and orthogneiss should have formed in the tectonic setting of a magmatic arc. This arc started to be separated from Gondwana by the formation of a continental back-arc basin when the Iapetus Ocean was still subducted below Gondwana 490-500 Ma ago. As an alternative to this view and in order to account for our observed trace element signature, we suggest that the invoked oceanic island-arc setting, of which only the protolith of the eclogite was part of (see section 4.6), occurred within the Rheic Ocean when intraoceanic subduction happened 385 Ma (Martínez Catalán et al., 2009) or 450-420 Ma (Matte, 1998) ago.

4.8.2. Petrogenesis of the eclogite

Peak pressure conditions around 22.5 kbar at 540 °C were derived for the eclogite (M_2 stage). These conditions are compatible with the observed mineral paragenesis and the composition of (specific domains of) these minerals: early garnet (Gt_1-Gt_2), omphacite (Om_1-Om_2), quartz, rutile, talc, and phengite (highest Si content of Ph_1). However, lawsonite, which should be a member of the M_2 mineral assemblage according to the PERPLE_X calculations (Fig. 4.7), is lacking. The lack of lawsonite in eclogite is typical for the entire Iberian massif (Tsujimori et al., 2006) and is here explained by the easy breakdown of this hydrous phase at rising temperature towards stage M_3. Peak pressure conditions of 21 kbar at 580 °C (Rodríguez et al., 2003) and 26 kbar at 650 °C (López-Carmona et al., 2014b) were reported for other eclogites of the MTZ. Especially the latter P-T estimate differs from our finding, but it is possible that different eclogite bodies have experienced somewhat different P-T conditions.

A metamorphic stage M_1, before stage M_2, is still recognizable by inclusion minerals in the garnet core. These minerals are biotite, hornblende (Am_1), and (clino)zoisite, which are typical for the amphibolite facies. Although we could not determine precise P-T conditions for M_1, we assume temperatures close to 500 °C and pressures below 11 kbar (see the boundaries of phases in Fig. 4.8e) for this metamorphic stage. Thus, a more or less isothermal burial path towards M_2 is likely. Along such a path, considerable amounts of omphacite (core Om_1 with XNa = 0.35-0.42 pfu) could have formed above pressures of 11 kbar by breakdown of the aforementioned inclusion minerals. The (inner) rim (XNa content = 0.43-0.48 pfu, Om_2) of zoned omphacite (Fig. 4.4e) followed at or near peak pressure conditions. Before reaching these conditions ($P \geq 20$ kbar) only little garnet should have been present (Fig. 4.8c) and, thus, most of the garnet grew (mainly at the expense of chlorite) close to the pressure peak and also during early exhumation. Consequently, the P-T path could be well constrained for these conditions.

During metamorphism from stage M_2 to stage M_3 (Fig. 4.7 and Fig. 4.8e) the content of clinopyroxene decreased and a barroisitic amphibole (Am_2-Am_3) formed instead. The H_2O, necessary for such a reaction, was possibly provided by the breakdown of lawsonite (see above), but (additional) water could have been allocated by the corresponding subduction environment (see below and, e.g., Massonne, 2012). At stage M_3, the minerals

Am_3, Gt_4, quartz, rutile, phengite (Ph_2 with the lowest Si content pfu analyzed), and probably paragonite were in equilibrium at the determined P-T conditions of 16 kbar and 620 °C (Fig. 4.8f). At stage M_4 cracks in the garnet seem to have been infiltrated by a hydrous fluid which caused an enrichment of Mg along such cracks also in inner domains of the garnet (see Fig. 4.3c). The thus modified garnet compositions are very similar to those of the outer rim of garnet (Gt_4). The temperature during this event could have been as high as 670 °C and, thus, would represent the thermal peak of eclogite metamorphism. The corresponding pressure might have been as low as 13 kbar in analogy to the corresponding P-T estimate for the surrounding gneiss (see below). The here derived peak temperature is, in fact, compatible with that given by López-Carmona et al. (2014b). But these authors assigned it to the peak pressure, whereas we found clear hints at a late stage temperature peak. Thus, López-Carmona et al. (2014b) suggested, in fact, a clockwise P-T loop as given in Fig. 4.7, but these authors assumed an isothermal decompression in contrast to our findings.

A retrograde evolution (M_5) is hardly discernable in the studied eclogite. Only little omphacite was replaced by a symplectite composed of plagioclase + amphibole (Am_4) + diopsidic clinopyroxene. If little paragonite would have formed during stage M_4, then it was completely decomposed at M_5. The minor retrogression indicates that an influx of hydrous fluid, if it happened at all at $P < 13$ kbar, must have ceased still at relatively high temperatures.

4.8.3. Petrogenesis of the gneiss

As there was no considerable change of the mineral assemblage during the whole metamorphism, the growth history of garnet and phengite was the basis for the deduction of a P-T path (Fig. 10c). As noted by Massonne (2015b), only rough P-T paths can be derived for HP metagranites since, for instance, Si contents in phengite can become geobarometrically insensitive at high pressures. The studied gneiss, however, tends to be rather a granodiorite, so that ca. 1 vol.% of garnet formed early. This amount of garnet represents the (original) inner core. After two corrosion events (see the irregularly shaped boundaries in the element maps of Fig. 4.5b, c) each followed by a newly grown garnet generation, the garnet volume was reduced to quantities below 1 vol.%. Nevertheless, a rough P-T path could be derived using the compositions of the remaining garnet

generations. The determined metamorphic peak (garnet rim) of 13-15 kbar and 600-670 °C is consistent with a previous estimate by Gil Ibarguchi (1995: 655 ± 30 °C, 15.5 ± 1 kbar, see also Fig. 4.10f) for a gneiss from the MTZ. This author applied the GRIPS barometer and garnet-biotite exchange thermometry. In addition, Rodríguez et al. (2003) used petrographic observations to constrain the mylonitization in felsic gneisses of the MTZ to 500-600 °C at maximum pressures of ca. 15 kbar due to the absence of omphacite in these rocks. Even if such a clinopyroxene would be pure jadeite, a (minimum) pressure of ca. 16 kbar at 600 °C or 18 kbar close to 700 °C is required for its formation. The corresponding reaction curve (jadeite + quartz = albite) is well defined by high-pressure experiments and, for this reason, was even used as experimental calibration curve (Johannes, 1978). Thus, a second line of evidence exists for peak pressures of the garnet-bearing gneiss being not as high as that of the studied eclogite. The possibility that jadeite-rich clinopyroxene had formed, but was completely decomposed during retrogression is unlikely. In the Sesia zone of the central Alps, omphacite and jadeite are still abundant in HP metagranodiorite and metagranite, respectively, despite subsequent retrogression events (Compagnoni & Maffeo, 1973; Koons, 1986).

According to our petrographic observations, clinozoisite-epidote (GEp_1 and GEp_2) was present in the studied gneiss during the whole metamorphism, but it occurs only in a small P-T area in the pseudosection of Figure 4.9. Thus, we checked if the selected Fe^{3+} content for the calculation of this P-T pseudosection was possibly too low. In P-T pseudosections, calculated for 20, 30 and 40 % of total Fe being Fe^{3+}, the clinozoisite-epidote field did, however, extend only little. Thus, we conclude that eventually minor contents of REE stabilize this phase or that the thermodynamic data for clinozoisite-epidote have to be revised.

4.8.4. Geodynamic model for the metamorphism of the studied rocks

As outlined in the section 4.2, a number of age data (Ar-Ar in phengite, U-Pb in zircon, Rb-Sr in biotite and plagioclase) were published for the MTZ and neighboring Variscan complexes so that we can rely in early Variscan events effecting metamorphism in the NW part of the Iberian Peninsula. These events have climaxed in a HP metamorphism in the time interval between 370 and 365 Ma (e.g., Rodríguez et al., 2003; López-Carmona et al., 2014a). There are also younger ages of (1) 350 ± 2 Ma, obtained

from zircon in eclogite of the Agualada Unit located close to the MTZ (Abati et al., 2010), (2) 353 ± 2 Ma based on $^{40}Ar/^{39}Ar$ dating of phengite from a HP gneiss of the MTZ (Rodríguez et al., 2003), and (3) 352 ± 3 Ma (Rb-Sr in biotite and plagioclase: Santos Zalduegui et al., 1995) for a metagranodiorite of the MTZ. These late metamorphic ages could possibly correspond to our late eclogitic stage M_4. Thus, we suggest that the studied eclogite and gneiss met at Earth's depths of ca. 45-50 km (~13 kbar), according to the derived P-T paths (Fig. 4.11), about 350-355 Ma ago.

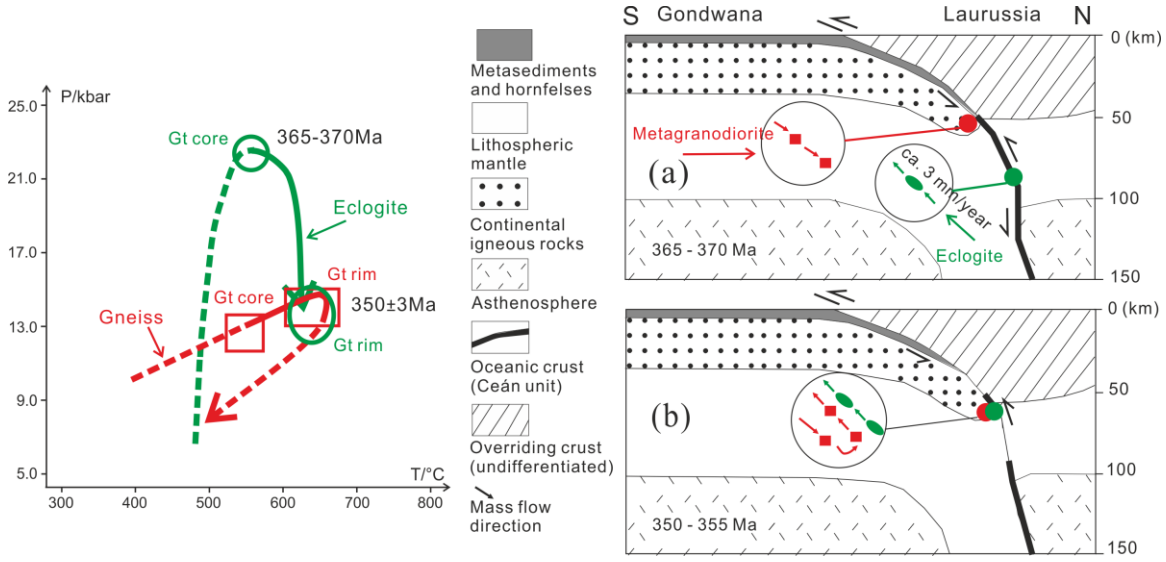

Fig. 4.11. Left hand side: P-T-t paths of eclogite and gneiss as shown in Figures 4.8f and 4.10d. Right hand side: sketch for the tectonic evolution of eclogite and granodioritic gneiss (strongly modified after Rodríguez et al., 2003) of the MTZ. (a) During subduction of the Rheic Ocean below Gondwana, eclogitic slices were involved in the upwards directed flow of a subduction channel at depths of ca. 80 km. The gneiss reached maximal depths of ca. 50 km. (b) Both rock types met at around 45-50 km and were exhumed together.

Two types of tectonic models exist for the closure of the Rheic Ocean in the range of the Iberian Peninsula. The first type of these models suggests that this ocean completely developed at the Laurussia margin based on the appearance of diverse ophiolite sequences in northern Spain (Martínez Catalán et al., 1996, 2007, 2009; Arenas et al., 2009; Díez Fernández et al., 2011, 2012a, 2012b; Díez Fernández & Martínez Catalán, 2012). Another type of these models proposed that the Rheic Ocean was subducted below Laurussia followed by continental (Gondwana) subduction (Rodríguez et al., 2003;

Ballèvre et al., 2012; Rubio Pascual et al., 2013). However, for the relatively well constrained time frame (380-350 Ma) all published tectonic models for the Variscan orogeny of the NW Iberian Peninsula cannot fully explain our new findings. In order to consider the two different types of HP metamorphism (peak P: 22.5 kbar for the eclogite, 13 kbar for the gneiss) and a late common evolution of the studied rocks, we propose the geodynamic model of Figure 4.11, which is based on the one by Rodríguez et al. (2003) with respect to the subduction direction. However, the opposite subduction direction seems to us to be possible as well, but has no influence on the following principal findings. For our model we assume, as in aforementioned geodynamic models, that the oceanic crust of the Rheic Ocean was already completely subducted during early Variscan times. However, it is already questionable if the studied eclogite represents this oceanic crust (see section 4.6 and section 4.8.1.). Alternatively, it is more likely that an island arc, of which the protolith of the studied eclogite was part of, was first accreted to the continental plate (Laurussia or possibly Gondwana?) and then transported after subduction erosion with the downgoing slab to great Earth's depth. This view is evidenced by an early more or less isothermal P-T path from metamorphic stage M_1 to stage M_2 for the eclogite. Our observations (inclusions in garnet, compositional zonation of garnet and omphacite) exclude an early path along a low geotherm as typical, for instance, for subducted oceanic crust. At Earth's depths around 80 km (~22.5 kbar) eclogite slices were involved in the upwards directed mass-flow of a subduction channel (see, e.g., Massonne, 2012). Typically, such eclogite slices are heated at these depths as they approach the wall to the overlying mantle wedge (e.g., Massonne & Kopp, 2005). This is compatible with the P-T path of the eclogite. Furthermore, a period of time of around 15 million years as suggested by published age data (peak P at 370-365 Ma, late eclogite stage at 352-353 Ma) is more than sufficient to transport the invoked eclogite slice with the upwards directed mass-flow to depths corresponding to 45-50 km (see, e.g., Massonne, 2012).

The studied gneiss could have been part of the continental margin of the plate (Gondwana) approaching Laurussia (or vice versa?). At least, we do not see any contradiction to the position of a Cambro-Ordovician magmatic arc, of which the studied orthogneiss could have been part of (see section 4.6), at this continental margin. This

margin was subducted to depths of 45-50 km during the continent-continent collisional process. Such burial depths reached during such a process seem to be quite common and can be related to a continent-microcontinent collision (see, e.g., Massonne & Calderón, 2008; Massonne & Toulkeridis, 2012) as well as a collision of larger continental plates (e.g. Liu et al., 2007; Massonne, 2014, 2015a; Iaccarino et al., 2015). At depths of 45-50 km both studied rock types came together and were from then on in contact with each other during the entire subsequent exhumation (Fig. 4.11).

4.9. Conclusions

The detailed study resulted in a relatively precise P-T path for the eclogite and a less precise path for the adjacent gneiss. These paths demonstrate that both rocks, although now in direct contact to each other, had experienced a different early P-T evolution. Thus, the frequently uttered opinion that such a contact proves a common P-T history of eclogite and gneiss was disproved. A similar finding was presented, for instance, by Willner et al. (2000), Braga et al. (2007), and Štípská et al. (2012). Only the exhumation history of the studied rocks from depths of 45-50 km was a common one. The structural inventory of the two adjacent rock types (eclogite and gneiss) does not confirm the tectonic emplacement of an eclogite body in the country rock (at ca. 13 kbar) because a late structural overprint, as reported by Díez Fernández and Martínez Catalán (2012), destroyed all earlier structures. Thus, the early evolution of both studied rocks (burial, prograde metamorphism, early exhumation) is only preserved in minerals such as garnet but not in macroscopically discernable tectonic structures.

Furthermore, our new results contribute significantly to a better understanding of the collisional situation in early Variscan times for the northwestern portion of the Iberian Peninsula. Since the existing various geodynamic models for this region are not fully compatible with our new findings, we presented a revised one, which also agrees with previously reported geochronological and geochemical data. For the future, the reconstruction of further detailed P-T paths for rocks of the MTZ is essential to further improve the collisional model for the Variscan orogeny in southwestern Europe.

5. Clockwise and anticlockwise P-T paths of eclogite-facies rocks from the 'La Pioza' land site of the Malpica-Tuy shear zone, NW Spain

by

Botao Li, Hans-Joachim Massonne*, Joachim Opitz

Institut für Mineralogie und Kristallchemie, Universität Stuttgart, Azenbergstr. 18, D-70174 Stuttgart, Germany

*corresponding author: H.-J. Massonne, Tel.: +49-711-68581225,

Fax: +49-711-68581222, * e-mail: h-j.massonne@mineralogie.uni-stuttgart.de

In preparation for submission

Highlights:

Anticlockwise and clockwise P-T paths of eclogites were recognized in Variscan NW Spain

Protoliths of eclogites from a km2-sized area are from various geotectonic settings

Contrasting P-T paths were caused by processes in a subduction channel

Abstract: The Malpica-Tuy shear zone (MTZ) in northwestern Spain is a key area for the understanding of geodynamic processes during the early collision of Gondwana and Laurussia. To better understand this collisional situation in Variscan times, we deciphered mass-flow paths in terms of pressure (P) and temperature (T) for 5 samples (three eclogites, a garnet-bearing glaucophanite and a tonalitic gneiss) occuring at the 'La Pioza' land site in the central MTZ. In addition, the protoliths of these rocks were elucidated. Three contrasting P-T paths resulted from the application of P-T pseudosections, calculated with PERPLE_X, and Zr-in-rutile geothermometry: (1) Two eclogites and the gneiss yielded a similar anticlockwise P-T path. Especially one of these eclogites recorded an extended path from 565-590 ºC and 5-8.5 kbar to peak temperatures of 650 ºC at 17-20 kbar and further to peak pressures of 23-26 kbar at 610-645 ºC. (2) A clockwise P-T loop was derived for an eclogite starting at 565-590 ºC and 16-19 kbar and ending at 595-640 ºC and 22-25 kbar. (3) The clockwise P-T path of the glaucophanite showed a temperature increase from 590-610 ºC to 665 ºC in the pressure range 18-22

kbar. Major and trace element geochemical features demonstrate that one eclogite and the glaucophanite were calc-alkaline igneous rocks. Two eclogites showed a tholeiitic nature. The tonalitic gneiss shows a subalkaline affinity. All metamafic rocks are characterized by a Nb anomaly. The protoliths of the eclogites with calc-alkaline affinity and the gneiss were related to a magmatic arc formed in Late Cambrian times according to previous age dating results. The protoliths of the eclogites with tholeiitic affinity were related to basalt/gabbro of thickened oceanic crust (island arc in the Rheic Ocean). The contrasting P-T paths and different nature of the protoliths are explained by different upwards-directed mass flows and, thus, mixing of various types of rocks in a subduction channel. Our findings also support the hypothesis that the MTZ represents subduction-related rocks embedded in high-pressure orthogneisses from the downgoing tip of a continental plate during initial continent-continent collision.

Keywords: Eclogite-facies rock; Malpica-Tuy shear zone; Garnet zonation; Zr-in-rutile geothermometry; Contrasting P-T paths; Tholeiitic protolith.

5.1. Introduction

Eclogite-facies metamorphic rocks have attracted geoscientists for a long time because they can provide valuable information on the thermal characteristics of paleo-subduction zones and, possibly, the early stage of a continent-continent collision after complete subduction of the oceanic plate in between. This information is obtained by detailed studies of the mineral compositions in such rocks and the subsequent application of geothermobarometric methods. Early geothermobarometry on eclogites has frequently resulted in a single pressure (P) - temperature (T) datum, which was, generally, assigned to peak metamorphic conditions. A simple clockwise P-T loop through such conditions was usually presented in older petrological works (e.g. Ernst and Dal Piaz, 1978; Jamtveit, 1987; Hirajima et al., 1988; Zhang et al., 1995; Wain, 1997). Recent studies, which intensely addressed the complex zonation of minerals such as garnet and phengite in eclogite frequently resulted, with the rare exception of anti-clockwise paths (Willner et al., 2004; Vignaroli et al., 2005), in clockwise P-T loops as well. However, various conclusions on the genesis of eclogite can be drawn from different shapes of such loops. The early part of a P-T path, constrained either by mineral compositions or inclusion minerals, can be nearly isobaric (Massonne and Kopp, 2005) or isothermal (Li

and Massonne, 2016). The latter case can be related to tectonic erosion of the continental crust overriding the subduction zone (see also Massonne, 2012). In other instances, the early path can be first nearly isothermal and then change to a section characterized by clearly increasing temperatures at moderately increasing pressures (Petrie et al., 2016) or vice versa with the nearly isothermal pressure increase before the metamorphic peak (Wei et al., 2015). The late section of the P-T path can be isothermal (Du et al., 2014; Janák et al., 2012) or can show a considerable cooling at decreasing pressures (Lü et al., 2007; Massonne, 2012, 2013). The latter type of late section might be responsible for a good preservation of eclogite.

In addition to the different shapes of P-T paths, it was noted, for instance, by Kadarusman et al. (2007) and Krebs et al. (2011) that eclogite bodies, occurring in a single unit, can show different P-T paths. These authors reported that the studied blocks of eclogite and blueschist occur in a serpentinite melange. In only km^2-large gneiss areas, but possibly in different units, eclogite bodies with different P-T evolutions were also found (e.g. in the Sulu terrane, E China: Zhu et al., 2007; in a limited area of the southern Dabie Shan, E China: compare Massonne, 2012, and Wei et al., 2015; in the Tian Shan of NW China: Tian & Wei, 2013). In other instances, bodies of eclogite can have experienced similar P-T conditions in an extended gneiss area (e.g. in NE Sardinia, Italy: Giacomini et al., 2005; Cruciani et al., 2011; Cruciani et al., 2012). Country-rocks, such as gneisses, and embedded eclogite bodies can show similar (e.g. NW Spain: Albert et al., 2012) or different P-T paths (e.g. Willner et al., 2000; Săbău and Massonne, 2003; Massonne, 2012; Li and Massonne, 2016). In the latter cases, the eclogite bodies must have been tectonically inserted in the country rocks. On the contrary, geoscientists often believe that country rocks and embedded eclogite bodies must have experienced the same P-T evolution (Kaneko et al., 2003; Xu et al., 2006).

We will demonstrate in this paper that eclogite bodies assembled in a km^2-large area, called land-site 'La Pioza', of the central Variscan Malpica-Tuy (also written Tui) shear zone (MTZ, Fig. 5.1) have experienced conditions along different P-T paths, which are clock-wise and even anti-clockwise. In fact, it is known for a long time that in the MTZ different high-pressure (HP) metamorphic rocks occur (Díez Fernández et al., 2011), but in previous works, the whole eclogite-facies area was treated as one tectonic block

(Rodríguez et al., 2003; López-Carmona et al., 2010, 2013; Díez Fernández et al., 2011), which is in contrast to our new findings. In addition, it was already recently proven for the northern MTZ that eclogite was significantly deeper subducted than surrounding HP gneisses (Li and Massonne, 2016).

5.2. Geological setting

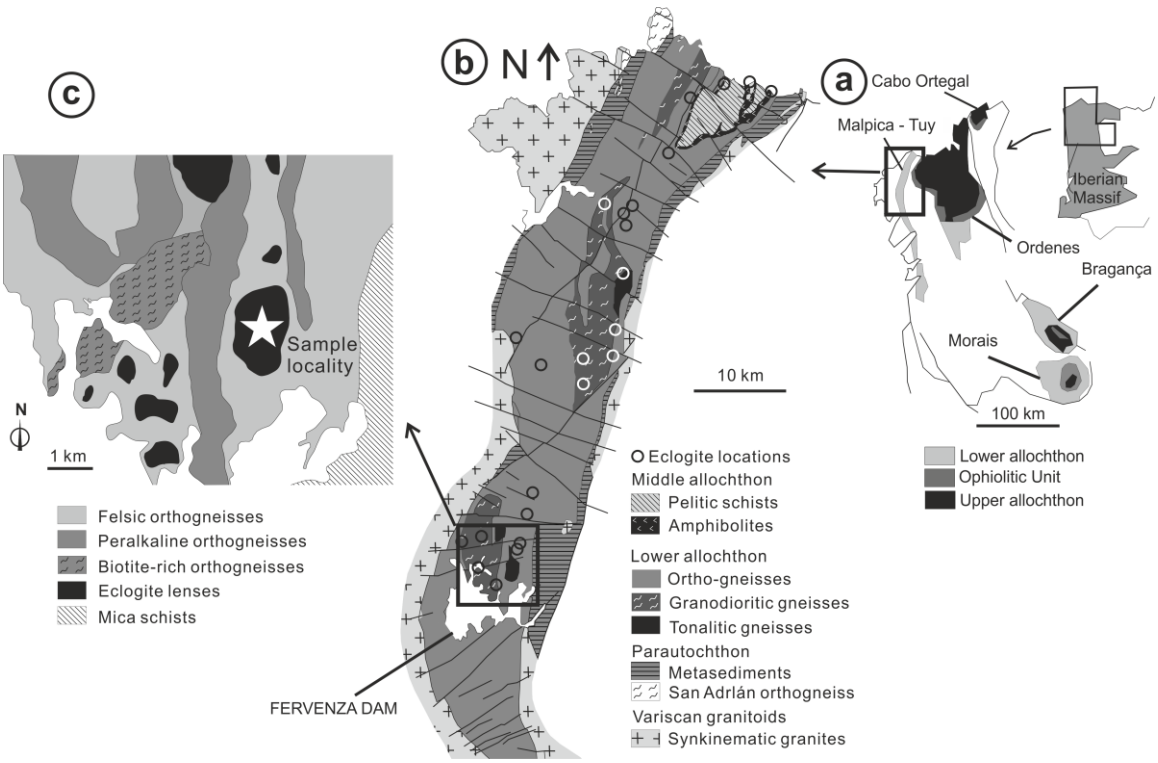

Fig. 5.1. (a) Geological frame of the Malpica-Tuy shear zone (MTZ) located in the Palaeozoic orogenic belt of NW Iberia modified after Santos Zalduegui et al. (1995); (b) geological map of the MTZ modified after López-Carmona (2013) showing the eclogite locations given by Gil Ibarguchi & Ortega Gironés (1985); (c) detalied geological map of the sampling area modified after Rivas Koslowski (1995) and Rodríguez et al. (2003).

The Iberian Massif in southwestern Europe is part of the Variscan orogen which formed by the collision of Laurussia and Gondwana (Andonaegui et al., 2012; Díez Fernández et al., 2011, 2012a; Díez Fernández and Martínez Catalán, 2012). In the northwestern Iberian Massif, five allochthonous complexes are preserved in late synformal structures (Fig. 5.1): three of them are exposed in Galicia (Cabo Ortegal, Órdenes, and MTZ) and two in the Portuguese region of Trás-os-Montes (Bragança and Morais complexes). In these allochthonous complexes, several crustal slices with

different origin were distinguished. These slices are from the top to the bottom the so-called upper, ophiolitic, and basal units. The upper unit consists of exotic terranes with Gondwanan affinity; the ophiolitic unit is considered to represent a collisional suture, whereas the basal unit is interpreted to be the most external continental margin of Gondwana (Abati et al., 2010; Andonaegui et al., 2012).

The MTZ is the westernmost of the European Variscan allochthonous complexes (Fig. 5.1). It is mainly composed of the basal unit (Díez Fernández et al., 2012a; Díez Fernández and Martínez Catalán, 2012). Some authors subdivided the MTZ in an upper subunit and a lower subunit (Rodríguez et al., 2003; López-Carmona et al., 2013). The upper subunit (Ceán unit), which was ascribed to the aforementioned ophiolitic unit, has oceanic affinity and is composed of pelitic schists and N-MORB-derived metabasic rocks (Fig. 5.1b). The lower subunit (Malpica-Tuy unit) consists of variably deformed and recrystallized granitoids, metasediments and sparse metabasites. The contact between upper and lower subunits is marked by a several meter thick zone of mylonites and ultramylonites located at the base of the Cambre amphibolites (Díez Fernández et al., 2011; López-Carmona et al., 2013)

Rocks of the Ceán unit developed almost entirely under blueschist-facies conditions (López-Carmona et al., 2010, 2013; Díez Fernández et al., 2011). P-T paths of chloritoid-glaucophanite schists, lawsonite blueschists and blueschist-facies metapelites were deduced by using isochemical phase diagrams (pseudosections), indicating peak conditions of 500 ºC at 17-18 kbar, 560 ºC at 22 kbar, and 520 ºC at 21-22 kbar, respectively (López-Carmona et al., 2010, 2013, 2014a).

Rocks of the Malpica-Tuy unit record intermediate temperatures of the eclogites facies (Díez Fernández et al., 2011). Prograde P-T paths for an eclogite body and its surrounding granodioritic gneiss in the northernmost Malpica-Tuy unit have been derived by using pseudosction modelling and traditional geothermobarometry (Li and Massonne, 2016). The isothermal burial path of the eclogite reached peak pressure conditions of 22.5 kbar at 540 °C. The subsequent exhumation path passed through P-T conditions of 21 kbar and 575 °C and 13.5 kbar and 625 °C. The latter data represent the peak P-T conditions of the gneiss (Li and Massonne, 2016). Peak pressure conditions of 21 kbar at 600 °C (Rodríguez et al., 2003) and 26 kbar at 650 °C (López-Carmona et al., 2014b)

were reported for other eclogites of the MTZ. Gil Ibarguchi (1995) gave peak conditions of 655 ± 30 °C and 15.5 ± 1 kbar, using conventional geothermometry, for an orthogneiss of the MTZ. Rodríguez et al. (2003) estimated peak conditions of 580 °C at 21 kbar and 500-600 °C at a maximal pressure of 15 kbar for a metatonalite and a felsic gneiss, respectively, using garnet-phengite-omphacite geothermobarometry. The HP metamorphism occurred mainly in the time interval between 365 and 370 Ma (van Calsteren et al., 1979; Santos Zalduegui et al., 1995; Martínez Catalán et al., 1996; Rodríguez et al., 2003; Abati et al., 2010; López-Carmona et al., 2014a).

A pre-Variscan magmatism happened between 470-500 Ma (Abati et al., 2010; Rodríguez et al., 2007), which produced two associations (Floor, 1967; Arps, 1970; Díez Fernández et al., 2012b): a calc-alkaline group including tonalites, granodiorites and alkaline-granites (high-K), and an alkaline association with alkaline and peralkaline granites and quartz syenites. According to the chemical compositions of the orthogneisses, the protoliths of the basal unit were formed in the context of a peri-Gondwanan magmatic arc (calc-alkaline granitoids) at 490-500 Ma, affected by subsequent rifting leading to the alkaline-peralkaline suite at 470-475 Ma during the opening of the Rheic Ocean (Abati et al., 2010). In contrast, the protoliths of metamafic rocks are still ambiguous, but because of similar ages of calc-alkaline gneiss and eclogite (Abati et al., 2010), and the co-occurrence of both types of rocks in the field (Rodríguez et al., 2003), the magmatism of the eclogitic protoliths in the MTZ was also assigned to the calc-alkaline suite.

Metamafic rocks are present only in the central to northern part of the lower subunit in the MTZ. These rocks as well as tonalitic/eclogitic gneiss occur mostly as lenses and boudins within orthogneisses (Gil Ibarguchi and Ortega Gironés, 1985; Santos Zalduegui et al., 1995; Rodríguez et al., 2003; Abati et al., 2010). Abundant eclogite bodies and adjacent rocks were sampled at and north of the northern shore of the Fervenza reservoir (Fig. 5.1c). We selected three different eclogite samples (130893, Sp96-41a and 18193), a glaucophanite (Sp96-41b) and a tonalitic gneiss (18195) for further detailed studies. These samples are all from the same eclogitic-facies area at the land-site 'La Pioza'. This km2-sized area represents the largest exposure of accumulated eclogite bodies north of the Fervenza reservoir and probably in the MTZ at all.

5.3. Analytical Methods

5.3.1. Whole-rock analyses

All five samples were crushed and milled to obtain homogeneous powders for whole-rock analyses. Major elements were analyzed on lithium borate glass-disks (prepared from 0.6 g sample powder and 3.6 g Li-borate = Spectromelt®) by X-ray fluorescence (XRF) spectrometry with a PHILIPS PW2400 XRF spectrometer. This instrument had been calibrated by using numerous geostandards. Both, XRF and laser ablation inductively-coupled plasma mass spectrometry (LA-ICP-MS), were used for the determination of trace elements. Powder of each sample was pressed to a disk (prepared with 12 g sample powder and 3 g wax-C) for the XRF determination. Lithium borate glass-disks (0.6 g sample powder + 3.6 g Spectromelt®) were analyzed by LA-ICP-MS employing a Cetac LSX-213 system with a wavelength of 213 nm combined with an Agilent 7700s ICP-MS. Laser sampling was performed in a He-Ar atmosphere (He = 300 and Ar = 800 ml/min). Spot size, laser shot frequency, and laser energy were 150 μm, 20 Hz, and 20 %, respectively. Four hundred fifty shots were used for each analysis. The external calibration standards were a DLH-7 glass from the P&H Developments Ltd. Company and a NIST 612 glass. Silicon was used as internal standard, employing the absolute content of this element previously measured by XRF spectroscopy. For a quality check of the applied method, we used glass-disks prepared from Spectromelt® and diorite (DR-N) or zinnwaldite (ZW-C) reference standards from the Service d'Analyse des Roches et des Minéraux du CNRS. For trace elements, we used the results from the LA-ICP-MS analyses for contents below 30 ppm and for Ba as they are more precise than the corresponding results from the XRF spectroscopy, due to, for instance, spectral overlap with other elements (e.g. BaLα- with TiKα-radiation). With the exception of Ba, we used the mean values of both analytical methods for element concentrations above 30 ppm.

5.3.2. Electron microprobe analyses of minerals

Garnet, white mica, and other silicates were analyzed with a CAMECA SX100 electron microprobe (EMP) with 5 wavelength-dispersive spectrometers. The conditions for these analyses were 15 kV acceleration voltage, 10 or 15 nA beam current, and approximately 2 minutes total counting time (a detailed description of the analytical

Table 5.1. Representative EMP analyses (in wt%) of garnet in the five studied rocks. The garnet structural formula (double unit) was calculated on the basis of 24 O, 10 six- and eight-fold coordinated cations. b.d.l. = below detection limit.

Sample	130893			18193			sp96-41a		sp96-41b			18195	
Garnet	core	mantle	rim	core	mantle	rim	core	rim	core	mantle	rim	core	rim
wt%													
SiO_2	37.76	37.94	39.35	37.52	38.74	38.67	39.84	40.14	37.64	37.10	38.69	37.61	38.49
TiO_2	0.14	0.21	0.03	0.08	0.02	0.05	0.13	0.09	0.05	0.14	0.03	0.07	0.02
Al_2O_3	21.35	21.32	22.27	21.55	21.96	22.09	22.74	22.98	21.43	21.18	21.94	21.55	22.01
Cr_2O_3	0.04	0.04	0.01	0.01	0.01	b.d.l.	0.13	0.01	0.03	0.08	0.01	0.01	b.d.l.
Fe_2O_3	0.21	0.47	b.d.l.	0.65	0.46	0.70	0.52	0.20	0.99	0.96	0.64	0.64	1.17
FeO	27.79	25.65	22.51	25.68	24.60	24.59	19.64	19.09	24.86	23.26	22.44	24.83	24.45
MnO	1.33	0.33	0.23	0.47	0.39	0.52	0.57	0.50	1.64	0.91	0.14	1.73	0.31
MgO	2.27	5.15	8.26	3.98	6.90	6.08	11.04	10.28	6.64	8.51	11.80	3.85	7.64
CaO	9.54	8.25	6.91	10.23	7.49	9.05	6.98	8.47	6.49	5.33	2.80	9.98	6.80
Na_2O	0.03	0.01	0.03	0.03	0.07	0.04	0.05	0.04	b.d.l.	b.d.l.	0.03	0.08	0.44
Total	100.45	99.37	99.59	100.18	100.65	101.78	101.65	101.81	99.79	97.47	98.52	100.35	101.32
pfu													
Si	5.96	5.95	6.05	5.80	5.91	5.82	5.84	5.89	5.78	5.76	5.87	5.81	5.74
Ti	0.02	0.02	0.00	0.01	0.00	0.01	0.01	0.01	0.01	0.02	0.00	0.01	0.00
Al	3.97	3.94	4.04	3.92	3.95	3.92	3.93	3.98	3.88	3.88	3.93	3.93	3.87
Cr	0.00	0.00	0.00	0.00	0.00	0.00	0.01	0.00	0.00	0.01	0.00	0.00	0.00
Fe^{3+}	0.02	0.06	0.00	0.08	0.05	0.08	0.06	0.02	0.11	0.11	0.07	0.07	0.13
Fe^{2+}	3.67	3.36	2.89	3.32	3.14	3.10	2.41	2.34	3.19	3.02	2.85	3.21	3.05
Mg	0.53	1.20	1.89	0.92	1.57	1.37	2.41	2.25	1.52	1.97	2.67	0.89	1.70
Ca	1.61	1.39	1.14	1.69	1.22	1.46	1.10	1.33	1.07	0.89	0.46	1.65	1.09
Mn	0.18	0.04	0.03	0.06	0.05	0.07	0.07	0.06	0.21	0.12	0.02	0.23	0.04
Na	0.01	0.00	0.01	0.01	0.02	0.01	0.01	0.01	0.00	0.00	0.01	0.03	0.13
pyrope	0.09	0.20	0.32	0.15	0.20	0.23	0.40	0.37	0.25	0.33	0.45	0.15	0.28
grossular	0.27	0.23	0.19	0.28	0.26	0.24	0.18	0.22	0.18	0.15	0.08	0.28	0.18
almandine	0.61	0.56	0.49	0.55	0.52	0.52	0.40	0.39	0.53	0.50	0.47	0.53	0.53
spessartine	0.03	0.01	0.01	0.01	0.01	0.01	0.01	0.01	0.04	0.02	0.00	0.04	0.01

Table 5.2. EMP analyses (in wt%) of various minerals from sample 18193, Sp96-41b and 18195. Structural formulae were calculated as follows: Phengite (Ph): O = 11; clinopyroxene (Om): O = 6 and 4 cations; amphibole (Am: glaucophane = Gl and barroisite = Ba) = 46 valencies, sum of cations - (K+Ba+Ca+Na) = 13; (clino)zoisite-epidote (Ep) = 25 valencies, Mn is trivalent; plagioclase (Pl): O = 8. b.d.l. = below detection limit.

sample	18193					Sp96-41b				18195					
minerals	Ph	Ph	Om	Am	Ep	Gl	Ba	Om	Pl	Ph	Ph	Om	Am	Ep	Pl
comments	early	late								early	late				
SiO_2	50.26	48.32	55.98	40.26	38.04	55.45	48.24	55.40	66.92	46.48	49.71	56.58	43.08	38.63	68.68
TiO_2	0.93	0.48	0.08	0.09	0.17	0.15	0.34	0.07	b.d.l.	0.44	0.28	0.12	0.36	0.12	b.d.l.
Al_2O_3	25.81	29.90	11.15	16.97	28.96	12.15	14.66	11.22	20.32	28.02	27.92	12.98	14.23	28.66	19.25
$(FeO)_{tot}$	2.43	1.74	4.53	18.51	5.08	6.61	7.93	5.42	0.44	3.49	1.77	4.06	13.81	6.37	0.31
MnO	0.04	b.d.l.	b.d.l.	0.22	b.d.l.	0.01	0.03	0.02	b.d.l.	0.60	b.d.l.	0.02	0.10	0.09	b.d.l.
MgO	3.63	2.87	8.20	7.73	0.08	14.14	14.33	7.74	0.06	2.65	3.37	7.01	10.96	0.12	b.d.l.
CaO	0.91	0.00	13.15	10.74	23.79	2.28	5.43	12.27	1.50	0.01	b.d.l.	11.29	10.39	23.32	0.39
Na_2O	2.19	1.13	6.66	2.48	0.01	6.46	5.42	7.19	10.87	1.18	0.98	8.08	3.17	0.05	11.78
K_2O	8.73	9.89	0.05	0.55	b.d.l.	0.05	0.12	b.d.l.	0.02	8.75	10.29	0.07	0.69	b.d.l.	0.05
BaO	0.41	0.36	b.d.l.	b.d.l.	b.d.l.	b.d.l.	b.d.l.	b.d.l.	0.02	0.46	0.47	b.d.l.	0.02	b.d.l.	b.d.l.
H_2O	4.43	4.45		2.02	1.91	2.21	2.16			4.32	4.45		2.03	1.94	
Total	99.76	99.14	99.80	100.28	98.59	99.52	98.67	99.34	100.15	96.41	99.25	100.20	98.84	99.29	100.45
pfu															
Si	6.808	6.506	1.995	5.980	2.981	7.513	6.687	1.981	2.932	3.224	3.352	1.991	6.357	2.992	2.992
Ti	0.095	0.048	0.002	0.010	0.010	0.016	0.035	0.002	0.000	0.023	0.014	0.003	0.040	0.007	0.000
Al	4.121	4.745	0.468	2.971	2.675	1.940	2.394	0.473	1.049	2.291	2.219	0.538	2.474	2.616	0.988
Fe^{3+}	0.000	0.000	0.000	0.813	0.333	0.634	0.919	0.060	0.016	0.102	0.000	0.028	0.406	0.412	
Fe^{2+}	0.275	0.196	0.135	1.486		0.040	0.000	0.102		0.101	0.100	0.092	1.299		
Mn	0.004	0.000	0.000	0.028	0.000	0.001	0.003	0.001	0.000	0.035	0.000	0.001	0.012	0.005	0.000
Mg	0.733	0.577	0.435	1.711	0.009	2.857	2.961	0.413		0.275	0.339	0.368	2.411	0.014	
Ca	0.132	0.001	0.502	1.709	1.998	0.331	0.807	0.470	0.070	0.001	0.000	0.426	1.644	1.935	0.018
Na	0.576	0.295	0.460	0.714	0.001	1.698	1.457	0.499	0.924	0.159	0.128	0.551	0.906	0.008	0.995
K	1.509	1.699	0.002	0.104		0.009	0.022	0.000	0.001	0.774	0.885	0.003	0.130		0.003
Ba				0.022	0.019	0.000	0.000			0.012	0.013		0.001		
H	2.000	2.000		2.000	1.000	2.000	2.000			2.000	2.000		2.000	1.000	

conditions and errors are given by Massonne, 2012).

The rutile analyses were also performed with the EMP with a beam current of 100 nA and an acceleration voltage of 15 kV. The contents of Nb, Zr, Fe, Cr, Si, and Ti were determined. When SiO_2 contents were above 0.3 wt%, the corresponding analyses were discarded as these data were probably influenced by nearby silicates (Zack et al., 2004). In case of Fe_2O_3 contents above 0.6 wt%, the analyses were also abandoned, because ilmenite, a replacement product of rutile, could have disturbed the results. Analytical 1σ-errors were about ± 35 ppm according to counting statistics.

Back-scattered electron (BSE) images were taken with the EMP to document specific textural features. X-ray maps for specific mineral grains were also produced with the EMP. For the mapping, Mn, Ca, Mg, Fe, and Y were considered for garnet. Mg, Fe, Ti, Na, and Ba radiation intensities were mapped for white mica. For clinopyroxene and amphibole Ca instead of Ba was considered. The parameters for the X-ray mapping were 1 or 2 μm step width, 50-100 ms per 12 step, 15 kV accelerating voltage, and 30 nA beam current for white mica, 50 nA for clinopyroxene and amphibole, and 60 nA for garnet.

For the calculation of structural formulae of minerals and the molar fractions of mineral components from EMP analyses, the computer program CALCMIN (Brandelik, 2009) was used. Representative EMP analyses of minerals in the studied rocks are given in Tables 5.1 and 5.2.

5.4. Sample descriptions

The mineral contents (vol.%) of the five selected samples (see section 5.2) are given in Table 5.3. For the subsequent description, we used the contents of elements per formula unit (pfu) and the following parameters for the chemical compositions of minerals: (1) XMg = Mg/(Mg + Mn + Fe^{2+}), (2) XPis = Fe^{3+}/(Fe^{3+} + Al) for (clino)zoisite-epidote (subsequently only named epidote), and (3) XNa = Na/(Na+K+Ca) for plagioclase.

5.4.1. Eclogites

The studied eclogites display a fine- to medium-grained granoblastic texture composed mainly of garnet (up to 0.6 mm in diameter), omphacite (around 0.06 mm × 0.04 mm) and amphibole (Fig. 5.2a). Eclogite 18193 contains more quartz (up to 10

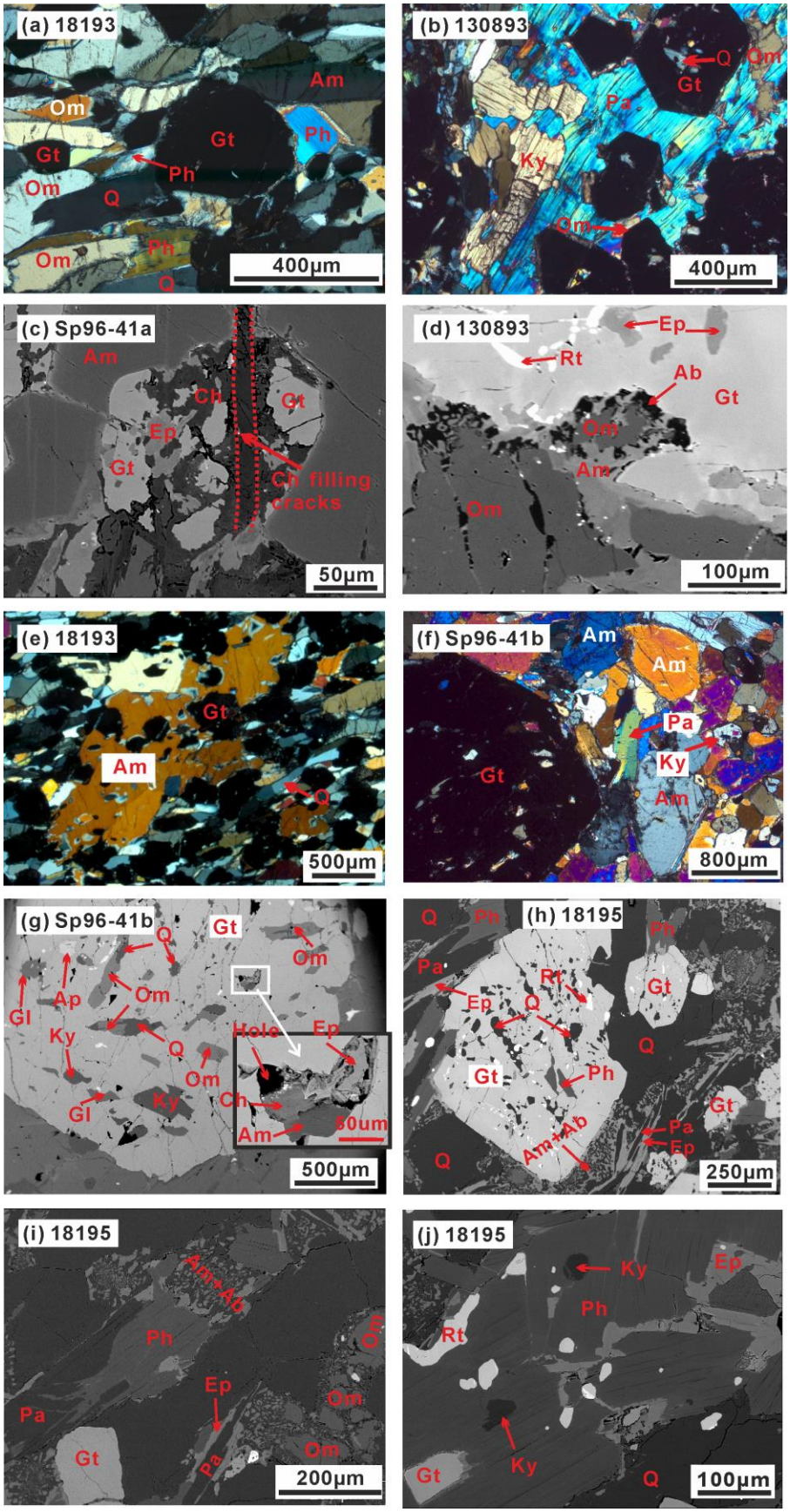
(a) 18193
Am
Om
Gt
Ph
Gt
Ph
Om
Q
Om
Ph
Q
400μm
(b) 130893
Q
Om
Gt
Pa
Ky
Om
400μm
(c) Sp96-41a
Am
Ch
Gt
Ep
Gt
Ch filling cracks
50μm
(d) 130893
Ep
Rt
Ab
Gt
Om
Am
Om
100μm
(e) 18193
Gt
Am
Q
500μm
(f) Sp96-41b
Am
Am
Pa
Ky
Gt
Am
800μm
(g) Sp96-41b
Q
Gt
Om
Gl
Ap
Om
Ky
Q
Hole
Ep
Om
Ky
Gl
Ch
Am
50um
500μm
(h) 18195
Q
Ph
Ph
Pa
Rt
Gt
Ep
Q
Q
Gt
Ph
Gt
Pa
Ep
Q
Am+Ab
250μm
(i) 18195
Am+Ab
Ph
Om
Ep
Pa
Om
Gt
Om
Pa
200μm
(j) 18195
Ky
Ep
Ph
Rt
Gt
Ky
Q
100μm

Fig. 5.2. Photomicrographs under crossed polarizers (a, b, e and f) and back-scattered electron images (c, d, and g-j). (a) Major minerals in sample 18193 are garnet (Gt), omphacite (Om), and amphibole (Am); (b) layers of paragonite (Pa) with inclusions of garnet, kyanite (Ky), and omphacite occur in sample 130893; (c) epidote (Ep) and chlorite (Ch) replaced garnet in sample Sp96-41a; chlorite also fills cracks in garnet; (d) symplectites of amphibole and plagioclase (Pl) around omphacite in sample 130893; (e) Coarse-grained amphibole and abundant quartz (Q) in sample 18193; (f) porphyroblastic garnet in Sp96-41b; (g) numerous inclusions (mainly kyanite, omphacite and glaucophane = Gl) in such garnet; (h) bimodal size distribution of garnet grains in sample 18195; (i) sample 18195: omphacite relics surrounded by a symplectite of amphibole + plagioclase as well as paragonite with epidote and anhedral phengite (Ph) at its grain margin; (j) garnet, kyanite, and rutile (Rt) inclusions in phengite of sample 18195.

vol.%) than the other two eclogites (Fig. 5.2a, e). Sample 130893 displays paragonite bands (Fig. 5.2b) with garnet, omphacite, and kyanite inclusions. Compared to the other eclogite samples, eclogite Sp96-41a shows more late-stage cracks, which are oriented and filled mainly with chlorite (Fig. 5.2c). All eclogites contain symplectites (Fig. 5.2d), mainly composed of amphibole and albite, around omphacite. Small garnet grains can be replaced by epidote and chlorite (Fig. 5.2c). In garnet of sample 130893, no inclusion was found in the core, but inclusions of epidote, amphibole, albite, and rutile occur in the mantle (Fig. 5.2d). Garnet of sample 18193 only contains inclusions of rutile. In garnet of sample Sp96-41a, inclusions of minerals were observed in both mantle and rim. These minerals are kyanite, amphibole, omphacite, quartz, phengite and rutile. Amphibole appears in the matrix either as small platy grains (around 0.4 mm × 0.1 mm, see Fig. 5.2a) or subhedral to anhedral porphyroblasts being up to 3 mm long (Fig. 5.2e). There are small flakes (around 0.03 mm × 0.02 mm) of phengite in eclogites 18193 (Fig. 5.2a) and Sp96-41a (Fig. 5.2f). No phengite was found in sample 130893. Epidote occurs in the matrix as anhedral grains (up to 0.08 mm).

The extended core of garnet in sample 130893 contains ca. 61 mol% almandine, 9 mol% pyrope, 27 mol% grossular (+ andradite), and 3 mol% spessartine components ($Alm_{61}Pyr_{9}Grs_{27}Sps_{3}$). The mantle composition is $Alm_{56}Pyr_{20}Grs_{23}Sps_{1}$ with a pyrope-rich and grossular-poor outermost rim ($Alm_{48.5}Pyr_{32}Grs_{19}Sps_{0.5}$) as shown in

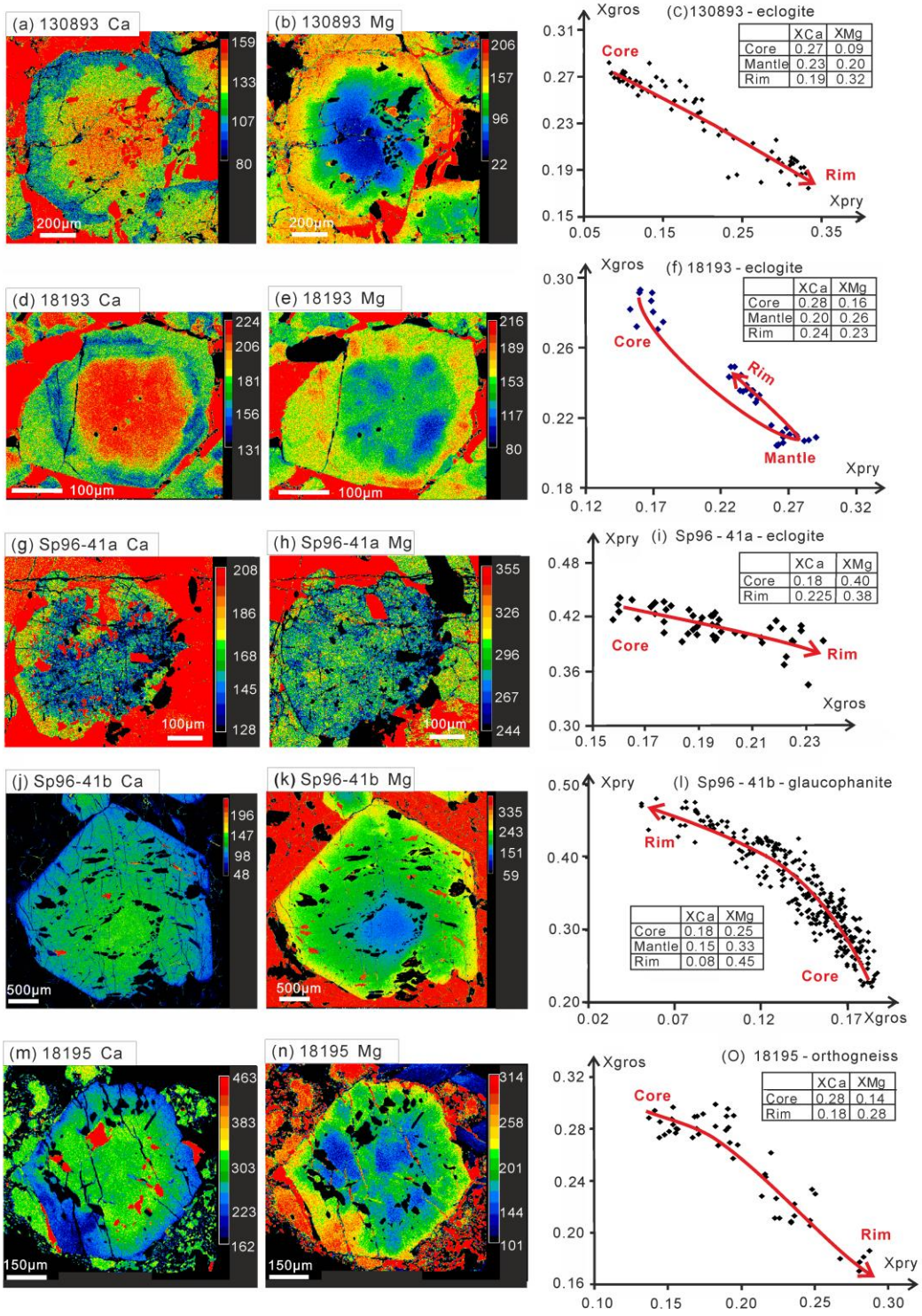

Fig. 5.3. Distribution maps for Ca and Mg in garnet and results of spot analyses of garnet in terms of molar fractions of pyrope (Xpyr) versus grossular (+ andradite) (Xgros) obtained with a CAMECA SX100 EMP from eclogite 130893 (a-c), eclogite 18193 (d-f), eclogite Sp96-41a (g-i), glaucophanite Sp96-41b (j-l) and gneiss 18195 (m-o).

Figure 5.3a-c. In sample 18193 the garnet composition varies as follows (Fig. 5.3 d-f): core ($Alm_{55.5}Pyr_{15.5}Grs_{28}Sps_1$), mantle ($Alm_{52.6}Pyr_{20.4}Grs_{26}Sps_1$), outermost rim ($Alm_{52}Pyr_{23}Grs_{24}Sps_1$). Core and rim compositions of garnet in sample Sp96-41a are $Alm_{40.6}Pyr_{40}Grs_{18.4}Sps_1$ and $Alm_{39}Pyr_{37.5}Grs_{22.5}Sps_1$, respectively (Fig. 5.3 h-j).
Phengite shows contents from 3.25 to 3.41 Si pfu and 3.28-3.41 pfu in samples 18193 and Sp96-41a, respectively. The early-stage phengite has higher silica contents than the late-stage one in both rocks.

Amphibole inclusions (XMg ~ 0.6) in garnet are mainly pargasite. This phase in the matrix (XMg = 0.37-0.82, 0.44-0.82 and 0.70-1.00 in 130893, 18193 and Sp9641a, respectively) includes calcic and sodic-calcic (magnesiotaramite, magnesiokatophorite, actinolite, magnesiohornblende, tremolite and barroisite) amphibole.

Omphacite grains in sample 130893 show somewhat higher Mg and Ca and lower Na and Fe^{2+} contents in the core (early omphacite: 43-49 mol% jadeite, 37-41 mol% diopside, and ~ 10 mol% hedenbergite components = $Jd_{43-49}Diop_{37-41}Hed_{10}$; a few mol%, resulting as total of other components such as orthopyroxene and aegirine, are not integrated in this formula), than in the rim (late omphacite: $Jd_{47-51}Diop_{34-37}Hed_{10-12}$). Omphacite core compositions in sample 18193 are lower in Mg and Ca and higher in Fe^{2+} ($Jd_{39-43}Diop_{40-42}Hed_{8-12}$) than those of the rim ($Jd_{39-43}Diop_{42-45}Hed_{5-8}$). Omphacite grains in sample Sp96-41a show no obvious chemical zoning from core to rim with $Jd_{24-36}Diop_{50-65}Hed_{2-7}$. The calculated aegirine component in omphacite of the three samples is between 2 and 6 mol%.

The Fe^{3+} contents of epidote enclosed in garnet are higher (XPis = 0.16-0.19) than those of matrix epidote (XPis = 0.12-0.15) in sample 130983. In Sp96-41a, epidote appears mainly in the matrix with XPis between 0.03 and 0.16. A few epidote inclusions are found in garnet with low Fe^{3+} contents (XPis ~ 0.03). In 18193, epidote only occurs as anhedral retrograde mineral in the matrix with XPis between 0.10 and 0.31.

5.4.2. Glaucophanite

The glaucophanite (Sp96-41b) has a fine-grained porphyroblastic texture (Fig. 5.2f). It mainly consists of garnet and amphibole (Table 5.3). Kyanite, paragonite, albite and omphacite are minor phases. Chlorite, epidote, rutile, ilmenite, and apatite are accessories.

Garnet forms porphyroblasts with diameters between 2 and 4 mm. It contains abundant inclusions (Fig. 5.2g) of quartz, amphibole, kyanite, paragonite, omphacite, epidote, apatite, chlorite, and rutile. The core composition of garnet is $Alm_{53.1}Pry_{25.4}Grs_{18}Sps_{3.5}$. Grossular component gradually decreases and the pyrope component increases (Fig. 5.3 j-l) from core to mantle ($Alm_{50.5}Pry_{32.5}Grs_{15}Sps_{2}$) and rim ($Alm_{47.5}Pry_{44.5}Grs_{7.5}Sps_{0.5}$).

Table 5.3. Major minerals and their model proportion (vol.%) for eclogites, glaucophanite and metatonalitic gneiss from the central Malpica-Tuy zone. "-": not found.

Sample	Lithology	Gt	Om	Am	Ep	Ph	Pa	Bt	Pl	Q	Ky	Rt
130893	eclogite	36	36	6	8	-	5	-	<2	<1	2	2
18193	eclogite	35	33	12	<1	2	-	-	2	10	-	3
Sp96-41a	eclogite	30	32	28	2	1	-	-	1	1	1	1
Sp96-41b	glaucophanite	30	1	41	<1	-	6	-	4	<1	15	1
18195	gneiss	16	12	14	4	8	10	<1	10	23	3	1

Amphibole is unoriented and fine-grained ranging in size from 0.05 to 0.8 mm. This phase is mostly glaucophane and appears in garnet and in the matrix (XMg = 0.98-1 and XCa = Ca pfu/2 = 0.06-0.23). Also barroisite occurs as inclusion in garnet (XMg = 0.9-0.97, XCa = 0.25-0.65) and as retrograde mineral in the matrix (XMg = 0.84-0.89, XCa = 0.25-0.72).

Omphacite ($Jd_{39-49}Diop_{30-40}Hed_{5-9}$) only appears as inclusion in garnet. Kyanite, paragonite, and quartz also occur in the matrix. Anhedral albite (XNa = 0.90-0.97) mainly grew along amphibole boundaries. Only one epidote (XPis = 0.17-0.20) grain was found. This grain together with chlorite (XMg = 0.74-0.77) and glaucophane (XMg = 1, XCa = 0.07) formed a polyphase inclusion in the garnet mantle (Fig. 5.2g).

5.4.3. Tonalitic gneiss

The studied tonalitic gneiss (18195) is fine-grained and slightly foliated. It contains garnet, amphibole, omphacite, albite, quartz, phengite, epidote, paragonite, and kyanite (Table 5.3) and accessory amounts of rutile, biotite, ilmenite, chlorite, and apatite.

Garnet is euhedral or rounded and shows a bimodal grain size distribution (Fig. 5.2h). Most garnet is fine-grained with diameters between 0.2 and 0.6 mm. Occasionally, garnet occurs as porphyroblast (1-2 mm) with numerous inclusions of quartz, phengite (Si around 3.38 pfu), epidote (XPis = 0.03-0.12), amphibole (XMg = 0.50-0.67), paragonite,

and rutile. The two types of garnet exhibit a similar compositional zonation with an increase of pryrope and a decrease of grossular and spessartine from core to rim (Fig. 5.3m-o). The mean core and rim compositions are $Alm_{54}Pry_{14.4}Grs_{27.6}Sps_4$ and $Alm_{53}Pry_{28.4}Grs_{18}Sps_{0.6}$, respectively.

Omphacite ($Jd_{47-53}Diop_{33-39}Hed_{3-7}$) is almost completely transformed to symplectites of amphibole and albite (Fig. 5.2i). The calculated aegirine component is 6-9 mol%.

Phengite shows a subhedral to anhedral shape with grain sizes between 0.2 and 1.0 mm (Fig. 5.2h, j). Inclusions in phengite are kyanite, garnet, and rutile (Fig. 5.2j). The Si content of phengite is usually between 3.22 (rim) and 3.35 pfu (core). Small flaky paragonite (0.01-0.03 mm, XNa = (Na/(Ca + Ba + Na + K) = 0.85-0.91) is often surrounded by epidote (Fig. 5.2i). Anhedral epidote (XPis = 0.22-0.27) in the matrix usually occurs along paragonite and garnet boundaries (Fig. 5.2j). Ca-amphibole (XMg = 0.55-0.73) and albite (XNa = 0.97-0.99) form the aforementioned symplectites. Small and anhedral biotite occurs at grain boundaries of phengite. Quartz is anhedral with grain sizes between 0.1 and 1 mm (Fig. 5.2h-j).

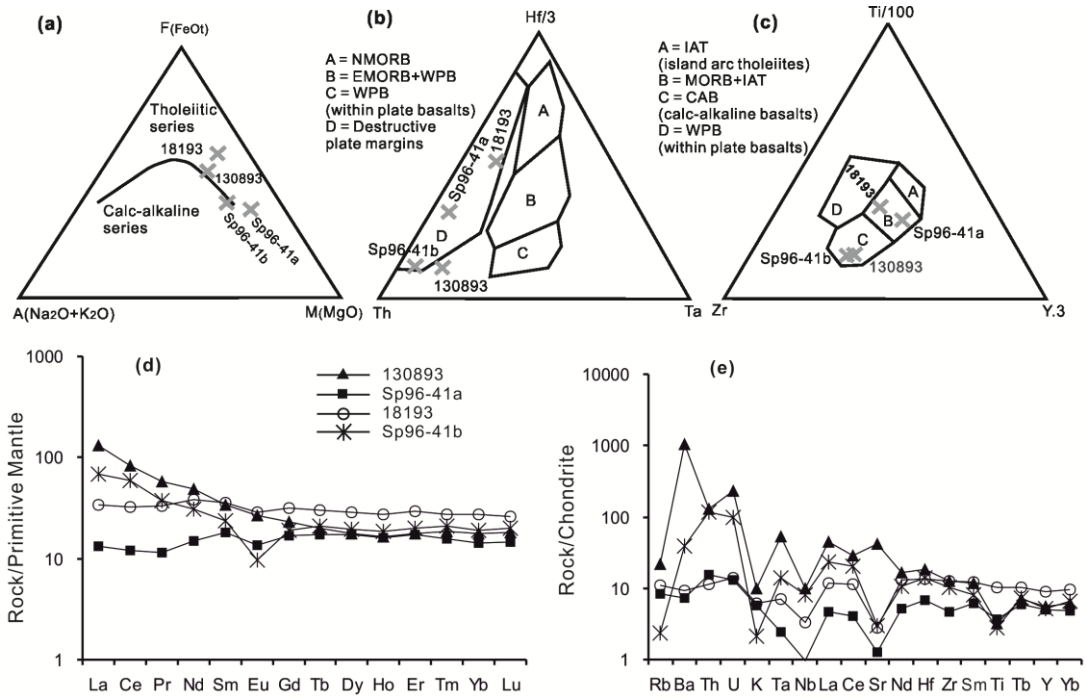

Fig. 5.4. Plots of bulk-rock data of three eclogites (samples 130893, 18193, Sp96-41a) and glaucophanite Sp96-41b in (a) the A-F-M ternary diagram by Irvine & Baragar (1971); (b) the Th-Ta-Hf ternary diagram by Wood et al. (1979); (c) the Ti-Zr-Y

ternary diagram by Pearce & Cann (1973) and (d) and (e) trace element diagrams normalized against chondrite after Sun & McDonough (1989).

5.5. Bulk-rock compositions and protolith nature

The studied sample 18195 has the typical composition of a tonalite (Table 5.4). Thus, it is called in this paper tonalitic or eclogitic gneiss, following the terminology by Rodríguez et al. (2003). The igneous protolith had a subalkaline nature according to the K_2O versus SiO_2 diagram (not shown here) by Peccerillo and Taylor (1976).

The four metamorphosed mafic rocks investigated in detail have similar basaltic compositions based on the major element (SiO_2 = 46.65-49.6 wt%; K_2O+Na_2O = 2.45-4.0 wt%; Le Bas, 1986). To elucidate their magmatic affinity, we used discrimination diagrams for major and trace elements. The AFM ternary diagram (Fig. 5.4a) after Irvine and Baragar (1971) demonstrates that the protolith of eclogite 18193 belongs to the tholeiitic series, whereas the compositions of the other metamafic rocks plot at the boundary between tholeiitic and calc-alkaline series. In the applied Ti-Zr-Y diagram (Pearce and Cann, 1973) and Th-Ta-Hf diagram (Wood et al., 1979) shown in Figure 5.4b and c, the compositions of 130893 and Sp96-41b are located in the fields for calc-alkaline basalts/gabbros (destructive plate margin) whereas those of 18193 and Sp96-41a plot in the fields for island arc tholeiite (IAT). In the rare-earth element (REE) diagram of Fig. 5.4d, the 4 samples can be divided into three groups. Samples 130893 and Sp96-41b are strongly light REE (LREE) enriched ($(Ce/Yb)_N$ = 3.1 and 4.8, $(La)_N$ = 130 and 68). Sample 18193 shows no enrichment of the LREE with $(Ce/Yb)_N$ = 1.2 and $(La)_N$ = 34. Sample Sp96-41a is LREE depleted with $(Ce/Yb)_N$ = 0.85 and $(La)_N$ = 13.4. In addition, this rock exhibits a slight middle-REE enrichment with $(Gd/Ce)_N$ = 1.4 and $(Gd/Yb)_N$ = 1.2. All metamafic samples show at least a slight Eu anomaly (130893: 0.96, 18193: 0.86, Sp96-41a: 0.77, Sp96-41b: 0.4), probably because of plagioclase fractionation in the original magma.

The primitive mantle-normalized spider diagram (Fig. 5.4e) after Sun and McDonough (1989) demonstrates an enrichment in large-ion lithophile elements (LILE) for samples 130893 and Sp96-41b, in contrast to samples Sp96-41a and 18193. All four metamafic samples show a negative Nb anomaly suggesting an origin of their protolith in a supra-subducton zone setting, i.e. a continental or oceanic arc setting.

Table 5.4. Bulk-rock analyses for the studied rocks determined by X-ray fluorescence spectrometry = XRF (major and trace elements) and laser-ablation (ICP) mass-spectrometry = LA (trace elements). b.d.l. = below detection limit. The units for major elements and trace elements are wt% and ppm, respectively.

Rock type	Eclogite		Eclogite		Eclogite		Glaucophanite		Metatonalite	
Sample No.	130893		18193		Sp96-41a		Sp96-41b		18195	
SiO_2	46.65		49.16		49.37		49.60		63.86	
Al_2O_3	19.8		14.69		15.78		20.41		15.16	
MnO	0.17		0.22		0.16		0.13		0.12	
MgO	6.12		6.40		11.69		11.25		3.34	
CaO	10.89		9.69		11.10		2.68		5.14	
Na_2O	3.32		2.65		2.27		3.95		3.10	
K_2O	0.30		0.18		0.18		0.07		0.81	
TiO_2	0.66		2.06		0.71		0.57		0.42	
P_2O_5	0.09		0.18		0.03		0.06		0.004	
Fe_2O_3	10.72		14.29		8.71		10.77		6.62	
total	98.73		99.52		99.99		99.48		98.61	
ppm	XRF	LA	XRF	LA	XRF	LA	XRF	LA	XRF	LA
Rb	14.5	14.0	5.0	6.86	4.0	5.34	0.5	1.49	15.5	23.3
Ba	7963	6426	67	59.9	50.5	46.1	288	248	382	331
K	2507	2457	1384	1519	1486	1411	581	534	7150	7054
Th	19.0	11.1	2.0	0.95	b.d.l.	1.30	6.5	9.78	8.5	5.52
U	4.0	4.90	b.d.l.	0.29	b.d.l.	0.27	b.d.l.	2.07	b.d.l.	1.06
Nb	11.0	7.03	8.5	2.34	6.0	0.70	9.5	5.68	11.0	4.52
Ta	3.0	2.15	3.5	0.29	2.0	0.10	2.5	0.58	2.0	0.62
La	32.0	29.6	5.0	8.12	3.0	3.17	14.5	16.1	6.5	7.84
Ce	55.0	48.1	13.0	19.9	2.5	7.35	35.0	37.0	10.5	16.5
Pr	1.5	5.51	b.d.l.	3.13	b.d.l.	1.09	1.0	3.53	1.0	1.54
Sr	819	960	52.0	66.9	22.0	31.6	56.5	71.3	100	128
Nd	9.0	22.7	17.0	17.8	8.0	6.94	8.5	14.6	4.0	6.53
Zr	103	176	114	165	40.0	65.3	90.0	140	63.5	101
Hf	b.d.l.	5.63	b.d.l.	4.12	b.d.l.	2.11	b.d.l.	4.33	b.d.l.	2.98
Sm	2.0	5.15	3.0	5.45	5.5	2.76	1.5	3.58	1.0	1.52
Eu		1.55		1.68		0.78		0.56		0.32
Gd		4.71		6.53		3.47		3.90		1.79
Tb		0.75		1.12		0.65		0.78		0.34
Dy		4.49		7.31		4.38		4.95		2.72
Y	26.0	24.4	40.5	42.3	22.0	24.1	22.5	23.7	15.0	15.5
Ho		0.93		1.55		0.92		1.04		0.62
Er		2.93		4.81		2.87		3.28		1.90
Tm		0.47		0.70		0.40		0.53		0.30
Yb	4.0	2.99	9.0	4.68	2.0	2.40	2.0	3.24	2.0	2.22
Lu		0.46		0.66		0.37		0.51		0.30

Additional discrimination diagrams were used to further clarify the tectonic setting of the protoliths of the metamafic rocks. In the Zr/Y-Zr diagram (Fig. 5.5a) by Pearce (1983), 130893 and Sp96-41b plot in the continental arc field, Sp96-41a in the oceanic arc field, and 18193 at the boundary between these fields. In the Nb/La-La/Sm diagram (Fig. 5.5b) by John et al. (2003), samples 18193 and Sp96-41a appear in the oceanic arc field, whereas 130893 and Sp96-41b are close to the continental arc field.

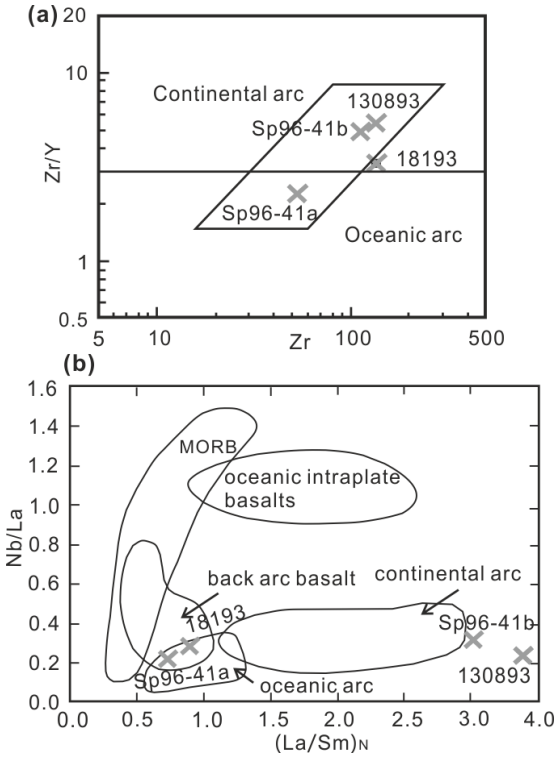

Fig. 5.5. Plots of bulk-rock data of three eclogites (samples 130893, 18193, Sp96-41a) and glaucophanite Sp96-41b in (a) the Zr/Y-Zr diagram by Pearce (1983); (b) the Nb/La-$(La/Sm)_N$ diagram by John et al. (2003).

5.6. Zr in rutile

For the geothermometric application of the Zr contents in rutile, we used the calibration by Tomkins et al. (2007). In addition, we focused on rutile included in garnet and omphacite (called here "included rutile"), but also considered rutile in the matrix ("matrix rutile"). Diffusional resetting has the effect that matrix rutile shows lower Zr contents than included rutile (Zack and Luvizottow, 2006; see also Taylor-Jones and Powell, 2015), whereas the shielding effect by porphyroblasts (garnet or pyroxene) avoids this resetting. Thus, the Zr-in-rutile thermometer is capable of recording high to

ultra-high-T conditions (e.g. Zhang et al., 2010; Ewing et al., 2013), especially peak temperatures that could not be recorded by any other thermometer. In all five samples, matrix rutile and included rutile record similar Zr contents (Fig. 5.6). For this reason, we conclude that the Zr contents in rutile did not experience diffusional resetting in our samples.

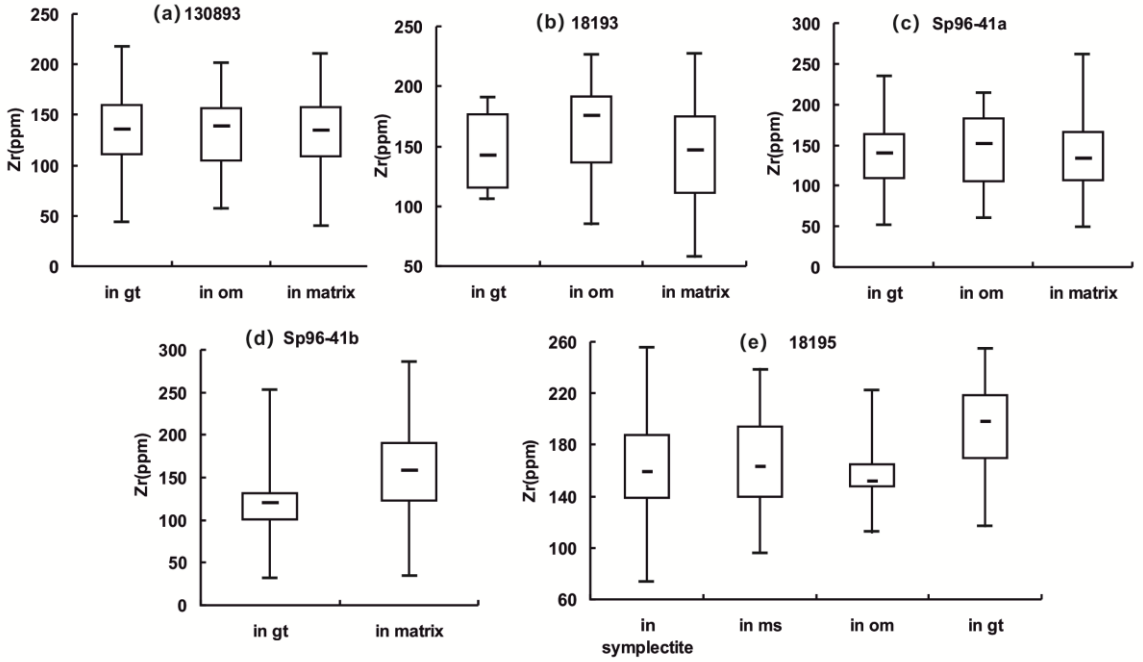

Fig. 5.6. Zr concentrations in rutile from all studied 5 samples sorted according to different appearances. Bottom and top of the boxes represent the first and third quartiles. The bar inside the box refers to the median.

In the eclogites, rutile is enclosed in garnet (Fig. 5.2d), omphacite, amphibole, symplectite replacing omphacite, and along grain boundaries between garnet, epidote, omphacite, amphibole, and kyanite. Subhedral (enlongated) or euhedral (round) small (6-20 μm in length or diameter) and subhedral large grains (100-300 μm in length) are found as included rutile and matrix rutile. Ilmenite lamellae are common in rutile, but were avoided when analyzing rutile. Two groups (low and high Zr contents) could be distinguished (Table 5.5) for each sample. These groups include measured Zr contents between 30-150 ppm (low Zr group) and 150-270 ppm (high Zr group). The mean values of the groups are around 110 ppm and 175 ppm yielding temperatures close to 640°C and 675 °C, respectively, at P = 26 kbar (T ~ 550 and 585 °C at P = 4 kbar).

In the glaucophanite Sp96-41b, rounded and enlongated rutile grains occur in both garnet and matrix (Fig. 5.6d). Only grains with sizes < 25 µm were found. Again two groups (low Zr contents: 23-150 ppm, high Zr: 151-253 ppm) (Table 5.5) of rutile occur in the core and rim of garnet. The high Zr rutile only appears in the garnet rim. The mean values of low- (Zr = 112 ± 27 ppm) and high-Zr (Zr = 187 ± 25 ppm) rutile yield a temperature of 660 ± 16 °C and 692 ± 9 °C, respectively, at P = 26 (Table 5.5).

Table 5.5. Zr contents in rutile and resulting temperatures related to P = 4 kbar and P = 26 bar. The temperatures were calculated using the equation for α-quartz given by Tomkins et al. (2007). The errors are related to 1σ for mean Zr contents and temperatures.

			mean Zr content	P = 4 kbar	P = 26 kbar
130893	low Zr contents	31-150 ppm	111 ± 29 ppm	550 ± 21 °C	637 ± 23 °C
	high Zr contents	151-237 ppm	173 ± 18 ppm	582 ± 8 °C	672 ± 8 °C
18193	low Zr contents	55-140 ppm	109 ± 21 ppm	551 ± 14 °C	638 ± 16 °C
	high Zr contents	141-235 ppm	175 ± 22 ppm	583 ± 9 °C	673 ± 9 °C
Sp96-41a	low Zr contents	50-150 ppm	110 ± 26 ppm	550 ± 17 °C	637 ± 19 °C
	high Zr contents	151-267 ppm	182 ± 27 ppm	586 ± 10 °C	676 ± 11 °C
Sp96-41b	low Zr contents	23-150 ppm	112 ± 27 ppm	571 ± 14 °C	660 ±16 °C
	high Zr contents	151-253 ppm	187 ± 25 ppm	600 ± 8 °C	692 ± 9 °C
18195	low Zr contents	67-180 ppm	143 ± 25 ppm	581 ± 11 °C	672 ± 13 °C
	high Zr contents	181-267 ppm	213 ± 22 ppm	606 ± 7 °C	700 ± 8 °C

Rutile in gneiss 18195 is as large as 40 µm. This mineral can be enclosed in garnet (Fig. 5.2h), omphacite, phengite (Fig. 5.2j), and symplectite around omphacite (Fig. 5.2i). Contents of Zr (67-267 ppm) are similar in rutile enclosed in the different minerals (Fig. 5.6e). Low- (67-180 ppm) and high-Zr (181-267 ppm) rutile occur in both core and rim of garnet. Ilmenite lamellae are common and some rutile grains in the symplectite are surrounded by titanite. The average values of low- (Zr = 143 ± 25 ppm) and high-Zr (Zr = 213 ± 22 ppm) rutile yield temperatures of 672 ± 13 °C and 700 ± 8 °C, respectively, at P = 26 kbar (Table 5.5).

5.7. P-T pseudosections

5.7.1. Calculation method for P-T pseudosections

P-T pseudosections were calculated using the software package PERPLE_X (see Connolly, 2005; update downloaded in August 2011 from the internet site

http://www.perplex.ethz.ch/) and the internally consistent thermodynamic data set (Holland and Powell, 1998 and updates) for minerals and H_2O (model CORK: Holland and Powell, 1991). The following solution models were applied from the downloaded version of the PERPLE_X file solution-model.dat: Chl(HP) for chlorite, Ep(HP) for epidote, feldspar for plagioclase and K-feldspar, GlTrTsPg for amphibole, Gt(HP) for garnet, Ctd(HP) for chloritoid, hCrd for cordierite, IlGkPy for ilmenite, MtUl(A) for magnetite, Mica(M) for paragonite with maximal 50% muscovite component, Omph(HP) for clinopyroxene, Opx(HP) for orthopyroxene, Pheng(HP) for phengite with maximal 50% paragonite component, St(HP) for staurolite, Stlp(M) for stilpnomelane, T for talc and TiBio(HP) for Biotite. Other phases such as rutile were considered as pure phase. The end-members tip, tbi, ann1, qfm, mthm, h2oL, ab, rieb, mrb, cumm, grun, and mic were excluded (see, e.g., Massonne, 2014). In addition, zo was excluded when the content of O_2 in the bulk-rock composition was above zero.

Table 5.6. Bulk-rock compositions from X-ray fluorescence spectrometry (Table 5.4) after modification (M1) for PERPLE_X calculations (see text). Compositions M2 refer to the subtraction of garnet core (+ mantle) compositions as explained in the text.

	130893		18193		Sp96-41a		Sp96-41b		18195	
	M1	M2	M1	M2	M1	M2	M1	M2	M1	M2
SiO_2	44.28	48.21	47.21	47.76	46.56	50.31	46.75	50.73	61.02	61.32
Al_2O_3	18.79	18.23	14.11	13.82	14.88	12.57	19.56	19.20	14.49	14.41
MnO	0.16	0.02	0.22	0.20	0.15	0.01	0.13	0.00	0.11	0.10
MgO	5.81	6.12	6.15	6.22	11.03	11.32	10.61	11.85	3.19	3.17
CaO	10.23	10.9	9.08	9.04	10.43	12.05	2.46	1.39	4.86	4.80
Na_2O	3.15	4.54	2.54	2.66	2.14	2.95	3.72	4.98	2.97	3.00
K_2O	0.29	0.41	0.18	0.18	0.17	0.23	0.07	0.09	0.78	0.79
TiO_2	0.63	0.88	1.97	2.06	0.67	0.88	0.54	0.72	0.40	0.40
FeO	9.16	3.19	12.35	11.85	7.39	3.14	8.67	3.54	5.69	5.51
O_2			0.21	0.20	0.08	0.03				
H_2O	7.50	7.50	6.00	6.00	6.50	6.50	7.50	7.50	6.50	6.50
total	100.0	100.0	100.0	100.0	100.0	100.0	100.0	100.0	100.0	100.0

As the system Na_2O-K_2O-CaO-FeO-O_2-MnO-MgO-Al_2O_3-SiO_2-TiO_2-H_2O was considered, we reduced the natural compositions to it (Table 5.6). For this purpose, the following principles were applied according to Massonne et al. (2013): (1) CaO was

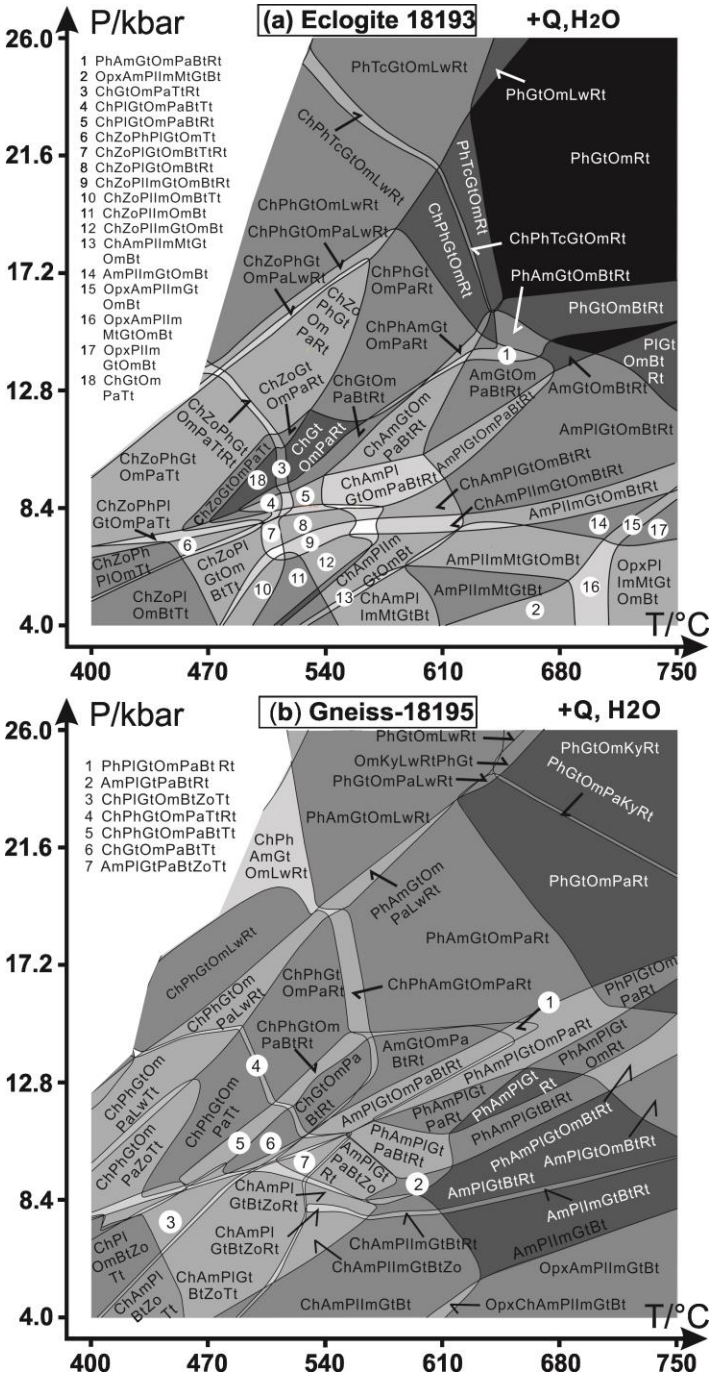

Fig. 5.7. P-T pseudosections calculated for the modified compositions of eclogite 18193 and glaucophanite Sp96-41b (Table 5.6, M_1) with the computer software package PERPLE_X (see text). The greytones of P-T fields refer to the variance (the darker the higher) of the corresponding mineral assemblage (+H_2O and quartz). Very small P-T fields are not labeled. Abbreviations are the same as in Fig. 5.2 and: botite (Bt), chloritoid (Ctd), ilmenite (Im), K-feldspar (Kf), lawsonite (Lw), magnetite (Mt), clinopyroxene (Om), orthopyroxene (Opx), plagioclase (Pl), stilpnomelane (Stlp), talc (Tc), titanite (Tt) and (clino)zoisite-epidote (Zo).

reduced according to the phosphorus contents in the rocks assuming that all phosphorus is bound in apatite, $Ca_5(PO_4)_3(OH)$. (2) The H_2O contents were enhanced to 6-7.5 wt% to permit the formation of a free hydrous fluid phase at relatively low temperatures. (3) The O_2 content was approximated according to estimated amounts of Fe^{3+} in the minerals and their modal contents of a rock. As this content can have a significant influence on the derivation of P-T conditions (see, e.g., Petrie et al., 2016), an independent control of these approximated values was achieved by calculating T-X_{O2} pseudosections at an estimated pressure. These pseudosections were contoured by isopleths for pyrope and grossular components in garnet.

In order to approach the effective bulk-rock composition for a late metamorphic stage (Table 5.6) at which the garnet rim formed, we subtracted the chemical composition of the garnet core (+ mantle in case of samples 13089 and Sp96-41b) from the bulk-rock composition (see, e.g., Marmo et al., 2002; Groppo and Rolfo, 2008). We subtracted 28 vol.%, 27 vol.%, 25 vol.%, 20 vol.%, 10 vol.% of the average garnet core (+mantle) composition from the bulk-rock of 130893, Sp96-41a, Sp96-41b, 18193, and 18195, respectively. Thus, we calculated altogether 10 P-T pseudections (2 for each sample) for the P-T range of 4-26 kbar and 400-750 ºC. As examples for the results of these calculations, we show only two of them (Fig. 5.7), one for eclogite 18193 and the other for tonalitic gneiss 18195. All P-T pseudosections were contoured by isopleths for the molar fractions of garnet components (grossular and pyrope, Fig. 5.8). In addition, examples for the contouring with isopleths for the modal content of garnet are shown in Figure 5.9.

5.7.2. Results of the calculated P-T pseudosections compared with petrographic observations

The calculated assemblages at eclogite-facies conditions (garnet-omphacite-quartz-phengite-H_2O) can include lawsonite (all samples), talc (in 18193, Sp96-41a, Sp96-41b), and chloritoid (Sp96-41b). However, these phases were not observed in the studied rocks. Thus, they were either replaced by phases such as garnet, clinopyroxene, amphiboles, quartz and epidote during a late metamorphic event or the P-T paths for the studied rocks did not cross the P-T fields containing them. On the contrary, kyanite appears in all P-T pseudosections, except for sample 18193, at eclogite

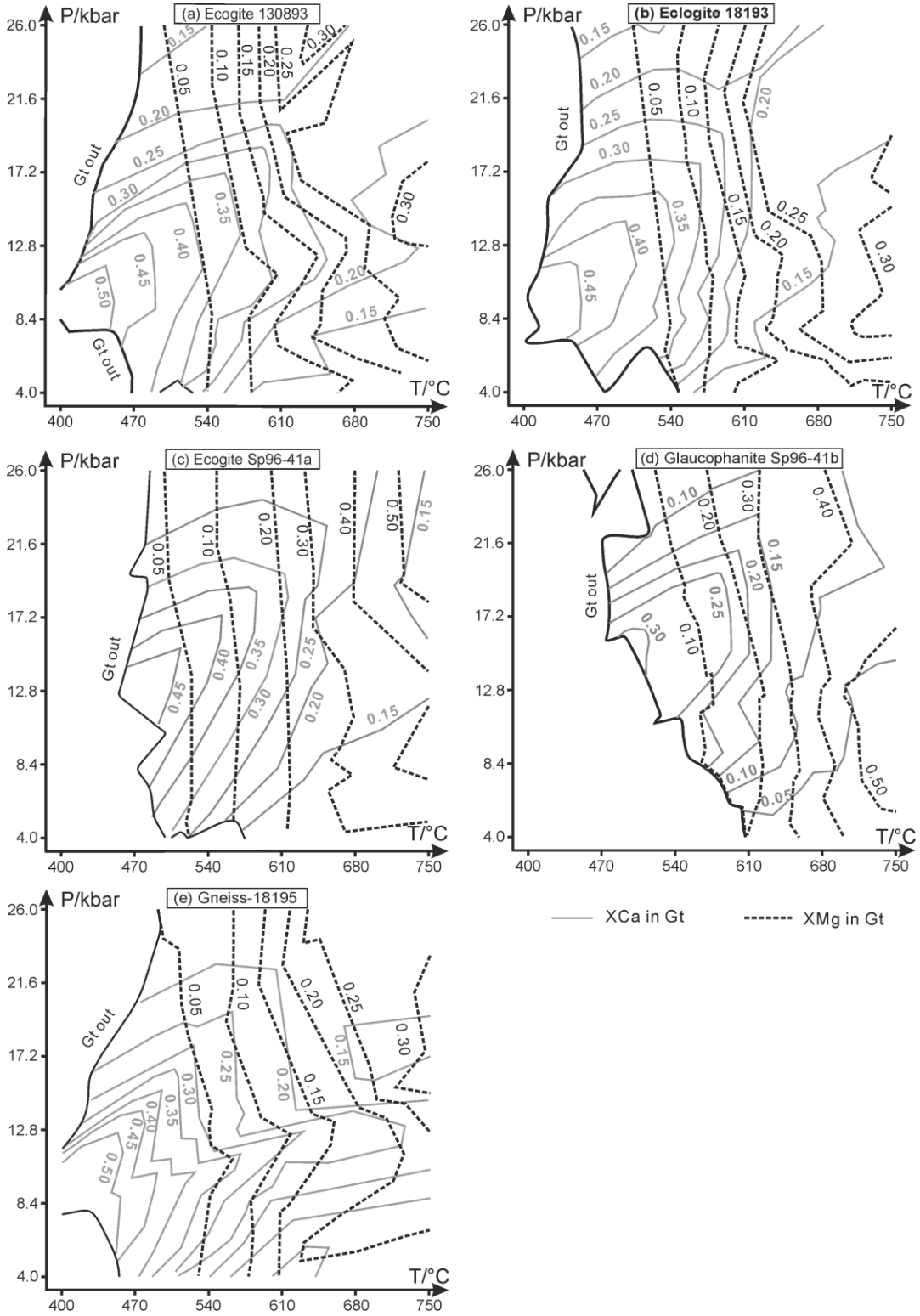

Fig. 5.8. Contouring of P-T pseudosections (see Fig. 5.7, those for samples 130893, Sp96-41a and Sp96-41b are not shown) by isopleths of the molar fractions of garnet components (grossular: XCa; pyrope: XMg).

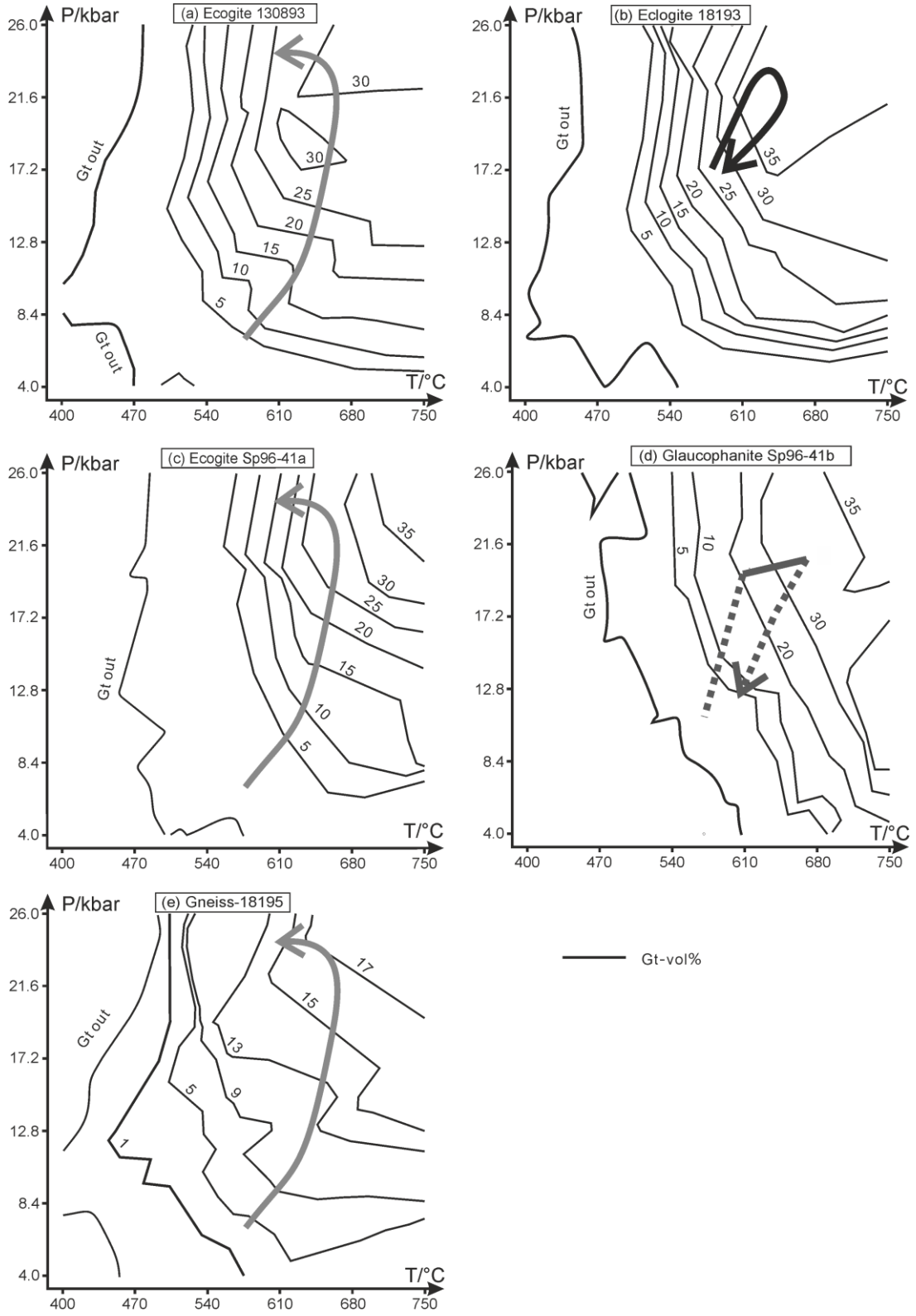

Fig. 5.9. Contouring of P-T pseudosections (see Fig. 5.7, those for samples 130893, Sp96-41a and Sp96-41b are not shown) by isopleths for the modal contents of garnet.

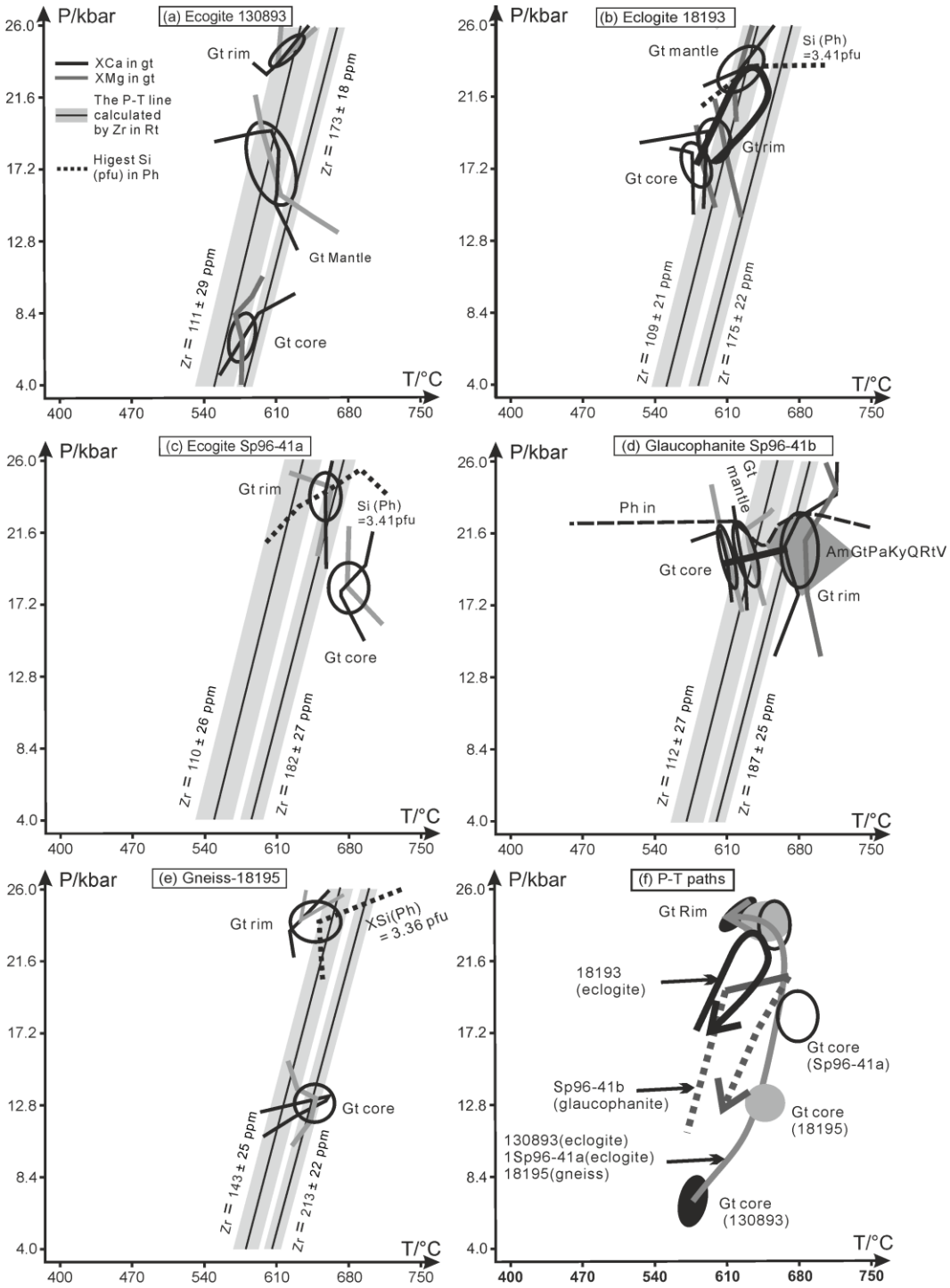

Fig. 5.10. (a-e) P-T estimates (ellipses, see also text) on the basis of intersecting isopleths for the compositions of the core, mantle, and rim of garnet (see Fig. 5.8)**.** The isopleths for garnet rims were calculated on the basis of effective bulk rock compositions (= bulk rock composition minus garnet core, see text). The straight lines result from the application of the Zr-in-rutile thermometer after Tomkins et al. (2007). The shaded areas around these straight lines refer to the 2σ errors. (f) Three different P-T paths (solid lines) for the studied rocks result. The dashed lines indicate uncertain parts of these paths.

facies conditions and was, indeed, observed in the corresponding rocks (Table 5.3). No paragonite and especially phengite, observed in the eclogites and the tonalitic gneiss, occurs in the P-T pseudosections at high T and low P (<15 kbar) due to dehydration reactions. Biotite, plagioclase and (clino)zoisite-epidote always appear at low P in accordance with the observation that they are late (see Fig. 5.2c, d, i) or early stage minerals. Amphibole occurs at pressures lower than 15 kbar in the P-T pseudosections for the three eclogites. In the P-T pseudosection for the glaucophanite, clinopyroxene only appears in a small range at pressures between 8 and18 kbar and at T <580 ºC. On the contrary, amphibole is present over almost the entire P-T pseudosection. In the P-T pseudosection for the gneiss, clinopyroxene appears at P > 18 kbar and T > 620 ºC. At these conditions amphibole is absent. Amphibole occurs at lower temperatures (T < 620 ºC) at high pressures or at T > 620 °C and lower pressures (P < 15 kbar) (Fig. 5.7b). This is compatible with the derived P-T path (see below) and the observation that amphibole has formed in the gneiss only in symplectites around omphacite (Fig. 5.2i).

5.7.3. P-T conditions

The subsequent quotation of P-T conditions is based on intersections (sometimes only approachs) of isopleths, mainly of garnet components. Due to analytical errors (see the data clouds in Fig. 5.10), we estimated a P-T range instead of quoting the exact P-T date resulting from the given mineral (garnet) composition. This range is defined by possible intersections of different mineral compositions within these analytical errors. In the corresponding graphs we present so-called error ellipses with the most likely P-T date in their center instead of the P-T ranges (or box) mentioned below. In addition, it is worthy of note that the uncertainties of the thermodynamic data, used for the derivation of P-T conditions, contribute to an additional error of the derived P-T conditions.

Eclogite 130893

The intersection of isopleths for the garnet core (XCa = 0.27, XMg = 0.09; Fig. 5.3c) in the P-T pseudosection for eclogite 130893 suggests that it grew in the range 565-590 ºC and 5.0-8.5 kbar (Figs. 5.8a, 5.10a). At this stage the oxygen content of the bulk rock was related to about 10 % of the iron being trivalent (subsequently: O_2 ~ 10%) according to a 'best-fit' approach in the constructed T-X_{O2} pseudosection for P = 7 kbar (not shown here). The corresponding isopleths for the garnet mantle (around XCa= 0.23, XMg = 0.20)

can intersect in a wide P -T range (580-630 ºC and 15-20 kbar) for the same O_2 content in the bulk rock. The isopleths for the garnet rim (XCa = 0.19, XMg = 0.32, O_2 ~ 10%) suggest that it grew at 610-640 ºC and 23.8-26.0 kbar (Figs. 5.8a, 5.10a).

According to the garnet elemental maps (Fig. 5.3a, b), the original garnet (core + mantle), was corroded resulting in a significant reduction of the garnet modal content before the formation of the garnet rim. The remaining content of garnet (core + mantle) after corrosion is ~ 30 vol.% (Fig. 5.9a) and, thus, yields a minimum pressure of ~ 18 kbar at 665 ºC.

Eclogite 18193

The intersections of isopleths for the compositions of the garnet core (XCa = 0.28, XMg = 0.16, Fig. 5.3f), mantle (XCa = 0.20, XMg = 0.26), and rim (XCa = 0.24, XMg = 0.23) in eclogite 18193 suggest garnet growth at 565-590 ºC and 16-19 kbar (core), 580-610 ºC and 17.5-20 kbar (mantle), and 595-640 ºC and 22-25 kbar (rim) (Figs. 5.8b, 10b). The corresponding P-T ranges were obtained for O_2 ~ 15% (garnet core and mantle, Table 5.6) and 30% (garnet rim) according to the aforementioned T-X_{O2} pseudosections (not shown here). The isopleth for the highest Si content (3.41 pfu) in phengite is compatible with the P-T range deduced for the garnet mantle (Fig. 5.10b).

According to the garnet elemental maps (Fig. 5.3d, e), the original garnet (core + mantle), was corroded resulting in a reduction of the garnet modal content to 35 vol.% before the formation of the garnet rim. This content points to a minimum pressure of ~ 18.5 kbar at 620 ºC (Fig. 5.9b).

Eclogite Sp96-41a

The isopleths for the compositions of the garnet core (XCa = 0.18, XMg = 0.40, Fig. 5.3i) and rim (XCa = 0.225, XMg = 0.38) intersect in the P-T ranges 650-700 ºC, 17-20 kbar and 640-675 ºC, 23-25 kbar, respectively (Figs. 5.8c, 10c). These intersections were obtained for O_2 ~ 10 %. The isopleth for the highest Si content (3.41 pfu) in phengite is compatible with the P-T range, in which the garnet rim grew. The isopleth for the lowest Si content (3.28 pfu) in phengite points to a lower metamorphic pressure (e.g. 13kbar around 580 °C) than derived for the growth of the garnet rim.

On the basis of garnet elemental maps (Fig. 5.3g, h) no or very little corrosion happened before the growth of the garnet rim. The modal content of the garnet core

derived from these maps is approximately 27 vol.%, which yields a pressure of ~ 21kbar at 670 ºC according to the isopleths of Fig. 5.9c. The isopleth for the entire garnet volume of 30 vol.% points to ~ 22 kbar at 675 ºC (Fig. 5.9c).

Glaucophanite Sp96-41b

According to the intersections of garnet isopleths at O_2 ~ 0%, core (XCa = 0.18, XMg = 0.25) and mantle (XCa = 0.15, XMg = 0.33) of garnet (Fig. 5.3) in the glaucophanite grew at 590-610 ºC, 18-22 kbar and 605-640 ºC, 18-22 kbar, respectively (Figs. 5.8d, 10d). The isopleths for XCa = 0.08 and XMg = 0.45 of the garnet rim cross the P-T field of the observed assemblage amphibole-garnet-paragonite-kyanite-quartz-rutile (Fig. 5.10d). Because of this match, this assemblage equilibrated with the garnet rim at 665-695 ºC and 18-22 kbar.

On the basis of garnet elemental maps (euhedral garnet core, see Fig. 5.3j, k) no or very little corrosion happened before the growth of the garnet rim. The modal content of garnet (only core+mantle) is ~25 vol.% and yields a pressure of 19.5 kbar at 635 °C (Fig. 5.10d). Thus, the corresponding isopleth for the given garnet volume is compatible with the above derived pressure range of 18-22 kbar. The isopleth for the entire garnet volume of 30 vol.%, points to ~ 19.5 kbar at 660 ºC (Fig. 5.9d).

Tonalitic gneiss 18195

The isopleths for the garnet rim (XCa = 0.18, XMg = 0.28, Fig. 5.3o) and the cluster of the highest Si contents (3.36 pfu) in phengite define peak pressure conditions of P = 23-25 kbar at 630-675 ºC (Figs. 5.8e, 10e). The garnet core (XCa = 0.28, XMg = 0.14) grew at 630-665 ºC and 11.5-14 kbar according to the correponding isopleths calculated for O_2 ~ 0 % confirmed by the modal content of garnet (only core) estimated to be ~ 10 vo.l% (Fig. 5.9e). The entire garnet volume (16 %) would be compatible with ~ 21.5 kbar at ~ 670 ºC, but this pressure is somewhat lower than the pressure range estimated from the garnet rim composition and the highest Si content in phengite (see above).

5. 8. Discussion

5.8.1. Protoliths and their geotectonic environments

Geochemical data for the four metamorphosed mafic rocks plot at or above the MORB-OIB array (Fig. 5.4a) suggesting a more or less strong contamination of mantle magmas by continental material before forming the igneous protoliths. This is typical for

calc-alkaline rocks of magmatic arcs, to which also the geochemical data of samples 130893 and Sp96-41b, plotted into the applied discrimination diagrams (Figs. 5.4b, c and 5.5a, b), point to. In addition, the relative enrichment in Th (although a relatively mobile element during metamorphism) and depletion in HFSE such as Nb (Fig. 5.4e) give evidence for suprasubduction zone settings, in which the protoliths of samples 130893 and Sp96-41b were involved in. However, samples 18193 and Sp96-41a show rather a tholeiitic affinity and are not characterized by high contents of LILE (Fig. 5.4c, e). Thus, they might be only weakly affected by continental material (see John et al., 2004; Andonaegui et al., 2016) and, therefore, the protoliths of these samples could belong to an oceanic arc setting. However, eclogites showing flat REE pattern as samples 18193 and Sp96-41a could also be metamorphosed oceanic crust (see, e.g., Massonne & Czambor, 2007), as basaltic melts, building this crust, were usually formed in a depleted mantle.

A similar conclusion, as drawn here for eclogite 130893 and glaucophanite Sp96-41b, was presented by Abati et al. (2010) and Díez Fernández et al. (2012b) based on zircon dating for other calc-alkaline rocks (gneisses and eclogites) of the MTZ. The continental magmatic arc proposed by these authors formed at ca. 490-500 Ma. Abati et al. (2010) and Díez Fernández et al. (2012b) additionally suggested that an alkaline to peralkaline magma suite formed at 472 ± 2 Ma (dated by Rodríguez et al., 2007), which is ~20 Ma younger than the calc-alkaline magma suite formed in the same tectonic unit as assumed by these authors. However, our investigated tholeiitic HP rocks 18193 and Sp96-41a show different geochemical features compared to the aforementioned calc-alkaline and alkaline-peralkaline igneous protoliths. The features of these HP rocks are rather similar to that of an eclogite body in the northern MTZ reported by Li and Massonne (2016). These authors proposed that the protolith of this eclogite body belonged to the above invoked oceanic island-arc setting. Furthermore, Li and Massonne (2016) speculated that this setting occurred in the Rheic Ocean and was formed by intraoceanic subduction. It is noteworthy, that Andonaegui et al. (2016) reported tholeiitic metamorphic rocks in the Órdenes complex (Fig. 5.1), located east of the MTZ, showing similar geochemical characteristics (e.g., negative Nb anomaly, data plot in the oceanic arc field of the Zr/Y-Zr diagram) as our samples 18193 and Sp96-41b. Unfortunately,

these authors were not able to decisively locate the protoliths of these rocks from the Órdenes complex in their model of the Late Cambrian continental arc.

The tonalitic gneiss 18195 shows a subalkaline affinity as metatonalites from the 'La Pioza' land site analyzed by Abati et al. (2010). These authors deduced a magmatic age (494±3 Ma) which is identical with those of other calc-alkaline or subalkaline (see Arculus, 2003) rocks from the MTZ (Díez Fernández et al., 2012b). Thus, we suggest that the protolith of sample 18195 formed in the same continental arc unit as calc-alkaline eclogite 130893 and glaucophanite Sp96-41b.

5.8.2. P-T paths

The thermodynamic calculations of pseudosections, including their contouring with various modal and chemical parameters, yielded peak pressures at about 24 ± 2 kbar (section 5.7.3) for four of the five studied samples. Only for the glaucophanite a lower peak pressure of 20 ± 2 kbar was derived, which is, however, still clearly in the P-T field of the eclogite facies. For these HP conditions, the results from the Zr-in-rutile thermometry (section 5.6.) and the temperatures obtained from the thermodynamic calculations of pseudosections are broadly compatible. For the glaucophanite and eclogite Sp96-41a, both methods yielded peak temperatures between 665-700 °C. For the other three studied rocks, these temperatures obtained from the Zr-in-rutile thermometry are c. 20-35 °C higher than those derived from the pseudosections (e.g. 640 °C and 675 °C at 26 kbar for eclogite 130893).

The applied geothermobarometry (see sections 6. and 7.3) results in an anticlockwise P-T path (eclogites 130893 and Sp96-41a, gneiss 18195) and two different clockwise P-T paths which are depicted in Figure 5.10f. The anticlockwise P-T path starts at 565-590 ºC and 5-8.5 kbar (eclogite 130893) or at significantly higher P-T conditions: 650 ºC and 17-20 kbar (eclogite Sp96-41a). Thus, it might be that the anticlockwise paths for two eclogites and the gneiss are only similar but not identical. Nevertheless, the anticlockwise path reached peak pressures of 23-26 kbar at 610-675 ºC, although this temperature range might also signalize that the peak temperatures for the three rocks were not identical (peak T for 130893 was lower than for Sp96-41a).

Eclogite 18193 shows a clockwise P-T path, which starts at 565-590 ºC and 16-19 kbar and reaches peak conditions at 595-640 ºC and 22-25 kbar. This path is

characterized by a temperature increase between 5 °C and 10 °C per one kbar and, thus, a gradient of only 2-3 °C/km. The glaucophanite shows another type of clockwise P-T path, which is characterizes by a significantly higher gradient (T increase from c. 600 ºC to 665 ºC at nearly constant pressure) and a peak pressure of only 20 ± 2 kbar (see above). Excepting this path, all other P-T paths derived here show a nearly isothermal burial, which is most obvious for eclogite 130893. However, the corrosion event discernable in the element distribution maps of garnet (Fig. 5.3a, b) from this rock suggests that a simple burial to depths of 80 km (~ 25 kbar), which would lead to continuous growth of garnet, cannot have taken place. An alternative could be two different prograde paths each followed by retrogression: the first prograde path reached solely peak conditions of ~ 7 kbar and 580 °C, whereas only the subsequent one led to HP conditions. In spite of this consideration, a nearly isothermal prograde path for an eclogite of the MTZ was already reported by Li and Massonne (2016). This path is clockwise with peak pressure conditions of 22.5 kbar and, thus, similar to the rocks studied here. Maximum temperatures, were, however, lower (somewhat less than 600°C at pressures > 20 kbar). Other clockwise P-T paths for eclogites of the MTZ were reported by Rodríguez et al. (2003: peak pressure of 21 kbar at 580 °C), López-Carmona et al. (2014b: 26 kbar at 650 °C), and Gil Ibarguchi (1995: 675 ± 30 ºC at a mimimal pressure of 16 ± 1 kbar). The peak temperatures estimated by the latter author are similar to those deduced here.

The peak temperature for the tonalitic gneiss 18195 (630-675 °C) is significantly higher than that of 580ºC at 21 kbar reported by Rodríguez et al. (2003) for an eclogitic gneiss of the central MTZ. Peak temperature conditions of 655 ± 30 °C (at a minimal pressure of 15.5 ± 1 kbar) derived by Gil Ibarguchi (1995) for a HP orthogneiss are compatible with our results. The HP gneiss from the northern MTZ studied by Li and Massonne (2016) experienced, in fact, a peak temperature (625 °C) almost as high as derived for sample 18195, but the peak pressures of these gneisses differ significantly (13.5 versus 24 kbar). This requires further comments. The tonalitic gneiss 18195 is part of the 'La Pioza' eclogite assembly and not identical to the surrounding gneisses which are more felsic (named granitic and perakaline gneisses by Rodríguez et al., 2003 as well as felsic and biotite-rich orthogneisses by Rivas-Koslowski, 1995) and contain only occasionally garnet. The modal content of garnet in an ordinary gneiss changes with P-T

conditions as was quantitatively worked out by Massonne (2009). On this basis, this author concluded, for instance, that the frequently garnet-free gneisses of the Sulu ultrahigh-pressure (UHP) terrane, which do not contain Na-rich clinopyroxene either, have never experienced UHP and probably HP conditions neither. A similar conclusion can be drawn here: it is unlikely that the widespread, garnet-poor, sodic clinopyroxene-free country rocks surrounding the 'La Pioza' eclogite assembly have experienced pressures in excess of 15 kbar. However, this petrographic hint has to be further constrained by further studies.

5.8.3. Geotectonic implications from the deduced P-T paths

This study has demonstrated that the rocks of the 'La Pioza' eclogite assembly have experienced HP conditions (> 18 kbar). However, the P-T paths of these rocks differ from each other being clockwise and anticlockwise probably with peak temperatures which are slightly distinct. In addition, the prograde path of the studied rocks with anticlockwise path is rather characterized by nearly isothermal pressure increase, which is untypical for subducted oceanic crust. Furthermore, the geotectonic environment of the protoliths of the studied rocks is different (see above: continental magmatic arc, oceanic island-arc). Previous models such as those by Martínez Catalán et al. (1996), Arenas et al. (2009), Díez Fernández et al. (2011, 2012a, 2012b), Rodríguez et al. (2003), and Rubio Pascual et al. (2013), including that by Ballèvre et al. (2012) related to the extension of Variscan NW Spain to the French Armorican Massif, do not account for the above features because coherency of crustal sections was anticipated. However, this coherency is even not valid for the solely km^2-sized area of the 'La Pioza' eclogite assembly. Only the recently presented geodynamic model by Li and Massonne (2016) for the Iberian Gondwana margin in late Paleozoic times offers a scenario where HP rocks come together at a late stage of a collisional evolution after experiencing metamorphic conditions along different P-T paths. We modified this scenario to account for our new findings.

A central element of our geodynamic scenario (Fig. 5.11) is the subduction channel, which is located between downgoing (oceanic) slab and overlying mantle wedge. In this subduction channel various HP-UHP rocks are subject of the upwards-directed forced mass-flow (e.g., Massonne, 2012). The concept of this channel flow is based on 2-dimensional numerical modeling experiments as presented, for instance, by Gerya et al.

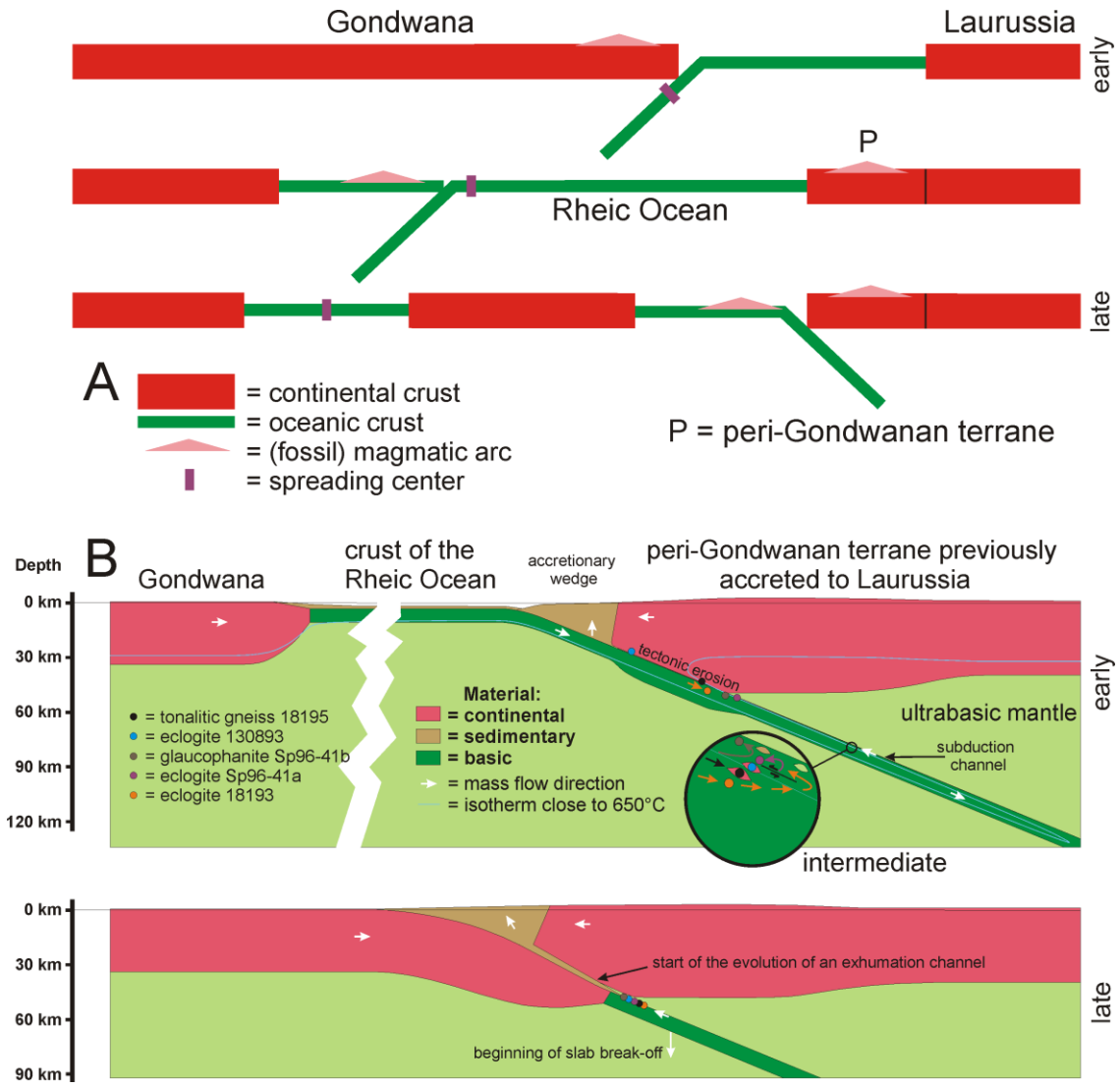

Fig. 5.11. Two-dimensional geodynamic scenario to explain the metamorphic evolution of the studied rocks. (A) Sketch to show the closure and opening of oceans between Gondwana and a continental plate north of it (here called Laurussia, see text) in Paleozoic times (Cambrian to Devonian) due to an apparently migrating spreading center (the center is fixed but the plates move). (B) Subduction and tectonic erosion resulting in HP rocks which were brought together in the upwards-directed mass flow of the subduction channel. This scenario, originally presented by Massonne (2012), was modified also to account for the subduction of an island arc (thickened oceanic crust). For the further evolution of the rocks in the exhumation channel between the colliding continental plates see Massonne (2012). For the geodynamic scenario related to the contact of the studied rocks with felsic HP rocks of the downgoing continental slab see Li and Massonne (2016).

(2002). These experiments as well as previous considerations of the thermal structure of a subduction zone (Toksöz et al., 1971) demonstrate that there is a considerable lateral thermal gradient from the hot mantle wedge to the cold downgoing slab. Thus, a P-T path of an eclogite, which shows a nearly isobaric heating before reaching peak P-T conditions, can be explained by a nearly lateral approach to the hot mantle wedge in a subduction zone as was suggested by Massonne and Kopp (2005: prograde path from 480 °C, 25 kbar to 720 °C, 27 kbar). On the contrary, a P-T path of a HP-UHP rock, which is characterized by an anticlockwise loop with cooling close to the peak pressure as derived here for eclogites 130893 and Sp96-41a as well as gneiss 18195, should be the result of the opposite movement (away from the mantle wedge). Thus, it is hypothesized that the somewhat different P-T paths at pressures > 15 kbar, including peak pressures and temperatures, of the 'La Pioza' rocks reflect diverse movements of rock volumes from the downgoing slab to the subduction channel and within this channel at depths of about 60 to 80 km (Fig. 5.11b). These rock volumes might stem from the subducted oceanic crust (Rheic Ocean) thickened by the formation of an island arc (samples 18193 and Sp96-41a, see section 5.8.1), but also from the margin of the overriding continental plate where a magmatic arc had been previously settled (Fig. 5.11a). At least, eclogite 130893, for which a nearly isothermal burial path starting at a pressure of about 7 kbar (~ 25 km Earth's depth at which a temperature for the early stage of 130893 of about 575 °C prevailed) was derived, is a clear candidate for the latter protolith source. It is hypothesized that this metabasic rock was involved in the subduction by tectonic erosion as the eclogite from the northern MTZ studied by Li and Massonne (2016). This erosional event could have been caused by the subduction of thickened oceanic crust (Fig. 5.11b) as proposed by Kay et al. (2005) for the late Tertiary subduction along the western margin of the South American plate.

The above invoked involvement of rocks from both island arc and continental magmatic arc in the here relevant HP metamorphism requires the consideration of early Paleozoic subduction and opening of oceans between Gondwana and a continental plate which is called here for simplicity Laurussia (actually formed after the Iapetus Ocean was closed at the end of the Silurian). Previous authors (e.g., Matte, 1998; Rodríguez et al., 2003; Arenas et al., 2009, 2014) had proposed an ocean between Gondwana and a part of

the plate which became Laurussia later. The subduction of the corresponding oceanic plate was accompanied by the formation of a magmatic arc at the margin of Gondwana. We assume that the spreading center of this ocean was also subducted and was then responsible for the formation of a new ocean (Rheic Ocean) between the separated part of Gondwana (a peri-Gondwanan terrane) and the remaining Gondwana plate (Fig. 5.11). After a considerable evolution of the Rheic Ocean an intraoceanic subduction occurred, leading to the formation of an island arc within this ocean. Again, the spreading center was subducted below Gondwana and the Rheic Ocean could not be extended anymore. The remaining part of this ocean was finally completely subducted below Laurussia in late Devonian times. During this process, the aforementioned island arc was also subducted and, thus, could meet with the fossil magmatic arc of the peri-Gondwanan terrane. This scenario, although speculative, would at least explain the concourse of rocks from both arcs.

5.9. Conclusions

The detailed study of HP rocks from the 'La Pioza' land site, including those reported recently by Li & Massonne (2016) from the northern MTZ, has resulted in the following findings: (1) HP rocks from the MTZ are not part of coherent crustal sections. These rocks were tectonically mixed still at HP conditions. (2) Concerning rocks which had experienced pressures in excess of 18 kbar, this mixing occurred already in the subduction channel. (3) Some of the rocks studied here and by Li & Massonne (2016) were transported into the subduction zone by tectonic erosion.

These findings are based on the derivation of P-T paths, but are additionally supported by the different geotectonic nature (island arc, continental magmatic arc) of the protoliths according to the study of the geochemical features of major and trace elements. The geodynamic scenario of Figure 5.11 offers an explanation why such rocks from different geotectonic environments can be involved in the same subduction zone where they meet in its subduction channel.

6. Metamorphic evolution of eclogite- and amphibolite-facies metapelites from the Ceán unit, Malpica-Tuy shear zone in NW Spain

by

Botao Li, Hans-Joachim Massonne*

Institut für Mineralogie und Kristallchemie, Universität Stuttgart, Azenbergstr. 18, D-70174 Stuttgart, Germany

*corresponding author: H.-J. Massonne, Tel.: +49-711-68581225,

Fax: +49-711-68581222, * e-mail: h-j.massonne@mineralogie.uni-stuttgart.de

In submission

Highlights:

Prograde path of high-pressure metapelite of the Ceán unit points to tectonic erosion

Metapelite of the northern Malpica-Tuy zone experienced different peak pressures

Monazite ages confirm Upper Devonian to late Carboniferous metamorphic events

Abstract: Metapelites from the northern Malpica-Tuy shear zone (Ceán unit) were studied to decipher their pressure-temperature (P-T) evolution, based on chemically zoned garnet, phengite and other minerals, using P-T pseudosections. In addition, monazite ages were determined with the electron microprobe. The two studied chloritoid schists experienced peak P-T conditions around 21 kbar at 570 °C and a subsequent isothermal exhumation. The prograde path is characterized by a pressure increase of about 8 kbar starting at temperatures of 450-500 °C and, thus, points to a tectonic erosion event caused by a subducting (oceanic) slab. A staurolite-andalusite bearing schist experienced only peak pressures of 9 kbar at a temperature around 570 °C since garnet and potassic white mica with Si contents above 3.2 per formula unit are lacking. This rock might represent metamorphosed sediments that were originally at the surface of the downgoing continental plate. These metasediments were tectonically mixed at the

subducted channel and then exhumed together to form the upper portion of the Malpica-Tuy shear zone. The ages of one hundred eleven monazite analyses are in the range of 307-385 Ma and, thus, confirm previously determined Upper Devonian to late Carboniferous metamorphic events.

Key words: Metapelite, Malpica-Tuy shear zone, Monazite age, Garnet, P-T pseudosection

6.1. Introduction

In order to better understand the processes during continent-continent collision, rocks, occurring in suture zones between the collided plates, are worth to be investigated in detail. The Malpica-Tuy (also Tui) shear zone (MTZ), located in the northwestern Iberian Peninsula (Fig. 6.1), is such a suture zone that resulted from the collision of northern Gondwana (or peri-Gondwanan microcontinents) with Laurussia (e.g. Matte 2001; Nance et al., 2010; Schulmann et al., 2014). Our recent study on adjacent eclogite and gneiss from the Malpica-Tuy unit of the MTZ demonstrated that both rock types had experienced different early metamorphic and peak-pressure conditions (Li & Massonne, 2016). This result is in contrast to a coherent crustal section of this unit suggested in previous works (Martínez Catalán et al., 1996; Rodríguez et al., 2003; Rubio Pascual et al., 2013). Our new finding resulted in suggestions for a modified geodynamic model for the Variscan collision in northwestern Iberia. This motivated us to have a closer look to the Ceán unit which overlies the Malpica-Tuy unit and is also considered as a coherent unit with oceanic affinity (López-Carmona et al. 2010, 2013; Díez Fernández et al., 2011).

The main target of our work was to decipher P-T conditions of various metapelites from the Ceán unit and to compare the results in order to draw conclusions on the geodynamic evolution of these rocks and tectonic models explaining this evolution. The strategy, applied in this work to reach the wanted results, involved (1) the precise determination of the variable composition of minerals, especially the relation of textural position and chemical zonation, with the electron microprobe (EMP),(2) the calculation of P-T pseudosections and their contouring with relevant modal and chemical parameters, and (3) the construction of P-T paths using the contouring of the pseudosection and the analyzed mineral compositions (see, e.g., for metapelites Massonne & Calderón, 2008;

Massonne & Toulkeridis, 2012; Cruciani et al., 2013). In addition, the determination of monazite ages with the EMP was achieved in order to relate specific metamorphic events to time. This combined strategy was already successfully applied to metapelites by Balen et al. (2015) and Massonne (2014, 2016).

It turned out again, that metamorphic rocks with significantly different peak pressures occur in the same unit. On the one hand, rocks from the Ceán unit with easily discernable chloritoid and garnet have experienced high-pressure (HP: > 10 kbar) conditions (17-23 kbar: Arenas et al., 1995; López-Carmona et al., 2010). On the other hand, abundant garnet-free metapelites of this unit were subject to medium-pressure (MP: 5-10 kbar at temperatures around 500 °C) metamorphism only. Thus, the Ceán unit is not as coherent as assumed by previous authors (e.g. López-Carmona et al., 2013; Díez Fernández et al., 2011) and requires a modified geodynamic scenario compared to earlier ones.

6.2. Geological setting

Five allochthonous metamorphic complexes (MTZ, Cabo Ortegal, Órdenes, Bragança and Morais complexes) occur in the northwestern Iberian Massif (Fig. 6.1a) that is part of the European Variscan orogen formed by the collision of Laurussia and Gondwana (Andonaegui et al., 2012; Díez Fernández et al., 2011, 2012; Díez Fernández & Martínez Catalán, 2012). In these complexes, several crustal slices with different origin were distinguished. These slices are the so-called upper, ophiolitic, and basal units from the top to the bottom. The upper unit consists of exotic terranes with Gondwanan affinity; the ophiolitic unit is considered to represent a collisional suture, whereas the basal unit is interpreted to be the most external continental margin of Gondwana (Abati et al., 2010; Andonaegui et al., 2012).

The MTZ (Fig. 6.1b) is the westernmost allochthonous complex in the northwestern Iberian Massif. This complex is mainly composed of the basal unit (Díez Fernández et al., 2012; Díez Fernández & Martínez Catalán, 2012). However, some authors subdivided the MTZ in a lower continental and an upper oceanic subunit (Ceán unit: Rodríguez et al., 2003; López-Carmona et al., 2013). The contact between these subunits is marked by a several meter thick zone of mylonites and ultramylonites located at the base of the Cambre amphibolites (Díez Fernández et al., 2011; López-Carmona et al., 2013). The

lower subunit (also called Malpica-Tuy unit) consists of variably deformed and recrystallized granitoids, metasediments and sparse metabasites (Fig. 6.1b). The upper subunit (Ceán unit), which is ascribed to the aforementioned ophiolitic unit, may be metamorphosed during a subduction event. The exhumation included the thrusting over the continental subunit. In the Armorican Massif of Brittany, western France, similar units occur (Ballèvre et al., 2014). The lower continental subunit can be correlated with the Champtoceaux complex (Ballèvre et al., 1994, 2009) and the upper oceanic subunit with the Île de Groix metabasites and metasediments (Shelley & Bossiére, 1999; Ballèvre et al., 2003).

The Ceán unit crops out mainly along a coastal strip east of the town of Malpica (Fig. 6.1b). This unit is composed of (1) a sequence of massive finely foliated amphibolites with lawsonite-pseudomorphs and a thicker metasedimentary sequence (Arps, 1981) "consisting of pelitic schists (Ceán Schists) and minor intercalations of ampelites, lydites and carbonates" (López-Carmona et al., 2010). These rocks developed almost entirely under blueschist-facies conditions (López-Carmona et al., 2010, 2013; Díez Fernández et al., 2011). Rodríguez et al. (2003) pointed out that no eclogite-facies assemblages have been found in rocks of the Ceán unit. Peak metamorphic conditions of 14-18 kbar at temperatures below 550 °C were given by Rodríguez Aller (2005) for these rocks. P-T paths of chloritoid-glaucophanite schists, lawsonite blueschists and blueschist-facies metapelites were deduced by using isochemical phase diagrams (pseudosections), resulting in peak conditions of 500 ºC at 17-18 kbar, 560 ºC at 22 kbar, and 520ºC at 21-22 kbar, respectively (López-Carmona et al., 2010, 2013, 2014). These conditions experienced by country rocks (gneisses) from the Malpica-Tuy unit, occurring close to the Ceán unit, are around 13.5 kbar and 625 °C (Li and Massonne, 2016). Eclogite bodies embedded in these gneisses were subject to significantly higher pressures of 22.5 kbar at 540 °C (Li and Massonne, 2016). Peak P-T conditions determined for rocks from the Ile de Groix are 17-23 kbar at 450-525 ºC and 12-16 kbar at 450 ºC for the blueschist-facies event in the Upper unit and Lower unit, respectively (Bosse et al., 2002;Ballèvre et al., 2003; El Korh et al., 2009). Previous dating of phengite in schists from the Ceán unit have yielded $^{40}Ar/^{39}Ar$ plateau ages of ca. 365 and 350 Ma (Rodríguez et al., 2003; López-Carmona et al., 2014). The older age was interpreted as the age of the peak

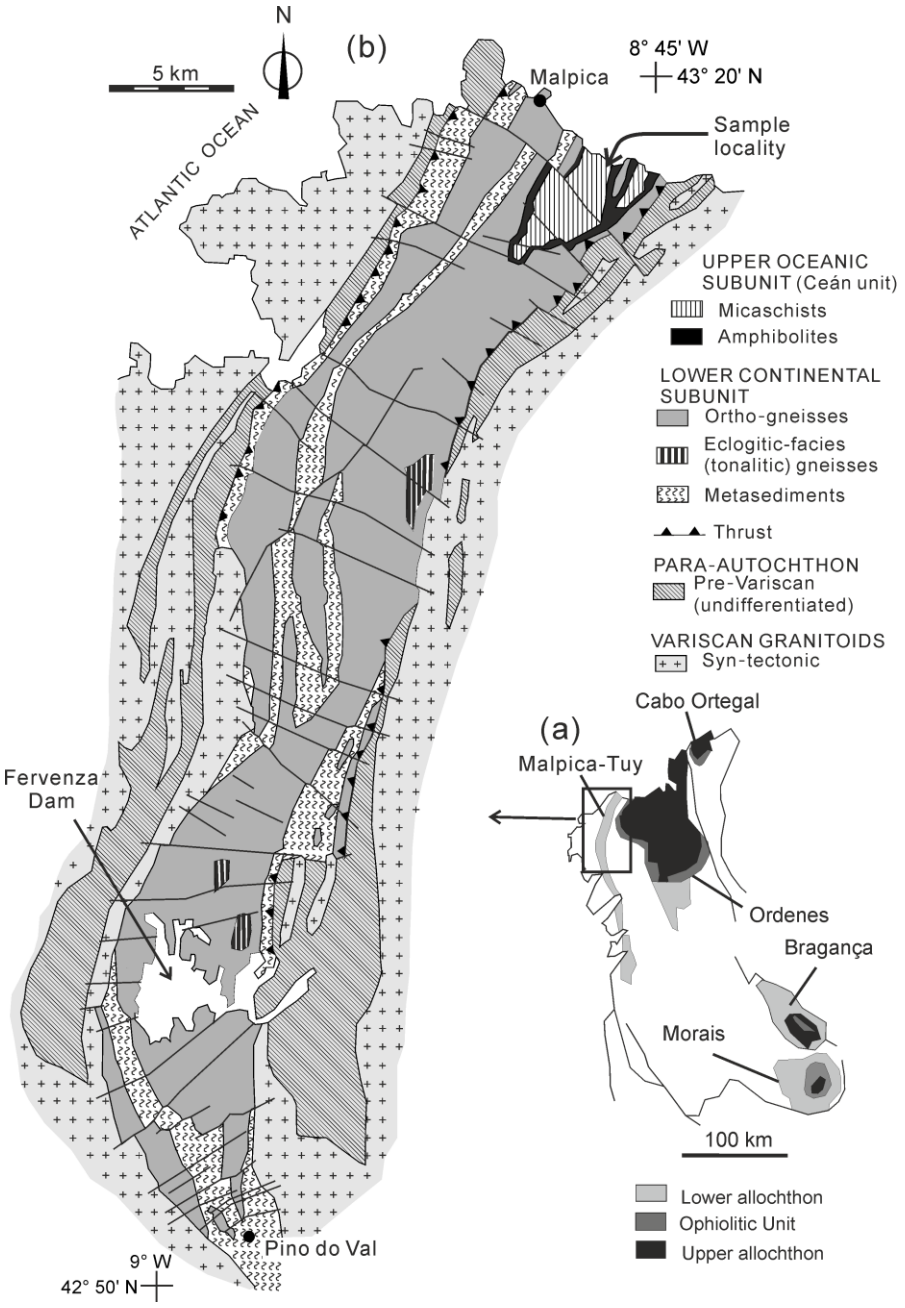

Fig. 6.1. (a) Geological frame of the Malpica-Tuy shear zone (MTZ) located in the Palaeozoic orogenic belt of NW Iberia modified after Santos Zalduegui et al. (1995). (b) Geological map of the MTZ after Rodríguez et al. (2003).

blueschist facies metamorphism in agreement with the HP event at 365-370 Ma dated for rocks from the Malpica-Tuy unit (Van Calsteren et al., 1979; Santos Zalduegui et al., 1995; Rodríguez et al., 2003; Abati et al., 2010). The younger age was considered as a cooling age. Similar ages (Rb-Sr: 345-353 Ma; $^{40}Ar/^{39}Ar$: 358-366 Ma; U-Pb titanite: 366

± 33 Ma) were obtained from the blueschists of the Ile de Groix (Bosse et al., 2005; El Korh et al., 2012). Older ages, obtained on zircon (around 480 Ma and 546-647 Ma), were reported by El Korh et al. (2012) and referred to magmatic emplacement in the Early Ordovician and inherited grains from a Cadomian basement.

6.3. Sampling and petrography

At the beach of O Riás, ca. 7 km southeast of Malpica, rocks of the Ceán unit (Fig. 6.1b) are exposed along cliffs. Large rounded pebbles of these rocks are lying below these cliffs. Numerous samples were hit from large, but flat, oval-shaped (minimum of the long axis: 30 cm) pebbles during excursions in the years 1993 and 1996. In the paper, we focus on two silvery metapelites with easily discernable chloritoid and a metapelite in which staurolite was detected in thin-section. The chloritoid schists (sample numbers Sp96-39j and Sp96-39k) were collected from the western margin of the beach of O Riás (N43°17’39”, W8°44’56”). The staurolite-bearing sample (Sp96-38w) was taken from the eastern side of the beach (N43°17’36”, W8°44’44”), ca. 300 m east of the Sp96-39 locality.

6.3.1. Staurolite-andalusite bearing schist 38w

The staurolite-andalusite bearing schist mainly contains muscovite (40 vol.%), biotite (20 vol.%), quartz (17 vol.%), chlorite (12 vol.%), plagioclase (6 vol.%), K-feldspar (2 vol.%) and andalusite (1 vol.%). Accessory minerals are staurolite, tourmaline, apatite, ilmenite and monazite. Most euhedral muscovite (mean size 0.5×0.05 mm^2), and subhedral to anhedral biotite (mean size 0.2×0.03 mm^2) build up a well-developed extensive foliation, but some mica grains are oblique to the main foliation (Fig. 6.2a) indicating two deformational events. Recrystallized fine-grained quartz is anhedral to subhedral with sizes mainly between 0.1 and 0.4 mm. Quartz-rich layers with thicknesses of 0.5-3 mm, alternate with mica layers. Porphyroblastic plagioclase with an average size of 0.5 mm is elongated along the main foliation, commonly associated with muscovite and chlorite in pressure shadows (Fig. 6.2a).

The rock is significantly retrograded, for instance, discernable by randomly oriented chlorite with average size of 0.2-0.05 mm (Fig. 6.2a). K-feldspar appears in late undeformed veins with width of ca. 0.2 mm (Fig. 6.2c). Porphyroblastic euhedral

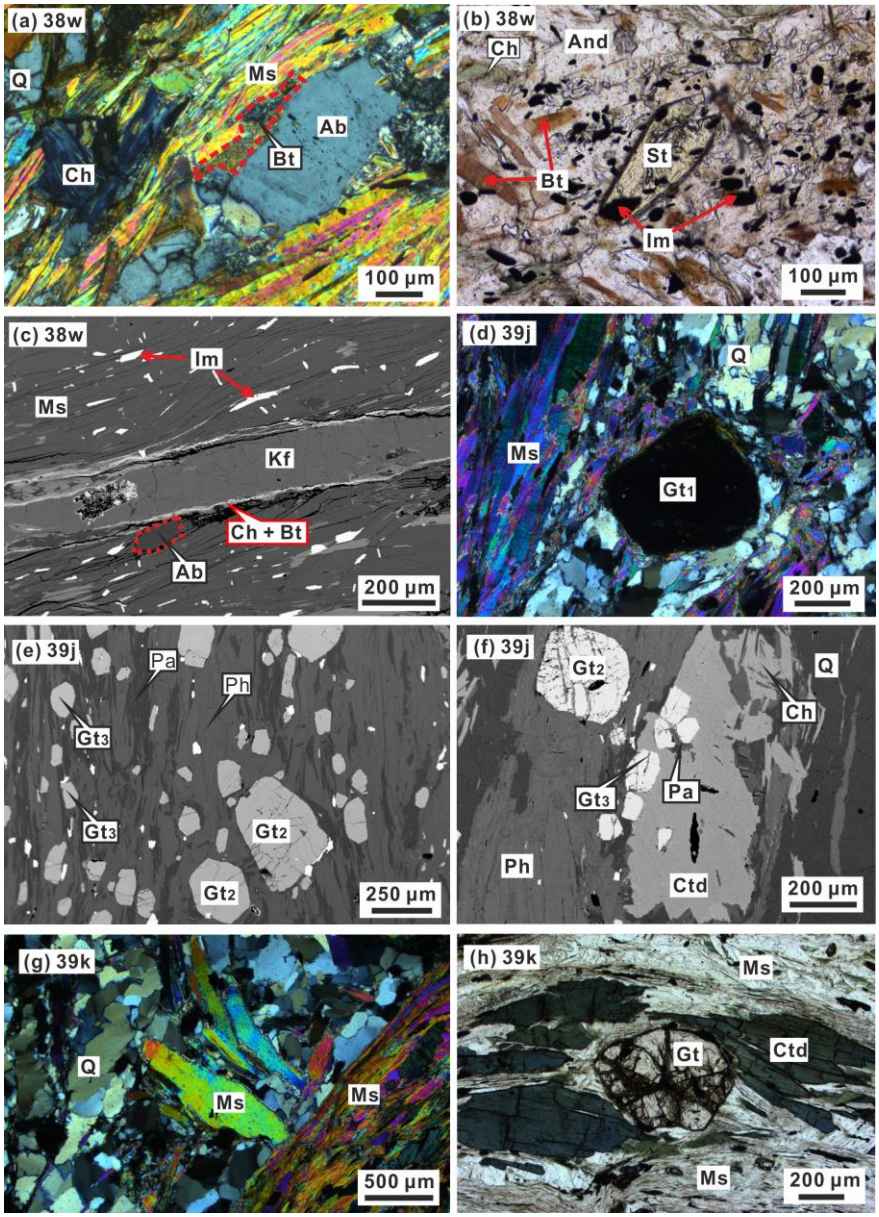

Fig. 6.2. Photomicrographs of the staurolite-andalusite bearing shist 38w (a-c), chloritoid schist 39j (d-f) and chloritoid schist 39k (g-h). (a) Under crossed polarized light (CPL): porphyroblastic albite (Ab), randomly oriented chlorite (Ch) and subhedral biotite (Bt). (b) Under plane polarised light (PPL): porphoroblastic andalusite (And) with numerous inclusions and chlorite (Ch) fills in cracks. (c) BSE image showing K-feldspar (Kf) vein and ilmenite (Im) in matrix. (d) CPL: quartz (Q) domains with largest garnets (Gt_1) and phyllosilicate domains. (e) BSE image: phyllosilicate domains with middle-sized garnets (Gt_2) and smallest garnets (Gt_3). (f) BSE image: enlongated chloritoid (Ctd) along foliation with garnet (Gt) and paragonite (Pa) inclusions. (g) CPL: coarse-grained muscovite (Ms) is perpendicular to the main foliation. (h) CPL: chloritoid and garnet in phyllosilicate domain.

andalusite being as large as 1 cm (Fig. 6.2b) contains numerous inclusions of staurolite, white mica, biotite, plagioclase, tourmaline, quartz and ilmenite. Chlorite fills cracks in andalusite. Staurolite is prismatic with local corrosion and 0.05-0.3 mm in length (Fig. 6.2b). Only a few staurolite grains were found to be not enclosed in andalusite but surrounded by muscovite in the matrix.

6.3.2. Chloritoid schist 39j

The major minerals in sample 39j are white mica (30 vol.%: muscovite-phengite and paragonite, see below), garnet (25 vol.%), chloritoid (12 vol.%), quartz (25 vol.%), and chlorite (6 vol.%). Accessory minerals are epidote, plagioclase, tourmaline, apatite, rutile, ilmenite and magnetite. Layers of oriented white mica (mean size 0.9×0.3 mm^2) and chlorite (mean size 0.6×0.1 mm^2) define the main foliation (Fig. 6.2d). Quartz layers with thickness of 0.5-5 mm, consisting mainly of fine-grained quartz (mean diameter 0.1 mm) slightly elongated along the main foliation, alternate with phyllosilicate layers (Fig. 6.2d).

Three groups of garnet can be distinguished according to grain size and textural position (Fig. 6.2d-f). The average size of rare (5 % of all garnet) large and euhedral garnet (Gt_1), occurring in quartz domains, is 0.5 mm. Middle-sized garnet (mean 0.3 mm, Gt_2) appears in phyllosilicate layers and is euhedral or elongated oblique to the foliation. Small garnet (0.05 mm, Gt_3) is distributed in phyllosilicate domains and elongated along the foliation. All garnet is marginally replaced and locally entirely wrapped by potassic white mica, chlorite and quartz. Chlorite and late potassic white mica fill garnet fractures. The inclusions in garnet (Gt_1 and Gt_2) cores are epidote, potassic white mica and rutile.

Chloritoid is elongated along the main foliation being up to 2 mm in length (Fig. 6.2f). Grain boundaries are irregularly replaced by chlorite and potassic white mica. Garnet (Gt_3), white mica and quartz are enclosed in chloritoid.

Occasionally, plagioclase was found along boundaries of white mica flakes. Epidote is only included in garnet. Apatite and ilmenite were found only in the matrix. Magnetite in the matrix is as large as 30 μm. This mineral also fills late-stage cracks in the rock. Rutile only occurs as inclusion in garnet and ilmenite.

6.3.3. Chloritoid-bearing schist 39k

The major minerals in sample 39k are garnet (20 vol.%), white mica (27 vol.%:

muscovite-phengite and paragonite, see below), quartz (30 vol.%), chloritoid (15 vol.%), and chlorite (5 vol.%). Accessory minerals are epidote, plagioclase, tourmaline, apatite, rutile, ilmenite and magnetite. All minerals show similar sizes and textures as in sample 39j. However, a few differences were observed: (1) A few large muscovite laths (up to 2 mm) appear with an orientation oblique and perpendicular to the main foliation (Fig. 6.2g). (2) Garnet appears only in phyllosilicate domains (Fig. 6.2h) with a bimodal grain size distribution (averages 0.6 and 0.15 mm for Gt_2 and Gt_3, respectively; Gt_1 was not observed). The large garnet is euhedral. The small garnet is euhedral or elongated along the foliation. (3) Chloritoid can be as large as 3.5 mm. (4) No Fe (hydroxy)oxides occur. (5) Epidote occurs not only in garnet, but also in the matrix with an average size of 0.1 mm, especially in phyllosilicate domains, and is elongated along the foliation.

6.4. Analytical methods

Garnet, white mica, chloritoid, chlorite, staurolite, biotite, epidote, plagioclase and tourmaline were quantitatively analyzed with a CAMECA SX100 electron microprobe (EMP) with 5 wavelength-dispersive spectrometers. The conditions for these analyses were 15 kV acceleration voltage, 10 or 15 nA beam current, and approximately 2 minutes total counting time. A detailed description of the analytical conditions and errors (for 15 nA) are given by Massonne (2012). For the calculation of the structural formula of a specific mineral and the molar fractions of mineral components from EMP analyses, the computer program CALCMIN (Brandelik, 2009) was used.

The analytical procedure, applied here with the EMP to determine the composition and age of monazite, was described by Massonne et al. (2012) and Massonne (2014). This procedure results in a good agreement with monazite ages obtained by other mass spectrometric methods (see Massonne, 2016; van Leeuwen et al., 2016; Waizenhöfer & Massonne, in review). A wide range of elements (Si, P, S, Ca, Y, La, Ce, Pr, Nd, Sm, Eu, Gd, Pb, Th, U) were analyzed. A beam current of 150 nA was used. The 1 sigma uncertainty was calculated by error propagation of the 1σ of the counting rates of the peak and background intensities of the relevant elements. As monazite compositions in the studied sample contains 2.5-7 wt% ThO_2, a 1-sigma error between 7 and 13 Ma often resulted for the single analysis. The age and corresponding error of all monazite analyses were calculated with the Mincalc programme (Bernhardt, 2007).

Back-scattered electron (BSE) images were taken with the EMP to document specific textural features. X-ray maps for garnet, potassic white mica and chloritoid were also produced with the EMP. The elements Mn, Ca, Mg, Fe and Y were considered for the simultaneous production of X-ray maps of garnet using 15 kV accelerating voltage and 60 nA beam current. X-ray maps for potassic white mica (Mg, Fe, Ti, Na, Ba) and chloritoid (Fe, Mn, Zn, Mg) were produced with 15 kV accelerating voltage and 30 nA and 40 nA beam current, respectively. Other parameters for the X-ray mapping were 1 or 2 µm step width and 50-100 ms per step.

6.5. Mineral chemistry

Representative EMP analyses of minerals in the studied rocks are given in Tables 6.1 (diverse minerals without garnet) and 6.2 (only garnet).

6.5.1. Staurolite-andausite bearing schist (38w)

All white mica in sample 38w is muscovite. According to chemical compositions, two generations were noted. The first generation, being identical with the core of grains, has higher Si contents (3.07-3.11 pfu) than the late generation (Si = 3.01-3.04 pfu) frequently occuring as rims of grains. Biotite is characterized by XMg = $(Mg/(Mg + Fe^{2+})$ between 0.32 and 0.37 and Si contents between 2.60 and 2.67 pfu. Plagioclase is albite with XNa = Na/(Na + K + Ca) = 0.96-1.00. K-feldspar is characterized by XK = K/(K + Na + Ca) = 0.96-1.00.

Both types of staurolite, enclosed in andalusite and in the matrix, contain low Mg contents between 0.05 and 0.10 in regard to XMg = $Mg/(Mg + Fe^{2+} + Zn + Mn)$. However, the sum of $Mg + Fe^{2+} + Zn + Mn$ is significantly below the ideal value of 4 (Table 6.2), so that probably Li contents play a major role. All chlorite shows a narrow range of composition with XMg = Mg/(Mg + Fe + Mn) between 0.35 and 0.42. Tourmaline contains about 1.5-2.6 wt % of Na2O and less than 8 wt % of CaO.

Table 6.1. EMP analyses (in wt %) of various minerals from sample 38w, 39j and 39k. Structural formulae were calculated as follows: Phengite: O = 11; (clino)zoisite-epidote = 25 valencies, Mn is trivalent; staurolite: numbers of ions on the basis of 49 (O, OH); Ctd: numbers of ions on the basis of 14 (O, OH). b.d.l. = below detection limit.

sample	38w			39j					39k					
minerals	Ph	Ph	St	Ph	Ph	Ctd	Ctd	Ep	Ph	Ph	Ctd	Ctd	Ep	Ep
comments	early	late		early	late	early	late		early	late	early	late	in gt	in matrix
SiO_2	46.90	46.35	29.44	50.88	47.52	23.69	23.88	37.31	49.75	47.11	23.45	24.24	34.99	34.99
TiO_2	0.26	0.27	0.04	0.15	0.30	b.d.l.	0.01	0.05	0.16	0.09	0.01	0.06	0.03	0.06
Al_2O_3	35.12	35.43	57.63	27.81	33.22	40.24	39.73	23.09	27.58	34.13	39.25	40.04	22.37	23.21
$(FeO)_{tot}$	1.36	1.50	8.75	3.36	2.46	24.70	26.01	13.15	4.35	3.20	25.77	25.79	13.70	11.75
MnO	b.d.l.	0.01	0.26	b.d.l.	0.05	0.33	0.49	0.78	0.01	b.d.l.	0.48	0.43	1.41	0.29
MgO	0.79	0.75	0.36	2.94	1.24	3.78	2.61	b.d.l.	2.72	0.88	3.35	2.93	0.11	0.03
CaO	0.02	b.d.l.	b.d.l.	b.d.l.	b.d.l.	b.d.l.	b.d.l.	22.81	b.d.l.	0.01	b.d.l.	b.d.l.	20.57	22.16
Na_2O	1.20	1.24	b.d.l.	0.30	1.09	b.d.l.	b.d.l.	0.00	0.44	1.48	b.d.l.	b.d.l.	0.04	b.d.l.
K_2O	9.92	10.11	b.d.l.	10.44	9.64	b.d.l.	b.d.l.	b.d.l.	10.65	9.26	b.d.l.	b.d.l.	b.d.l.	b.d.l.
BaO	0.17	0.13	b.d.l.	0.19	0.14	b.d.l.	b.d.l.	b.d.l.	0.17	0.13	b.d.l.	b.d.l.	b.d.l.	b.d.l.
ZnO	b.d.l.	b.d.l.	1.24	b.d.l.	b.d.l.	b.d.l.	b.d.l.	b.d.l.	b.d.l.	b.d.l.	b.d.l.	b.d.l.	b.d.l.	b.d.l.
H_2O	4.53	4.52	1.06	4.52	4.52	7.39	7.28	1.89	4.46	4.53	7.32	7.35	1.81	1.80
Total	100.3	100.3	98.8	100.6	100.2	100.1	100.0	99.1	100.3	100.8	99.6	100.9	95.0	94.3
pfu														
Si	3.105	3.078	8.304	3.374	3.155	1.921	1.966	2.964	3.341	3.117	1.922	1.978	2.904	2.917
Ti	0.013	0.014	0.007	0.008	0.015			0.003	0.008	0.004		0.004	0.002	0.004
Al	2.740	2.773	19.15	2.173	2.599	3.845	3.855	2.162	2.183	2.662	3.791	3.850	2.188	2.280
Fe^{3+}	0.000	0.000				0.155	0.145	0.874	0.014		0.208	0.142	0.951	0.819
Fe^{2+}	0.075	0.083	2.063	0.186	0.137	1.521	1.646	0.000	0.230	0.177	1.558	1.617		
Zn			0.258											
Mn	0.000	0.000	0.062		0.003	0.023	0.034	0.047	0.001		0.033	0.030	0.089	0.019
Mg	0.078	0.074	0.152	0.290	0.122	0.456	0.320	0.000	0.273	0.087	0.409	0.357	0.013	0.004
Ca	0.001	0.000						1.942	0.000	0.000			1.830	1.979
Na	0.153	0.159		0.038	0.140				0.058	0.190			0.007	
K	0.838	0.856		0.883	0.816				0.912	0.782				
Ba	0.004	0.003		0.005	0.004				0.005	0.003				
H	2.0	2.0	2.0	2.0	2.0	4.0	4.0	1.0	2.0	2.0	4.0	4.0	1.0	1.0

Table 6.2. Representative EMP analyses (in wt %) of garnet in the samples 39j and 39k. The garnet structural formula (double unit) was calculated on the basis of 24 O, 10 sixand eight-fold coordinated cations. Molar fractions of garnet components are given at the bottom.

sample	39j				39k	
comment	inner core	outer core	Inner rim	Outer rim	core	rim
SiO_2	36.86	36.97	36.58	36.84	36.06	36.85
TiO_2	0.15	0.08	0.05	0.04	0.05	0.03
Al_2O_3	20.14	21.05	20.16	21.11	20.77	21.12
Cr_2O_3	0.04	0.03	0.01	0.05	0.02	0.01
Fe_2O_3	1.94	0.78	1.31	0.43	1.22	0.86
FeO	16.40	28.78	30.56	32.67	24.60	32.57
MnO	18.32	5.41	2.87	1.74	10.80	2.40
MgO	0.40	0.62	1.24	2.09	0.94	1.65
CaO	7.44	7.90	6.76	5.51	6.50	6.10
Na_2O	0.02	0.05	0.03	0.02	0.01	0.03
Total	101.7	101.7	99.6	100.5	101.0	101.6
pfu						
Si	5.846	5.817	5.912	5.838	5.675	5.771
Ti	0.017	0.009	0.006	0.005	0.006	0.004
Al	3.763	3.904	3.840	3.943	3.853	3.898
Cr	0.005	0.003	0.001	0.007	0.003	0.001
Fe3	0.231	0.092	0.159	0.051	0.144	0.101
Fe2	2.175	3.787	4.129	4.330	3.238	4.265
Mg	0.095	0.146	0.298	0.494	0.221	0.386
Ca	1.264	1.331	1.170	0.936	1.097	1.024
Mn	2.460	0.720	0.393	0.233	1.440	0.318
Na	0.006	0.015	0.010	0.005	0.005	0.008
pyrope	0.016	0.024	0.050	0.082	0.037	0.064
grossular	0.211	0.222	0.195	0.156	0.240	0.053
spessartine	0.410	0.120	0.065	0.039	0.183	0.171
almandine	0.363	0.634	0.690	0.723	0.540	0.712

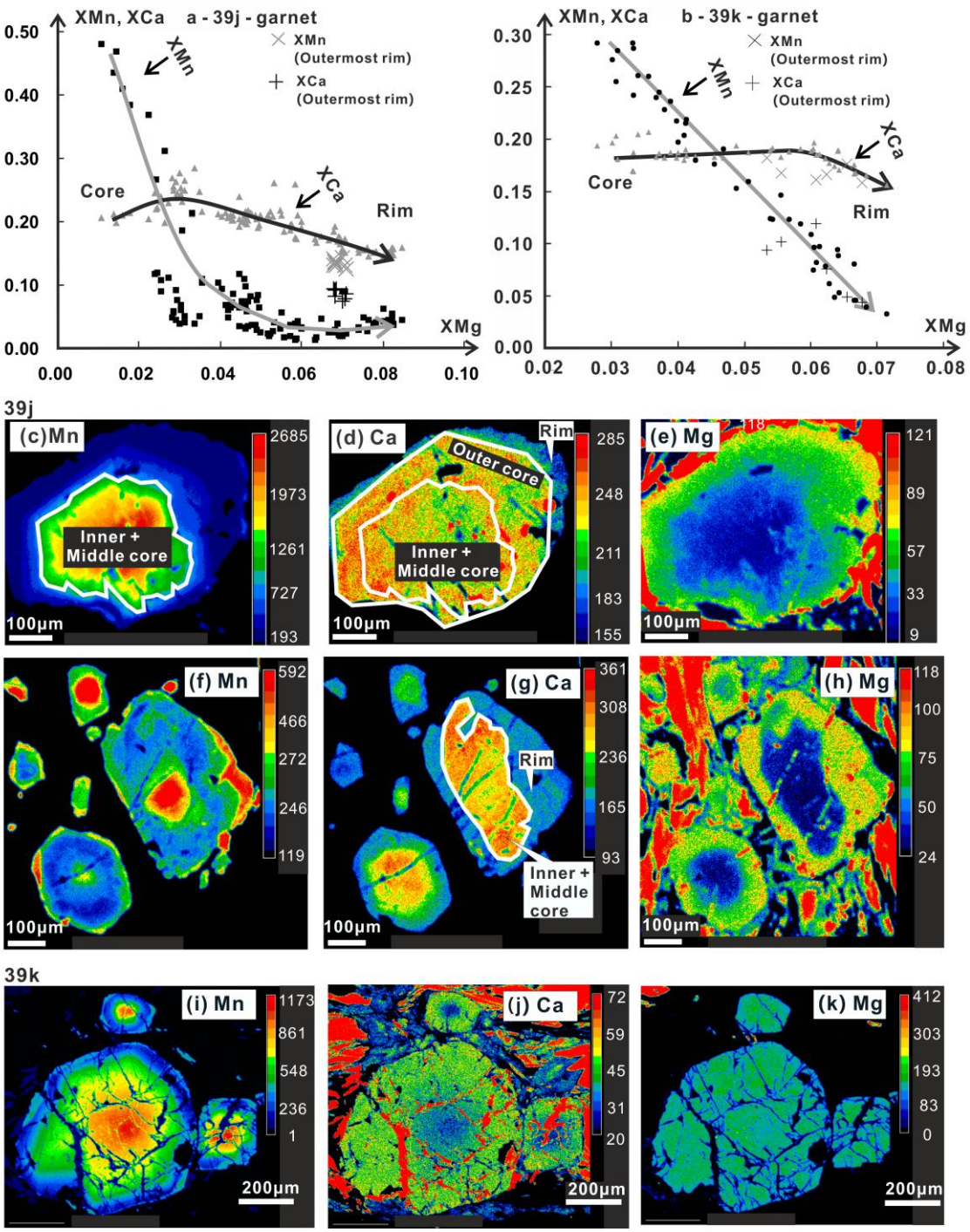

Fig. 6.3. (a,b) Analyses of garnet from chloritoid schists of 39j (a) and 39k (b) in terms of molar fractions of pyrope (XMg) versus grossular (+ andradite) (XCa) and spessertine (XMn) obtained with a CAMECA SX100 EMP. (b-h) Mn, Ca and Mg concentration maps of large, middle-sized, small garnets in sample 39j. (i-k) Mn, Ca and Mg concentration maps of garnets in sample 39k.

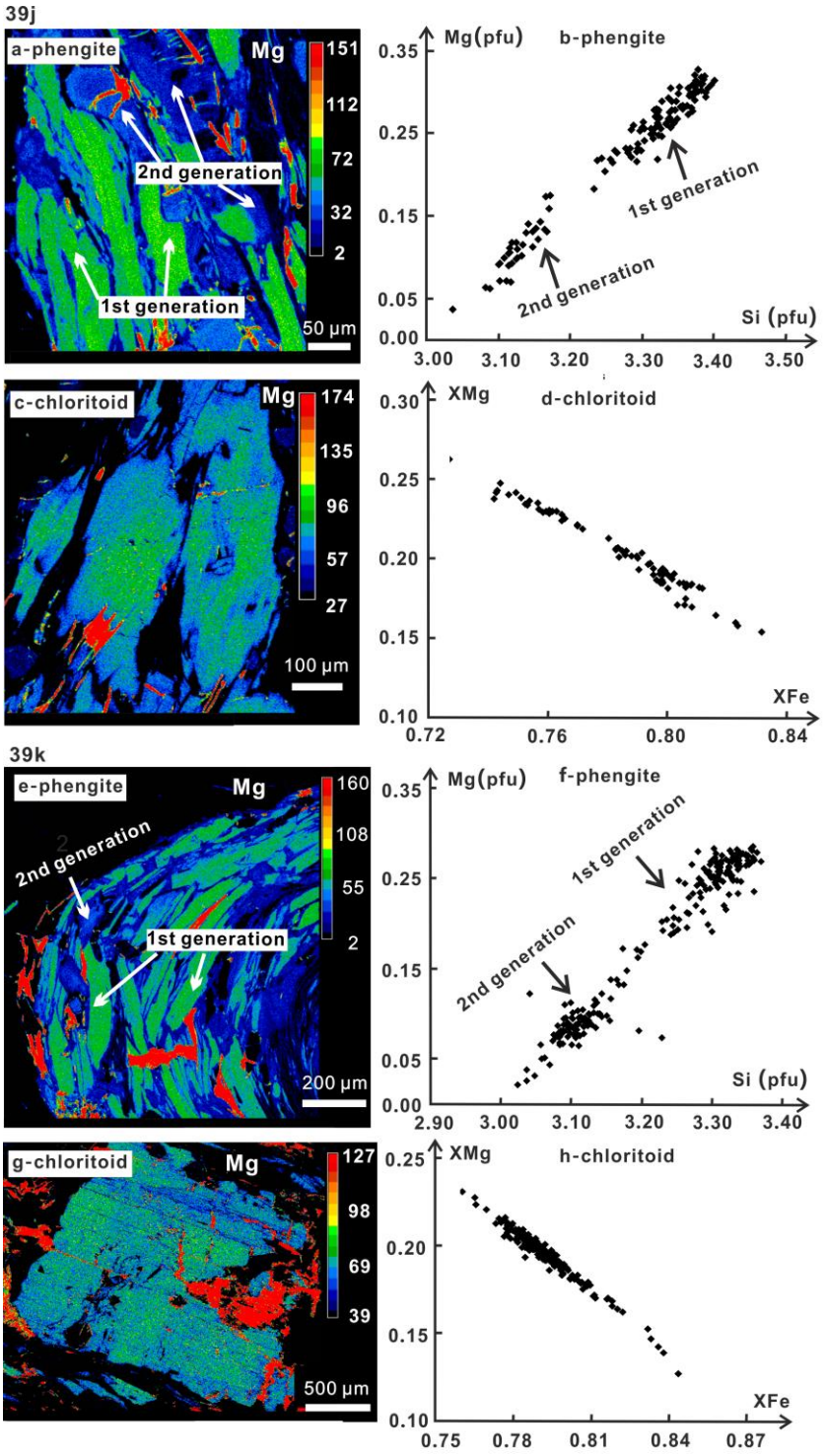

Fig. 6.4. Mg concentration maps obtained with a CAMECA SX100 EMP of white mica (a, e) and chloritoid (c, g). (b, f) White Mica (phengite) analyses obtained with an EMP in terms of Mg (pfu) versus Si (pfu). (d, h). Chloritoid analyses obtained with an EMP in terms of XMg (pfu) versus XFe.

6.5.2. Chloritoid schist (39j)

The composition of garnet in terms of XMn, XMg and XCa is shown in Fig. 6.3a. X-ray maps of Ca, Mg, Mn for the three types of garnet (Gt_1, Gt_2 and Gt_3) are displayed in Fig. 6.3c-h. All three garnet types are chemically zoned with significant variation in the contents of almandine ($Alm_{22–75}$), spessartine ($Sps_{13–58}$), pyrope ($Prp_{1–8}$), and grossular ($Grs_{13–28}$) components. Gt_1 and Gt_2 show the same zonation with XMg and XFe increasing and XMn decreasing from core to rim. XCa first slightly increase in the core domain, but shows a significant decrease towards the rim. Average compositions of inner core, middle core, outer core, and rim domains of Gt_1 and Gt_2 are $Sps_{40}Pry_{1.5}Gros_{20}Alm_{38.5}$, $Sps_{15}Pry_3Gros_{22}Alm_{60}$, $Sps_7Pry_5Gros_{20}Alm_{68}$ and $Sps_4Pry_8Gros_{15}Alm_{73}$, respectively. In middle-sized garnet (Gt_2), the defined outer core did not grow, and resorption happened after the growth of the garnet middle core, which can be seen in Figures 6.2j and 6.3g. In large garnet (Gt_1) the resorption also occurred after the growth of the middle core domain, but an outer core domain developed showing a euhedral boundary (Figs. 6.2d, 6.3d).Small garnet (Gt_3), which is elongated along the foliation, has equal composions as the rim of Gt_1 and Gt_3 (Figs. 6.2e, 3f-h).

Potassic white mica of different textural position has been analyzed: large oriented mica, mica included in garnet and chloritoid, and late mica formed in garnet cracks. Oriented potassic white mica shows Si contents between 3.25 and 3.39 pfu in the core and 3.12 and 3.17 pfu at the rim (Fig. 6.4a, b). The later compositional range was found in mica in garnet cracks. Phengite included in garnet and chloritoid is characterized by Si contents of 3.25-3.35 pfu and ca. 3.30 pfu, respectively. Analyzed intergranular paragonite (mean size 0.5×0.1 mm^2) yields contents of muscovite component between 2 and 20 mol %.

Chloritoid porphyroblasts show zoning with XMg ranging from 0.24 (core) to 0.16 (rim) pfu (Fig. 6.4c, d). Mn contents are lower than 0.04 pfu. Chlorite in the matrix is characterized by XMg (Mg/(Mg + Fe^{2+} + Mn) between 0.39 and 0.45. Epidote in garnet and in the matrix contains pistacite component, $Ca_2Al_2Fe^{3+}Si_3O_{12}(OH)$, ranging from 27-31 mol %. XNa of plagioclase is 0.98-1.00.

6.5.3. Chloritoid schist (39k)

Coarse- and fine-grained garnet (Gt_2 and Gt_3) shows the same elemental zonation (Fig. 6.3i-k). Except locally developed outermost rims ($Sps_{12}Pry_{6.3}Gros_{17}Alm64.7$) in both types of garnet, average compositions are $Sps_{25}Pry_{3.5}Gros_{18.5}Alm_{53}$ and $Sps_5Pry_{6.5}Gros_{17}Alm_{71.5}$ of garnet core and rim, respectively (Fig. 6.3b).

Potassic white mica has been analyzed in the following textural positions: oriented mica, unoriented coarse mica (Fig. 6.2g), mica included in chloritoid, and mica in garnet cracks. The unoriented coarse mica and cores in oriented mica are phengite with Si contents between 3.24 and 3.36 pfu (Fig. 6.4e). These contents of rims of oriented mica and deformed margins of the unoriented coarse mica are between 3.06 and 3.19 pfu (Fig. 6.4f). Mica included in chloritoid contains Si between 3.14 and 3.35 pfu. Mica in garnet cracks is muscovite with Si around 3.05 pfu. The analyses of paragonite, occurring in mica layers, show variable contents of muscovite component (2-14 mol %).

Porphyroblastic chloritoid shows no clear zonation (Fig. 6.4g). XMg ranges between 0.15 and 0.22 pfu. However, the lower XMg values were detected rather at the boundaries of chloritoid grains. Mn contents are below 0.04 pfu. Chlorite in the matrix is characterized by XMg between 0.30 and 0.41. Epidote in garnet shows higher Fe^{3+} contents (28-33 mol % pistacite component) than epidote in the matrix (25-28 mol %). Plagioclase is albite with XNa = 0.98-1.00.

6.6. P-T data

6.6.1. Calculation method

P-T pseudosections were calculated with PERPLE_X (see Connolly, 2005; update in August 2011 downloaded from the internet site http://www.perplex.ethz.ch/) and the internally consistent thermodynamic data set (Holland & Powell, 1998; and their updates) for minerals and H_2O (model CORK: Holland & Powell, 1991). The following solid-solution models (see file solution model of the PERPLE_X software), which are based on works, for instance, by Anderson & Lindsley (1988), Fuhrman & Lindsley (1988), Powell & Holland (1999), and Massonne (2010), were used for calculating P-T pseudosections for the three metapelites: Carp(M) for carpholite, Chl(HP) for chlorite, Ctd(HP) for chloritoid,, Ep(HP) for epidote, feldspar for plagioclase and K-feldspar,

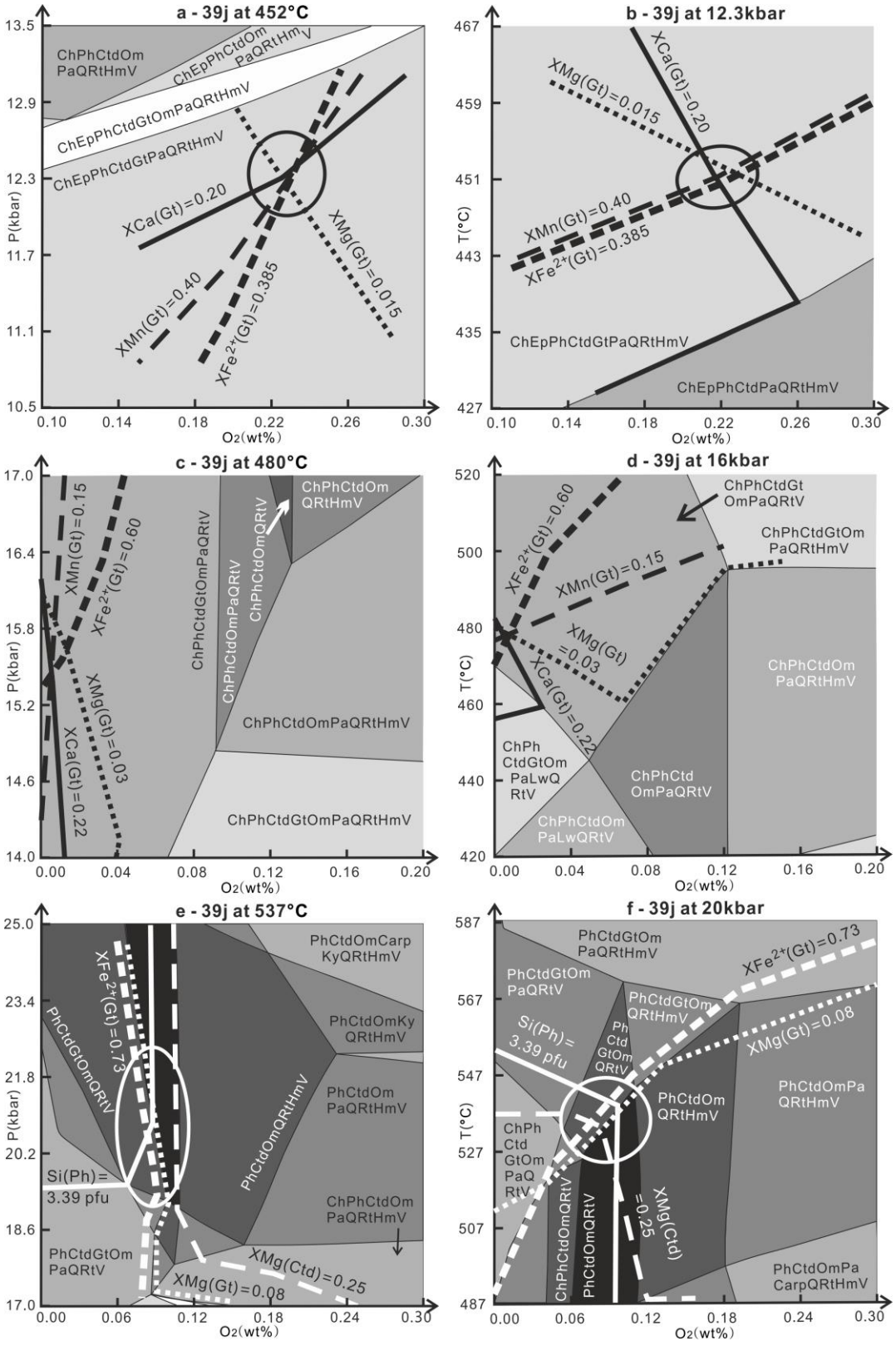

Fig. 6.5. P-O_2 and T-O_2 pesudosections calculated on fixed temperatures for O_2

conditions of garnet inner core (a, b), outer core (c, d) and outer rim (e, f) in sample 39j. Abbreviations are the same as in Fig. 6.2 and carpholite (Carp), clinopyroxene (Om), hematite (Hm), lawsonite (Lw), magnetite (Mt), paragonite (Pa), plagioclase (Pl), rutile (Rt), stilpnomelane (Stlp), H_2O (V) and (clino)zoisite-epidote (Ep). The greytones of P-T fields are related to the variance (the darker the higher) of the corresponding mineral assemblage (+ H_2O and quartz), which is also used for the following pseudosections.

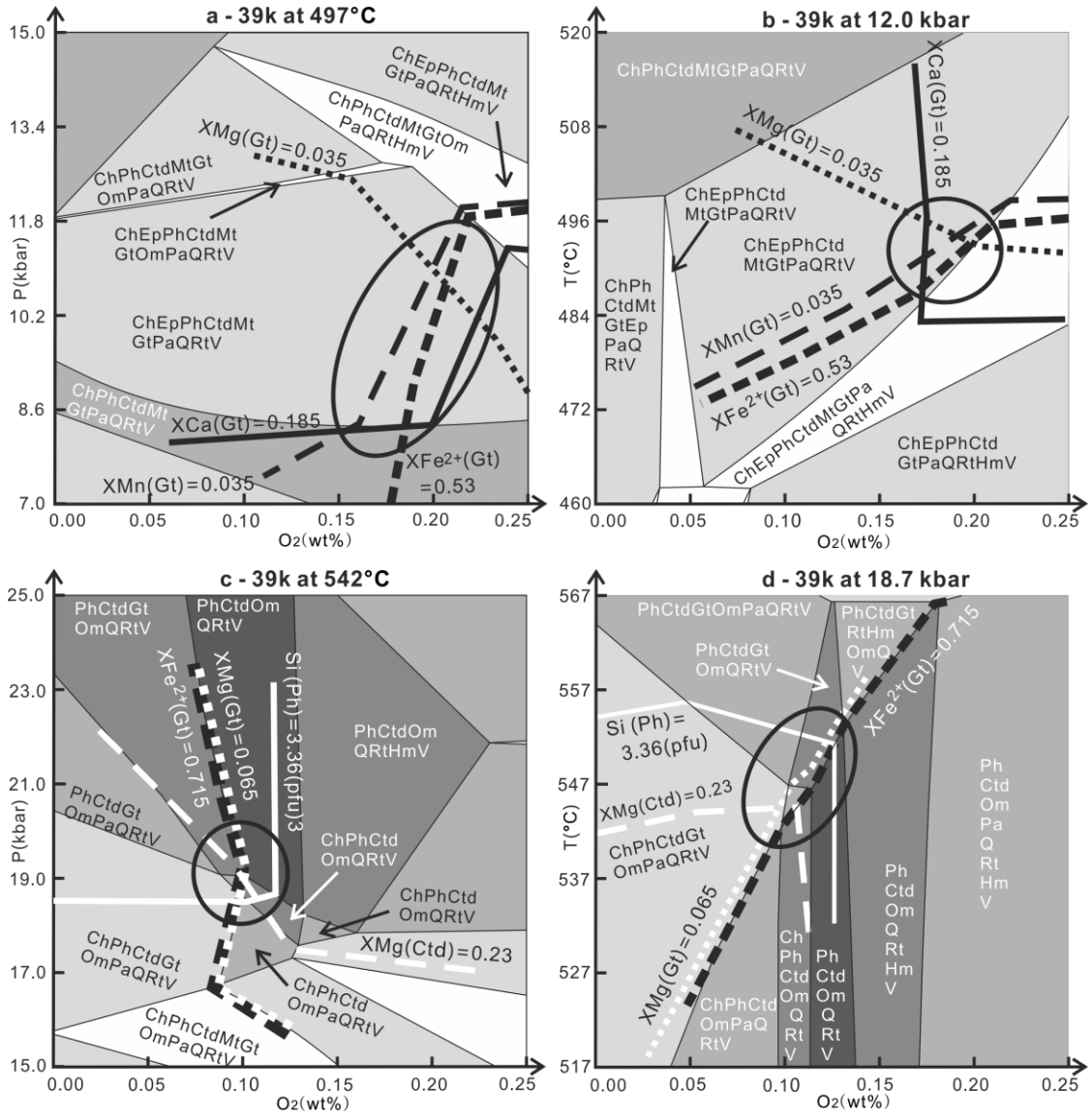

Fig. 6.6. P-O_2 and T-O_2 pesudosections calculated for fixed temperature and pressure, respectively, to determine the O_2 contents in sample 39k relevant to the garnet core (a, b) and rim (c,d). Abbreviations as in Figs. 2 and 5. For greytones of P-T fields see Fig. 6.5.

Table 6.3. Bulk-rock analyses for the studied rocks determined by X-ray fluorescence spectrometry (XRF), and modified bulk-rock compositions for the calculation of P-T, T-X and P-X pseudosections (Pseu.). XRF: Original results. M_1 (in sample 38w, 39j and 39k) and M_2 (in 39j with different O_2 content compared to M_1) are compositions before subtracting the garnet core. M_3 in 39j and M_2 in 39k are the compositions after subtraction of the garnet core.

	38w		39j				39k		
	XRF	M_1	XRF	M_1	M_2	M_3	XRF	M_1	M_2
SiO_2	59.40	52.76	59.61	58.76	58.90	59.65	53.89	58.73	59.32
Al_2O_3	20.58	25.05	20.55	20.25	20.30	20.31	25.58	20.34	20.38
MnO	0.21	0.09	0.30	0.30	0.30	0.06	0.09	0.21	0.01
MgO	1.69	2.18	1.77	1.74	1.75	1.78	2.22	1.67	1.69
CaO	0.38	0.04	0.46	0.32	0.32	0.10	0.11	0.30	0.17
Na_2O	0.92	1.01	0.79	0.78	0.78	0.81	1.04	0.91	0.93
K_2O	3.97	5.02	4.00	3.94	3.95	4.07	5.13	3.92	4.01
TiO_2	0.71	0.99	0.74	0.73	0.73	0.75	1.01	0.70	0.71
P_2O_5	0.06		0.10				0.05		
Fe_2O_3	8.47		8.41				7.79		
FeO		6.86		7.46	7.48	6.89		7.53	7.17
O_2		0.00		0.22	0.00	0.08		5.50	5.50
H_2O		6.00		5.50	5.50	5.50		0.18	0.10
total	96.39	100.00	96.73	100.00	100.00	100.00	96.91	100.00	100.00
Pseu.		Fig. 6.7		Fig. 6.5a Fig. 6.5b Fig. 6.8a	Fig. 6.5c Fig. 6.5d Fig. 6.8b	Fig. 6.5e Fig. 6.5f Fig. 6.9a		Fig. 6.6a Fig. 6.6b Fig. 6.10a	Fig. 6.6c Fig. 6.6d Fig. 6.11a

Gt(HP) for garnet, hCrd for cordierite, IlGkPy for ilmenite, MtUl(A) for magnetite, GlTrTsPg for amphibole, Mica(M) for paragonite with maximal 50% muscovite component, Omph(HP) for clinopyroxene, Opx(HP) for orthopyroxene, Pheng(HP) for phengite with maximal 50% paragonite component, St(HP) for staurolite, Stlp(M) for stilpnomalane, T for talc and TiBio(HP) for biotite. In addition, quartz, rutile, Al-silicates, lawsonite, and cordierite were considered as pure phases. We excluded mica (tip, tbi, ann1), feldspar (ab, mic), amphibole (rieb, mrb, cumm, grun) and melt (h2oL) components and the O_2 buffers qfm and mthm. For instance, these mica components were neglected because of their untrustworthiness (Massonne, 2014). When the bulk rock composition included O_2, zoisite (zo) was additionally excluded.

6.6.2. Effective bulk-rock composition and ferric iron contents

The PERPLE_X calculations were undertaken in the system Na_2O-K_2O-CaO-FeO-O_2-MnO-MgO-Al_2O_3-SiO_2-TiO_2-H_2O. The bulk-rock compositions (Table 6.3) were correspondingly modified (see Massonne et al., 2013). (1) CaO was reduced according to the phosphorus contents in the rocks, which were related to ideally composed apatite (Ca_5 $(PO_4)_3(OH)$). (2) The H_2O content were enhanced to 6, 5.5, and 5.5 wt% for samples 38w, 39j, and 39k, respectively, to permit the formation of a free hydrous fluid phase at relatively low temperatures.

In order to approach the effective bulk-rock composition for a late metamorphic stage at which the garnet rim formed, we subtracted the chemical composition of the garnet core from the bulk-rock composition (see, e.g., Marmo et al., 2002; Groppo & Rolfo, 2008). According to the aforementioned X-ray maps for garnet, 3 vol.% of an average chemical composition of the garnet core, analyzed with the EMP (see below), were subtracted from the bulk rock of samples 39j and 39k. The results of this procedure are shown in Table 6.3.

P-T pseudosections can be considerably influenced by the selected content of Fe^{3+} or O_2. This was demonstrated for metapelites by Boger et al. (2012), Korhonen et al. (2012), Lòpez-Carmona et al. (2013), Lo Pò & Braga (2014), and Massonne (2014). Thus, the relevant Fe^{3+} or O_2 content should be estimated as accurate as possible. In this work, P-O_2 and T-O_2 pseudosections at constant temperature and pressure, respectively, were used to estimate the Fe^{3+}/Fe^{2+} ratio of each metamorphic stage for samples 39j and 39k (Figs. 6.5, 6.6) considering a reasonable intersection, for instance, of the three garnet isopleths for XCa, XFe, and XMg of a selected garnet composition. For sample 39j, such intersections in P-O_2 and T-O_2 pseudosections (Fig. 6.5c,d) occur at absence of ferric iron (Table 6.3, bulk-rock composition 39j-M_2) for middle garnet core composition ($Sps_{15}Pry_3Gros_{22}Alm_{60}$). The same is true for the outer core composition ($Pry_5Gros_{20}Alm_{68}$) of garnet (P-O_2 and T-O_2 pseudosections are not shown). For the garnet inner core ($Sps_{40}Pry_{1.5}$ $Gros_{20}Alm_{38.5}$) the Fe^{3+} content is around 26.5 % of the total iron (= 0.20-0.24 wt% O_2; Table 6.3, 39j-M_1) as demonstrated by the P-O_2 and T-O_2 pseudosections (Fig. 6.5a,b). This content for the bulk rock, related to the garnet rim stage, is around 10 % (O_2 content between 0.06-0.12 wt%; Table 6.3, 39j-M_3), using

isopleths of XMg (0.08) and XFe (0.73) in garnet, the highest Mg content in chloritoid (XMg = 0.25) and the highest Si content in phengite (3.39 pfu) in P-O_2 and T-O_2 pseudosections (Fig. 6.5e,f). For sample 39k, the Fe^{3+} content is around 21.5 % of the total iron (O_2 contents between 0.15 and 0.23 wt%; Table 6.3, 39k-M_1) for the early garnet core ($Sps_{25}Pry_{3.5}Gros_{18.5}Alm_{53}$) as shown in P-$O_2$ and T-O_2 pseudosections of Figure 6.5 a and b. An Fe^{3+} content of about 12.5 % of the total iron (O_2 between 0.06-0.12 wt%; Table 6.3, 39k-M_2) was obtained for the metamorphic stage of the garnet rim using isopleths of XMg (0.065) and XFe (0.715) in garnet, the highest Mg content in chloritoid (XMg = 0.23) and the highest Si content in phengite (Si = 3.36 pfu) in the P-O_2 and T-O_2 pseudosections of Figure 6.6 c and d). For sample 38w, O_2 was neglected (Table 6.3, 38w-M_1) according to the criteria: (1) absence of magnetite and (2) low amounts of ferric iron in minerals (Iaccarino et al., 2015).

6.6.3. Results

Six P-T pseudosections were worked out in detail for the modified compositions given in Table 6.3 (M_1, M_2 and M_3) considering the P-T ranges 1-10 kbar at 450-650 °C (38w-M_1, Fig. 6.7) and 4-25 kbar at 400-600 °C (39j-M_{1-3}, Figs. 6.8, 6.9; 39k-M_{1-2}, Figs. 6.10, 6.11). These pseudosections were contoured by isopleths of molar fractions of garnet (only samples 39j and 39k), XMg in staurolite (only sample 38w), XMg in chlorite, Si in phengite, and XMg in chloritoid (only samples 39j and 39k). These isopleths were used to define P-T conditions. The angle between the intersecting isopleths affects the extension of error ellipses, which were drawn around the intersections in Figures 6.7 to 6.11 arbitrarily considering compositional errors for the corresponding minerals.

For the staurolite-andalusite bearing schist 38w the intersection (Fig. 6.7e) of isopleths for core compositions (highest Si content in muscovite = 3.11 pfu, highest XMg = 0.10 in staurolite) suggests P-T conditions of 7-9 kbar and 560-580 °C (stage I). Staurolite with lowest XMg (0.05) (close to its lower pressure limit), muscovite with low Si contents (3.04 pfu) and the upper pressure limit of andalusite result in P-T conditions of 1.5-2.8 kbar and 500-530 °C (stage II).

Three P-T pseudosections for somewhat different compositions (see above) of chloritoid schist 39j (Table 6.3, 39j-M_1, M_2 and M_3) were used to decipher the P-T

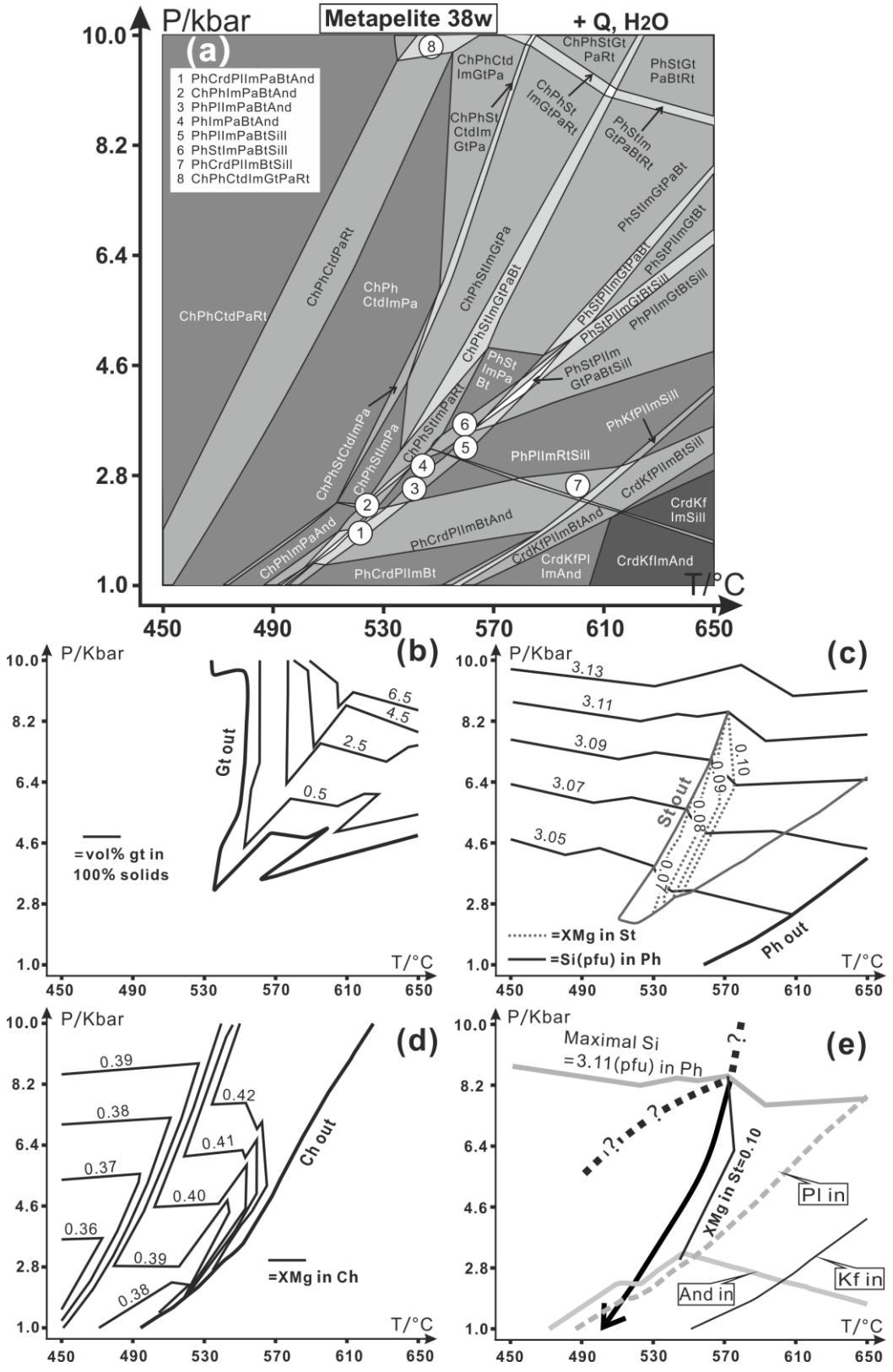

Fig. 6.7. (a) P-T pseudosection calculated for the modified composition of staurolite-andalusite schist 38w (Table 6.3, 38w-M_1) with PERPLE_X (see text). (b)

Isopleths for the modal contents of garnet. (c) Isopleths of Si contents in phengite. (d) XMg isopleths in chlorite. (e) XMg isopleths in staurolite, mineral phase boundaries and reconstructed P-T path, solid line is certain part, and dashed black lines are uncertain part. Abbreviations as in Figures 6.2 and 6.5 and andalusite (And), cordierite (Crd), sillimanite (Sill) and staurolite (St). For greytones of P-T fields see Figure 6.5.

conditions of the formation of the inner core, middle core, outer core, and rim (peak pressure metamorphism) domains of garnet and the late metamorphic stage (stage III). In the P-T pseudosections (Fig. 6.8a, b) for 39j-M_1 and -M_2 the intersections of isopleths for the inner core ($Sps_{40}Pry_{1.5}$ $Gros_{20}Alm_{38.5}$), middle core ($Sps_{15}Pry_3Gros_{22}Alm_{60}$), and outer core ($Pry_5Gros_{20}Alm_{68}$) of garnet occur at the P-T conditions 440-470 °C and 12-14.5 kbar, 485-510 °C and 12.5-17 kbar, and 490-520 °C and 16-20 kbar, respectively. Thus, the garnet core grew along a prograde P-T evolution (stage I). P-T conditions of 550-570 °C and 19-23 kbar (Fig. 6.9a) are suggested for peak pressure metamorphism (stage II) based on intersecting isopleths of XMg (0.08) and XFe (0.73) in the garnet rim (Fig. 6.9b, c), the highest Mg content in chloritoid (XMg = 0.25) (Fig. 6.9d) and the highest Si content in phengite (3.39 pfu) (Fig. 6.9c) in the P-T pseudosection for composition 39j-M_3. The P-T conditions of stage III were derived using isopleths of the lowest Mg content in chloritoid (XMg = 0.17), the highest Si content in late muscovite (3.17 pfu) (Figs. 6.4a, 6.9c) and the highest Mg content in chlorite (XMg = 0.45) (Fig. 6.9e) and the P-T pseudosection for composition 39j-M_3. Conditions of 555-575 °C and 8.5-12.5 kbar result (Fig. 6.9a).

Two P-T pseudosections (Fig. 6.10a, 6.11a) for somewhat different compositions (see above) of chloritoid schist 39k (Table 6.3, 39k-M_1 and -M_2) were used to estimate the P-T conditions for the formation of the garnet core and rim (peak pressure metamorphism = stage II) and the late metamorphic stage (stage III). The intersection of isopleths (Fig. 6.10b, c) for the garnet core ($Sps_{25}Pry_{3.5}Gros_{18.5}Alm_{53}$) suggests P-T conditions of 480-510 °C at 8-13 kbar (stage I). P-T conditions of 555-585 °C and 18-24 kbar result for stage II (Fig. 6.11a) by intersecting isopleths of XMg (0.065) and XFe (0.715) in garnet (Fig. 6.11 b, c), the highest Mg content in chloritoid (XMg = 0.23) (Fig. 6.11d) and the highest Si content in phengite (3.36 pfu) (Fig. 6.11c). For the derivation of P-T conditions of stage III, we considered isopleths of the lowest Mg content in chloritoid

(XMg = 0.15), the highest Si content in late muscovite (3.19 pfu) and the highest Mg content in chlorite (XMg = 0.41). P-T conditions of 535-560 °C and 9.5-13 kbar result for this stage (Fig. 6.11a).

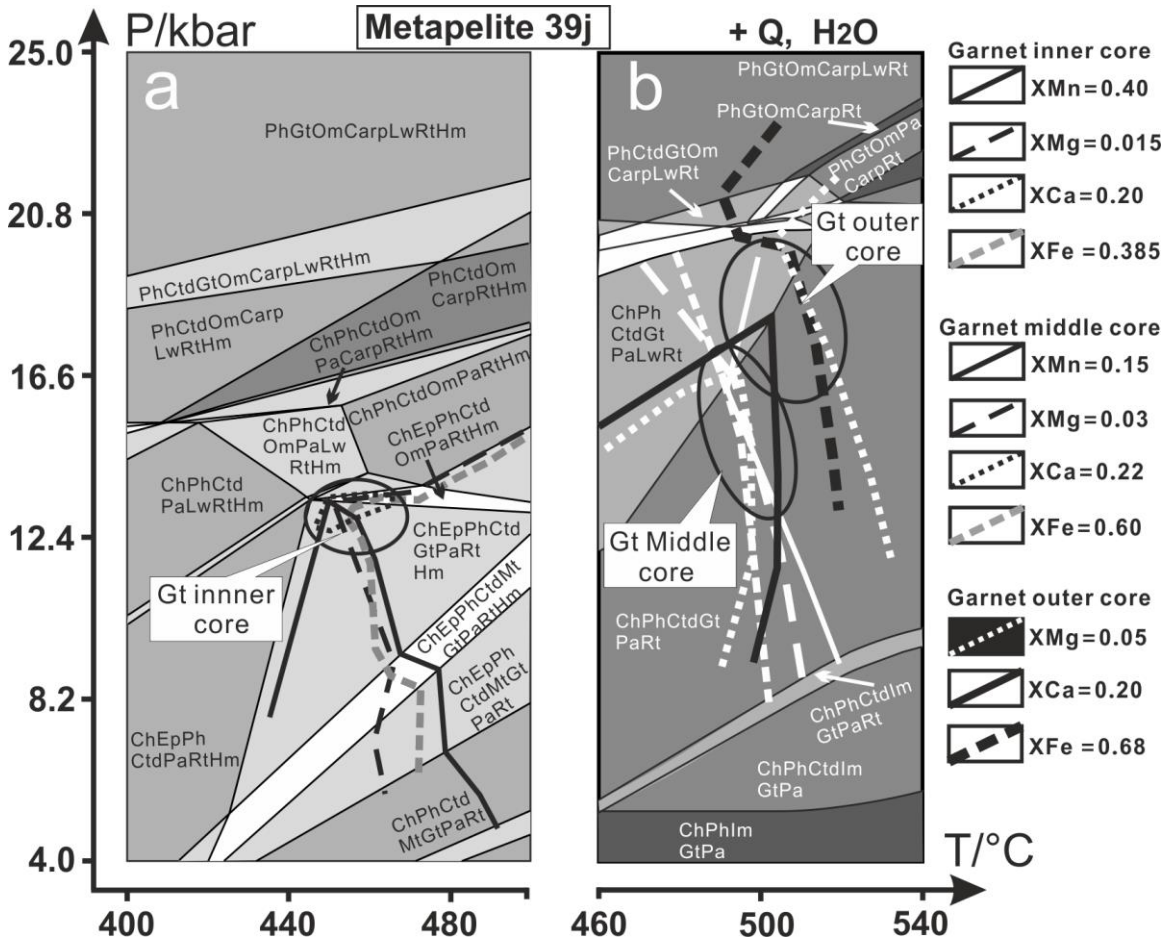

Fig. 6.8. P-T pseudosections calculated for modified compositions of chloritoid schist 39j (Table 6.3, a: 39j-M_1. b: 39j-M_2) with the computer software package PERPLE_X (see text). The isopleths of garnet compositions were contoured on the corresponding pseudosections. Abbreviations as in Figures 6.2 and 6.5. For greytones of P-T fields see Figure 6.5.

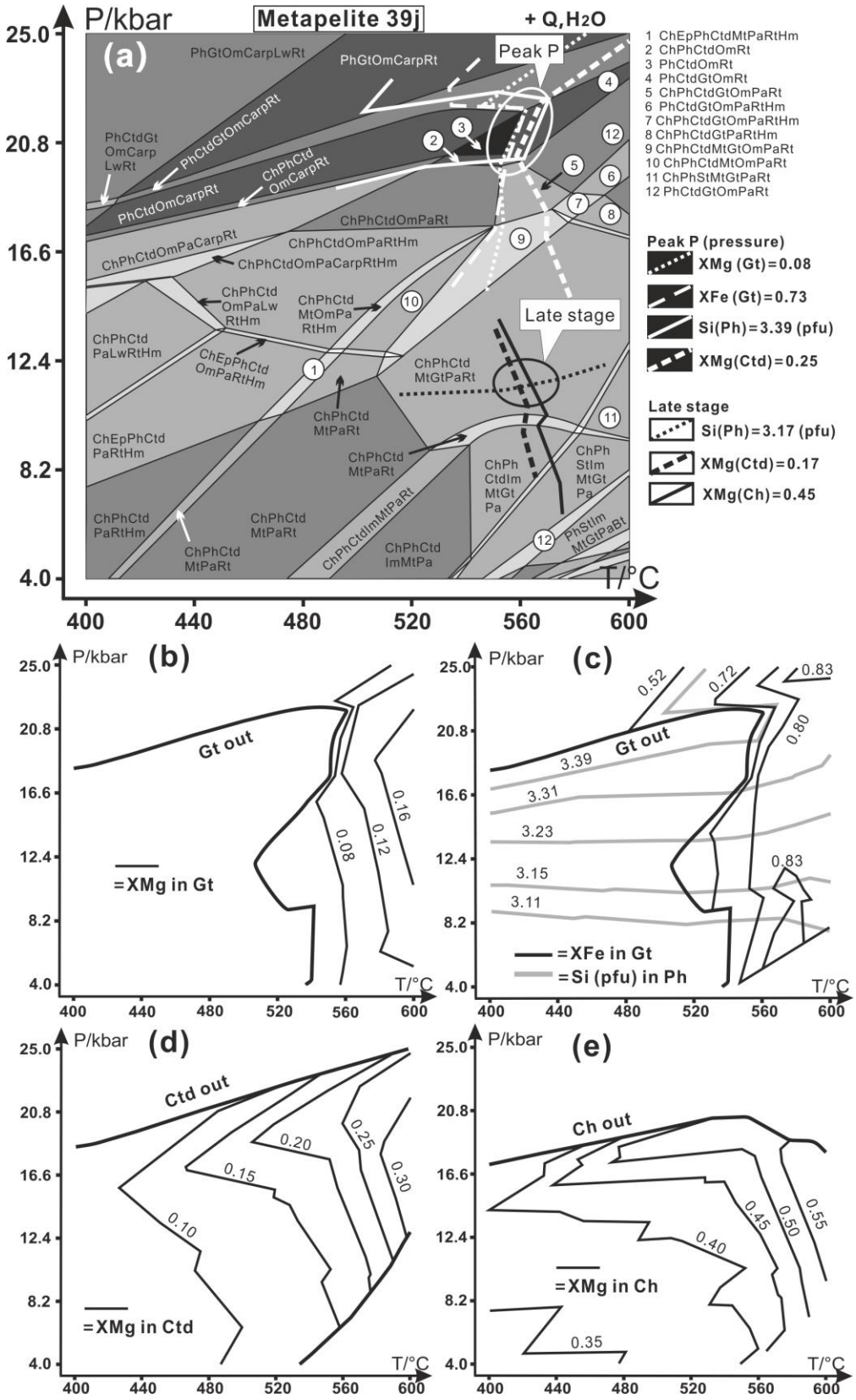

Fig. 6.9. (a) P-T pseudosection calculated for the modified composition chloritoid schist

(Table 6.3, 39j-M_3) with the computer software package PERPLE_X (see text). (b) Isopleths of XMg in garnet. (c) Isopleths of Si contents in phengite and XFe in garnet. (d) XMg isopleths in chloritoid. (e) XMg isopleths in chlorite. Abbreviations are the same as in Fig. 6.2, Fig. 6.5 and Fig. 6.7.

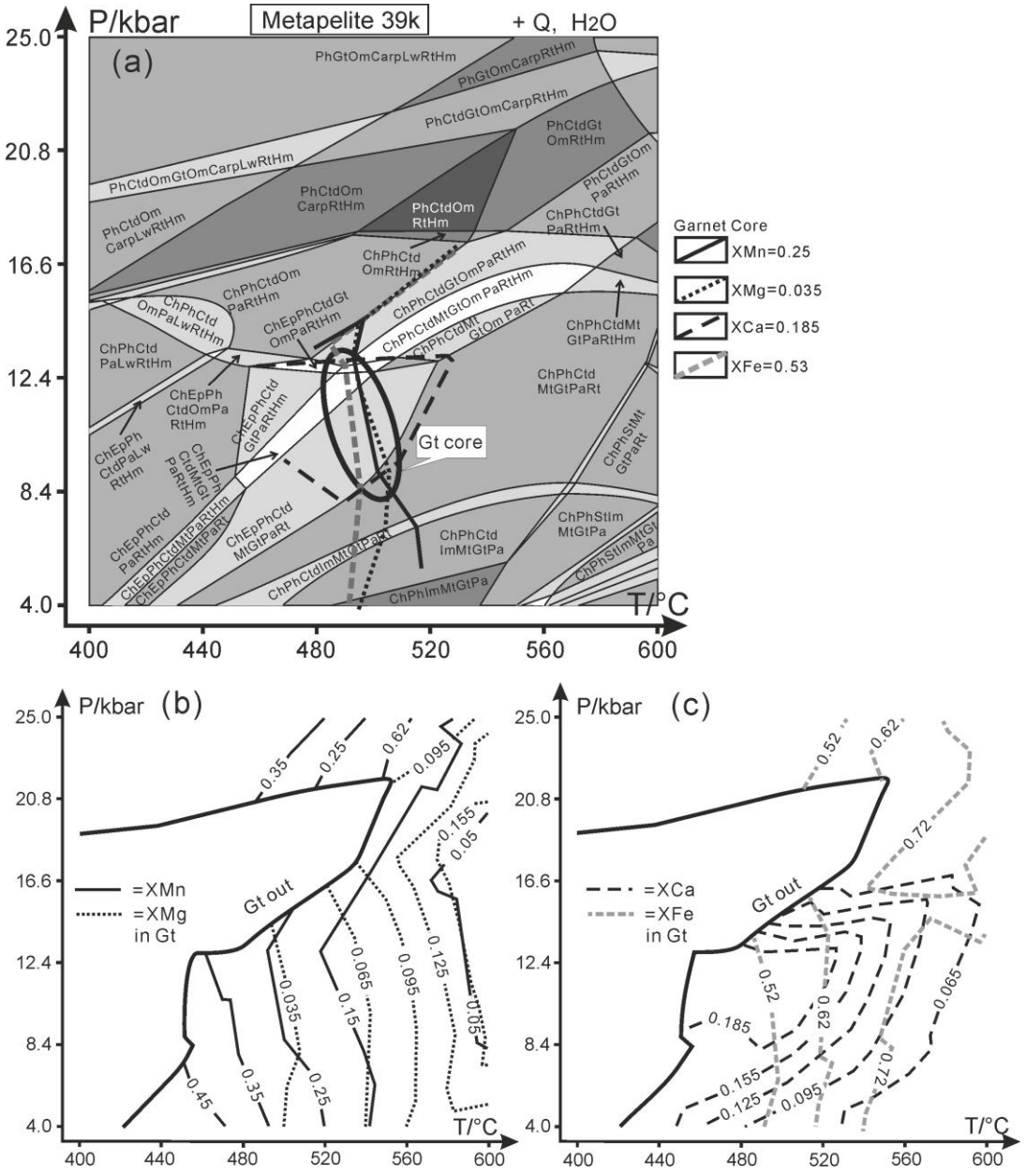

Fig. 6.10. (a) P-T pseudosection calculated for a modified composition of chloritoid schist 39k (Table 6.3, 39k-M_1) with PERPLE_X (see text). (b, c) Isopleths of XMn, XMg, XCa and XFe in garnet. Abbreviations as in Figures 6.2, 6.5 and 6.7. For greytones of P-T fields see Figure 6.5.

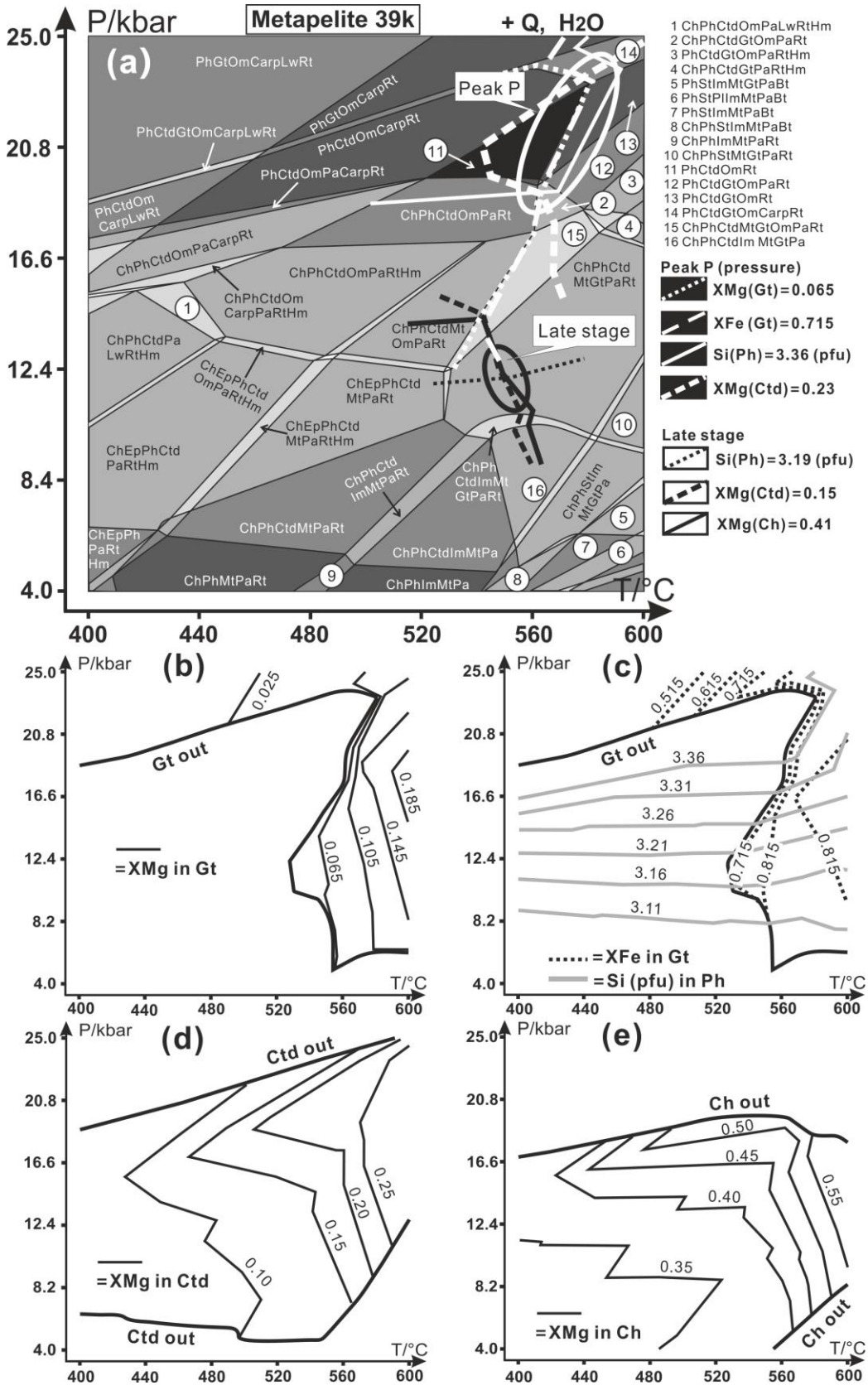
P/kbar
Metapelite 39k
+ Q, H2O
(a)
PhGtOmCarpLwRt
PhGtOmCarpRt
PhCtdGtOmCarpLwRt
PhCtdOmCarpRt
PhCtdOmPaCarpRt
PhCtdOm CarpLwRt
ChPhCtdOmPaRt
ChPhCtdOmPaCarpRt
ChPhCtdOmPaRtHm
ChPhCtdOm CarpPaRtHm
ChPhCtd MtGtPaRt
ChPhCtdPa LwRtHm
ChPhCtdMt OmPaRt
ChEpPhCtd OmPaRtHm
ChEpPhCtd MtPaRt
ChEpPhCtd MtPaRtHm
ChEpPhCtd PaRtHm
ChPhCtd ImMtPaRt
ChPh CtdImMt GtPaRt
ChPhStIm MtGtPa
ChPhCtdMtPaRt
ChEpPh PaRt Hm
ChPhCtdImMtPa
ChPhMtPaRt
ChPhImMtPa
Peak P
Late stage
T/°C
1 ChPhCtdOmPaLwRtHm
2 ChPhCtdGtOmPaRt
3 PhCtdGtOmPaRtHm
4 ChPhCtdGtPaRtHm
5 PhStImMtGtPaBt
6 PhStPlImMtPaBt
7 PhStImMtPaBt
8 ChPhStImMtPaBt
9 ChPhImMtPaRt
10 ChPhStMtGtPaRt
11 PhCtdOmRt
12 PhCtdGtOmPaRt
13 PhCtdGtOmRt
14 PhCtdGtOmCarpRt
15 ChPhCtdMtGtOmPaRt
16 ChPhCtdIm MtGtPa
Peak P (pressure)
XMg(Gt)=0.065
XFe (Gt)=0.715
Si(Ph)=3.36 (pfu)
XMg(Ctd)=0.23
Late stage
Si(Ph)=3.19 (pfu)
XMg(Ctd)=0.15
XMg(Ch)=0.41
(b)
Gt out
0.025
0.185
0.145
0.105
0.065
=XMg in Gt
(c)
0.515
0.615
0.715
3.36
3.31
3.26
3.21
3.16
3.11
0.715
0.815
=XFe in Gt
=Si (pfu) in Ph
(d)
Ctd out
0.25
0.20
0.15
0.10
=XMg in Ctd
(e)
Ch out
0.50
0.45
0.40
0.35
0.55
=XMg in Ch

Fig. 6.11. (a) P-T pseudosection calculated for a modified composition of chloritoid schist 39k (Table 6.3, 39k-M_2) with PERPLE_X (see text). (b) Isopleths of XMg in garnet. (c) Isopleths of Si contents in phengite and XFe in garnet. (d) XMg isopleths in chloritoid. (e) XMg isopleths in chlorite. Abbreviations as in Figures 6.2, 6.5 and 6.7. For greytones of P-T fields see Figure 6.5.

6.7. U-Th-Pb monazite dating

One hundred eleven EMP analyses were achieved on 18 grains of monazite in sample 38w (staurolite-andalusite bearing schist). The monazite grains are ca.5-25 µm in diameter and located in mica (Fig. 6.12a, b) and quartz (Fig. 6.12e, f) domains and enclosed in andalusite (Fig. 6.12c, d). According to BSE images, most grains show patchy zoning (Fig. 6.12b, d, f). Clusters of monazite grains (Fig. 6.12c, d) point to the replacement of a precursor mineral that was probably allanite (see, e.g., Massonne, 2016).

The obtained ages and chemical data are summarized in Fig. 6.12g. The ages range between 307 and 385 Ma. Probably due to numerous mixed analyses of different monazite domains, different age groups are not clearly discernable. However, 5 populations with age maxima (= mean values) at 379 Ma (A), 367 Ma (B), 355 Ma (C), 339 Ma (D), and 320 Ma (E) are likely (Fig. 6.12g) applying a histogram analysis using the Isoplot program (Ludwig, 2003). In addition, ThO_2 to UO_2 ratios (Fig. 6.12j) were considered to discriminate between the five populations. However, only the older populations A to C showed lower ThO_2/UO_2 (ranges and means with a 1 sigma error: 8.3-12.2, 9.1 ± 2.5 for A; 7.5-17.4; 13.5 ± 5.7 for B; 6.7-15.0; 11.4 ± 3.2 for C) than the younger populations D and E (4.4-36.5, 16.0 ± 6.2 for D; 7.4-34.5, 17.2 ± 6.1 for E). The La to Gd (Fig. 6.12i) ratio and Y_2O_3 content (Fig. 6.12h), potential discriminators for monazite populations (e.g. Massonne 2014, 2016), yielded only fairly constant average values for the five populations: (1) ranges and means for La/Gd (with a 1 sigma error): 10.6-12.4, 11.7 ± 0.6 for A; 10.8-16.8, 13.6 ± 1.6 for B; 7.4-15.1, 11.2 ± 2.2 for C; 8.0-15.4, 13 ± 1.9 for D; 10.0-16.5, 12.9 ± 1.9 for E and (2) ranges and means for Y_2O_3 (with a 1 sigma error): 0.91-1.13 wt%, 1.10 ± 0.08 wt. % for A; 0.73-1.09 wt%, 0.86 ± 0.17 wt% for B; 0.87-1.14 wt%, 1.02 ± 0.08 wt% for C; 0.45-1.26 wt% 0.87 ± 0.16 wt% for D; 0.43-1.55 wt%, 0.87 ± 0.23 wt% for E.

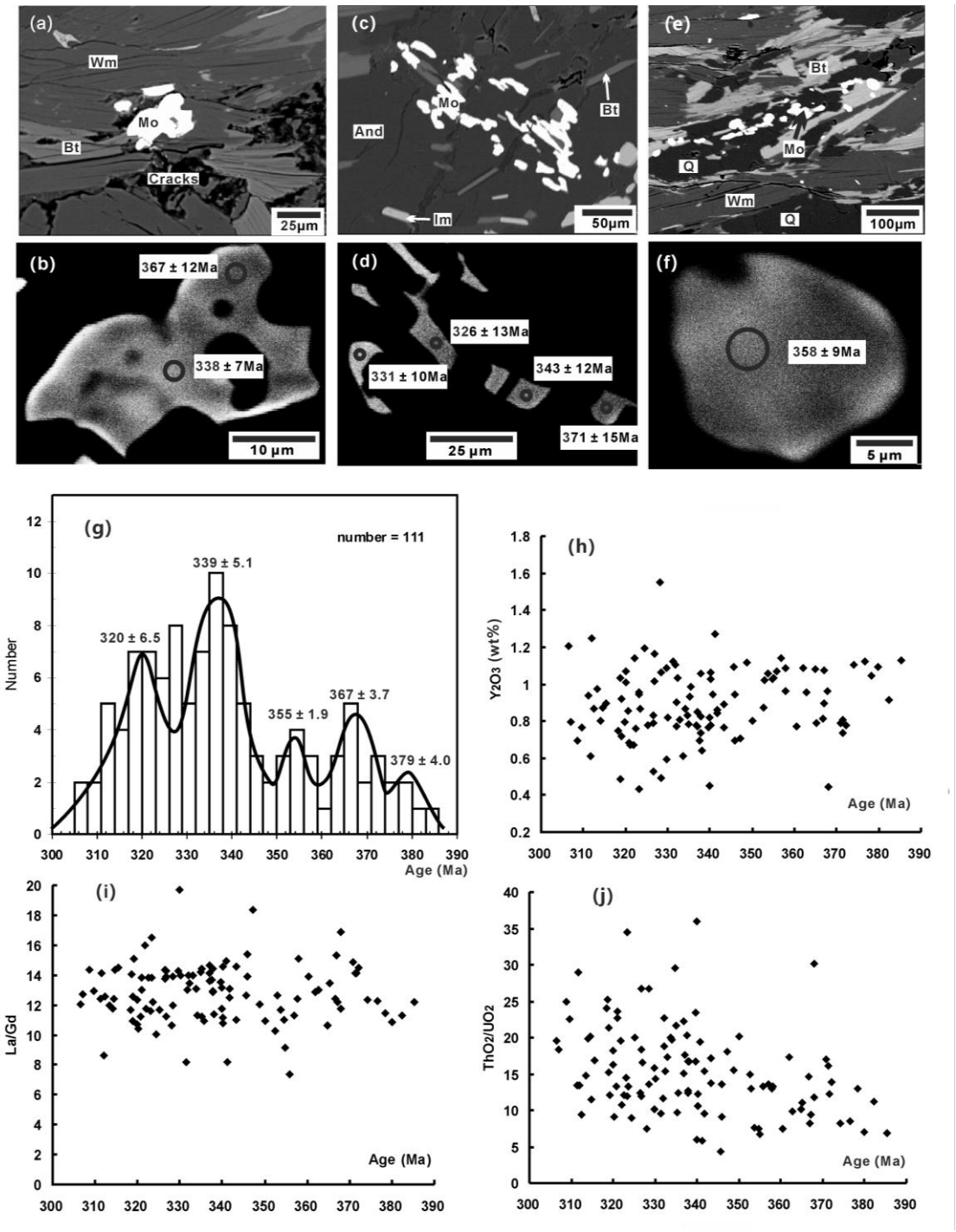

Fig. 6.12. BSE images show monazite (white) in sample Sp96-38w. (a, b) Monazite in mica domains. (c, d) Monazite cluster in andalusite. (e, f) Monazite cluster in quartz domains. (b, d, f) are high-contrast BSE images showing patchy zonation in monazite. (g) Age histogram. (h) Y_2O_3 contents versus age (Ma). (i) La to Gd ratios versus age (Ma). (j) ThO_2 to UO_2 ratios versus age (Ma).

6.8. Discussion

6.8.1. Comparison between calculated and observed mineral assemblages

For sample 38w two P-T conditions were reconstructed using mineral compositions (see: section 6.6.3). The calculated mineral assemblage at stage I is chlorite + potassic white mica + staurolite + chloritoid + ilmenite + garnet (2.5 vol.%) + paragonite + quartz. Early muscovite, staurolite and ilmenite are included in andalusite (Fig. 6.2b), but no chloritoid, garnet and paragonite were observed in the rock. Similar to Lo Pò et al. (2016), the lack of these minerals can be explained by their replacement (including early muscovite partially) by late chlorite with XMg = 0.35-0.42, muscovite with Si = 3.01-3.04 pfu and biotite during early retrograde metamorphism towards stage II. The calculated assemblage of this stage, chlorite + muscovite + ilmenite + paragonite + biotite + andalusite + quartz is realized in the rock with the exception of paragonite. Chlorite (observed XMg = 0.35-0.42), occurring in both calculated assemblages, can be exclusively related to stage II because the calculated XMg (0.50) for stage I is significantly higher than the observed one. In addition, the random orientation of chlorite and its occurrence in cracks (Fig 6.2a, b) also indicate a late formation of chlorite.

The calculated mineral assemblage for sample 39j at peak pressure conditions (stage II) is phengite + chloritoid + garnet + Na-clinopyroxene + rutile + quartz (see the P-O_2, T-O_2 and P-T pseudosections of Figs. 6.5e, f and 6.9a). This assemblage is broadly consistent with petrographic observations. For instance, rutile was found to be included in the garnet rim. The only problematic mineral is Na-clinopyroxene as it is lacking in the rock. We assume that this mineral was replaced by other minerals during retrograde metamorphism, because Na-clinopyroxene is not stable in the rock below 12 kbar according to the pseudosection calculations. The calculated assemblage for sample 39k at stage II is the same as for 39j (see pseudosections of Figs. 6.6c, 6.6d and 6.11a) and also fits the petrographic observations reported in section 6.3.3. Again rutile is, for instance, included in the garnet rim: The lack of Na-clinopyroxene is explained as for sample 39j.

The calculated mineral assemblage for stage III of both samples 39j and 39k is chlorite + phengite + chloritoid + magnetite + garnet +paraganite + rutile (Figs. 6.9a, 6.11a). This assemblage occurs in both samples; however, rutile was transformed to ilmenite after stage III.

6.8.2. P-T evolution

Both studied chloritoid schists 39j and 39k experienced the same peak P-T conditions around 21 kbar at 550-585 °C. These rocks also developed the same mineral assemblage at these conditions and experienced an identical retrograde evolution to P-T conditions of 535-575 °C and 8.5-13 kbar (Fig. 6.13). The here derived conditions are similar to those reported by López-Carmona et al. (2014) also for chloritoid schists from the Ceán unit. These authors estimated peak conditions of 22 kbar and 560 °C and an early retrograde path to 10-11 kbar and 550-560 °C. Blueschists from the Upper unit of the Íle de Groix experienced peak P-T conditions of 17-23 kbar at 450-525 ºC (Ballèvre et al., 2003; El Korh et al., 2009), thus, confirming the assumed correlation of the Ceán unit of the MTZ and the Upper unit of the Íle de Groix (see Ballèvre et al., 2014).

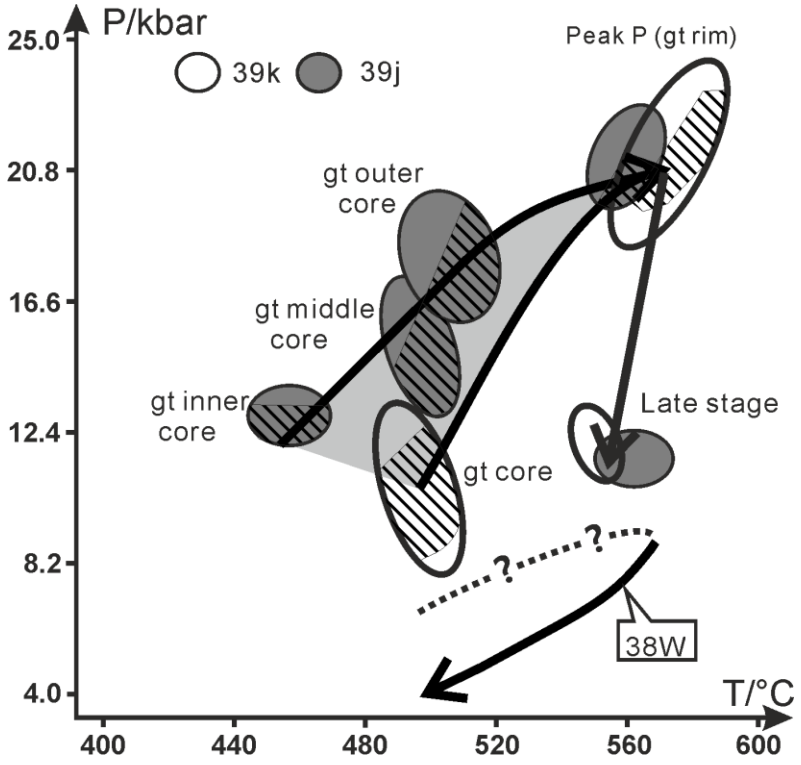

Fig. 6.13. P-T paths for chloritoid schists 39j and 39k. The solid and dashed lines indicate certain and uncertain sections, respectively. Ellipses relate to P-T estimates on the basis of intersecting isopleths (see text). On the basis the identical assemblages in corresponding P-O_2, T-O_2 and P-T pseudosections, the P-T conditions in filled ellipses (inclined lines) should be more precise than in open ellipses.

A major difference between the P-T derivations by Lopez-Carmona et al. (2014) and this study concerns the prograde path for the chloritoid schists of the Ceán unit. These authors assumed a nearly isobaric prograde heating path starting at 430°C (20 kbar). This path was calculated on the basis of a P-T peudosections and intersecting isopleths of XCa in early garnet and the highest Si content in phengite. Our study suggests a considerable burial from depths of ~ 40 km (10-11 kbar) at temperatures between 450 and 500°C (Fig. 6.13) based on garnet compositions alone. The assumption of coexisting early garnet with high Si phengite may be incorrect, but, eventually, all these prograde paths are correct which would, however, require an unusual geotectonic environment differing from shear subduction of sediments on top of a downgoing oceanic plate. At least, our prograde paths resemble those determined by Li & Massonne (2016) and Li et al. (in prep.) for diverse HP rocks, mainly eclogites, from the MTZ. Thus, we follow the interpretations for these prograde paths given by these authors: material from the overlying plate was scraped off during the subduction of an oceanic slab. This process, called tectonic erosion, was also proposed, for instance, by Massonne (2012) and Petrie et al. (2016) for similar geotectonic environments based on pseudosection modeling. This implies that the Ceán unit is not as coherent as suggested by López-Carmona et al. (2010, 2013) and Díez Fernández et al. (2011), who assumed that this unit represents an undisturbed upper part of oceanic crust. Recently, Li & Massonne (2016) already demonstrated that the Malpica-Tuy unit of the MTZ is also not a coherent unit because eclogite occurring near Malpica had experienced significantly higher peak pressures than surrounding orthogneiss. In addition, the studied staurolite-andalusite-bearing rock (38w) gives no evidence for a peak pressure higher than 10 kbar (Fig. 6.13). In fact, we cannot completely rule out that all evidence for HP metamorphism was erased in this rock, but the complete disappearance of garnet and potassic white mica with Si contents > 3.2 pfu seems to us to be unlikely. Furthermore, the analyzed monazite in sample 38w shows constantly higher Y contents than 0.5 wt% (as Y_2O_3), frequently even above 1 wt%. In the presence of garnet, which would appear at higher pressure than 10 kbar in significant quantities at temperatures around 550 °C (Fig. 6.7b), lower Y contents in monazite (close to zero) would be expected as argued by Massonne (2012, 2016).

In summary, the Ceán unit consists of metapelites which had experienced different

P-T paths and came from different geotectonic environments. The chloritoid schists are, in fact, geochemically characterized to be part of oceanic crust, but it is possible that they were first part of the base of an accretionary wedge from which they were tectonically eroded. Finally they met at deep subduction levels (~ 70 km corresponding to 21 kbar) and were exhumed together (see P-T paths in Fig. 6.13) probably by the upwards-directed mass flow of a subduction channel (see Massonne, 2012; Li et al., in prep.) as diverse eclogites from the MTZ. At higher levels, additional metasediments, which were never subducted such as our sample 38w, were involved in the Ceán unit before it was transported as a whole on top of the underlying Malpica-Tuy unit of the MTZ.

6.8.3. Interpretation of monazite ages

Although five age populations are shown in Figure 6.12a based on histogram analysis with Isoplot, only two generations can be distinguished applying compositional data of monazite (section 7.): (1) an older generation yielding ages between 385 and 350 Ma and (2) a younger generation with ages between 349 and 307 Ma. On overlap of these age ranges must be considered due to the error of a single age determination (see section 6.4.). Based on previous age determinations of metamorphic rocks from the Ceán and adjacent units including those from Brittany (see section 6.2.), the here determined older ages are compatible with the collisional event amalgamating northern Gondwana and Laurussia after closure of the Rheic ocean (see the age interpretations by van Calsteren et al., 1979; Santos Zalduegui et al., 1995; Martínez Catalán et al., 1996; Rodríguez et al., 2003; Abati et al., 2010; López-Carmona et al., 2014). In this context, the HP metamorphism of the Ceán unit (prograde and early exhumation of our samples 39j and 39k) occurred and, thus, it is likely that MP (38w) and the addressed HP rocks came together before 350 Ma. The younger monazite ages are related to retrograde events. In sample 38w the formation of andalusite porphyroblasts demonstrates that such events at low pressures had a major imprint on this rock.

6.9. Conclusions

The detailed study of HP and MP metapelites from the beach of O Riás (Ceán unit of the MTZ), has resulted in the following findings: (1) the Ceán unit is not as coherent as suggested by López-Carmona et al. (2010, 2013) and Díez Fernández et al. (2011), who

assumed that this unit represents an undisturbed upper part of oceanic crust. However, it is likely that chloritoid schists were first part of the overlying plate in a collisional setting (e.g. the base of an accretionary wedge) from which they were tectonically eroded. Finally these rocks met at deep subduction levels (~ 70 km corresponding to 21 kbar) and were exhumed together probably by the upwards-directed mass flow of a subduction channel (see Massonne, 2012; Li et al., in prep.) as diverse eclogites from the MTZ. (2) Medium-pressure metapelites, which were never subducted such as our sample 38w, experienced peak pressure conditions around 8 kbar at temperatures of 560-580 °C and were involved in the Ceán unit before it was transported as a whole on top of the underlying Malpica-Tuy unit of the MTZ. (3) The ages obtained by one hundred eleven monazite analyses confirm previously determined Upper Devonian to late Carboniferous metamorphic events. Ages between 385 and 350 Ma are compatible with the collisional event amalgamating northern Gondwana and Laurussia. Ages below 350 Ma refer to retrograde events.

7. Final conclusions

The thesis presents detailed P-T paths of 12 samples from the lower continental subunit (MTU: 5 eclogites, 3 orthogneisses and 1 glaucophanite) and upper oceanic subunit (Ceán unit: two chloritoid schist and 1 staurolite-bearing schist) in the MTZ. In addition, the magmatic environment of tholeiitic and calc-alkaline rocks was elucidated and metamorphic ages were determined. Findings on dating, metamorphic evolution and protolith character were combined. The new results contribute significantly to a better understanding of the collisional situation in early Variscan times for the northwestern portion of the Iberian Peninsula. Since the existing various geodynamic models for this region are not fully compatible with the new findings, a revised one (section 4.8.4) is presented, which also agrees with previously reported geochronological and geochemical data.

The results on one eclogite block and its surrounding gneiss from the northern MTZ highlight that both rocks had experienced a different early P-T evolution (see section 4.7). Thus, the frequently uttered opinion that a pristine contact between eclogite and gneiss proves a common P-T history of both rock types was disproved. Only the exhumation history of the studied rocks from depths of 45-50 km was a common one.

The detailed study of 3 types of eclogite, one glaucophanite and one metatonalitic gneiss from an occurrence in the center of the MTZ results in three different relatively precise P-T paths, from which the following was concluded: (1) HP rocks from the MTZ are not part of coherent crustal sections. These rocks were tectonically mixed still at HP conditions. (2) Concerning rocks which had experienced pressures in excess of 18 kbar, this mixing occurred already in the subduction channel. (3) Some of the rocks studied here were transported into the subduction zone by tectonic erosion. These findings are additionally supported by the different geotectonic nature (island arc, continental magmatic arc) of the protoliths according to the study of the geochemical features of major and trace elements.

The detailed study of HP (>10 kbar) and medium-pressure (5-10 kbar) metapelites from the beach of O Riás in the Ceán unit resulted in the following findings (see section 6.9): (1) the Ceán unit is not as coherent as suggested by López-Carmona et al. (2010,

2013) and Díez Fernández et al. (2011), who assumed that this unit represents an undisturbed upper part of oceanic crust. However, it is possible that chloritoid schists were first part of the base of an accretionary wedge from which they were tectonically eroded. Finally they met at deep subduction levels (~ 70 km corresponding to 21 kbar) and were exhumed together probably by the upwards-directed mass flow of a subduction channel as the studied eclogite from Punta Palerón (see section 4.8.4) of the northern MTZ. (2) The studied medium-pressure metapelite, which was never subducted because of peak pressure conditions of 7-9 kbar at 560-580 °C, was involved in the Ceán unit before this unit was transported as a whole on top of the underlying MTU of the MTZ. (3) The ages of one hundred eleven monazite analyses are in the range of 307-385 Ma and, thus, confirm previously determined Upper Devonian to late Carboniferous metamorphic events.

8. References

Abati, J., Gerdes, A., Suárez, J.F., Arenas, R., Whitehouse, M.J., Fernández, R.D. (2010). Magmatism and early-Variscan continental subduction in the northern Gondwana margin recorded in zircons from the basal units of Galicia, NW Spain. Geological Society of America Bulletin, 122,

Ai, Y. (1994). A revision of the garnet-clinopyroxene Fe^{2+}-Mg exchange geothermometer. Contributions to Mineralogy and Petrology, 115, 467-473.

Albert, R., Arenas, R., Sánchez-Martínez, S., Gerdes, A. (2012). The eclogite facies gneisses of the Cabo Ortegal Complex (NW Iberian Massif): Tectonothermal evolution and exhumation model. Journal of Iberian Geology, 38, 389-406.

Allaz, J., Selleck, B., Williams, M.L., Jercinovic, M.J. (2013). Microprobe analysis and dating of monazite from the Potsdam Formation, New York: A progressive record of chemical reaction and fluid interaction. American Mineralogist, 98, 1106-1119.

Anderson, D.J. & Lindsley, D.H. (1988). Internally consistent solution models for Fe-Mg-Mn-Ti oxides: Fe-Ti oxides. American Mineralogist, 73, 714-726.

Andonaegui, P., Castiñeiras, P., González Cuadra, P., Arenas, R., Sánchez Martínez, S., Abati, J., Díaz García, F., Martínez Catalán, J.R. (2012). The Corredoiras orthogneiss (NW Iberian Massif): Geochemistry and geochronology of the Paleozoic magmatic suite developed in a peri-Gondwanan arc. Lithos, 128, 84-99.

Andonaegui, P., Sánchez-Martínez, S., Castiñeiras, P., Abati, J., Arenas, R. (2015). Reconstructing subduction polarity through the geochemistry of mafic rocks in a Cambrian magmatic arc along the Gondwana margin (Órdenes Complex, NW Iberian Massif). International Journal of Earth Sciences, 104, 1-13. 219-235.

Andonaegui, P., Sánchez-Martínez, S., Castiñeiras, P., Abati, J., Arenas, R. (2016). Reconstructing subduction polarity through the geochemistry of mafic rocks in a Cambrian magmatic arc along the Gondwana margin (Órdenes Complex, NW Iberian Massif). International Journal of Earth Sciences, 105, 713-725.

Aranovich, L.Y., Lavrenteva, I.V., Kosyakova, N.A. (1988). Biotite-garnet and biotite-orthopyroxene geothermometers: correction for the variable Al-content in biotite. Geokhimiya, 5, 668-676.

Arculus, R.J. (2003). Use and abuse of the terms calcalkaline and calcalkalic. Journal of Petrology, 44, 929-935.

Arenas, R., Abati, J., Martínez Catalán, J.R., Garcia, F.D., Pascual, F.J.R. (1997). P-T evolution of eclogites from the Agualada Unit (Órdenes Complex, northwest Iberian Massif, Spain): implications for crustal subduction. Lithos, 40, 221-242.

Arenas, R., Fernández, R.D., Martínez, S.S., Gerdes, A., Fernández-Suárez, J., Albert, R. (2014). Two-stage collision: exploring the birth of Pangea in the Variscan terranes. Gondwana Research,

25, 756-763.

Arenas, R., Martínez, S.S., Castiñeiras, P., Jeffries, T.E., Fernández, R.D., Andonaegui, P. (2009). The basal tectonic mélange of the Cabo Ortegal Complex (NW Iberian Massif): a key unit in the suture of Pangea. Journal of Iberian Geology, 35, 85-125.

Arps, C.E.S. (1970). Petrology of a part of the Western Galician basement between the Rio Jallas and the Ria de Arosa (NW Spain) with emphasis on zircon investigations. Leidse Geologische Mededelingen, 46, 57-116.

Arps, C.E.S. (1981). Amphibolites and other metamorphic mafic rocks of the blastomylonitic graben in Western Galicia, NW Spain: field relations and petrography. Leidse Geologische Mededelingen, 52, 57-71.

Balen, D., Massonne, H.-J. Petrinec, Z. (2015). Collision-related Early Paleozoic evolution of a crustal fragment from the northern Gondwana margin (Slavonian Mountains, Tisia Mega-Unit, Croatia): Reconstruction of the P-T path, timing and paleotectonic implications. Lithos, 232, 211-228.

Ballèvre, M., Fourcade, S., Capdevila, R., Peucat, J.J., Cocherie, A., Fanning, C.M. (2012). Geochronology and geochemistry of Ordovician felsic volcanism in the southern Armorican Massif (Variscan belt, France): Implications for the breakup of Gondwana. Gondwana Research, 21, 1019-1036.

Barreiro, J.G., Catalán, J.R.M., Arenas, R., Castiñeiras, P., Abati, J., García, F.D., Wijbrans, J.R. (2007). Tectonic evolution of the upper allochthon of the Órdenes complex (northwestern Iberian Massif): Structural constraints to a polyorogenic peri-Gondwanan terrane. Geological Society of America Special Papers, 423, 315-332.

Bingen, B. & van Breemen, O. (1998). U-Pb monazite ages in amphibolite-to granulite-facies orthogneiss reflect hydrous mineral breakdown reactions: Sveconorwegian Province of SW Norway. Contributions to Mineralogy and Petrology, 132, 336-353.

Bohlen, S.R. & Liotta, J.J. (1986). A barometer for garnet amphibolites and garnet granulites. Journal of Petrology, 27, 1025-1034.

Braga, R., Massonne, H.-J., Morten, L. (2007). An early metamorphic stage for the Variscan Ulten Zone gneiss (NE Italy): evidence from mineral inclusions in kyanite. Mineralogical Magazine, 71, 691-702.

Brandelik, A. (2009). CALCMIN – an EXCEL™ Visual Basic application for calculating mineral structural formulae from electron microprobe analyses. Computers & Geosciences, 35, 1540-1551.

Braun, I., Montel, J.M., Nicollet, C. (1998). Electron microprobe dating of monazites from high-grade gneisses and pegmatites of the Kerala Khondalite Belt, southern India. Chemical Geology, 146, 65-85.

Brouwer, P. (2006). Theory of XRF. Almelo, Netherlands: PANalytical BV, pp. 11-14.

Carswell. D.A. (1990). Eclogie Facies Rocks. Chapman &Hall, New York, pp. 1-13.

Casini, L. & Oggiano, G. (2008). Late orogenic collapse and thermal doming of the northern Gondwana margin incorporated in the Variscan Chain: a case study from the Ozieri Metamorphic Complex, northern Sardinia, Italy. Gondwana Research, 13, 396-406.

Cherniak, D.J., Manchester, J., Watson, E.B. (2007). Zr and Hf diffusion in rutile. Earth and Planetary Science Letters, 261, 267-279.

Cherniak, D.J., Watson, E.B., Grove, M., Harrison, T.M. (2004). Pb diffusion in monazite: a combined RBS/SIMS study. Geochimica et Cosmochimica Acta, 68, 829-840.

Cocks, L.R.M. & Torsvik, T.H. (2011). The Palaeozoic geography of Laurentia and western Laurussia: a stable craton with mobile margins. Earth-Science Reviews, 106, 1-51.

Compagnoni, R. & Maffeo, B. (1973): Jadeite-bearing metagranites l.s. and related rocks in the Mount Mucrone Area (Sesia-Lanzo Zone, Western Italian Alps). Schweizerische Mineralogische und Petrographische Mitteilungen, 53, 355-378.

Connolly, J.A.D. (1990). Multivariable phase diagrams: an algorithm based on generalized thermodynamics. American Journal of Science, 290, 666-718.

Connolly, J.A.D. (2005). Computation of phase equilibria by linear programming: a tool for geodynamic modeling and its application to subduction zone decarbonation. Earth and Planetary Science Letters, 236, 524-541.

Connolly, J.A.D. & Kerrick, D.M. (1987). An algorithm and computer program for calculating composition phase diagrams. Calphad, 11, 1-55.

Connolly, J.A.D. & Petrini, K. (2002). An automated strategy for calculation of phase diagram sections and retrieval of rock properties as a function of physical conditions. Journal of Metamorphic Geology, 20, 697-708.

Cruciani, G., Franceschelli, M., Groppo, C. (2011). P-T evolution of eclogite-facies metabasite from NE Sardinia, Italy: insights into the prograde evolution of Variscan eclogites. Lithos, 121, 135-150.

Cruciani, G., Franceschelli, M., Groppo, C., Spano, M.E. (2012). Metamorphic evolution of non-equilibrated granulitized eclogite from Punta de li Tulchi (Variscan Sardinia) determined through texturally controlled thermodynamic modelling. Journal of Metamorphic Geology, 30, 667-685.

Dasgupta, S., Sengupta, P., Guha, D., Fukuoka, M. (1991). A refined garnet-biotite Fe-Mg exchange geothermometer and its application in amphibolites and granulites. Contributions to Mineralogy and Petrology, 109, 130-137.

de Jong, K. (2003). Very fast exhumation of high-pressure metamorphic rocks with excess ^{40}Ar and inherited ^{87}Sr, Betic Cordilleras, southern Spain. Lithos, 70, 91-110.

Díez Fernández, J. & Martínez Catalán, J.R. (2012). Stretching lineations in high-pressure belts: the

fingerprint of subduction and subsequent events (Malpica-Tui complex, NW Iberia). Journal of the Geological Society, 169, 531-543.

Díez Fernández, R., Castiñeiras, P., Barreiro, J.G. (2012b). Age constraints on Lower Paleozoic convection system: magmatic events in the NW Iberian Gondwana margin. Gondwana Research, 21, 1066-1079.

Díez Fernández, R., Martínez Catalán, J.R., Arenas, R., Abati, J. (2011). Tectonic evolution of a continental subduction-exhumation channel: Variscan structure of the basal allochthonous units in NW Spain. Tectonics, 30, TC3009.

Díez Fernández, R., Martínez Catalán, J.R., Arenas, R., Abati, J. (2012a). The onset of the assembly of Pangaea in NW Iberia: Constraints on the kinematics of continental subduction. Gondwana Research, 22, 20-25.

Díez Fernández, R., Martínez Catalán, J.R., Gerdes, A., Abati, J., Arenas, R., Fernández-Suárez, J. (2010). U-Pb ages of detrital zircons from the Basal allochthonous units of NW Iberia: Provenance and paleoposition on the northern margin of Gondwana during the Neoproterozoic and Paleozoic. Gondwana Research, 18, 385-399.

Díez Fernández, R., Martínez Catalán, J.R., Gómez Barreiro, J., Arenas Martín, R. (2012c). Extensional flow during gravitational collapse: a tool for setting plate convergence (Padrón migmatitic dome, Variscan belt, NW Iberia). Journal of Geology, 120, 83-103.

Du, J.X., Zhang, L.F., Shen, X.J., Bader, T. (2014). A new P-T-t path of eclogites from Chinese southwestern Tianshan: constraints from P-T pseudosections and Sm-Nd isochron dating. Lithos, 200, 258-272.

Ellis, D.J. & Green, D.H. (1979). An experimental study of the effect of Ca upon garnet-clinopyroxene Fe-Mg exchange equilibria. Contributions to Mineralogy and Petrology, 71, 13-22.

Endo, S., Wallis, S.R., Tsuboi, M., Aoya, M., Uehara, S.I. (2012). Slow subduction and buoyant exhumation of the Sanbagawa eclogite. Lithos, 146, 183-201.

Ernst, W.G., & Dal Piaz, G.V. (1978). Mineral paragenesis of eclogitic rocks and related mafic schists of the Piemonte ophiolite nappe, Breuil-St. Jacques area, Italian Western Alps. American Mineralogist, 63, 621-640.

Ewing, T.A., Hermann, J., Rubatto, D. (2013). The robustness of the Zr-in-rutile and Ti-in-zircon thermometers during high-temperature metamorphism (Ivrea-Verbano Zone, northern Italy). Contributions to Mineralogy and Petrology, 165, 757-779.

Ferry, J.M., & Watson, E.B. (2007). New thermodynamic models and revised calibrations for the Ti-in-zircon and Zr-in-rutile thermometers. Contributions to Mineralogy and Petrology, 154, 429-437.

Ferry, J.T. & Spear, F.S. (1978). Experimental calibration of the partitioning of Fe and Mg between

biotite and garnet. Contributions to mineralogy and petrology, 66, 113-117.

Finger, F., Roberts, M.P., Haunschmid, B., Schermaier, A., Steyrer, H.P. (1997). Variscan granitoids of central Europe: their typology, potential sources and tectonothermal relations. Mineralogy and Petrology, 61, 67-96.

Floor, P. (1967). Petrology of an aegirine-riebeckite gneiss-bearing part of the Hesperian Massif: the Galiñeiro and sourrounding areas, Vigo, Spain. Leidse Geologische Mededelingen, 36, pp. 164.

Foster, G., Kinny, P., Vance, D., Prince, C., Harris, N. (2000). The significance of monazite U-Th-Pb age data in metamorphic assemblages; a combined study of monazite and garnet chronometry. Earth and Planetary Science Letters, 181, 327-340.

Franke, W. (1989). Variscan plate tectonics in Central Europe-current ideas and open questions. Tectonophysics, 169, 221-228.

Fuenlabrada, J.M., Arenas, R., Díez Fernández, R., Sánchez Martínez, S., Abati, J., López Carmona, A. (2012). Sm–Nd isotope geochemistry and tectonic setting of the metasedimentary rocks from the basal allochthonous units of NW Iberia (Variscan suture, Galicia). Lithos, 148, 196-208.

Fuenlabrada, J.M., Arenas, R., Martínez, S.S., García, F.D., Castiñeiras, P. (2010). A peri-Gondwanan arc in NW Iberia: I: isotopic and geochemical constraints on the origin of the arc—a sedimentary approach. Gondwana Research, 17, 338-351.

Fuhrman, M.L. & Lindsley, D.H. (1988). Ternary-feldspar modeling and thermometry. American Mineralogist, 73, 201-215.

Gao, X.Y., Zheng Y.F., Chen Y.X. (2012). Dehydration melting of ultrahigh-pressure eclogite in the Dabie orogen: evidence from multiphase solid inclusions in garnet. Journal of Metamorphic Geology, 30, 193-212.

Gerya, T.V., Stöckhert, B., Perchuk, A.L. (2002). Exhumation of high-pressure metamorphic rocks in a subduction channel: A numerical simulation. Tectonics, 21, 6-1–6-19.

Giacomini, F., Bomparola, R.M., Ghezzo, C. (2005). Petrology and geochronology of metabasites with eclogite facies relics from NE Sardinia: constraints for the Palaeozoic evolution of Southern Europe. Lithos, 82, 221-248.

Gil Ibarguchi, J.I. (1995). Petrology of jadeite metagranite and associated orthogneiss from the Malpica-Tuy allochthon (Northwest Spain). European Journal of Mineralogy, 7, 403-416.

Gil Ibarguchi, J.I., Mendia, M., Girardeau, J., Peucat, J.J. (1990). Petrology of eclogites and clinopyroxene-garnet metabasites from the Cabo Ortegal Complex (northwestern Spain). Lithos, 25, 133-162.

Gil Ibarguchi, J.I. & Ortega Gironés, E. (1985). Petrology, structure and geotectonic implications of glaucophane-bearing eclogites and related rocks from the Malpica-Tuy (MT) Unit, Galicia, Northwest Spain. Chemical Geology, 50, 145-162.

Godard, G. (2009). Two orogenic cycles recorded in eclogite-facies gneiss from the Southern

Armorican Massif (France). European Journal of Mineralogy, 21, 1173-1190.

Green, T.H. & Adam, J. (1991). Assessment of the garnet-clinopyroxene Fe-Mg exchange thermometer using new experimental data. Journal of Metamorphic Geology, 9, 341-347.

Green, T.H. & Hellman, P.L. (1982). Fe-Mg partitioning between coexisting garnet and phengite at high pressure, and comments on a garnet-phengite geothermometer. Lithos, 15, 253-266.

Groppo, C. & Rolfo, F. (2008). Counterclockwise P-T evolution of the Aghil Range: Metamorphic record of an accretionary melange between Kunlun and Karakorum (SW Sinkiang, China). Lithos, 105, 365-378.

Groppo, C., Rolfo, F., Liu, Y.C., Deng, L.P., Wang, A.D. (2015). P-T evolution of elusive UHP eclogites from the Luotian dome (North Dabie Zone, China): How far can the thermodynamic modeling lead us?. Lithos, 226, 183-200.

Guillot, S., De Sigoyer, J., Lardeaux, J.M., Mascle, G. (1997). Eclogitic metasediments from the Tso Morari area (Ladakh, Himalaya): Evidence for continental subduction during India-Asia convergence. Contributions to Mineralogy and Petrology, 128, 197-212.

Hirajima, T., Banno, S., Hiroi, Y., Ohta, Y. (1988). Phase petrology of eclogites and related rocks from the Motalafjella high-pressure metamorphic complex in Spitsbergen (Arctic Ocean) and its significance. Lithos, 22, 75-97.

Holland, T.J.B. (1980). The reaction albite = jadeite + quartz determined experimentally in the range 600-1200 degrees C. American Mineralogist, 65, 129-134.

Holland, T. & Powell, R. (1991). A compensated-Redlich-Kwong (CORK) equation for volumes and fugacities of CO_2 and H_2O in the range 1 bar to 50 kbar and 100-1600 °C. Contributions to Mineralogy and Petrology, 109, 265-273.

Holland, T.J.B. & Powell, R. (1998). An internally consistent thermodynamic data set for phases of petrological interest. Journal of metamorphic Geology, 16, 309-343.

Horváth, P., Balen, D., Finger, F., Tomljenović, B., Krenn, E. (2010). Contrasting P-T-t paths from the basement of the Tisia Unit (Slavonian Mts., NE Croatia): Application of quantitative phase diagrams and monazite age dating. Lithos, 117, 269-282.

Hynes, A. & Forest, R.C. (1988). Empirical garnet-muscovite geothermometry in low-grade metapelites, Selwyn Range (Canadian Rockies). Journal of Metamorphic Geology, 6, 297-309.

Iaccarino, S., Montomoli, C., Carosi, R., Massonne, H.-J., Langone, A., Visonà, D. (2015). Pressure-temperature-time-deformation path of kyanite-bearing migmatitic paragneiss in the Kali Gandaki valley (Central Nepal): Investigation of Late Eocene-Early Oligocene melting processes. Lithos, 231, 103-121.

Irvine, T. & Baragar, W. (1971). A guide to the chemical classification of the common volcanic rocks. Canadian Journal of Earth Sciences, 8, 523-548.

Jahn, B.-M. (1999). Sm-Nd isotope tracer study of UHP metamorphic rocks: Implications for

continental subduction and collisional tectonics. International Geology Review, 41, 859-885.

Jakes, P., & Gill, J. (1970). Rare earth elements and the island arc tholeiitic series. Earth and Planetary Science Letters, 9, 17-28.

Jamtveit, B. (1987). Metamorphic evolution of the Eiksunddal eclogite complex. Western Norway, and some tectonic implications. Contributions to Mineralogy and Petrology, 95, 82-99.

Janák, M., Ravna, E.J.K., Kullerud, K. (2012). Constraining peak P-T conditions in UHP eclogites: calculated phase equilibria in kyanite- and phengite-bearing eclogite of the Tromsø Nappe, Norway. Journal of Metamorphic Geology, 30, 377-396.

Johannes, W. (1978). Pressure comparing experiments with NaCl, AgCl, talc, and pyrophyllite assemblies in a piston cylinder apparatus. Neues Jahrbuch für Mineralogie Monatshefte, 1978, 84-92.

Johannes, W., Bell, P.M., Mao, H.K., Boettcher, A.L., Chipman, D.W., Hays, J.F., Newton, R.C., Seifert, F. (1971). An interlaboratory comparison of piston-cylinder pressure calibration using the albite-breakdown reaction. Contributions to Mineralogy and Petrology, 32, 24-38.

John, T., Schenk, V., Haase, K., Scherer, E., Tembo, F. (2003). Evidence for a Neoproterozoic ocean in south-central Africa from mid-oceanic-ridge-type geochemical signatures and pressure-temperature estimates of Zambian eclogites. Geology, 31, 243-246.

John, T., Scherer, E.E., Haase, K., Schenk, V. (2004). Trace element fractionation during fluid-induced eclogitization in a subducting slab: trace element and Lu-Hf-Sm-Nd isotope systematics. Earth and Planetary Science Letters, 227, 441-456.

Kadarusman, A., Massonne, H.-J., van Roermund, H., Permana, H., Munasri, (2007). P-T evolution of eclogites and blueschists from the Luk Ulo Complex of Central Java, Indonesia. International Geology Review, 49, 329-356.

Kaneko, Y., Katayama, I., Yamamoto, H., Misawa, K., Ishikawa, M., Rehman, H.U., Kausar, A.B., & Shiraishi, K. (2003). Timing of Himalayan ultrahigh-pressure metamorphism: sinking rate and subduction angle of the Indian continental crust beneath Asia. Journal of Metamorphic Geology, 21, 589-599.

Kay, S.M., Godoy, E., Kurtz, A. (2005). Episodic arc migration, crustal thickening, subduction erosion, and magmatism in the south-central Andes. Geological Society of America Bulletin, 117, 67-88.

Kelsey, D.E., Powell, R., Wilson, C.J.L., Steele, D.A. (2003). (Th + U)-Pb monazite ages from Al-Mg-rich metapelites, Rauer Group, East Antarctica. Contributions to Mineralogy and Petrology, 146, 326-340.

Kirchner, K.L., Behr, W.M., Loewy, S., Stockli, D.F. (2016). Early Miocene subduction in the western Mediterranean: Constraints from Rb-Sr multimineral isochron geochronology. Geochemistry, Geophysics, Geosystems. In press.

Kleemann, U. & Reinhardt, J. (1994). Garnet-biotite thermometry revised: the effect of Al^{VI} and Ti in

biotite. European Journal of Mineralogy, 6, 925-941.

Klemd, R., John, T., Scherer, E.E., Rondenay, S., Gao, J. (2011). Changes in dip of subducted slabs at depth: petrological and geochronological evidence from HP-UHP rocks (Tianshan, NW-China). Earth and Planetary Science Letters, 310, 9-20.

Koons, P.O. (1986). Relative geobarometry from high-pressure rocks of quartzofeldspathic composition from the Sesia Zone, Western Alps, Italy. Contributions to Mineralogy and Petrology, 93, 322-334.

Kouketsu, Y., Enami, M., Mizukami, T. (2010). Omphacite-bearing metapelite from the Besshi region, Sambagawa metamorphic belt, Japan: Prograde eclogite facies metamorphism recorded in metasediment. Journal of Mineralogical and Petrological Sciences, 105, 9-19.

Krebs, M., Schertl, H.-P., Maresch, W.V., Draper, G. (2011). Mass flow in serpentinite-hosted subduction channels: P-T-t path patterns of metamorphic blocks in the Rio San Juan mélange (Dominican Republic). Journal of Asian Earth Sciences, 42, 569-595.

Krogh, E.J. (1980). Geochemistry and petrology of glaucophane-bearing eclogites and associated rocks from Sunnfjord, western Norway. Lithos, 13, 355-380.

Krogh, E.J. (1981). Compatible P-T conditions for eclogites and surrounding gneisses in the Kristiansund area, western Norway. Contributions to Mineralogy and Petrology, 75, 387-393.

Krogh, E.J. (1988). The garnet-clinopyroxene Fe-Mg geothermometer—a reinterpretation of existing experimental data. Contributions to Mineralogy and Petrology, 99, 44-48.

Krogh, E.J. & Råheim, A. (1978). Temperature and pressure dependence of Fe-Mg partitioning between garnet and phengite, with particular reference to eclogites. Contributions to Mineralogy and Petrology, 66, 75-80.

Kroner, U. & Romer, R.L. (2013). Two plates—many subduction zones: the Variscan orogeny reconsidered. Gondwana Research, 24, 298-329.

Krs, M., Pruner, P., Man, O. (2001). Tectonic and paleogeographic interpretation of the paleomagnetism of Variscan and pre-Variscan formations of the Bohemian Massif, with special reference to the Barrandian terrane. Tectonophysics, 332, 93-114.

Lanari, P., Riel, N., Guillot, S., Vidal, O., Schwartz, S., Pêcher, A., Hattori, K. (2013). Deciphering high-pressure metamorphism in collisional context using microprobe-mapping methods: application to the Stak eclogitic massif (NW Himalaya). Geology, 41, 111-114.

Lavrenteva, I.V. & Perchuk, L.L. (1981). Phase correspondence in the system biotite-garnet: experimental data. Doklady Akademii Nauk SSSR, 260, 731-734.

Le Bas, M.J., Le Maitre, R.W., Streckeisen, A., Zanettin, B. (1986). A chemical classification of volcanic rocks based on the total alkali-silica diagram. Journal of Petrology, 27, 745-750.

Leake, B.E., Woolley, A.R., Arps, C.E.S., Birch, W.D., Gilbert, M.C., Grice, J.D., Hawthorne, F.C., Kato, A., Kisch, H.J., Krivovichev, V.G., Linthout, K., Laird, J., Mandarino, J.A., Maresch, W.V.,

Nickel, E.H., Rock, N.M.S., Schumacher, J.C., Smith, D.C., Stephenson, N.C.N., Ungaretti, L., Whittaker, E.J.W., and Guo, Y.Z. (1997). Nomenclature of amphiboles: report of the subcommittee on amphiboles of the International Mineralogical Association, commission on new minerals and mineral names. American Mineralogist, 82, 1019-1037.

Li, B. & Massonne, H.-J. (2016). Early Variscan P-T evolution of an eclogite body and its adjacent orthogneiss from the northern Malpica-Tuy shear-zone in NW Spain. European Journal of Mineralogy, DOI: 10.1127/ejm/2016/0028-2569, First Published on July 17, 2016.

Li, B., Massonne, H.-J., Opitz, J., in prep. Clockwise and anticlockwise P-T paths of eclogite-facies rocks from the 'La Pioza' land site of the Malpica-Tuy shear zone, NW Spain.

Liu, Y., Siebel, W., Massonne, H.-J., Xiao, X. (2007). Geochronological and petrological constraints for the tectonic evolution of the central Greater Himalayan Sequence in the Kharta area, southern Tibet. Journal of Geology, 115, 215-230.

Llana-Fúnez, S. & Marcos, A. (2001). The Malpica-Lamego Line: a major crustal-scale shear zone in the Variscan belt of Iberia. Journal of Structural Geology, 23, 1015-1030.

Lo Pò, D., Braga, R., 2014. Influence of ferric iron on phase equilibria in greenschist facies assemblages: the hematite-rich metasedimentary rocks from the Monti Pisani (Northern Apennines). Journal of Metamorphic Geology 32, 371-387.

Lo Pò, D., Braga, R., Massonne, H.-J., Molli, G., Montanini, A. Theye, T. (2016). Fluid-induced breakdown of monazite in medium-grade metasedimentary rocks of the Pontremoli basement (Northern Apennines, Italy). Journal of Metamorphic Geology, 34, 63-84.

López-Carmona, A. (2013). Roches du faciès des schistes bleus du Complexe de Malpica-Tui (NO du Massif Ibérique). Doctoral dissertation, Université de Rennes 1, pp. 55.

López-Carmona, A., Abati, J., Pitra, P., Lee, J.K. (2014a). Retrogressed lawsonite blueschists from the NW Iberian Massif: P-T-t constraints from thermodynamic modelling and $^{40}Ar/^{39}Ar$ geochronology. Contributions to Mineralogy and Petrology, 167, 1-20.

López-Carmona, A., Abati, J., Pitra, P., Lee, J.K.W., Fernández-Suárez, J., Gutiérrez-Alonso, G. (2014b). P-T-t constraints and geodynamic implications from blueschists and eclogites of the north Gondwanan margin in Iberia (Malpica-Tui complex, Galicia). Gondwana 15, Abstract Vol., 100, http://igcp591.org/downloads/Gondwana15_Abstracts.pdf.

López-Carmona, A., Abati, J., Reche, J. (2010). Petrologic modeling of chloritoid-glaucophane schists from the NW Iberian Massif. Gondwana Research, 17, 377-391.

López-Carmona, A., Pitra, P., Abati, J. (2013). Blueschist-facies metapelites from the Malpica-Tui Unit (NW Iberian Massif): phase equilibria modelling and H_2O and Fe_2O_3 influence in high-pressure assemblages. Journal of Metamorphic Geology, 31, 263-280.

Lü, Z., Zhang, L.F., Qü, J.F., Li, H.F. (2007). Petrology and metamorphic P-T path of eclogites from Habutengsu, southwestern Tianshan, Xinjiang. Acta Petrologica Sinica, 23, 1617-1626.

Marmo, B.A., Clarke, G.L., Powell, R. (2002). Fractionation of bulk rock composition due to porphyroblast growth; effects on eclogite facies mineral equilibria, Pam Peninsula, New Caledonia. Journal of Metamorphic Geology, 20, 151-165.

Martínez Catalán, J.R., Arenas, R., Abati, J., Sánchez Martínez, S., Diaz Garcia, F., Fernández Suárez, J., González Cuadra, P., Castiñeiras, P., Gómez Barreiro, J., Díez Montes, A., González Clavijo, E., Rubio Pascual, F.J., Andonaegui, P., Jeffries, T.E., Alcock, J.E., Díez Fernández, R., López Carmona, A. (2009). A rootless suture and the loss of the roots of a mountain chain: the Variscan belt of NW Iberia. Comptes Rendus Geoscience, 341, 114-126.

Martínez Catalán, J.R., Arenas, R., Díaz García, F., Cuadra, P.G., Gómez-Barreiro, J., Abati, J., Castiñeiras, P., Fernández-Suárez, J., Martínez, S.S, Andonaegui, P., Clavijo, E.G., Díez Montes, A., Rubio Pascual, F. J., Aguado, B.V. (2007). Space and time in the tectonic evolution of the northwestern Iberian Massif: Implications for the Variscan belt. Geological Society of America Memoirs, 200, 403-423.

Martínez Catalán, J.R., Arenas, R., Diaz Garcia, F., Rubio Pascual, F.J., Abati, J., Marquinez, J. (1996). Variscan exhumation of a subducted Paleozoic continental margin: The basal units of the Ordenes Complex, Galicia, NW Spain. Tectonics, 1, 106-121.

Massonne, H.-J. (2009). Hydration, dehydration, and melting of metamorphosed granitic and quartz-dioritic rocks at high and ultrahigh pressure conditions. Earth and Planetary Science Letters, 288, 244-254.

Massonne, H.-J. (2010). Phase relations and dehydration behaviour of calcareous sediments at very-low to low grade metamorphic conditions. Periodico di Mineralogia, 79, 21-43.

Massonne, H.-J. (2012). Formation of amphibole and clinozoisite-(Clino)zoisite in eclogite owing to fluid infiltration during exhumation in a subduction channel. Journal of Petrology, 53, 1969-1998.

Massonne, H.-J. (2013). Constructing the pressure-temperature path of ultrahigh-pressure rocks. Elements, 9, 267-272.

Massonne, H.-J. (2014). Wealth of P-T-t information in medium-high grade metapelites: Example from the Jubrique Unit of the Betic Cordillera, S Spain. Lithos, 208, 137-157.

Massonne, H.-J. (2015). Derivation of P-T paths from high-pressure metagranites — examples from the Gran Paradiso Massif, western Alps. Lithos, 226, 265-279.

Massonne, H.J. (2016). Hydration of the lithospheric mantle by the descending plate in a continent–continent collisional setting and its geodynamic consequences. Journal of Geodynamics, 96, 50-61.

Massonne, H.-J. & Czambor, A. (2007). Geochemical signatures of Variscan eclogites from the Saxonian Erzgebirge, central Europe. Chemie der Erde – Geochemistry, 67, 69-83.

Massonne, H. J. & Calderón, M. (2008). P-T evolution of metapelites of the Guarguaráz Complex, Argentina — evidence for Devonian crustal thickening close to the western Gondwana margin.

Revista Geológica de Chile, 35, 215-231.

Massonne, H.-J. & Kopp, J. (2005). A low-variance mineral assemblage with talc and phengite in an eclogite from the Saxonian Erzgebirge, Central Europe, and its P-T evolution. Journal of Petrology, 46, 355-375.

Massonne, H.-J. & Schreyer, W. (1987). Phengite geobarometry based on the limiting assemblage with K-feldspar, phlogopite, and quartz. Contributions to Mineralogy and Petrology, 96, 212-224.

Massonne, H.-J. & Toulkeridis, T. (2012). Widespread relics of high-pressure metamorphism confirm major terrane accretion in Ecuador: a new example from the Northern Andes. International Geology Review, 54, 67-80.

Massonne, H.-J., Opitz, J., Theye, T., Nasir, S. (2013). Evolution of a very deeply subducted metasediment from As Sifah, northeastern coast of Oman. Lithos, 156, 171-185.

Matte, P. (1986). Tectonics and plate tectonics model for the Variscan belt of Europe. Tectonophysics, 126, 329-374.

Matte, P. (1991). Accretionary history and crustal evolution of the Variscan belt in Western Europe. Tectonophysics, 196, 309-337.

Matte, P. (1998). Continental subduction and exhumation of HP rocks in Paleozoic orogenic belts: Uralides and Variscides. Geologiska Föreningens i Stockholm Förhandlingar, 120, 209-222.

McKerrow, W.S., Mac Niocaill, C., Ahlberg, P.E., Clayton, G., Cleal, C.J., Eagar, R.M.C. (2000). The late Palaeozoic relations between Gondwana and Laurussia. Geological Society, London, Special Publications, 179, 9-20.

Möller, A., Hensen, B.J., Armstrong, R.A., Mezger, K. Ballèvre, M. (2003). U-Pb zircon and monazite age constraints on granulite-facies metamorphism and deformation in the Strangways Metamorphic Complex (central Australia). Contributions to Mineralogy and Petrology, 145, 406-423.

Morimoto, N., Fabries, J., Ferguson, A.K., Ginzburg, I.V., Ross, M., Seifert, F.A., Zussman, J., Aoki, K., Gottardi, G. (1988): Nomenclature of pyroxenes. American Mineralogist, 73, 1123-1133.

Nakamura, D. (2009). A new formulation of garnet-clinopyroxene geothermometer based on accumulation and statistical analysis of a large experimental data set. Journal of Metamorphic Geology, 27, 495-508.

Nakano, N., Osanai, Y., Owada, M., Satish-Kumar, M., Adachi, T., Jargalan, S., Yoshimoto, A., Syeryekhan, K., Boldbaatar, C.H. (2015). Multiple growth of garnet, sillimanite/kyanite and monazite during amphibolite facies metamorphism: implications for the P-T-t and tectonic evolution of the western Altai Range, Mongolia. Journal of Metamorphic Geology, 33, 937-958.

Nakano, N., Osanai, Y., Sajeev, K., Hayasaka, Y., Miyamoto, T., Minh, N.T., Owada, M., Windley, B. (2010). Triassic eclogite from northern Vietnam: inferences and geological significance. Journal of Metamorphic Geology, 28, 59-76.

Nance, R.D., Gutiérrez-Alonso, G., Keppie, J.D., Linnemann, U., Murphy, J.B., Quesada, C., Strachan, R.A., Woodcock, N.H. (2010). Evolution of the Rheic Ocean. Gondwana Research, 17, 194-222.

Ogenhall, E., 2010. Geological Evolution of the Supracrustal Palaeoproterozoic Hamrånge Group: A Svecofennian Case Study. PhD dissertation, Uppsala universitet, pp. 20-28.

Orellana, F.A., Gálvez, C.G., Roldán, M.T., García-Ruiz, C. (2013). Applications of laser-ablation-inductively-coupled plasma-mass spectrometry in chemical analysis of forensic evidence. TrAC Trends in Analytical Chemistry, 42, 1-34.

Parrish, R.R. (1990). U-Pb dating of monazite and its application to geological problems. Canadian Journal of Earth Sciences, 27, 1431-1450.

Pattison, D.R.M. & Newton, R.C. (1989). Reversed experimental calibration of the garnet-clinopyroxene Fe-Mg exchange thermometer. Contributions to Mineralogy and Petrology, 101, 87-103.

Pearce, J.A. (1983). Role of the sub-continental lithosphere in magma genesis at active continental margins. In: Hawkesworth C.J., Norry M.J. (eds), Continental basalts and mantle xenoliths. Shiva, Nantwich, 230-249.

Pearce, J.A., (2008). Geochemical fingerprinting of oceanic basalts with applications to ophiolite classification and the search for Archean oceanic crust. Lithos, 100, 14-48.

Pearce, J.A. & Cann, J.R. (1973). Tectonic setting of basic volcanic rocks determined using trace element analyses. Earth and Planetary Science Letters, 19, 290-300.

Pearce, T.H., Gorman, B.E., Birkett, T.C. (1975). The TiO_2-K_2O-P_2O_5 diagram: a method of discriminating between oceanic and non-oceanic basalts. Earth and Planetary Science Letters, 24, 419-426.

Peccerillo, A. & Taylor, S.R. (1976). Geochemistry of Eocene calc-alkaline volcanic rocks from the Kastamonu area, Northern Turkey. Contributions to Mineralogy and Petrology, 58, 63-81.

Perfit, M.R., Gust, D.A., Bence, A.E., Arculus, R.J., Taylor, S.R. (1980). Chemical characteristics of island-arc basalts: implications for mantle sources. Chemical Geology, 30, 227-256.

Petrie, M.B., Gilotti, J.A., McClelland, W.C., Massonne, H.-J., van Staal, C. (2016). The P-T-t path of eclogites in the St. Cyr klippe, Yukon, Canada: High-pressure metamorphism in an accreted terrane of the North American Cordillera. European Journal of Mineralogy, in press.

Platt, J.P., Anczkiewicz, R., Soto, J.I., Kelley, S.P., Thirlwall, M. (2006). Early Miocene continental subduction and rapid exhumation in the western Mediterranean. Geology, 34, 981-984.

Powell, R. & Holland, T.J.B. (1988). An internally consistent dataset with uncertainties and correlations: 3. Applications to geobarometry, worked examples and a computer program. Journal of metamorphic Geology, 6, 173-204.

Powell, R. & Holland, T. (1999). Relating formulations of the thermodynamics of mineral solid solutions: Activity modeling of pyroxenes, amphiboles, and micas. American Mineralogist, 84,

1-14.

Pullen, A., Kapp, P., Gehrels, G.E., Vervoort, J.D., Ding, L. (2008). Triassic continental subduction in central Tibet and Mediterranean-style closure of the Paleo-Tethys Ocean. Geology, 36, 351-354.

Ravna, K. (2000). The garnet-clinopyroxene Fe^{2+}-Mg geothermometer: an updated calibration. Journal of metamorphic Geology, 18, 211-219.

Ravna, E.J.K., Andersen, B., Jolivet, L., De Capitani, C. (2010). Cold subduction and the formation of lawsonite eclogite-constraints from prograde evolution of eclogitized pillow lava from Corsica. Journal of Metamorphic Geology, 28, 381-395.

Reed, S.J.B., (2005). Electron microprobe analysis and scanning electron microscopy in geology. Cambridge University Press: pp. 7-11.

Rivas-Kozlowski, M.M. (1995). Kristallinkartierung in der Malpica-Tuy-Zone (NW-Spanien) nördlich des Fervenza Stausees (Kommune Brandomil). Unpubl. Diploma mapping report, Ruhr-Universität Bochum, pp. 59.

Rodríguez Aller, J. (2005). Recristalización y deformación de litologías supracorticales sometidas a metamorfismo de alta presión (Complejo de Malpica-Tuy, NO del Macizo Ibérico). Ediciós do Castro, pp 572.

Rodríguez, J., Cosca, M.A., Gil Ibarguchi, J.I., Dallmeyer, R.D. (2003). Strain partitioning and preservation of $^{40}Ar/^{39}Ar$ ages during Variscan exhumation of a subducted crust (Malpica-Tui complex, NW Spain). Lithos, 70, 111-139.

Rodríguez, J., Paquette, J.L., Gil Ibarguchi, J.I. (2007). U-Pb dating of Lower Ordovician alkaline magmatism in the Gondwana margin (Malpica-Tui Complex, Iberian Massif): Latest continental events before oceanic spreading. In: Arenas, R., Martínez Catalán, J.R., Abati, J., Sánchez Martínez, S. (Eds.), The rootless Variscan suture of NW Iberia (Galicia Spain). Field trip guide and conference abstracts. International Geological Correlation Programme 497. The Rheic Ocean: Its origin, evolution and correlatives. Publicaciones del Instituto Geológico y Minero de España, pp. 163-164.

Rubio Pascual, F.J., Arenas, R., Díez Gárcía, F., Martínez Catalán, J.R., Abati, J. (2002). Contrasting high-pressure metabasites from the Santiago unit (Ordenes Complex, northwestern Iberian Massif, Spain). Geological Society of America Special Papers, 364, 105-124.

Rubio Pascual, F.J., Matas, J., Martín Parra, L.M. (2013). High-pressure metamorphism in the Early Variscan subduction complex of the SW Iberian Massif. Tectonophysics, 592, 187-199.

Săbău, G., & Massonne, H.-J. (2003). Relationships among eclogite bodies and host rocks in the Lotru metamorphic suite (South Carpathians, Romania): petrological evidence for multistage tectonic emplacement of eclogites in a medium-pressure terrain. International Geology Review, 45, 225-262.

Santos Zalduegui, J.F., Schärer, U., Gil Ibarguchi, J.I. (1995). Isotope constraints on the age and origin

of magmatism and metamorphism in the Malpica-Tuy allochthon, Galicia, NW Spain. Chemical Geology, 121, 91-103.

Scherrer, N.C., Engi, M., Gnos, E., Jakob, V., Liechti, A. (2000). Monazite analysis; from sample preparation to microprobe age dating and REE quantification. Schweizerische mineralogische und petrographische Mitteilungen, 80, 93-105.

Shelley, D. & Bossière, G. (2000). A new model for the Hercynian Orogen of Gondwanan France and Iberia. Journal of Structural Geology, 22, 757-776.

Smith, D.C., Kienast, J.R., Kornprobst, J., Lasnier, B. (1982). Eclogites and their problems: an introduction to the First Int. Eclogite Conf. Terra Cognita, 2, 283-296.

Smye, A.J., Warren, C.J. Bickle, M.J. (2013). The signature of devolatisation: Extraneous 40Ar systematics in high-pressure metamorphic rocks. Geochimica et Cosmochimica Acta, 113, 94-112.

Spear, F.S. (1995). Metamorphic phase equilibria and pressure-temperature-time paths. Washington: Mineralogical Society of America, pp. 17.

Štípská, P., Chopin, F., Skrzypek, E., Schulmann, K., Pitra, P., Lexa, O., Martelat, J.E., Bollinger, C. Žáčková, E. (2012). The juxtaposition of eclogite and mid-crustal rocks in the Orlica-Śnieżnik Dome, Bohemian Massif. Journal of Metamorphic Geology, 30, 213-234.

Sun, S.S. & McDonough, W.F. (1989). Chemical and isotopic systematics of oceanic basalts: implications for mantle composition and processes. Journal of the Geological Society, London, Special Publications, 42, 313-345.

Suzuki, K. & Adachi, M. (1991). Precambrian provenance and Silurian metamorphism of the Tsubonosawa paragneiss in the South Kitakami terrane, Northeast Japan, revealed by the chemical Th-U-total Pb isochron ages of monazite, zircon and xenotime. Geochemical Journal, 25, 357-376.

Taylor-Jones, K. & Powell, R. (2015). Interpreting zirconium-in-rutile thermometric results. Journal of Metamorphic Geology, 33, 115-122.

Tian, Z.L. & Wei, C.J. (2013). Metamorphism of ultrahigh-pressure eclogites from the Kebuerte Valley, South Tianshan, NW China: phase equilibria and P-T path. Journal of Metamorphic Geology, 31, 281-300.

Toksöz, M.N., Minear, J.W., Julian, B.R. (1971). Temperature field and geophysical effects of a downgoing slab. Journal of Geophysical Research, 76, 1113-1138.

Tomkins, H.S., Powell, R.., Ellis, D.J. (2007). The pressure dependence of the zirconium-in-rutile thermometer. Journal of Metamorphic Geology, 25, 703-713.

Tsujimori, T., Sisson, V.B., Liou, J.G., Harlow, G.E., Sorensen, S.S. (2006). Very-low temperature record of the subduction process: a review of worldwide lawsonite eclogites. Lithos, 92, 609-624.

van Calsteren, P.W.C., Boelrijk, N.A.I.M., Hebeda, E.H., Priem, H.N.A., Den Tex, E., Verdurmen,

E.A.T.H., Verschure, R.H. (1979). Isotopic dating of older elements (including the Cabo Ortegal mafic-ultramafic complex) in the Hercynian Orogen of NW Spain: Manifestations of a presumed Early Paleozoic mantle plume. Chemical Geology, 24, 35-56.

van der Wegen, G. (1978). Garnet-bearing metabasites from the blastomylonitic Graben, western Galicia, Spain. Scripta Geologica, 45, 1-95.

van Leeuwen, T., Allen, C.M., Elburg, M., Massonne, H.-J., Palin, J.M., Hennig, J. (2016). The Palu Metamorphic Complex, NW Sulawesi, Indonesia: Origin and evolution of a young metamorphic terrane with links to Gondwana and Sundaland. Journal of Asian Earth Sciences, 115, 133-152.

Vignaroli, G., Rosetti, F., Bouybaouene, M., Massonne, H.-J., Theye, T., Faccenna, C., Funiciello, R. (2005). A counter-clockwise P-T path for the Voltri Massif eclogites (Ligurian Alps, Italy). Journal of Metamorphic Geology, 23, 533-555.

Wain, A. (1997). New evidence for coesite in eclogite and gneisses: Defining an ultrahigh-pressure province in the Western Gneiss region of Norway. Geology, 25, 927-930.

Watson, E.B., Wark, D.A., Thomas, J.B. (2006). Crystallization thermometers for zircon and rutile. Contributions to Mineralogy and Petrology, 151, 413-433.

Wei, C., Cui, Y., Tian, Z. (2015). Metamorphic evolution of LT-UHP eclogite from the south Dabie orogen, central China: An insight from phase equilibria modeling. Journal of Asian Earth Sciences, 111, 966-980

Williams, M.L., Jercinovic, M.J., Terry, M.P. (1999). Age mapping and dating of monazite on the electron microprobe: deconvoluting multistage tectonic histories. Geology, 27, 1023-1026.

Willner, A.P., Krohe, A., Maresch, W.V. (2000). Interrelated P-T-t-d paths in the Variscan Erzgebirge dome (Saxony, Germany): Constraints on the rapid exhumation of high-pressure rocks from the root zone of a collisional orogen. International Geology Review, 42, 64-85.

Willner, A.P., Glodny, J., Gerya, T.V., Godoy, E., Massonne, H.-J. (2004). A counterclockwise PTt path of high-pressure/low-temperature rocks from the Coastal Cordillera accretionary complex of south-central Chile: constraints for the earliest stage of subduction mass flow. Lithos, 75, 283-310.

Winchester, J.A., & Team, P.T.N. (2002). Palaeozoic amalgamation of Central Europe: new results from recent geological and geophysical investigations. Tectonophysics, 360, 5-21.

Wood, D.A., Joron, J.L., Treuil, M. (1979). A re-appraisal of the use of trace elements to classify and discriminate between magma series erupted in different tectonic settings. Earth and Planetary Science Letters, 45, 326-336.

Wu, C.M., & Cheng, B.H. (2006). Valid garnet-biotite (GB) geothermometry and garnet-aluminum silicate-plagioclase-quartz (GASP) geobarometry in metapelitic rocks. Lithos, 89, 1-23.

Xiao, Y., Hoefs, J., van den Kerkhof, A.M., Fiebig, J., Zheng, Y. (2000). Fluid history of UHP metamorphism in Dabie Shan, China: a fluid inclusion and oxygen isotope study on the

coesite-bearing eclogite from Bixiling. Contributions to Mineralogy and Petrology, 139, 1-16.

Xu, Z., Zeng, L., Liu, F., Yang, J., Zhang, Z., McWilliams, M., Liou, J.G. (2006). Polyphase subduction and exhumation of the Sulu high-pressure-ultrahigh-pressure metamorphic terrane. Geological Society of America Special Paper, 403, 93-113.

Zack, T. & Luvizottow, G.L. (2006). Application of rutile thermometry to eclogites. Mineralogy and Petrology, 88, 69-85.

Zack, T., Moraes, R., Kronz, A. (2004). Temperature dependence of Zr in rutile: empirical calibration of a rutile thermometer. Contributions to Mineralogy and Petrology, 148, 471-488.

Zhang, G., Ellis, D.J., Christy, A.G., Zhang, L., Song, S. (2010). Zr-in-rutile thermometry in HP/UHP eclogites from Western China. Contributions to Mineralogy and Petrology, 160, 427-439.

Zhang, R.Y., Liou, J.G., Ernst, W.G. (1995). Ultrahigh-pressure metamorphism and decompressional P-T paths of eclogites and country rocks from Weihai, eastern China. Island Arc, 4, 293-309.

Zhu, Y.F., Massonne, H.-J., Theye, T. (2007). Eclogites from the Chinese Continental Scientific Drilling borehole, their petrology and different P-T evolutions. Island Arc, 16, 508-535.

Acknowledgements

Firstly, I would like to express my deepest gratitude to Prof. Hans-Joachim Massonne for his extensive work as my supervisor, and he gave me the best supervision. During my PhD work, he never criticized me on my bad work, but always was patient and silent to help me and encourage me in every way. He read though my manuscripts for publications many times for each, and did careful corrections again and again to improve them. He has also been a very dedicate guide for me. He supported me to go to geological field and international conferences, which allowed me to greatly broaden my scientific horizons. He is always at service and patient to answer every of my questions making sure that my work was always on the right track. His broad knowledge and calm personality have been very inspiring on my future work and life.

Secondly, I want to thank Prof. Joris van Slageren for participate to my dissertation as my second supervisor. He is a responsible professor, and he was caring on the progress of my PhD work, giving me good tips how to manage my work and prepare final exam.

Thirly, I want to mention the institute team. Dr. Thomas Theye taught me how to use the insruments of EMP and XRF, and I troubled him tens of thounds of times during my analytical work. He introduced books and papers to me from time to time. He is a good advisor, and he solved a lot of my scientific questions. I also want to give a big thank to Dr. Joachim Opitz, as others said “he taught us to enjoy sunshine everyday”. He always can find fun from stressful life, which makes the work place so happy. He is a kind of culture dictionary, and I know a lot of interesting stories about different countries from him. Another one of my most respective persons is Prof. Arne Willner. Everytime when I met him, he asked my work progress and gave me constructive suggestions. Dr. Tillmann Viefhaus is also a helpful person, he was enthuastic to give me valuable informations and I troubled him a lot about chemisty questions. I appreciate Volker Spieth for organizing so many times of lunch and dinner. He encouraged me to improve my English and plan my future. I thank Alexander Shopf for kindly providing his mother’s hause for my first year stay. In the beginning of my Phd study, he also helped a lot about my enrollment and EMP operation. Gelareh rahimi and Florian Waizenhoefer are thanked for unforgettable experiences of common study, field trip and dialy discussions. I also want to give my

deep gratitude to Bettina Wieland, Moritz Schmelz, Gisela Kwiatkowski, Matthias Leiss, and Zeljka Zigovecki Gobac for their help.

In such international environment here, I had also the opportunity to know interesting people from all over the world, giving me the curiosity about different cultures and point of views. It was priceless. Wentao Cao from USA, Deborah Lo Pò, Salvatore Iaccarino, Dario Fancello from Italy and Sérgio Benjamin Baggio from Brazil, became very close friends to me. We chatting, traveling, and eating during our leisure time, which are very unforgettable memories.

My parents are thanked for giving me total freedom for chasing my dream. I want to thank my boyfriend Xiao-Ping Yuan. He donated much emotional support and motivated me through my tough time.

China Scholarship Council is thanked for providing a four-year scholarship to undertake a PhD thesis work at Universitaet Stuttgart.